SCUOLA DI DOTTORATO
UNIVERSITÀ DEGLI STUDI DI MILANO-BICOCCA

Dipartimento di Biotecnologie e Bioscienze

Dottorato di Ricerca in Scienze della Vita Ciclo XXIX

Curriculum in Biotecnologie

The RNA processing proteins Xrn1 and Rrp6 regulate DNA damage checkpoint activation and telomere metabolism

Cesena Daniele

Matricola 718295

Tutore: Prof.ssa Longhese Maria Pia

Coordinatore: Prof. Vanoni Marco Ercole

ANNO ACCADEMICO 2015/2016

INDEX

Index

ABSTRACT

Abstract

Genome instability is one of the most pervasive characteristics of cancer cells. It can be due to DNA repair defects, failure to arrest the cell cycle and loss of telomere-end protection that lead to end-to-end fusion and degradation. Among the many types of DNA damage, the DNA Double Strand Break (DSB) is one of the most severe, because it can cause mutations and chromosomal rearrangements. Eukaryotic cells respond to DSBs by activating a checkpoint that depends on the protein kinases Tel1/ATM and Mec1/ATR, in order to arrest the cell cycle until DSBs are repaired. Mec1/ATR is activated by RPA-coated single-stranded DNA (ssDNA) that arises upon nucleolytic degradation (resection) of the DSB.

A similar checkpoint response is triggered when the natural ends of eukaryotic chromosomes lose their protection, resembling and being recognized as DSBs. This protection is provided by specialized nucleoprotein complexes called telomeres. Telomeric DNA consists of repetitive G-rich sequences that terminate with a 3'-ended single-stranded overhang (G-tail), which is important for telomere extension by telomerase. Several proteins, including the CST complex, are necessary to maintain telomere structure and length in both yeast and mammals.

Emerging evidences indicate that RNA processing proteins play critical, yet poorly understood, roles in genomic stability and telomere metabolism. We provide evidence that the *Saccharomyces cerevisiae* RNA decay factors Xrn1, Rrp6 and Trf4 facilitate activation of Mec1/ATR by promoting the generation of RPA-coated ssDNA at intrachromosomal DSBs. Xrn1 and Rrp6 are also required to activate a

Abstract

Mec1/ATR-dependent checkpoint at uncapped telomeres due to loss of the CST component Cdc13. Xrn1 promotes checkpoint activation by facilitating the generation of ssDNA at both DSBs and uncapped telomeres. Xrn1 exerts this function at DSBs by promoting the loading of the MRX complex, whereas how it does at uncapped telomeres remains to be determined. By contrast, DSB resection is not affected by the absence of Rrp6 or Trf4, but their lack impairs the recruitment of RPA, and therefore of Mec1, to the DSB. Rrp6 and Trf4 inactivation affects neither Rad51/Rad52 association nor DSB repair by homologous recombination (HR), suggesting that full Mec1 activation requires higher amount of RPA-coated ssDNA than HR-mediated repair. Finally, we demonstrate that Xrn1 maintains telomere length by promoting the association of Cdc13 to telomeres independently of ssDNA generation and exerts this function by downregulating the *RIF1* transcript.

Our results provide novel links between RNA processing and genome stability.

RIASSUNTO

Riassunto

L'instabilità genomica è una delle caratteristiche principali delle cellule tumorali e può essere causata da difetti nella riparazione del DNA, dal mancato arresto del ciclo cellulare e dalla perdita della protezione telomerica all'estremità dei cromosomi, che porta alla degradazione e alla fusione delle estremità. Tra i vari tipi di danno al DNA, le rotture della doppia elica del DNA (*Double-Strand Break* o DSB) rappresentano una delle lesioni più pericolose, poiché possono causare mutazioni o riarrangiamenti cromosomici. In presenza di DSBs, le cellule eucariotiche attivano un checkpoint, dipendente dalle protein chinasi Tel1/ATM e Mec1/ATR, che arresta il ciclo cellulare finché il danno non è stato riparato. Mec1/ATR è attivata dal DNA a singolo filamento (ssDNA) ricoperto da RPA che si forma dopo il processamento nucleolitico (*resection*) delle estremità del DSB.

Una simile risposta è attivata anche quando le estremità naturali dei cromosomi eucariotici perdono la loro protezione, generando delle estremità simili ad un DSB che vengono riconosciute dal checkpoint e dai meccanismi di riparazione. Questa protezione è fornita da complessi nucleoproteici specializzati, chiamati telomeri. Il DNA telomerico è costituito da sequenze ripetute ricche in G che terminano con una coda a singolo filamento sporgente in 3' (detta coda G), la quale è importante per l'estensione dei telomeri ad opera della telomerasi. Diverse proteine, tra cui il complesso CST, sono necessarie al mantenimento della struttura e della lunghezza dei telomeri sia in lievito che nei mammiferi.

Recenti dati sperimentali indicano che i fattori che processano l'RNA hanno un ruolo fondamentale nella stabilità del genoma e nel

metabolismo telomerico, anche se il meccanismo è ancora poco compreso. In questa tesi abbiamo dimostrato che in *Saccharomyces cerevisiae* le proteine che degradano l'RNA Xrn1, Rrp6 e Trf4 promuovono l'attivazione di Mec1/ATR facilitando la formazione di DNA a singolo filamento ricoperto da RPA ai DSB. Inoltre, Xrn1 e Rrp6 sono necessarie per attivare il checkpoint anche ai telomeri deprotetti a causa del malfunzionamento di Cdc13, una delle subunità del complesso CST coinvolto nella protezione dei telomeri. Xrn1 facilita la formazione di DNA a singolo filamento ai DSBs promuovendo il caricamento del complesso MRX, mentre come svolga questa funzione ai telomeri deprotetti rimane ancora da chiarire. Al contrario, la generazione di ssDNA ai DSBs non è influenzata dalla mancanza di Rrp6 o Trf4, ma la loro assenza ostacola il reclutamento di RPA e quindi di Mec1 al sito di danno. L'inattivazione di Rrp6 e Trf4 non influenza né l'associazione di Rad51/Rad52 ai DSB né la riparazione della rottura attraverso la ricombinazione omologa (*Homologous Recombination* o HR), suggerendo che la piena attivazione di Mec1 richieda più DNA a singolo filamento ricoperto da RPA di quanto ne sia richiesto per la riparazione attraverso la ricombinazione omologa. Infine, Xrn1, regolando negativamente il trascritto di *RIF1*, è coinvolto nel mantenimento della lunghezza dei telomeri promuovendo l'associazione di Cdc13 indipendentemente dalla formazione di DNA a singolo filamento.

In conclusione, i nostri risultati forniscono un nuovo collegamento tra il processamento dell'RNA e il mantenimento della stabilità del genoma.

INTRODUCTION

Maintaining genome integrity: the DNA Damage Response

Maintaining the integrity of the genome is crucial for all organisms. In fact, preservation of genomic integrity is a pre-requisite for proper cell function and faithful transmission of the genome to progeny. However, environmental factors and the chemical properties of DNA do not guarantee lifelong stability and proper functioning of the genome. It is estimated that each cell has approximately 10^4-10^5 lesions per day, which must be repaired to ensure genomic integrity. In eukaryotes, the mechanisms involved in maintaining genome integrity and in preventing the generation of potentially deleterious mutations are extremely sophisticated and they include a complex cellular response, called DNA Damage Response (DDR), highly conserved during evolution. The DDR is a network of cellular pathways that sense, signal and repair DNA lesions: they are able to detect the presence of DNA lesions and activate a specialized surveillance mechanism, known as DNA damage checkpoint, that coordinates the repair of the damage with cell cycle progression (Figure 1) (Ciccia and Elledge, 2010).

The biological significance of a functional DDR for human health is clearly illustrated by the severe consequences of inherited defects in DDR factors resulting in various diseases, including immune deficiency, neurological degeneration, premature aging, and severe cancer susceptibility (Jackson and Bartek, 2009). Taken advantage of the extreme conservation of DDR among eukaryotes, we can use model organisms, like the yeast *Saccharomyces cerevisiae*, to better characterize the molecular mechanisms of these pathways.

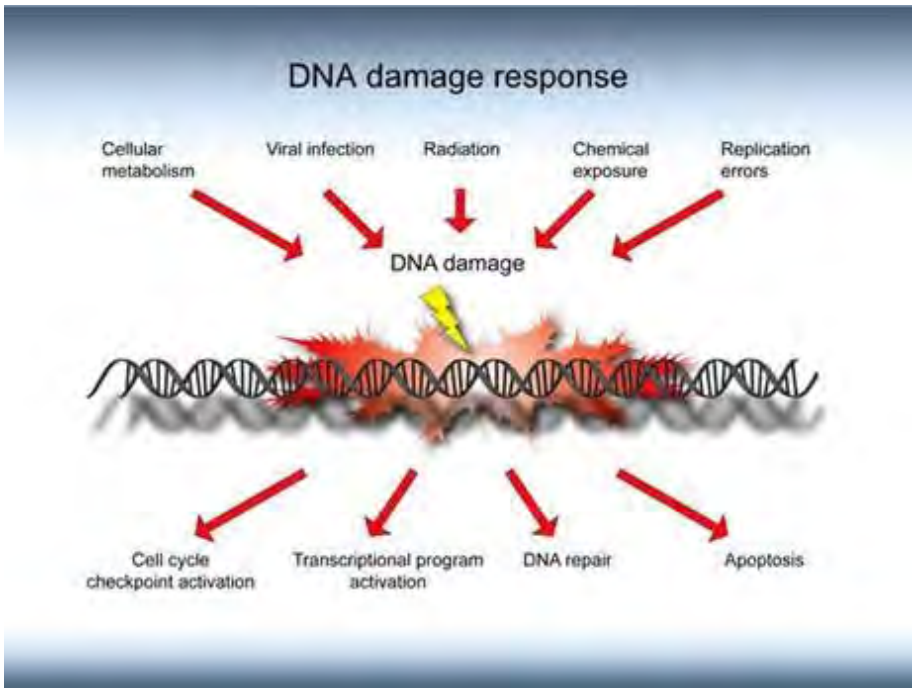

Figure 1. Cell response to DNA damage: causes and consequences. DNA damage caused by cellular metabolism, viral infection, radiation, chemical agents and errors during DNA replication induce the DNA damage response. The presence of DNA damage leads to: checkpoint activation, transcriptional program activation, DNA repair and apoptosis.

DNA Double-Strand Breaks (DSBs)

DNA double-strand breaks (DSBs) are among the most cytotoxic forms of DNA damage because failure to repair them can lead to loss of genetic information and chromosome rearrangements. DSBs are generated when the phospho-sugar backbones of both DNA strands are broken at the same position or in sufficient proximity to allow physical dissociation of the double helix into two separate molecules. DSBs are generated by the action of exogenous agents, such as ionizing radiation (IR) or radiomimetic chemicals that mimic the action of

ionizing radiation. The latter comprise several distinct classes of chemicals. These include base alkylating agents such as methyl methane sulfonate (MMS), as well as crosslinking agents that introduce covalent crosslinks between bases of the same (intrastrand) or complementary strands (interstrand or ICLs), including platinum derivatives and psoralens. In addition, DNA topoisomerase inhibitors induce the formation of single-strand breaks (SSBs) or DSBs by trapping topoisomerase-DNA intermediates during isomerization reactions. For example, the camptothecins and their derivatives (irinotecan and topotecan), which inhibit type IB topoisomerases, generate DSBs primarily during DNA replication. Drugs that generate DSBs are widely used in cancer chemotherapy since tumor cells are often more sensitive to DSBs than normal cells.

DSBs are also generated during normal cell metabolism. The reactive oxygen species (ROS) produced during cellular metabolism can oxidize bases and trigger both single and double strand breaks. Other physiological sources of endogenous DSBs include DNA replication and meiotic recombination, as well as programmed rearrangements of the immunoglobulin and T cell receptor loci during lymphoid cell development. DNA replication is thought to be the major source of DSBs in proliferating cells since the DNA intermediates at replication forks are fragile and susceptible to breakage. Notably, breaks can occur following DNA polymerase stalling, which leads to the generation of persistent single-strand DNA (ssDNA) intermediates. DNA polymerase stalling can also be induced by depleting the deoxyribonucleotides pool with ribonucleotide reductase inhibitors,

such as hydroxyurea (HU). Broken or collapsed replication forks containing ssDNA resemble DSBs at different stages of processing and are also a source of genomic instability if not properly repaired (Aparicio *et al.*, 2014).

DSBs can be repaired through two major conserved pathways: Non-Homologous End-Joining (NHEJ) and Homologous Recombination (HR). NHEJ directly rejoins together the two broken ends, whereas HR uses intact homologous duplex DNA sequences (sister chromatids or homologous chromosomes) as a template for accurate repair. An important factor governing the choice between the HR and NHEJ repair pathways is the phase of the cell cycle. HR is generally restricted to the S and G2 phases when DNA has replicated and the sister chromatid is available as a repair template. On the other hand, NHEJ operates throughout the cell cycle but seems to be more prevalent in the G1 phase. Making the right choice between NHEJ and HR is important to ensure genome stability (Symington and Gautier, 2011).

DSB repair pathways: Non-Homologous End-Joining (NHEJ)

NHEJ is a repair process that directly ligates two broken ends with little or no processing. If the ends are compatible, the enzyme DNA ligase directly reconstitutes the phosphodiester bond; but if, as is often the case, are not perfectly compatible, they are first processed by different protein and then relegated (Figure 2A). This makes the process prone to the loss of small stretches of DNA and therefore the NHEJ repair process is called error prone. It is highly efficient, but it can lead to

mutations at the joining sites, as well as inversions and translocations (Chiruvella *et al.*, 2013).

NHEJ is the main repair pathways in mammals and is conserved from yeast to humans. The initial step in NHEJ is the recognition and binding of the Ku heterodimer (composed of the Ku70 and Ku80 subunits) to the DSB. NHEJ is active only on blunt or minimally processed DNA ends, and therefore is inhibited by the nucleolytic degradation of the 5' strands (resection) that leads to HR. If cells are in the G1 cell cycle phase, the presence of Ku prevents resection and mediates recruitment of downstream NHEJ factors. Once Ku is bound to the DSB ends, it recruits the other NHEJ factors to the damage site, including DNA Ligase IV (Dnl4 in yeast and DNL4 in mammals) with its cofactor (Lif1 in yeast and XRCC4 in human) and XRCC4-like factor (Nej1 in yeast and XLF in human) (Davis and Chen, 2013). Given that most of the DNA damage generate ends not compatible, before the action of the DNA ligase, if necessary, there is processing of the DNA ends to create ligatable ends. Depending on the nature of the break, different DNA end processing enzymes may be required, including those that resect DNA ends, fill in gaps, remove blocking end groups, and make the ends ligatable. In mammals, Ku also recruits the DNA-PKcs, a member of the phosphoinositide 3-kinase related protein kinase (PIKK) family, which phosphorylates different substrates involved in NHEJ. In yeast, a DNA-PKcs homolog is missing and the function of this kinase is thought to be substituted by the Mre11/Rad50/Xrs2 (MRX) complex (MRE11/RAD50/NBS1 complex in mammals). This complex possesses several functions in NHEJ. First, through interaction with other NHEJ

proteins (Palmbos *et al.*, 2008), it functions as chaperone/adaptor of the NHEJ machinery coordinating interactions among its individual components. Second, it mediates DNA end-tethering (this function resembles that of DNA-PKcs in mammalian cells) (Ferrari *et al.*, 2015) and, finally, as the Mre11 nuclease and Rad50 ATPase activities are required to dissociate MRX and Ku70/80 complexes from DSBs (Wu *et al.*, 2008), it has also a role in terminating NHEJ process.

Mutations in components of NHEJ caused different diseases including hypersensitivity to IR and the Lig4 syndrome, a rare disorder caused by mutations in the gene encoding for the Ligase IV and characterized by immune deficiency, microcephaly, and developmental delay (Davis and Chen, 2013).

DSB repair pathways: Homologous Recombination (HR)

Homologous recombination is defined as the exchange of genetic information between donor and recipient DNA molecules with similar or identical sequence (Figure 2C-E). Availability of a homologous sequence for recombinational repair is mainly defined by ploidy and cell cycle phase. However, additional factors such as proximity of the donor and recipient sequences, chromatin structure, and nuclear compartmentalization also contribute to the availability of a sequence for HR (Mathiasen and Lisby, 2014). HR is the main repair pathways in yeast and is conserved from yeast to humans. Recombination is initiated upon the formation of ssDNA overhangs through a process termed DNA end resection, which is essential for all recombination mechanisms (Figure 3). Resection of DSBs commits their repair to HR

as it prevents ligation by the potentially more mutagenic NHEJ pathway (Symington and Gautier, 2011). The ssDNA is bound by replication protein A (RPA) to control its accessibility to the Rad51 recombinase. The barrier to Rad51-catalyzed recombination imposed by RPA can be overcome by a number of mediators, such as BRCA2 and Rad52, which serve to replace RPA with Rad51 on ssDNA, and the Rad51 paralogs Rad55-Rad57 (RAD51B-RAD51C-XRCC2-XRCC3 in human) which stabilize Rad51 filaments on ssDNA. The Rad51 nucleoprotein filament catalyzes the invasion into a homologous duplex to produce a displacement loop (D-loop). At this stage, additional anti-recombination functions are exerted by Srs2 (FBH1, PARI), which dissociates Rad51 filaments from ssDNA, and Mph1 (FANCM), which disassembles D-loops (Daley *et al.*, 2014). Upon Rad51-catalyzed strand invasion, the ATP-dependent DNA translocase Rad54 enables the invading 3' end to be extended by DNA polymerases to copy genetic information from the intact duplex DNA. Ligation of the products often leads to joint molecules (JMs), such as single- or double-Holliday junctions (s/dHJs) or hemicatenanes (HCs), which must be processed to allow separation of the sister chromatids during mitosis. JMs can be dissolved by the Sgs1-Top3-Rmi1 complex (STR) (BTR, BLM-TOP3a-RMI1-RMI2) (Bizard and Hickson, 2014) or resolved by structure-selective nucleases, such as Mus81-Mms4 (MUS81-EME1), Slx1-Slx4, and Yen1 (GEN1) (Wyatt and West, 2014). JM are resolved to produce crossover (CO) or non-crossover (NCO) products, depending on the manner in which the DNA strands are bound to each other. Mitotic cells favor recombination events that

lead to non-crossover events likely to avoid potentially detrimental consequences of loss of heterozygosity and translocations.

There are several pathways of DNA repair by homologous recombination. The first HR model for repair of a DSB is called the Double-Strand Break Repair (DSBR) model (or double Holliday Junction model), where the second end of DSB can be engaged to stabilize the D-loop structure (second-end capture), leading to the generation of a double-Holliday Junction (dHJ) (Mehta and Haber, 2014) (Figure 2C). In the second model, the invading strand can be displaced from the D-loop and anneals either with its complementary strand as in gap repair or with the complementary strand associating with the other end of the DSB. Since the model involves DNA synthesis followed by strand annealing, it is called Synthesis-Dependent Strand Annealing (SDSA) (Figure 2D). This repair mechanism is conservative, since ensures the production of only NCO product because no HJs are formed, thus SDSA mechanism is preferred over DSBR during mitosis. In the third model, the D-loop structure can assemble into a replication fork and copy the entire chromosome arm in single-ended invasion process called Break-Induced Replication (BIR) (Figure 2E). This mechanism is evoked more often when there is only one DNA end, either due to the loss of the other end or in the process of lengthening telomeres in telomerase-deficient cells. In BIR, the DSB end is nucleolytically processed similar to the resection that occurs in other DSB HR repair events. The single-strand tail then invades a homologous DNA sequence, often the sister chromatid or homolog chromosome, but sometimes a repeated sequence on a different chromosome. The invading end is used to copy

information from the invaded donor chromosome by DNA synthesis (Malkova and Ira, 2013).

All the above pathways require Rad51, with the exception of some forms of BIR. However, DSBs can also be repaired by pathways independent of Rad51 (e.g. NHEJ). One of these pathways is the Single-Strand Annealing pathway (SSA) (Figure 2B). SSA is restricted to repair of DNA breaks that are flanked by direct repeats that can be as short as 30 nt. Resection exposes the complementary strands of homologous sequences, which recombine resulting in a deletion containing a single copy of the repeated sequence. SSA is therefore considered to be highly mutagenic. The non-homologous single-stranded tails are removed by the Rad1-Rad10 endonuclease (XPF-ERCC1 in mammals) in a complex that includes both the Msh2-Msh3 mismatch repair proteins and "scaffold" proteins Slx4 and Saw1. After tail clipping, remaining gaps must be filled in by DNA synthesis and sealed by ligation. SSA requires the strand-annealing activity of Rad52 and is aided by the Rad52 homolog Rad59 (Mehta and Haber, 2014; Bhargava *et al.*, 2016).

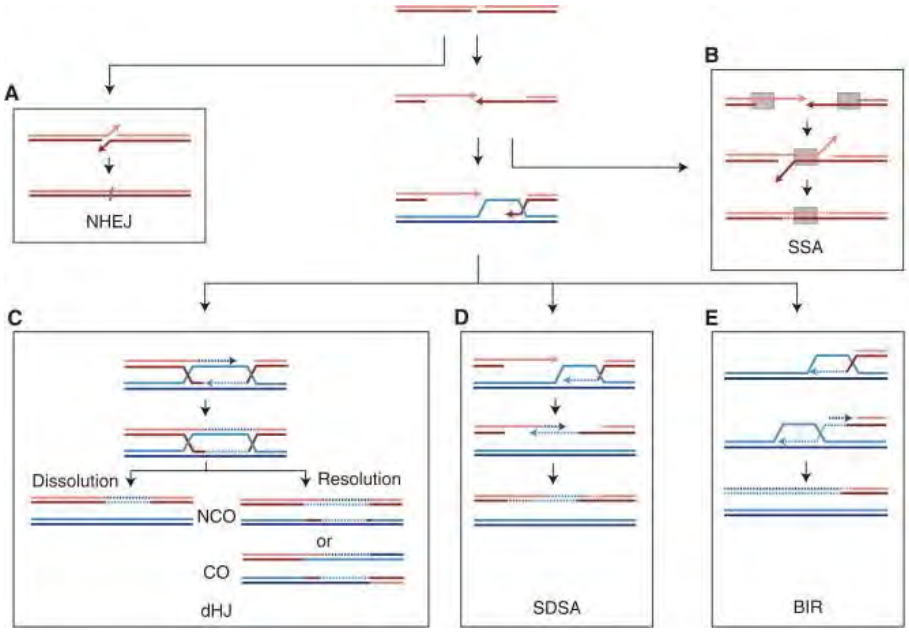

Figure 2. Pathways of DNA DSB repair. DSBs are processed by 5' to 3' end resection producing 3' single-stranded tails. A) NHEJ involves ligation of broken ends, with little or no base pairing. B) Single-Strand Annealing (SSA) takes place when resection reveals flanking homologous repeats that can anneal, leading to deletion of the intervening sequences. C) The double Holliday Junction (dHJ) pathway involves second end capture to stabilize the D-loop. The dHJ structure can be resolved either by helicase and topoisomerase-mediated dissolution to give non-crossover (NCO) or cleaved by HJ resolvases to produce both crossover (CO) or NCO outcomes. D) In Synthesis-Dependent Strand Annealing (SDSA), the newly synthesized strand dissociates from the D-loop and results in a NCO outcome with no change to the template DNA. E) BIR involves both leading and lagging strand synthesis and results in loss of heterozygosity or, if the template is located ectopically, a nonreciprocal translocation. Newly synthesized DNA is depicted as dashed lines in the same color as the template; arrowheads indicate 3' ends (Mehta and Haber, 2014).

Resection: a crucial step in DSB repair

The repair of DNA double-strand breaks by homologous recombination initiates by nucleolytic degradation of the 5' terminated strand of the DNA break. This leads to the formation of 3' tailed DNA, which serves as a substrate for the strand exchange

protein Rad51. The nucleoprotein filament then invades homologous DNA to drive template-directed repair. Long tracts of ssDNA are also required for activation of the DNA damage checkpoint response. Thus, identifying the proteins required and the underlying mechanism for DNA end resection has been an intense area of investigation.

Genetic studies in *S. cerevisiae* show that end resection takes place in two steps. Initially, a short oligonucleotide tract is removed from the 5' strand to create an early intermediate with a short 3' overhang. Then in a second step the early intermediate is rapidly processed generating an extensive tract of ssDNA. The first step is dependent on the highly conserved MRX complex and Sae2, while the second step employs the exonuclease Exo1 and the helicase Sgs1 with the endonuclease Dna2. Resection mechanisms are highly conserved between yeast and humans, and analogous machineries are found in prokaryotes as well (Cejka, 2015) (Figure 3).

Positive regulators of DSB resection

The MRX (Mre11, Rad50, Xrs2) complex in yeast or MRN complex (MRE11, RAD50, NBS1) in mammal initiates DSB resection together with the Sae2 protein (CtIP in human) (Clerici *et al.*, 2005). MRX has an affinity for DNA ends, and was shown to be one of the first proteins recruited to DSBs (Lisby *et al.*, 2004). It likely functions as a dimer (Hohl *et al.*, 2011) and it has both catalytic and structural roles in DNA end processing. The structural role of MRX involves recruitment of components belonging to the second long-range processing step (Zhu *et al.*, 2008; Mimitou and Symington, 2008; Cejka *et al.*, 2010; Shim *et*

al., 2010). Mre11 exhibits 3'-5' dsDNA DNA exonuclease activity and ssDNA endonuclease activity (Paull and Gellert, 1998; Trujillo *et al.*, 1998). It has been demonstrated that Sae2 strongly promotes the endonuclease of Mre11 within the MRX complex (Cannavo and Cejka, 2014). The preferential cleavage of the 5'-terminated DNA suggests that the Mre11 nuclease initiates DNA resection via its Sae2-promoted endonuclease, rather than exonuclease activity (Cannavo and Cejka, 2014). It has been proposed that MRX together with Sae2 can remove oligonucleotides from the 5' ends of the break, giving rise to short 3'-ended ssDNA tails of 50-200 nucleotides that are then subjected to extensive resection (Mimitou *et al.*, 2008; Zhu *et al.*, 2008) (Figure 3). Sae2 involvement in DSB processing is conserved among eukaryotes, as also its putative ortholog in humans CtIP has critical functions in DSB resection (Sartori *et al.*, 2007). The function of Sae2 in end resection requires its phosphorylation on Ser267 by Cyclin-Dependent Kinases (CDK) (Huertas *et al.*, 2008). In fact, a *sae2-S267A* mutant exhibits defective generation of 3'-ended ssDNA and reduced HR-mediated DSB repair. Therefore, the CDK dependent regulation of Sae2 activity represents one of the key control mechanisms ensuring that resection only takes place in the S/G2 phase of the cell cycle when a homologous template is available for repair. In addition to CDK, Sae2 is also regulated by the Mec1 and Tel1 kinases in response to DNA damage (Cejka, 2015).

The requirement for MRX and Sae2 in end resection depends upon the nature of DNA ends. The initial endonucleolytic cleavage of the 5' strands catalyzed by MRX and Sae2 is crucial for the processing of

"dirty" DNA ends such as those created after exposure to IR, CPT, bleomycin and methylating agents, where protein-DNA adducts or altered DSB ends structures must be removed to allow further processing. Conversely, resection of "clean" DSB ends, such as those generated by endonucleases, can occur also in the absence of MRX and Sae2 (Gobbini *et al.*, 2013). In fact, initiation of resection at an endonuclease-induced DSB is impaired in cells lacking MRX or Sae2, but once resection is initiated its rate is similar to that of wild type cells (Clerici *et al.*, 2005). It is worth noting that the defect in initiating resection is more severe in *mre11Δ* cells than in *sae2Δ* cells or *mre11* nuclease defective mutants, and this difference is likely due to reduced recruitment at DSBs of other proteins involved in resection (Sgs1, Dna2 and Exo1) rather than to a specific requirement for MRX to initiate resection (Gobbini *et al.*, 2013).

More extensive DSB resection is catalyzed by the 5'-3' exonuclease Exo1 and 5' flap endonuclease Dna2 that acts in concert with the 3'-5' RecQ helicase Sgs1 , acting in two partially redundant pathways (Mimitou *et al.*, 2008; Zhu *et al.*, 2008) (Figure 3). Inactivation of a single pathway results in only a minor resection defect, because the other pathway can effectively compensate. Major resection defects were only revealed when both pathways were inactivated simultaneously, for example in *sgs1Δ exo1Δ* double mutants (Zhu *et al.*, 2008; Mimitou and Symington, 2008). The extension of resection generates a longer ssDNA fragment 3' protruding necessary to activate the subsequent step of HR.

Sgs1 is a DNA helicase belonging to the RecQ family (Cejka and Kowalczykowski, 2010). Sgs1 translocates with a 3'-5' polarity on one DNA strand and unwinds DNA. Unwound ssDNA is coated by RPA, which directs the nucleolytic activity of Dna2 toward the 5'terminated DNA strand. Then the ssDNA formed by Sgs1-mediated DNA unwinding is degraded by the endonuclease Dna2, which is a CDK target in DSB resection (Chen *et al.*, 2011).

Dna2 is a bifunctional helicase-nuclease, which possess both 3'-5' and 5'-3' nuclease activities and a DNA helicase activity with a 5'-3' polarity. Dna2 must load on a free ssDNA end but then degrades DNA endonucleolytically, resulting in degradation products of 5-10 nucleotides in length (Zhu *et al.*, 2008; Cejka *et al.*, 2010).

Both Sgs1 and Dna2 have separate functions unrelated to DNA end resection. Sgs1 functions together with Top3 and Rmi1 to dissolve dHJs into NCO products, thereby preventing sister chromatid exchanges and chromosome instability. Dna2 is responsible for removing DNA flaps arising by strand displacement synthesis by DNA polymerase δ during lagging strand DNA synthesis. The Okazaki fragment processing function of Dna2 is essential, although the viability of *dna2Δ* mutants can be rescued by multiple mechanisms (Cejka, 2015).

Exo1 is an exonuclease with 5'-3' nuclease activity. Unlike the Dna2 nuclease that is specific for ssDNA, the nuclease activity of Exo1 degrades the 5'-terminated strand within dsDNA (Tran *et al.*, 2002). Therefore, Exo1 does not require a helicase partner to unwind DNA, and directly produces the required 3'-tailed DNA (Tran *et al.*, 2002).

Resection in humans occurs via two pathways, which are similar to those described for *S. cerevisiae*. In one of them, BLM, the human counterpart of Sgs1, and DNA2 physically interact and collaborate in 5'-3' resection of DNA ends, while MRN promotes resection by recruiting BLM to DNA ends. In addition, DNA2 also interacts with another RecQ family helicase, Werner (WRN). In the second pathway, MRN, RPA and BLM stimulate resection by promoting the action of human EXO1 to DNA ends, with BLM enhancing EXO1 affinity for DSB ends and MRN increasing EXO1 processivity (Nimonkar *et al.*, 2011).

DSB resection is also influenced by histone modifications and ATP-dependent chromatin remodeling reactions (Seeber *et al.*, 2013). For example, the chromatin remodeler Fun30 promotes DSB resection by removing Rad9 from the DSB ends. Interestingly, recent data indicate that Exo1- and Sgs1/Dna2-mediated DSB processing require distinct chromatin remodeling events (Adkins *et al.*, 2013). In fact, either removal of H2A-H2B dimers or incorporation of the histone variant H2A.Z markedly enhances Exo1 activity, suggesting that ATP-dependent chromatin-remodeling enzymes regulate Exo1-mediated resection. By contrast, resection by the Sgs1-Dna2 machinery remains efficient when chromatin fibers are subsaturated with nucleosomes, suggesting that initiation of resection by this pathway might simply require a nucleosome-free gap next to the DSB.

Negative regulators of DSB resection

DNA end resection is also negatively regulated to prevent that nucleolytic degradation takes place in a different phase of cell cycle

and to avoid the generation of excessive ssDNA. In particular, deletion of *YKU70* or *YKU80* allows DSB resection in *S. cerevisiae* G1 cells. Moreover, G1 cells lacking Ku show an increased recruitment of Mre11 at the DSB ends, whereas loss of MRX increases Ku binding (Gobbini *et al.*, 2013). These results suggest that Ku and MRX compete for binding to DSBs and that DSB-bound Ku limits the formation of ssDNA by impairing the loading and/or the activity of resection factors. Notably, resection of a single DSB in Ku-deficient G1 cells occurs independently of CDK activity, although it is limited to DNA regions close to the break site (Clerici *et al.*, 2008). This finding indicates that Ku is the principal rate-limiting factor for initiation of resection in G1, and its action is prevented in G2 by CDK-dependent phosphorylation events. The presence of the Ku complex bound at the DSB ends inhibits the nucleolytic processing catalyzed by Exo1 (Villa *et al.*, 2016). The absence of Ku suppresses the resection defect of *mre11Δ* and *sae2Δ* cells in an Exo1-dependent manner (Shim *et al.*, 2010; Mimitou and Symington, 2010; Foster *et al.*, 2011), indicating that Ku restricts Exo1-mediated resection. As Ku is bound very close to the DSB ends, the MRX-Sae2 clipping could allow Exo1 to initiate resection from a nick and this, in turn, would overcome the inhibition exerted by Ku on Exo1 activity (Figure 3). The negative regulation of Ku complex in DSB resection is conserved also in mammalian cells. Human Ku (KU70 and KU80) blocks EXO1-mediated DNA end resection. Unlike in yeast, the displacement of Ku from DNA ends is not mediated by the MRN complex (Sun *et al.*, 2012).

By contrast, Sgs1-Dna2 is unable to initiate end resection without MRX even in the absence of Ku, suggesting the existence of another inhibitory pathway. The resection activity of Sgs1-Dna2 is inhibited mainly by the Rad9 protein (Bonetti *et al.*, 2015; Ferrari *et al.*, 2015), which was originally identified as an adaptor in the DNA damage checkpoint pathway, linking the checkpoint kinases Mec1 and Tel1 to the activation of the effector kinases Rad53 and Chk1 (Pellicioli and Foiani, 2005). Rad9 is already bound to chromatin even in the absence of DNA damage by an interaction with methylated lysine 79 of histone H3 (H3-K79) (Grenon *et al.*, 2007; Lazzaro *et al.*, 2008) (Figure 3). Rad9 binding to the sites of damage is further strengthened by an interaction between its BRCT domain and histone H2A that has been phosphorylated on serine 129 (γH2A) by the checkpoint kinases Mec1 and Tel1 (Hammet *et al.*, 2007). Several lines of evidence indicate that Rad9 acts as a barrier toward end processing enzymes by restricting the access of Sgs1-Dna2 to the DSB ends. The lack of Rad9 suppresses the resection defect of Sae2-deficient cells, which show an increased amount of Rad9 bound very close to the DSB ends (Bonetti *et al.*, 2015; Ferrari *et al.*, 2015). The lack of Rad9 increases the resection efficiency also in a wild type context (Lazzaro *et al.*, 2008) and this rapid resection is mainly dependent on Sgs1, whose recruitment at DSBs is inhibited by Rad9 (Bonetti *et al.*, 2015; Ferrari *et al.*, 2015). The human structural and functional ortholog of Rad9 is 53BP1, a protein that interacts with histones and histone-binding proteins. Mammalian 53BP1 inhibits DSB resection promoted by CtIP in G1. DSB resection is allowed by the removal of 53BP1 from DSB ends, which is promoted

by the BRCA1 protein. Moreover, loss of 53BP1 partially rescues the HR defects of BRCA1 mutant cells, confirming that BRCA1 overcomes 53BP1 function at DSBs (Gobbini *et al.*, 2013).

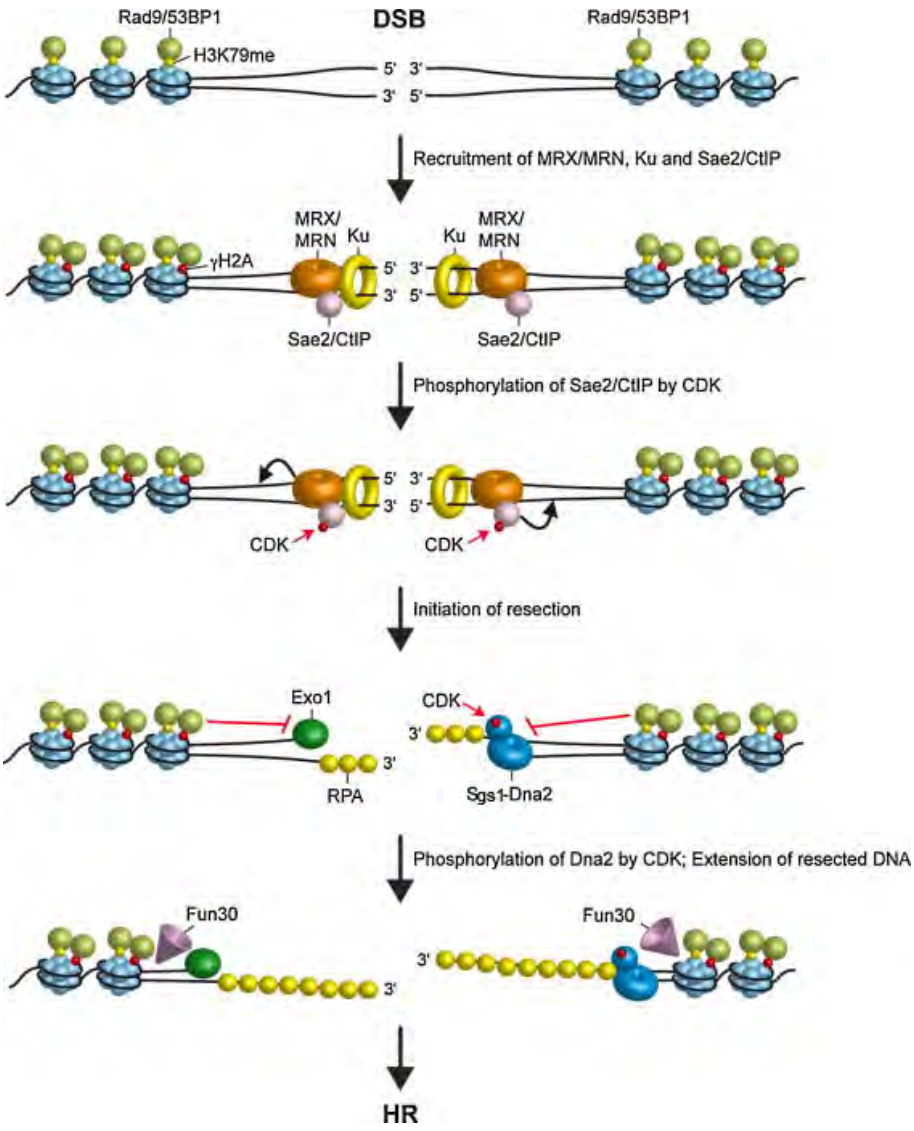

Figure 3. Model for DNA-end resection. MRX/MRN, Ku and Sae2/CtIP rapidly bind DNA ends. Upon phosphorylation of Sae2/CtIP by CDK, MRX/MRN and Sae2/CtIP catalyze the initial processing of the 5' strand. This clipping removes Ku or creates substrates that are no longer bound by Ku. The 5' strand is then extensively

processed through two parallel pathways governed by Exo1 and Sgs1 in concert with Dna2. MRX facilitates the extensive resection by promoting the recruitment of Exo1 and STR-Dna2. Extensive DSB resection is inhibited by the checkpoint adaptor protein Rad9/53BP1, which is bound to methylated histone H3 at lysine 79 (H3-79me) and histone H2A that has been phosphorylated at serine 129 (γH2A). The chromatin remodeler Fun30 promotes DSB resection by removing Rad9 from the DSB ends. The phosphorylation events are indicated as red dots (Gobbini *et al.*, 2013).

The DNA damage checkpoint

The DDR ensures the rapid detection and repair of DSBs in order to maintain genome integrity. Central to the DDR is the DNA damage checkpoint response (Figure 4). When activated by DNA damage, these sophisticated surveillance mechanisms induce transient cell cycle arrests, allowing sufficient time for DNA repair. Activation of the DNA damage checkpoint results in cell cycle arrest, activation of transcriptional programs, initiation of DNA repair or, if the damage is too severe, cellular senescence or programmed cell death (Ciccia and Elledge, 2010). Once repair is completed, the DNA damage checkpoint response is downregulated and cells re-enter the cell cycle in a process known as recovery. Alternatively, if the lesion is irreparable, cells may undergo adaptation and eventually re-enter the cell cycle in the presence of DNA damage (Finn *et al.*, 2012). In *S. cerevisiae*, DNA damage checkpoints operate at three distinct stages in the cell cycle. The G1 checkpoint arrests cells at the G1/S transition prior to START (Fitz Gerald *et al.*, 2002) before cells irreversibly commit to the next cell cycle. This transient arrest delays bud emergence, spindle pole body duplication and S phase entry, allowing time for DNA lesions to

be repaired before the onset of DNA replication (Fitz Gerald *et al.*, 2002). However, certain DNA aberrations such as alkylated DNA do not activate the G1 checkpoint and instead cells pass through START. Essentially, these lesions elicit a checkpoint response during S phase since they need to be converted to secondary lesions during DNA replication before being recognized by the checkpoint machinery (Segurado and Tercero, 2009). The intra-S phase checkpoint slows the rate of replication in response to DNA damage, coordinating fork repair mechanisms and cell cycle progression to ensure the fidelity and completion of replication before cells enter mitosis. The G2/M checkpoint arrests cells at the metaphase to anaphase transition, preventing cells from progressing through mitosis in the presence of DNA damage. The different DNA damage checkpoints share many components and are now known to target many aspects of cellular metabolism besides cell cycle transitions (Finn *et al.*, 2012).

These pathways are highly conserved from yeast to humans. Thus, significant findings in yeast, providing a comprehensive overview of how these signaling pathways function to orchestrate the cellular response to DNA damage and preserve genome stability in eukaryotic cells. Studies of cancer-predisposition syndromes and sporadic tumors in humans have identified mutations in many DNA damage checkpoint genes, underscoring the importance of the checkpoint response. Recent work has also shown that the checkpoint is activated in early cancerous lesions and may function more generally to prevent human tumorigenesis (Harrison and Haber, 2006).

The checkpoint pathways involve three major groups of proteins that act in concert to transduce the signal of damage in order to promote cell cycle arrest and DNA repair. These groups include: (a) sensor proteins that recognize damaged DNA directly or indirectly and signal the presence of alterations in DNA structure, initiating the transduction cascade; (b) transducer proteins, typically protein kinases, that relay and amplify the damage signal from the sensors by phosphorylating other kinases or downstream target proteins; and (c) effector proteins, which include the most downstream targets of the transducer protein kinases, and are regulated, usually by phosphorylation, to prevent cell cycle progression and initiate DNA repair (Figure 4).

The apical protein kinases in the checkpoint transduction cascade are members of a family of phosphoinositide 3-kinase-related kinases (PIKKs), which include the *S. cerevisiae* protein kinases Mec1 and Tel1, as well as their mammalian orthologs ATR and ATM, respectively (Ciccia and Elledge, 2010). In both yeast and mammals, Mec1 physically interacts with Ddc2 (ATRIP in mammals), which helps the recruitment of Mec1 to the DSB ends. By contrast, Tel1 activation depends on the MRX complex, which is required for Tel1 recruitment to the site of damage through direct interaction between Tel1 with Xrs2, as well as for Tel1 kinase activity. Whereas Tel1 is recruited on blunt DSB ends or DNA ends with short ssDNA tails, Mec1 recognizes RPA-coated ssDNA that results from resection of the DSB ends (Villa *et al.*, 2016).

Following DSB formation, binding of MRX to DNA ends promotes the recruitment of Tel1 to the DSB, which facilitates the removal of Ku from the DSB ends to prevent Ku-mediated end-joining and to facilitate resection of the DSB ends (Figure 4). Tel1 also promotes proper MRX association at DSBs needed for end tethering (Cassani *et al.*, 2016).

As the single-stranded tail generated by the resection machinery increases in length, it simultaneously potentiates Mec1/ATR activation and attenuates Tel1/ATM activation (Mantiero *et al.*, 2007; Shiotani and Zou, 2009). When DSB resection takes place, the resulting ssDNA-coated by RPA is recognized by Mec1-Ddc2. In addition, the 9-1-1 checkpoint clamp (Ddc1-Rad17-Mec3 in *S. cerevisiae*; RAD9-RAD1-HUS1 in humans) and clamp loader (Rad24-Rfc2-5 in *S. cerevisiae*; RAD17-RFC2-5 in humans) are recruited to RPA-coated ssDNA independently of the Mec1-Ddc2/ATR-ATRIP complex The 9-1-1 complex promotes Mec1-dependent phosphorylation of its targets and stimulates Mec1 kinase activity via a direct interaction with Ddc1 (Majka *et al.*, 2006).

Once loaded onto RPA-coated ssDNA, Mec1 phosphorylates H2A on serine 129 (γH2A). γH2A generation promotes the enrichment of Rad9 to the DSB ends, which inhibits DSB resection by counteracting Sgs1-Dna2 activity. Mec1 also phosphorylates Rad9 and these phosphorylation events create a binding site for the effector kinase Rad53 (CHK2 in mammals), which then undergoes in-trans autophosphorylation events required for Rad53 activation as a kinase. Once activated, Rad53 in turn inhibits DSB resection by

phosphorylating and inhibiting Exo1 and by promoting Rad9-mediated inhibition of Sgs1-Dna2 activity (Figure 4). Mec1 also activates another effector kinase Chk1, which is required only for the DNA damage G2/M checkpoint. On the contrary, CHK1 is the primary effector of both the DNA damage and replication checkpoints in vertebrates, with CHK2 playing a subsidiary role (Finn *et al.*, 2012).

Once activated, the checkpoint effector kinases phosphorylate several downstream targets, thus regulating a variety of cellular processes. One of the primary events governed by the checkpoint response is the cell cycle arrest, which is induced by the phosphorylation of different substrates depending on the cell cycle phase in which the DNA damage is detected. The arrest of the cell cycle is likely required to allow DNA repair to occur. Numerous proteins directly involved in this repair have been identified as targets of the checkpoint kinases (Putnam *et al.*, 2009).

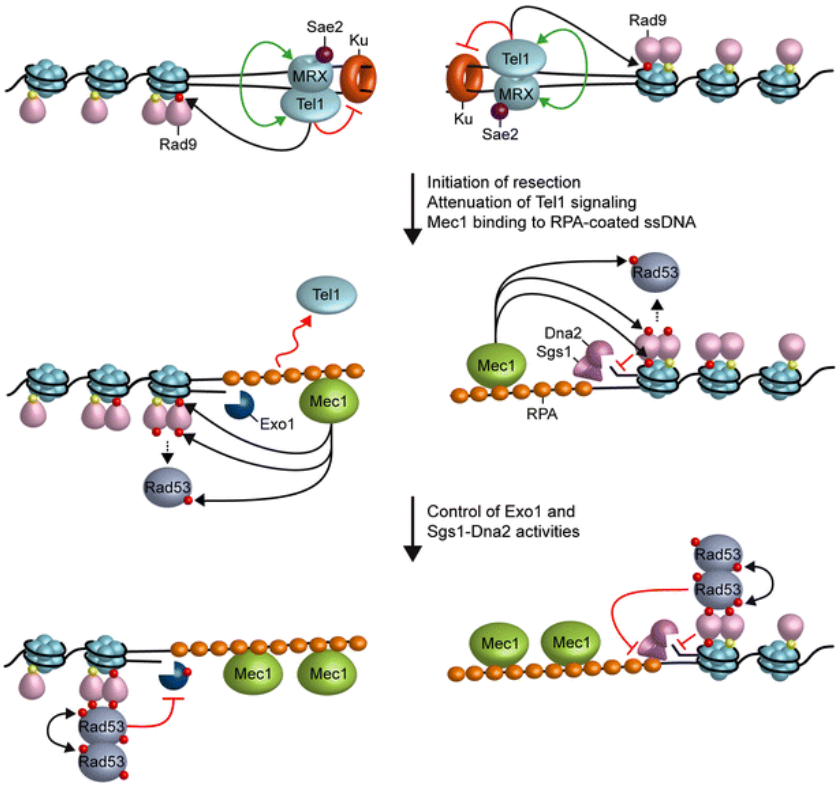

Figure 4. Interplays between end resection and checkpoint. Rad9 is bound to methylated histone H3 (*yellow dots*) even in the absence of DSBs. When a DSB occurs, the MRX complex and Sae2 localize to the DSB ends. MRX is required for the recruitment at DSBs of Tel1, which in turn stabilizes MRX retention at DSBs in a positive feedback loop (*double green arrows*). Tel1 promotes the removal of Ku from the DSB and the initiation of resection. Furthermore, it contributes to the recruitment of Rad9 to the DSB ends through γH2A generation (*red dots*). When DSB resection takes place, the resulting 3'-ended ssDNA attenuates Tel1 signaling activity and, once coated by RPA, allows activation of Mec1. Activated Mec1 contributes to γH2A generation that leads to a further enrichment of Rad9 at DSBs, which provides a barrier to the resection activity of Sgs1-Dna2. Mec1 also phosphorylates Rad9 and these phosphorylation events create binding sites for Rad53 molecules, which then undergo in-trans autophosphorylation and activation (*double black arrows*). Mec1-dependent phosphorylation of Rad53 allows further autoactivation. Once activated by Mec1, Rad53 counteracts DSB resection by phosphorylating and inhibiting Exo1 and by restricting the access to the DSB of Sgs1-Dna2 possibly by reducing Sgs1 binding to RPA-coated DNA. Phosphorylation events are indicated by *black arrows* and *red dots* (Villa *et al.*, 2016).

Maintaining genome integrity: protection and replication of the natural ends of linear chromosomes

The natural ends of eukaryotic chromosomes must be distinguished from intrachromosomal DSBs, which activate a DNA damage response (DDR) including checkpoint-mediated cell cycle arrest and DNA repair/recombination pathways. Protection of chromosome ends, referred to as capping, is achieved by packaging into specialized protective structures called telomeres (Wellinger and Zakian, 2012) (Figure 5).

A number of proteins bind the telomeric DNA and protect it from fusion, degradation, and recognition as a DSB that would otherwise lead to chromosome instability and cell death. Telomeric DNA in most eukaryotes consists of tandem arrays of short repeated sequences, which are guanine-rich in the strand running 5'-3' from the centromere towards the chromosome end. The G-rich strand at both ends of a chromosome extends over the C-strand to form a 3'-ended single-stranded G-rich overhang (G-tail) (Henderson and Blackburn, 1998). Most telomeric DNA is replicated by standard semiconservative DNA replication. As a result of the gap left by the DNA replication machinery after removal of the terminal RNA primer, telomeric DNA sequences become shorter with each round of DNA replication (the so called "end-replication problem"). In most eukaryotes, this loss of telomeric DNA is counteracted by a ribonucleoprotein enzyme called telomerase, which uses its RNA component as a template to add telomere repeats at the telomeric 3' overhang in a reverse transcriptase reaction (Greider and Blackburn, 1985). In mammalian

cells, the minimal catalytic core of telomerase consists of the telomerase reverse transcriptase (TERT) and the telomerase RNA (TERC). In *Saccharomyces cerevisiae*, the telomerase consists of the reverse transcriptase Est2, the template RNA *TLC1*, and two accessory proteins Est1 and Est3 (Wellinger and Zakian, 2012). *S. cerevisiae* telomerase is recruited to telomeres through an interaction between the telomerase subunit Est1 and Cdc13, a component of the CST complex (Nugent *et al.*, 1996; Evans and Lundblad, 1999; Pennock *et al.*, 2001; Bianchi *et al.*, 2004).

Telomeres can function both as tumor suppressors by limiting the number of cell divisions and as tumor promoters by inducing genome instability. Although telomerase is continuously expressed in unicellular eukaryotes, its expression is downregulated in most human somatic tissues (Kim *et al.*, 1994). The inability of the replication machinery to fully replicate DNA ends, coupled with low/absent telomerase activity, results in progressive telomere shortening that causes cells to stop dividing in a process called replicative senescence (Harley *et al.*, 1990; Lundblad and Szostak, 1989). In the absence of other genetic changes, these cells can remain in a quiescent state that essentially functions as an anticancer mechanism for long-lived species like humans. However, genetic alterations that cause a failure to activate the checkpoint response may allow additional cell divisions, during which the dysfunctional telomeres continue to erode until they eventually become too short to protect the chromosome termini from unscheduled DNA repair events. The cells then enter a period called “crisis”, during which the chromosomes ends undergo end-to-end

fusion events and enter a breakage-bridge fusion cycle that leads to genomic instability. Although cells entering this state can be eliminated by apoptosis, most cancer cells exhibit upregulation of telomerase activity, indicating that rare surviving cells can avert senescence and crisis by restabilizing telomeres (Counter *et al.*, 1992) (Figure 5).

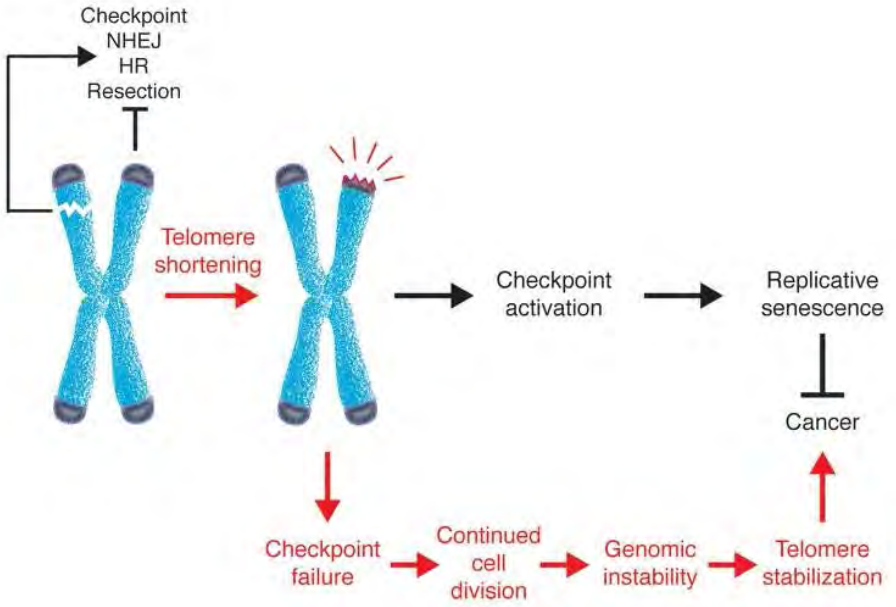

Figure 5. Telomere deprotection in carcinogenesis. Although intrachromomal DSBs elicit a checkpoint response and can be repaired, the natural chromosome ends are protected from fusion and degradation and do not activate the checkpoint. This protective function, referred to as capping, is due to proteins that bind the telomeric DNA. Loss of capping due to either deficiencies in capping proteins or loss of telomeric DNA induces a DNA damage checkpoint response that leads to cell cycle arrest and senescence, thus providing a potent anticancer mechanism. However, rare failure to activate the checkpoint may allow cells to undergo cell divisions during which uncapped telomeres can be subjected to unscheduled DNA repair events. The resulting genomic instability, coupled with activation of telomere restabilizing mechanisms, can drive the oncogenic process (Gobbini *et al.*, 2014).

Capping of Chromosome Ends

The ends of eukaryotic chromosomes are not subjected to DNA repair events and do not activate the DDR, despite being physical DNA ends. Several studies on *S. cerevisiae* and mammals have revealed that protein complexes with specificity for double-stranded and single-stranded telomeric DNA prevent the natural chromosome ends from being recognized as intrachromosomal DSBs (de Lange, 2009) (Figure 6). In *S. cerevisiae*, the telomeric ssDNA is bound by Cdc13, which can be found with Stn1 and Ten1 in a heterotrimeric complex called CST (Figure 6A). CST protects telomeric DNA from degradation; exposure of cells harboring *cdc13*, *stn1,* or *ten1* conditional alleles to restrictive conditions causes telomere degradation by progressive resection of the 5'-ended strand and a checkpoint-dependent cell cycle arrest. The 5'-3' exonuclease Exo1 appears to be the major nuclease that degrades telomeres in *cdc13* mutants (Maringele and Lydall, 2002) (Figure 7). As Cdc13 binding to the single-stranded telomeric DNA reduces the association of Mec1 with these DNA ends (Hirano and Sugimoto, 2007) and the CST complex bears a structural resemblance to the RPA complex, CST binding to the telomere has been proposed to prevent RPA recruitment and subsequent Mec1 activation (Gao *et al.*, 2007). A CST-like complex (Ctc1-Stn1-Ten1) has recently been identified in *S. pombe*, plants, and humans and shown to perform a similar function in telomere capping and telomerase regulation (Price *et al.*, 2010) (Figure 6B and C).

Double-stranded telomeric DNA in *S. cerevisiae* is bound by the Rap1-Rif1-Rif2 complex (Figure 6A) (Shi *et al.*, 2013). Loss of function of this

complex has less catastrophic consequences than CST inactivation; dysfunction of Rap1 or Rif2 leads to increased amounts of telomeric ssDNA and NHEJ-mediated fusion events (Marcand *et al.*, 2010). Generation of telomeric ssDNA in cells defective for Rif2 or Rap1 requires the MRX complex, suggesting that Rap1 and Rif2 prevent resection at telomeric ends by interfering with the association between MRX and telomeres (Figure 7). On the other hand, inactivation of Rap1 or Rif2 does not leads to checkpoint activation (Bonetti *et al.*, 2010), suggesting that the exposed telomeric ssDNA is still covered by Cdc13, which limits association of Mec1 with telomeres. Unlike Rif2 and Rap1, Rif1 is not involved in the prevention of telomeric fusions by NHEJ and plays a very minor role in protecting telomeres from degradation (Ribeyre and Shore, 2012). Instead, Rif1 prevents short telomeric ends from activating checkpoint-mediated cell cycle arrest by inhibiting the recruitment of checkpoint proteins to these ends (Xue *et al.*, 2011). Furthermore, it plays a unique role in supporting cell viability and prevents nucleolytic degradation in mutants defective in the CST complex (Anbalagan *et al.*, 2011). Interestingly, both CST and Rif1 physically and genetically interact with components of the polα-primase complex (Qi and Zakian, 2000) raising the possibility that Rif1 might promote the ability of CST to fill in the exposed telomeric ssDNA through activation/recruitment of the lagging-strand DNA replication machinery (Figure 7).

Degradation of telomeric DNA is also counteracted by the Ku complex, which acts in a different pathway from Rif2. In fact, while MRX is primarily responsible for nucleolytic degradation of telomeres in *rif2*Δ

cells (Bonetti *et al.*, 2010) Exo1 is the nuclease that degrades telomeric DNA in *yku70*Δ G1 cells (Maringele and Lydall, 2002). Interestingly, Ku protects telomeres in the G1 phase of the cell cycle, when the protective function of CST is dispensable (Vodenicharov *et al.*, 2010).

In vertebrates, telomeres are protected from eliciting the DDR and undergoing degradation or fusion events by a specialized group of proteins collectively called shelterin, which includes TRF1, TRF2, RAP1, TIN2, TPP1, and POT1 (Figure 6C). Although the shelterin complex represents a functional unit, the individual components have specific protective functions (de Lange, 2009). Inactivation of TRF2 in mouse embryo fibroblasts by either gene deletion or overexpression of a dominant-negative variant causes activation of ATM (Celli and de Lange, 2005), as well as accumulation of telomere-induced foci formed by DDR factors such as 53BP1, MRN, ATM, and the histone variant γH2AX (Takai *et al.*, 2003). Moreover, TRF2 also protects telomeres from NHEJ-mediated fusion events (Celli and de Lange, 2005). In mammals, the telomeric single-stranded overhang can fold back on the double-stranded part of the telomere to form a lariat structure, called a t-loop, which is predicted to prevent the binding of DNA repair/checkpoint proteins to the telomeric DNA. As TRF2 is required for the formation and/or maintenance of t-loops (Doksani *et al.*, 2013), TRF2-dependent remodeling of telomeres into t-loop structures might explain how TRF2 represses NHEJ and ATM signaling at telomeres.

Repression of ATR is performed by POT1 in humans and POT1a in mice (Hockemeyer *et al.*, 2005; Wu *et al.*, 2006). Based on the finding that POT1 specifically recognizes the telomeric ssDNA overhangs, it has

been proposed that POT1 and POT1a block ATR activation by preventing RPA binding to the telomeric ssDNA (Gong and de Lange, 2010). This switch from RPA to POT1 on telomeric ssDNA is promoted by the heterogeneous nuclear ribonucleoprotein A1 (hnRNPA1) protein through a mechanism that is regulated by telomeric repeat containing RNA (TERRA), a non-coding RNA that is transcribed from the telomeric C-rich strand (Flynn *et al.*, 2011). Inhibition of RPA binding by POT1 may also play an important role in preventing HR, which is repressed at telomeres in a redundant manner by POT1 and RAP1 (Wu *et al.*, 2006; Sfeir *et al.*, 2010).

Even when mouse telomeres are stripped of shelterin and Ku, complete loss of telomeric DNA does not occur unless the DNA damage response protein 53BP1 is also depleted (Sfeir and de Lange, 2012), suggesting that multiple pathways act in a highly redundant manner to block telomere degradation.

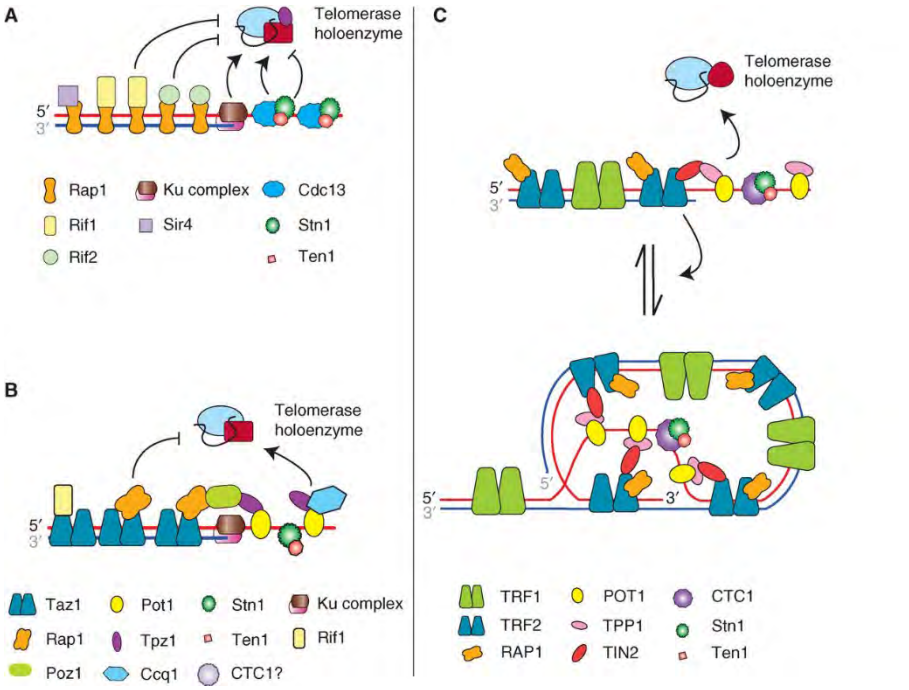

Figure 6. Model structures and associated proteins of budding yeast, fission yeast, and human telomeres. A) DNA structure and associated proteins of budding yeast telomeres. Arrows and blunt arrows denote upregulation and down-regulation of telomerase recruitment, respectively. B) DNA structure and associated proteins of fission yeast telomeres C) DNA structure and associated proteins of human telomeres (Webb *et al.*, 2013).

End processing at telomeres

Generation of telomeric G-strand overhangs occurs independently of telomerase action (Wellinger *et al.*, 1996; Dionne and Wellinger, 1998). Single-stranded overhangs at lagging-strand telomeres can potentially originate from the removal of the last RNA primer and/or from the inability of the polα-primase complex to efficiently initiate Okazaki fragment synthesis at the end of a linear DNA molecule. By contrast, leading-strand DNA synthesis generates blunt ended DNA termini. As 3’ single-stranded overhangs can be detected at both

daughter telomeres (Wellinger *et al.*, 1996; Makarov *et al.*, 1997), the C-strand of leading-strand telomeres should be processed by nucleases to generate 3' ended ssDNA overhangs. Interestingly, semiconservative replication of telomeres is a prerequisite for this C-strand degradation (Dionne and Wellinger, 1998), suggesting that the processing activities devoted to create G-tails are either directly associated with the replication fork machinery or are dependent on fork passage that allows their recruitment to chromosomal termini.

In human, it has been recently shown that lagging-strand telomeres have an almost mature single-stranded overhang size very soon after replication of the duplex telomeric DNA. By contrast, generation of G-rich single-stranded overhangs at human leading-strand telomeres is delayed, suggesting that apparently distinct processing activities act at the leading- and lagging-strand telomeres (Chow *et al.*, 2012). Furthermore, the final lagging RNA primer at the lagging-strand telomere has been shown not to be positioned at the very end of the chromosome, but to be randomly located ˜70–100 nucleotides from the end (Chow *et al.*, 2012). This finding implies that each round of DNA replication leaves up to 100 nucleotides of unreplicated DNA on each lagging-strand telomere.

In *S. cerevisiae*, single-stranded G-rich tails of 5-10 nt in length are present at telomeres throughout most of the cell cycle except in late S phase, when longer overhangs are detected (Soudet *et al.*, 2014). On lagging-strand ends, synthesis of the last primer initiates on the very last template nucleotides and primer length appears to match the required overhang length of about 10 nt. Therefore, after primer

removal, this end looks precisely like the parental telomere. Thus, for yeast, the end-replication problem really manifests itself on the leading-strand ends. On leading-strand ends, DNA synthesis proceed all the way to the end of the template, generating blunt-ends that are shown to be replication intermediates. The parental template strand then is resected by about 30-40 nt before being filled in again to leave a DNA end with a 3' overhang of about 10 nt (Soudet *et al.*, 2014).

The activities responsible for telomere processing in *S. cerevisiae* share common players with the machinery resecting DNA DSBs (Figure 7). The MRX complex has been shown to play an important role in the generation of the telomeric ssDNA (Diede and Gottschling, 2001; Bonetti *et al.*, 2009). Consistent with the notion that the blunt ends generated by leading-strand synthesis are resected to generate ssDNA, the MRX complex localizes preferentially at leading-strand telomeres (Faure *et al.*, 2010). Whether a MRX independent mechanism is processing the lagging-strand telomeres remains to be determined. As for DSB resection, MRX acts in the same pathway as the Sae2 protein to generate G-tails, and Sae2 function at telomeres needs phosphorylation on Ser267 by the cyclin-dependent kinase Cdk1 in *S. cerevisiae* (Figure 7) (Bonetti *et al.*, 2009). This requirement can explain why telomere resection can occur only in S and G2 phases of the cell cycle, when Cdk1 activity is high (Dionne and Wellinger, 1996; Frank *et al.*, 2006; Vodenicharov and Wellinger, 2006). However, the phospho-mimicking *sae2-S267D* allele does not bypass the Cdk1 requirement for degradation of the C-rich strand, suggesting that

other unknown Cdk1 targets contribute to regulate telomere processing (Bonetti *et al.*, 2009).

As MRX and Sae2 are required to initiate resection of modified ends, MRX/Sae2-dependent processing activities might be required to overcome unusual chromatin structures and/or protein-DNA complexes at telomeres that block the access of Exo1. Consistent with this hypothesis, MRX and Sae2 are not required for processing telomeres that are deprotected due to the lack of the CST complex, and whose extensive processing depends on Exo1 (Maringele and Lydall, 2002; Zubko *et al.*, 2004).

Although G-tails are short in *mre11Δ* cells, they still increase in length in late S/G2 phase (Larrivée *et al.*, 2004). Likewise, loss of Sae2 does not abolish ssDNA telomeric generation (Bonetti *et al.*, 2009), indicating that partially overlapping processing activities exist. Indeed, Sgs1 and Exo1 are responsible for the residual resection that occurs in a *sae2Δ* mutant (Bonetti *et al.*, 2009), indicating that Exo1 and Sgs1, acting in cooperation with Dna2, provide compensatory activities for processing telomeric ends when Sae2-MRX activity is compromised (Figure 7).

Remarkably, the nuclease activities that process mammalian telomeres are somewhat different from those involved in *S. cerevisiae* telomere processing. In mice, deletion of either NBS1 or BLM, the mammalian counterparts of Xrs2 and Sgs1, respectively, does not reduce the telomeric overhang signals, indicating that these proteins do not play a major role in telomere processing (Wu *et al.*, 2012). Instead, mammalian telomere processing depends on the nucleases

Apollo/SNM1B and Exo1 (Wu *et al.*, 2012). Apollo, which is recruited to telomeres by TRF2 (van Overbeek and de Lange, 2006), was shown to contribute to overhang generation specifically at leading-strand telomeres (Wu *et al.*, 2012). Unlike Apollo, Exo1 appears to exert its effect on both leading- and lagging-strand telomeres, as Exo1 deficiency results in 40 % reduction of the telomeric overhang signal at both newly synthesized telomeres (Wu *et al.*, 2012). It is so far unclear whether other nucleases in addition to Apollo contribute to telomere-end processing at mammalian telomeres, as it happens in yeast.

The differences between budding yeast and mammals in G-tail generation may be due to differences in the structure of telomeric DNA. The t-loop conformation of mammalian telomeres is thought to protect telomeric ends from the ATM-dependent checkpoint by inhibiting detection of the telomere by the mammalian equivalent of the MRX complex, MRN (MRE11-RAD50-NBS1) (Lazzerini Denchi and de Lange, 2007). As t-loop formation requires TRF2 (Doksani *et al.*, 2013), which is responsible for loading Apollo to the telomeric ends, one possibility is that mammalian telomeres have evolved a specialized mechanism that allows the generation of telomeric single-stranded overhangs in a TRF2 telomeric context. Consistent with this hypothesis, removal of the TRF1 and TRF2 shelterin subunits in cells lacking 53BP1 leads to increased telomeric ssDNA that depends on CtIP and BLM, the mammalian orthologs of Sae2 and Sgs1, respectively (Sfeir and de Lange, 2012).

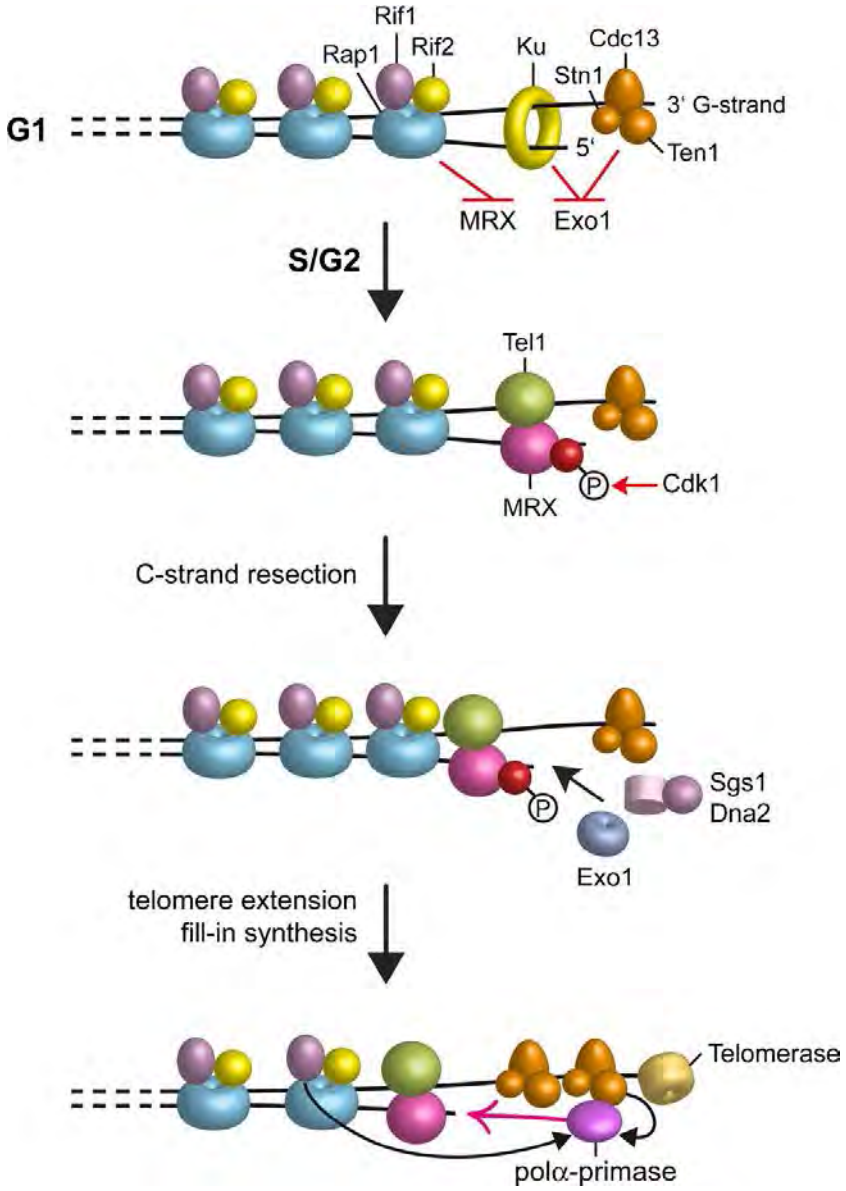

Figure 7. Telomere resection in *S. cerevisiae*. In G1, when Cdk1 activity is low, Ku and the CST complex protect telomeres from Exo1, while Rap1, Rif1 and Rif2 mainly act by preventing MRX access at telomeres. In S/G2, telomere resection can take place because Cdk1 activates Sae2-MRX, and Ku does not exert its inhibitory effect. Sgs1-Dna2 and Exo1 can provide compensatory activities to resect the 5' C-strand. The resulting telomeric ssDNA is covered by the CST complex. Then, Cdc13 allows telomerase action, and Rif1 assists the CST-mediated filling-in of the complementary C-strand by the polα–primase complex.

mRNA degradation pathways: deadenylation-dependent decay

Recent evidences indicate a role for RNA processing in the maintenance of genome integrity. An important aspect of RNA processing is mRNA degradation. Indeed, messenger RNA turnover is a critical modulator of gene expression and many mechanisms primarily devoted to regulating the stability of transcripts or the elimination of defective mRNAs exist. These pathways are well conserved among eukaryotes and generally converge to the degradation of mRNA by two exoribonucleases activities. One degrades transcripts from 5' to 3' direction and is dependent on XRN protein family members (Nagarajan *et al.*, 2013) and the other degrades transcripts from 3' to 5' direction through the activity of the multi-subunit exosome complex (Houseley *et al.*, 2006).

In general, the decay of most eukaryotic mRNAs occurs by three major pathways: 1) deadenylation-dependent 2) deadenylation-independent and 3) endonucleolytic cleavage-dependent decay.

As its name implies, the first rate-limiting step of deadenylation-dependent mRNA decay involves shortening of the poly(A) tail prior to 5' cap removal (i.e. decapping) and subsequent degradation (Figure 8). In budding yeast, the deadenylation step is performed by two main complexes, CCR4-NOT and PAN2-PAN3. The CCR4-NOT complex is a multifunctional protein assembly of 9 main subunits (10 subunits in human), 2 of which, CCR4 and Caf1, are deadenylases, while the other 7 subunits function as scaffold protein of the complex with distinct yet not fully characterized roles. The second deadenylation complex present in yeast, but also well conserved in higher eukaryotes, is a

heterotrimer formed by the PAN2 protein interacting with the homodimer of PAN3. The 3' exonuclease PAN2, the activity of which depends on the poly(A) binding protein Pab1, is responsible for the rapid removal of the first exposed adenine residues, leaving the poly(A) tail of around 65 nucleotides. After this, the poly(A) tail is slowly degraded by the CCR4 nuclease (Parker, 2012).

Following this deadenylation step, the mRNA can undergo degradation in either the 5' to 3' or 3' to 5' direction. The 5' to 3' degradation pathway requires that the 5'-cap structure of mRNAs is removed. This process is performed by the Dcp2 enzyme, which forms a complex with Dcp1 and hydrolyze the 5' cap structure to release m7GDP and a 5' monophosphate mRNA. Several decapping enhancers or activators are known to function to stimulate the rate of decapping either by directly stimulating the activity of Dcp2 or by inhibiting translation initiation. The best defined decapping activator, which is conserved in all eukaryotes, is the Lsm1-7-Pat1 complex, while other cofactors vary between organisms (Siwaszek *et al.*, 2014). Decapped (5' monophosphorylated) RNA is exposed to attack and complete degradation by Xrn1, a processive 5' to 3' exonuclease, highly conserved across species (Figure 8). Decapping and the 5' to 3' degradation are coupled, as Xrn1 nuclease interacts directly with the components of the decapping machinery (Siwaszek *et al.*, 2014). Xrn1 has two highly conserved domains that fold into the active region of the enzyme, which is then stabilized by interactions with additional domains (Nagarajan *et al.*, 2013). The active site of Xrn1 couples unwinding of duplexes to the processivity of the enzyme, which

explains how it can degrade through structures without a helicase. Indeed, Xrn1 appears to be able to degrade structured RNA by pulling the RNA through a channel that is wide enough for only a single strand, which causes duplex unwinding (Jinek *et al.*, 2011). A paralog of Xrn1 is Rat1, which is typically localized to the nucleus and functions in nuclear RNA processing and/or degradation pathways (Nagarajan *et al.*, 2013). However, Rat1 can substitute for Xrn1 when it is localized to the cytoplasm due to mutation, indicating that no Xrn1-specific protein-protein interactions are required for mRNA degradation (Johnson, 1997).

After deadenylation the mRNA can also be degraded in the 3' to 5' direction, primarily through the activity of the multi-subunit exosome complex (Kilchert *et al.*, 2016) (Figure 8). This macromolecular complex has a central core arranged in a ring consisting of six catalytically inactive 3' to 5' exoribonucleases, capped by three small RNA-binding proteins. Depending on the subcellular localization, the exosome core associates with catalytically active subunits: a distributive RNase D 3' to 5' exoribonuclease, Rrp6 (nucleus and nucleolus), and/or a processive RNase II 3' to 5' exoribonuclease Rrp44/Dis3 (cytoplasm and nucleus). In humans, there is an additional exosome-associated Dis3 homolog, called Dis3L, which is mainly localized in the cytoplasm (Kilchert *et al.*, 2016). The majority of substrates enter the barrel-like structure of the exosome through a pore at the centre of the cap and are channelled to the active site of Dis3 (Bonneau *et al.*, 2009). Moreover, RNA-unwinding activities are central to the regulation of the exosome, as they facilitate threading

of the RNA substrate through the narrow channel entrance (Hardwick and Luisi, 2013). In *S. cerevisiae*, two related conserved helicases, Mtr4 and Ski2, are required for RNA degradation in the nucleus and the cytoplasm, respectively. Both helicases are associated with accessory factors, which unwind the RNA and feed it into the exosome complex. Mtr4, for example, interacts with a non-canonical poly(A) polymerase (Trf4 or Trf5) and a RNA-binding protein Air1 or Air2 to form the Trf4/5-Air1/2-Mtr4 polyadenylation complex (TRAMP) (LaCava *et al.*, 2005), while Ski2 forms a complex with Ski3 and Ski8 proteins and interacts with the cytoplasmic exosome through Ski7 and Ski4 proteins (Parker, 2012). Finally, exosome-mediated 3' to 5' degradation in the cytoplasm is followed by hydrolysis of the remaining cap-structure by Dcs1 (DcpS in mammals), a "scavenger" type decapping enzyme (Liu *et al.*, 2004).

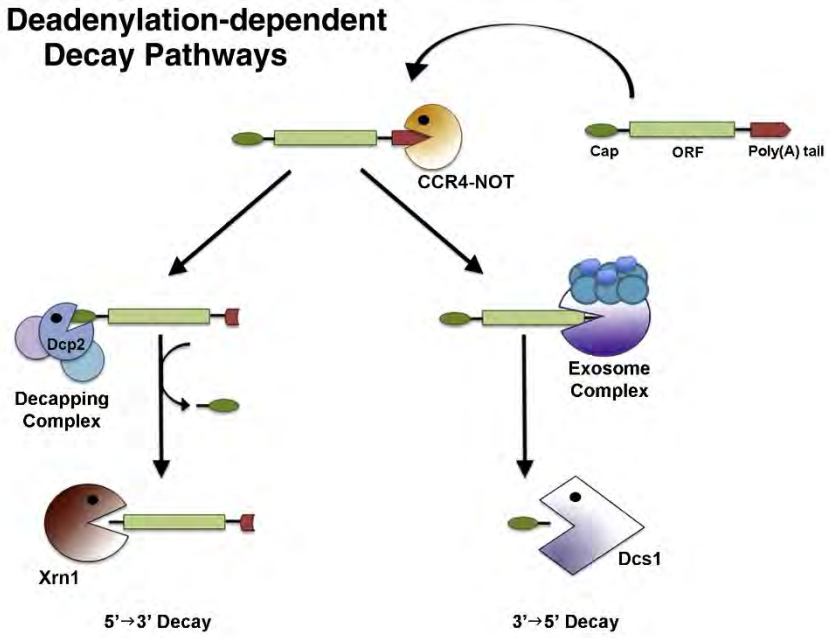

Figure 8. Mechanisms of mRNA degradation in eukaryotes: deadenylation-dependent pathway. Deadenylation activity of CCR4-NOT complex removes nearly all of the poly(A) tail. Following deadenylation, mRNAs can be degraded by either 5' to 3' or 3' to 5' decay pathways. In 5' to 3' decay, a decapping complex, typically containing Dcp2, hydrolyzes the 5' cap exposing the mRNA to exoribonuclease Xrn1. Alternatively, the deadenylated mRNA is degraded by the exosome complex in the 3' to 5' direction, and the 5' cap structure is hydrolyzed by the scavenger-decapping enzyme Dcs1 (Nagarajan *et al.*, 2013).

mRNA degradation pathways: deadenylation-independent and endonucleolytic cleavage-dependent decay

Another mRNA degradation mechanism involves the internal cleavage of mRNA to create unprotected 5' and 3' fragments that are substrates for exoribonucleolytic decay (Figure 9). While in *S. cerevisiae* mRNA degradation mainly depends on exoribonucleolytic decay from the ends, in other organisms many pathways utilize endoribonucleases (e.g. AGO, SMG6, and Rrp44/Dis3) (Tomecki and Dziembowski, 2010).

One example of this in both plants and animals occurs via small RNAs (20–30 nt long) acting as guides in silencing complexes by directing AGO proteins to specific target mRNAs (Valencia-Sanchez *et al.*, 2006). Endonucleolytic cleavage is achieved by an AGO slicer activity if the small RNA is highly complementary to the target, if not, other decay mechanisms that may be linked to translational inhibition can take place. If cleavage by AGO does occur, Xrn1 in humans or Xrn4 in plants degrade the 3' mRNA fragment while the 5' fragment is degraded by the exosome (Valencia-Sanchez *et al.*, 2006). In humans and *Drosophila melanogaster*, transcripts containing premature termination codons (PTCs) are degraded via a SMG6-mediated endonucleolytic mechanism, followed by exoribonucleolytic decay of the cleaved 5' and 3' fragments by the exosome and Xrn1 (Pacman in *D. melanogaster*), respectively (Eberle *et al.*, 2009).

Some mRNAs undergo 5' to 3' decay without the removal of poly(A) tail (e.g. *S. cerevisiae* transcripts recognized for nonsense-mediated decay, and *RPS28B* and *EDC1* mRNAs) (Peccarelli and Kebaara, 2014; Badis *et al.*, 2004; Muhlrad and Parker, 2005). As part of the cytoplasmic mRNA surveillance system, aberrant mRNAs, mainly NMD substrates, also predominantly undergo 5' to 3' degradation without the need for deadenylation (Peccarelli and Kebaara, 2014) (Figure 9).

The nonsense-mediated mRNA decay (NMD) pathway is a translation-dependent mRNA degradation pathway that recognizes and elicits the rapid degradation of select mRNAs that prematurely terminate translation. In cases where the mRNAs have a premature termination codon (PTC), degradation of these mRNAs by NMD prevents the

accumulation of potentially harmful truncated proteins. This pathway is highly conserved in all eukaryotes, from yeast to humans (Peccarelli and Kebaara, 2014). Three core *trans*-acting factors are required for a functional NMD pathway in all eukaryotes. These core NMD factors are the up-frameshift proteins Upf1, Upf2, and Upf3 and mutation or silencing of anyone of these three factors selectively stabilizes mRNAs that are regulated by NMD (He *et al.*, 1997). Upf1, a group 1 RNA helicase with ATPase activity, is the central regulator of the degradation pathway and is the most conserved of the Upf proteins, while Upf2 and Upf3 are responsible for regulating Upf1 function. Upf1 also associates with additional factors, including the eukaryotic translational release factors eRF1 and eRF3 (Czaplinski *et al.*, 1998). It is important to note that Upf1p plays additional roles distinct from NMD, including telomere maintenance, histone mRNA decay, genome stability, and advancement of the cell cycle (Chawla *et al.*, 2011; Kaygun and Marzluff, 2005; Azzalin and Lingner, 2006). In yeast, NMD targets can be recognized as targets due to the lack of factors bound downstream from the termination codon (Amrani *et al.*, 2004). In this model, known as the faux untranslated region (UTR) model, a ribosome terminating translation at a termination codon substantially upstream from the poly(A) tail terminates translation inefficiently. The faux-UTR model posits that NMD occurs because Pab1 or other factor bound to the poly(A) tail is not in close proximity to the terminating ribosome to enable interaction of Pab1 with eRF3, which is bound to the terminating ribosome and thus establishes the correct context for a normal translation termination event (Amrani *et al.*, 2006). In the

absence of correct translation termination, the Upf factors interact with the release factors, eRF1p and eRF3p, resulting in an aberrant translation termination event and NMD activation. NMD activation leads to the decapping of the mRNA by the Dcp1-Dcp2p complex, followed by 5' to 3' degradation of the mRNA by the exoribonuclease Xrn1p (Peccarelli and Kebaara, 2014).

In metazoans, additional factors are required for NMD such as the SMG proteins, which perform a variety of functions like regulating the phosphorylation state of Upf1 or showing an endonuclease activity in the case of SMG6. Additionally, the exon-junction complex (EJC) is a multiprotein complex that enhances NMD of mRNAs that undergo splicing (Popp and Maquat, 2013).

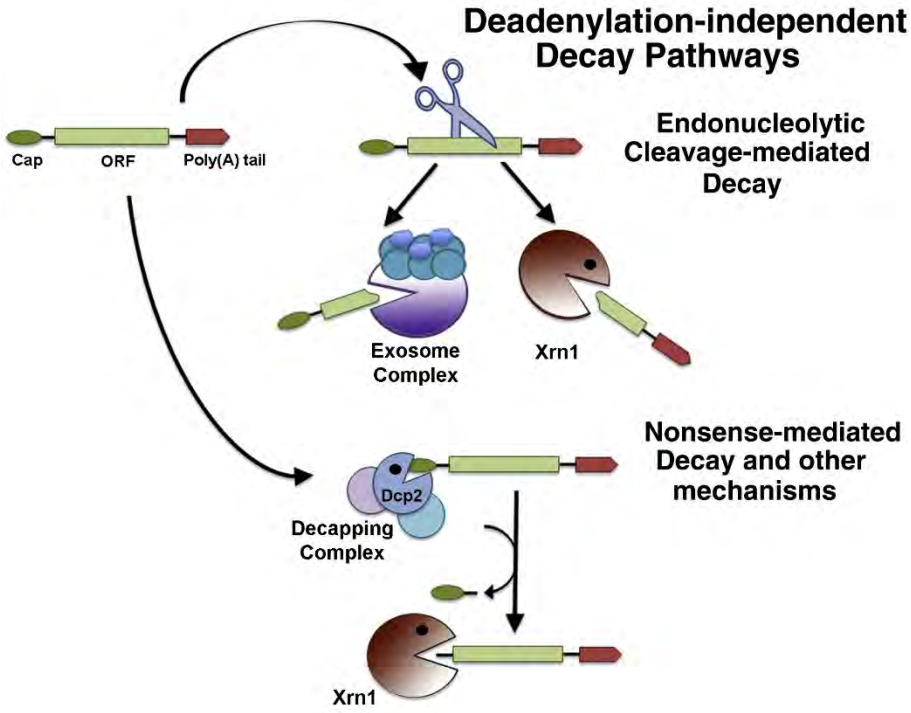

Figure 9. Mechanisms of mRNA degradation in eukaryotes: deadenylation-independent pathway. mRNA degradation can occur independent of deadenylation as in endonucleolytic cleavage (scissors) mediated decay and nonsense-mediated decay (NMD) pathways. Internal cleavage due to endonucleolytic activity results in 5' and 3' mRNA fragments with unprotected ends that are degraded by Xrn1 and the exosome complex, respectively. NMD targets (and certain long noncoding RNAs) bypass deadenylation and undergo 5' cap removal by the decapping complex followed by 5' to 3' degradation by Xrn1 (Nagarajan *et al.*, 2013).

Maintaining genome integrity: a role for RNA processing

Recent studies in mammalian cell lines and model organisms have implicated several aspects of RNA processing in the prevention of genome instability, showing that virtually every major aspect of RNA processing is potentially mutable to a genome instability phenotype, from transcript elongation to termination, 3' end processing, splicing, RNA transport, and RNA degradation (Chan *et al.*, 2014).

RNA processing defects are associated to increases in transcription-coupled DNA:RNA hybrid-mediated R-loop formation, which in turn constitute a major source of genome instability across species (Aguilera and García-Muse, 2012). For example in yeast, mutations in several RNA degradation proteins such as Xrn1 and Rrp6 have been found to increase R-loop formation and subsequent genome instability and transcription-associated hyper-recombination (Luna *et al.*, 2005; Gavaldá *et al.*, 2013; Wahba *et al.*, 2013). An R-loop is a three-strand nucleic acid structure formed by an DNA:RNA hybrid plus a displaced DNA strand (ssDNA), identical to the RNA molecule. R-loops are known to play important roles in gene expression regulation by influencing transcription termination, DNA methylation, and chromatin modification (Aguilera and García-Muse, 2012; Ginno *et al.*, 2013). Thus, the formation of R-loops could play a role in genome integrity both by creating a damage-prone site on the genome and by altering the expression of key genome maintenance proteins.

Significantly, regardless of R-loop formation, RNA processing defects can change gene expression patterns due to their effects on RNA levels. Producing more, less, or altered sets of mRNAs will influence the amount of protein produced and ultimately control the fate of the cell and the potential progression into disease (Lee and Young, 2013). An example of this effect is shown by the *XRN1* gene mutations in many organisms. Mutations in *S. cerevisiae XRN1* lead to reduced growth rates, reduced rates of diploid formation, decreased sporulation and deficiencies in meiotic homologous pairing of the DNA (Nagarajan *et al.*, 2013; Tishkoff *et al.*, 1995), while mutations in *XRN1*

can result in osteosarcoma in human (Zhang *et al.*, 2002). However, these phenotypes cannot completely exclude a direct effect of Xrn1 on particular targets.

Moreover, several RNA-binding proteins (RBPs) and RNA processing protein are directly involved in the maintenance of genome integrity and in DNA repair through interactions with nascent transcripts, non-coding RNAs (ncRNAs), damaged DNA, and DNA repair proteins (Dutertre *et al.*, 2014). Several RNA interacting proteins were reported to be located at sites of DNA lesions. Among these, some endoribonucleases have been implicated in the formation around the DSB of small noncoding RNAs that control DDR activation in both mammals and Arabidopsis (Francia *et al.*, 2012; Wei *et al.*, 2012). Furthermore, in mammals, the endoribonuclease Ago2 is required for the recruitment of the recombination protein Rad51 to the DSB ends (Gao *et al.*, 2014), while the exosome recruits the activation-induced cytidine deaminase (AID) to ssDNA regions generated at divergently transcribed loci in B cells (Pefanis *et al.*, 2014).

RNA processing proteins have also been implicated in telomere metabolism in both yeast and mammals, although the related mechanisms are poorly understood. In particular, the 5’ to 3’ exoribonuclease Xrn1 has been identified in genome-wide screenings for *Saccharomyces cerevisiae* mutants with altered telomere length (Askree *et al.*, 2004; Ungar *et al.*, 2009). Moreover, proteins belonging to the mammalian Nonsense-Mediated mRNA Decay (NMD) pathway have been found to bind telomeres and to control telomere length (Azzalin *et al.*, 2007; Chawla *et al.*, 2011). Similarly, the lack of the *S.*

cerevisiae NMD proteins was shown to cause telomere shortening by increasing the amount of Stn1 and Ten1, which in turn inhibit telomerase activity by interfering with Est1-Cdc13 interaction (Lew *et al.*, 1998; Dahlseid *et al.*, 2003; Addinall *et al.*, 2011; Holstein *et al.*, 2014). Furthermore, both Xrn1 and the nuclear exosome control degradation of the RNA component of human telomerase (Shukla *et al.*, 2016). Finally, Rat1 and the NMD pathway control the level of a new class of noncoding RNAs called TERRA (telomeric repeat-containing RNA), which are transcribed from the subtelomeric sequences and likely regulate telomere length (Luke *et al.*, 2008; Pfeiffer and Lingner, 2012; Iglesias *et al.*, 2011).

Despite the mechanistic understanding of how RNA processing defects could cause genome instability, their importance in oncogenesis is virtually unknown. It has become increasingly clear that some RNA processing factors are prevalently mutated in cancers and likely act as oncogenes or tumor suppressors (Chan *et al.*, 2014). However, the mechanistic link is usually unclear and the biological consequences of mutations across different RNA processing pathways are expected to vary.

This PhD thesis investigated the role(s) of the *S. cerevisiae* RNA processing proteins Xrn1 and Rrp6 in the cellular response to DNA DSBs and in the metabolism of telomeres.

RESULTS

(Manfrini *et al.*, 2015)

EMBO REPORTS

February 2015, Vol. 16, N° 2: 221-231.

doi: 10.15252/embr.201439458.

RNA-processing proteins regulate Mec1/ATR activation by promoting generation of RPA-coated ssDNA.

Nicola Manfrini[1], Camilla Trovesi[1], Maxime Wery[2], Marina Martina[1], Daniele Cesena[1], Marc Descrimes[2], Antonin Morillon[2], Fabrizio d'Adda di Fagagna[3], Maria Pia Longhese[1]

[1]Dipartimento di Biotecnologie e Bioscienze, Università di Milano-Bicocca, Milan, Italy.

[2]Institut Curie, CNRS UMR3244 Université Pierre et Marie Curie, Paris Cedex 05, France.

[3]IFOM Foundation-FIRC Institute of Molecular Oncology Foundation, Milan, Italy; Istituto di Genetica Molecolare, Consiglio Nazionale delle Ricerche, Pavia, Italy.

DNA double-strand breaks (DSBs) undergo 5'-3' nucleolytic degradation (resection) of their 5'-ending strands, to generate 3'-ended ssDNA overhangs, which are bound by the RPA complex (Longhese *et al.*, 2010). RPA-coated ssDNA enables the checkpoint kinase Mec1/ATR to recognize DSBs (Zou and Elledge, 2003) and facilitates the formation of continuous Rad51 filaments that initiate homologous recombination (HR) (Jasin and Rothstein, 2013). DSB resection is initiated by the MRX (Mre11-Rad50-Xrs2)/MRN (Mre11-Rad50-Nbs1) complex that acts in concert with Sae2/CtIP (Cannavo and Cejka, 2014; Mimitou and Symington, 2008; Zhu *et al.*, 2008). Subsequent long-range resection of the 5' strand can occur by one of two pathways that depend on either the 5'-3' exonuclease Exo1/hEXO1 or the Sgs1/BLM helicase in conjunction with the nuclease Dna2/hDNA2 (Mimitou and Symington, 2008; Zhu *et al.*, 2008).

Recent data indicate that RNA-processing proteins contribute to maintain genome stability either by controlling the turnover of specific transcripts or preventing accumulation of harmful DNA: RNA hybrids (Dutertre *et al.*, 2014). RNA processing can be directly involved in the DNA damage response (DDR), as some endoribonucleases have been implicated in the formation around the DSB of small noncoding RNAs that control DDR activation in both mammals and *Arabidopsis* (Francia *et al.*, 2012; Wei *et al.*, 2012). Furthermore, in mammals, the endoribonuclease Ago2 facilitates the recruitment of the recombination protein Rad51 to the DSB ends (Gao *et al.*, 2014), while the exosome recruits the activation-induced cytidine deaminase (AID)

to ssDNA regions generated at divergently transcribed loci in B cells (Pefanis *et al.*, 2014).

In *Saccharomyces cerevisiae*, RNA processing relies on a 5'-3' exoribonuclease activity that is due to the Xrn protein family, which comprises one cytoplasmic (Xrn1) and one nuclear enzyme (Rat1) (Nagarajan *et al.*, 2013). The nuclear exosome, whose activity is modulated by a set of cofactors including the poly(A) polymerase Trf4, is responsible for the 3'-5' RNA-processing activity, which depends on the exoribonuclease Rrp6 (Houseley *et al.*, 2006). Xrn1, Rrp6 and Trf4 have been shown to prevent DNA:RNA hybrid-mediated genome instability and transcription-associated hyperrecombination (Luna *et al.*, 2005; Gavaldá *et al.*, 2013; Wahba *et al.*, 2013). Furthermore, the lack of Trf4 leads to sensitivity to camptothecin (Sadoff *et al.*, 1995), while *XRN1* deletion impairs meiotic recombination (Tishkoff *et al.*, 1995). However, the precise DNA maintenance mechanisms involving these RNA decay factors remain poorly characterized. Here, we show that Xrn1, Rrp6 and Trf4 participate in the activation of the checkpoint kinase Mec1 by promoting the formation of RPA-coated ssDNA at DSB ends. These findings reveal a novel role for RNA decay factors in the maintenance of genome integrity.

Xrn1, Rrp6 and Trf4 are necessary for Mec1/ATR activation in response to a DSB

To investigate the role of Xrn1, Rrp6 and Trf4 in the DDR, yeast strains carrying the deletion of the corresponding genes were tested for sensitivity to DNA damaging agents. The *xrn1Δ*, *rrp6Δ* and *trf4Δ*

mutants were hypersensitive to the DSB-inducing agent phleomycin, with *xrn1Δ* cells showing the strongest sensitivity (Figure 10A), suggesting that the corresponding proteins are involved, directly or indirectly, in the cellular response to DSBs.

Next, we asked whether *xrn1Δ*, *rrp6Δ* and *trf4Δ* cells were defective in checkpoint activation in response to a single DSB. To address this question, we deleted *XRN1*, *RRP6* or *TRF4* in a haploid strain carrying the *HO* gene under the control of a galactose-inducible promoter. In this strain, induction of HO by galactose addition leads to the generation at the *MAT* locus of a single DSB that cannot be repaired by HR due to the lack of the homologous donor loci *HML* and *HMR* (Lee *et al.*, 1998). *HO* expression was induced by transferring to galactose wild-type, *xrn1Δ*, *rrp6Δ* and *trf4Δ* cells exponentially growing in raffinose. Checkpoint activation was monitored by following Rad53 phosphorylation, which is required for Rad53 activation and is detectable as a decrease of its electrophoretic mobility. As shown in Figure 10B, the amount of phosphorylated Rad53 after HO induction was much lower in *xrn1Δ*, *rrp6Δ* and *trf4Δ* than in wild-type cells. Furthermore, when the same strains were arrested in G1 with α-factor and then spotted on galactose-containing plates to induce HO, *xrn1Δ*, *rrp6Δ* and *trf4Δ* cells formed microcolonies with more than 2 cells more efficiently than similarly treated wild-type cells (Figure 10C), indicating a defect in DSB-induced cell cycle arrest.

Although *xrn1Δ*, *rrp6Δ* and *trf4Δ* cells slightly delayed the G1/S transition under unperturbed conditions (Figure 10D), their checkpoint defect was not due to altered cell cycle progression, as

xrn1Δ, *rrp6Δ* and *trf4Δ* were defective in Rad53 phosphorylation also when the HO cut was induced in G2-arrested cells that were kept arrested in G2 throughout the experiment (Figure 10E).

The requirement of Xrn1, Rrp6 and Trf4 for DSB-induced checkpoint activation was not locus specific, as *xrn1Δ*, *rrp6Δ* and *trf4Δ* cells were defective in Rad53 phosphorylation also when the HO-induced DSB was generated at the *LEU2* locus (Figure 10F). Neither it was influenced by the level of transcription of the DNA region in which the DSB occurs, as the amount of Rad53 phosphorylation in wild-type, *xrn1Δ*, *rrp6Δ* and *trf4Δ* cells after HO-induced DSB formation into the *LEU2* gene was similar to that detected when the DSB was generated into the *LEU2* gene lacking its promoter (Figure 11).

Xrn1 and Rrp6 promote checkpoint activation by acting as exoribonucleases. In fact, cells carrying the *xrn1-E176G* or the *rrp6-D238A* allele, encoding nuclease-defective Xrn1 (Page *et al.*, 1998) or Rrp6 (Burkard and Butler, 2000) variants, were as defective in HO-induced Rad53 phosphorylation as *xrn1Δ* and *rrp6Δ* cells, respectively (Figure 10G).

In *S. cerevisiae*, checkpoint activation in response to a single DSB is completely dependent on Mec1 (Mantiero *et al.*, 2007), suggesting that *xrn1Δ*, *rrp6Δ* and *trf4Δ* cells might be defective in Mec1 activation. Indeed, *xrn1Δ*, *rrp6Δ* and *trf4Δ* cells were defective in phosphorylation of the Mec1 specific target Ddc2 after HO induction (Figure 10H), indicating that the lack of Xrn1, Rrp6 or Trf4 impairs Mec1 signaling activity.

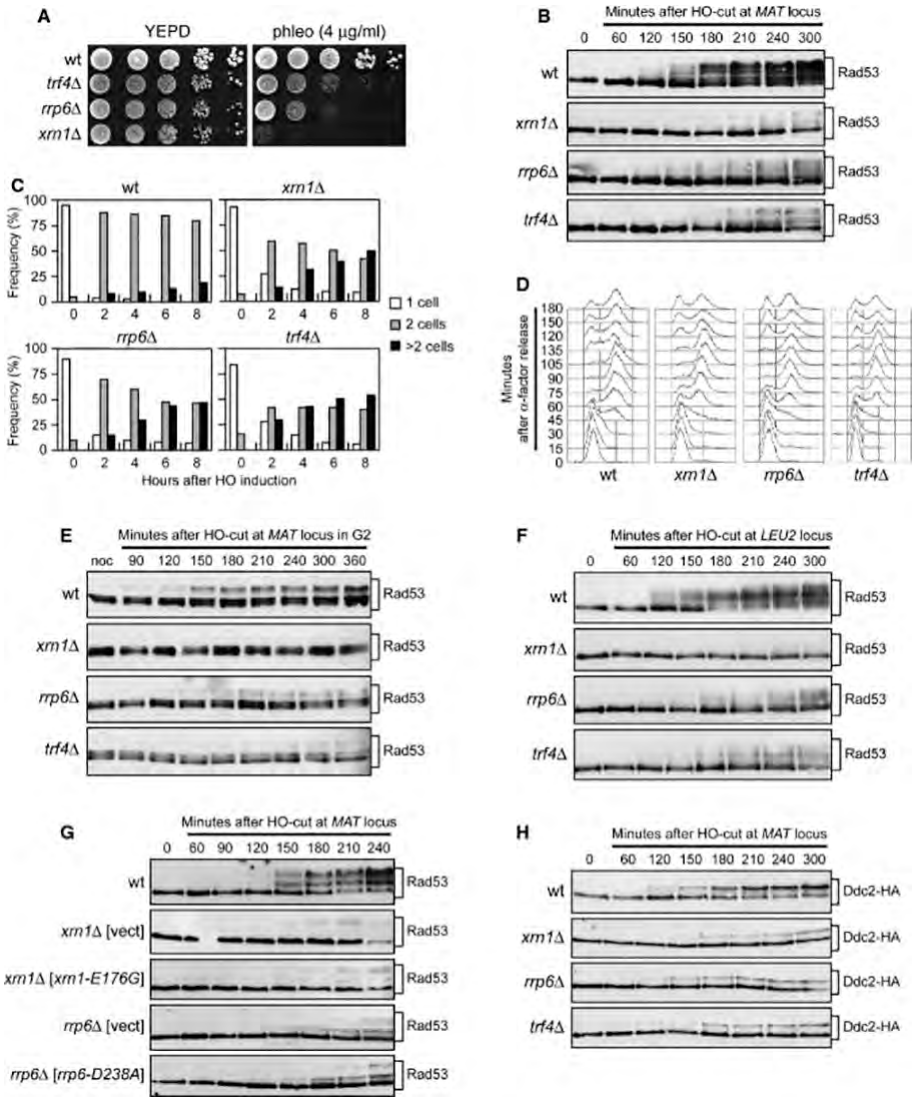

Figure 10. The lack of Xrn1, Rrp6 or Trf4 impairs Mec1 checkpoint signaling in response to a DSB. A) Sensitivity to phleomycin. Serial dilutions (1:10) of exponentially growing cell cultures were spotted out onto YEPD plates with or without phleomycin (phleo). B) Rad53 phosphorylation after a DSB at the *MAT* locus. YEPR exponentially growing cell cultures of JKM139 derivative strains, carrying the HO cut site at the *MAT* locus, were transferred to YEPRG at time zero. Protein extracts from samples taken at the indicated times after HO induction were subjected to Western blot analysis with anti-Rad53 antibodies. C) Checkpoint-mediated cell cycle arrest. G1-arrested JKM139 derivative cells were plated on galactose-containing plates at time zero. Two hundred cells for each strain were analyzed to determine the frequency of cells that were unbudded, large budded or

forming microcolonies with more than two cells. D) Analysis of cell cycle progression in unperturbed conditions. Cell cultures arrested in G1 with α-factor were released into YEPD at time zero. FACS analysis of DNA content. E) Checkpoint activation in G2-arrested cells. As in (B) except that HO was induced in nocodazole-arrested JKM139 derivative cells that were kept arrested in G2 in the presence of nocodazole throughout the experiment. F) Rad53 phosphorylation after a DSB at the *LEU2* locus. As in (B), but inducing HO expression in YFP17 derivative strains, which carry the HO cut site at the *LEU2* locus. G) Checkpoint activation. Protein extracts from JKM139 derivative strains containing the indicated centromeric plasmids were subjected to Western blot analysis with anti-Rad53 antibodies at different time points after HO induction. H) Ddc2 phosphorylation after a DSB at the *MAT* locus. Protein extracts from JKM139 derivative strains expressing fully functional Ddc2-HA were subjected to Western blot analysis with anti-HA antibodies at different time points after HO induction.

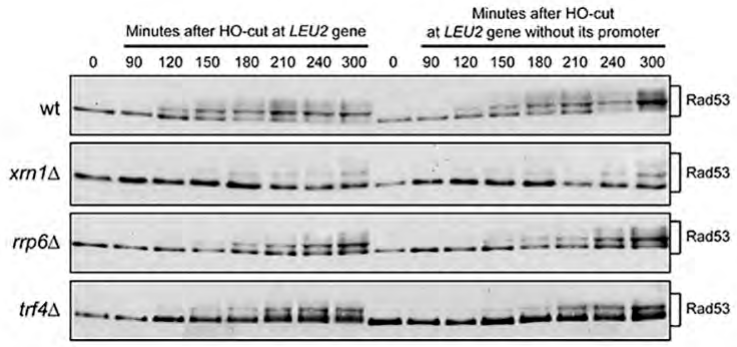

Figure 11. Rad53 phosphorylation after a DSB at the *LEU2* gene or at the *LEU2* gene lacking its promoter. Western blot analysis with anti-Rad53 antibodies of protein extracts from YFP17 derivative strains, carrying the HO-cut site at the *LEU2* gene or at the *LEU2* gene lacking its promoter. Samples were taken at the indicated times after transfer from YEPR to YEPRG (time zero).

Xrn1 promotes resection of DNA ends

While Xrn1 controls cytoplasmic RNA decay, RNA processing into the nucleus depends on its nuclear paralog Rat1 (Johnson, 1997). Targeting Rat1 into the cytoplasm by deleting its nuclear localization sequence (*rat1-ΔNLS*) restores Xrn1-like function in mRNA degradation (Johnson, 1997), prompting us to test whether it could restore Rad53 phosphorylation after DSB formation in *xrn1Δ* cells. Strikingly, expression of the *rat1-ΔNLS* allele on a centromeric plasmid, but not of wild-type *RAT1*, suppressed both the Rad53 phosphorylation defect (Figure 12A) and the hypersensitivity to phleomycin (Figure 12B) of *xrn1Δ* cells, indicating that Xrn1 controls checkpoint activation by acting in the cytoplasm.

Mec1 activation requires formation of RPA-coated ssDNA, which arises from 5' to 3' nucleolytic degradation of the DSB ends (Zou and Elledge, 2003). To assess whether the inability of *xrn1Δ* cells to activate Mec1/ATR could be related to defects in DSB resection, we directly monitored ssDNA generation at the DSB ends. Cells exponentially growing in raffinose were transferred to galactose to induce HO and genomic DNA was analyzed at different time points after HO induction. Because ssDNA is resistant to cleavage by restriction enzymes, 5' strand resection can be measured by following the loss of SspI restriction fragments by Southern blot analysis under alkaline conditions using a ssRNA probe that anneals to the unresected strand on one side of the break. The appearance of ssDNA intermediates was delayed in galactose-induced *xrn1Δ* cells compared to wild-type

(Figure 12C and D), indicating that the lack of Xrn1 impairs generation of ssDNA at the DSB ends.

DSB resection is under the control of several proteins, which act as positive (Mre11, Rad50, Xrs2, Dna2, Sgs1 and Exo1) or negative (Rad9) regulators (Longhese *et al.*, 2010). The resection defect of *xrn1Δ* was not due to lower amounts of the above proteins, as similar amounts of Mre11, Rad50, Xrs2, Sgs1, Exo1 and Rad9 proteins could be detected in both wild-type and *xrn1Δ* cells (Figure 13). The amount of Dna2 was higher in xrn1Δ than in wild-type cells (Figure 13), but this effect did not account by itself for the DSB resection defect of *xrn1Δ* cells, as DNA2 overexpression did not affect either checkpoint activation or generation of ssDNA at the DSB ends in wild-type cells (data not shown).

Xrn1 supports MRX function in DSB resection

As the lack of Xrn1 impairs initiation of DSB processing, which is known to require the MRX complex, we investigated whether it might affect MRX function. Epistasis analysis revealed that DSB resection in the *xrn1Δ mre11Δ* double mutant was as defective as in the *mre11Δ* single mutant (Figure 12C and D), indicating that Xrn1 and MRX promote DSB resection by acting in the same pathway. Chromatin immunoprecipitation (ChIP) and quantitative real-time PCR showed that Mre11 association at the HO-induced DSB was lower in *xrn1Δ* than in wild-type cells (Figure 12E). This decreased binding was not due to lower Mre11 protein level (Figure 13) or altered MRX complex formation (Figure 12F). Neither it was due to different resection

kinetics, as the lack of Xrn1 impaired Mre11 recruitment even when the DSB was induced in G1-arrested cells (Figure 12G), where DSB resection is very poor due to low Cdk1 activity (Ira *et al.*, 2004). Consistent with MRX being required to load Exo1 and Dna2 at the DSB (Shim *et al.*, 2010), Exo1 association at the HO-induced DSB was lower in *xrn1Δ* than in wild-type cells (Figure 12G), and similar results were obtained for Dna2 (data not shown). Thus, Xrn1 regulates DSB resection likely by promoting MRX recruitment to the DSB.

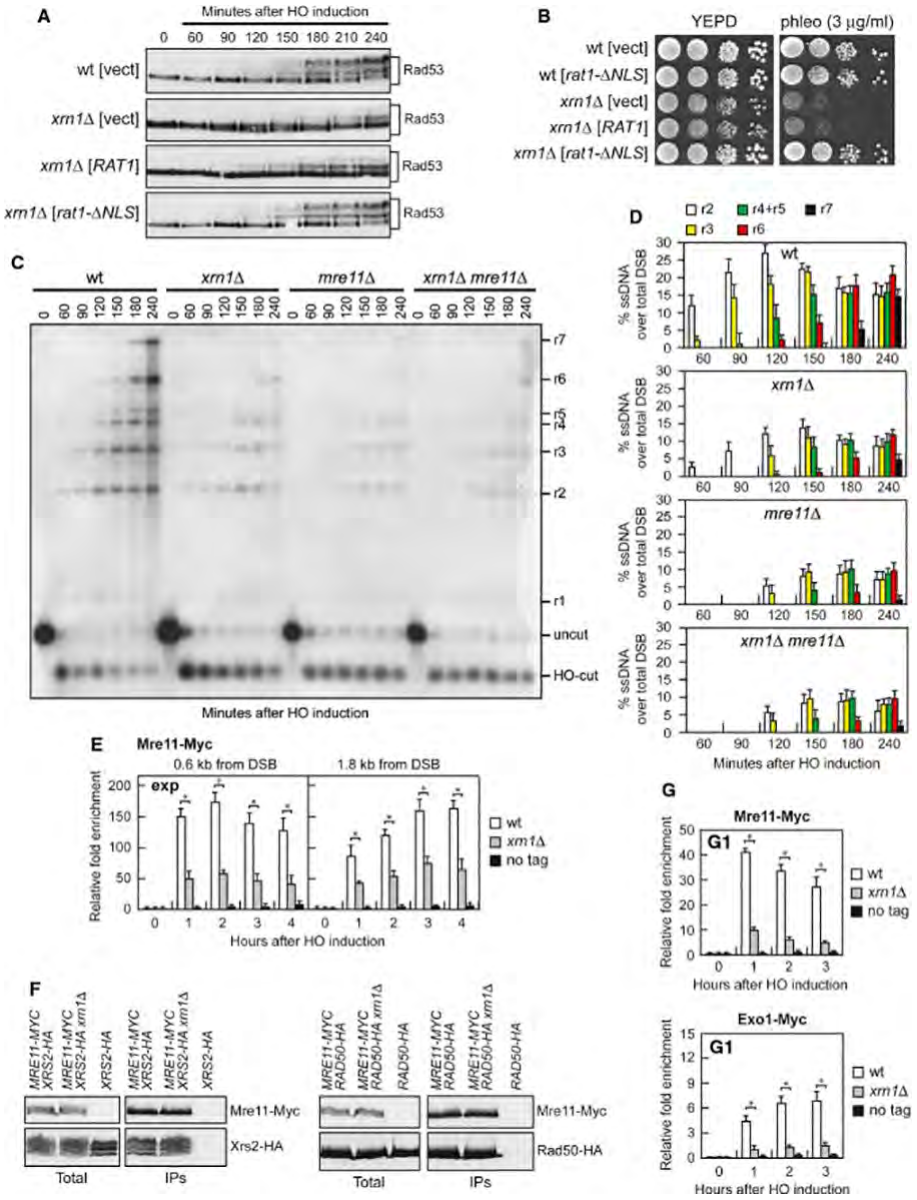

Figure 12. The lack of Xrn1 impairs DSB resection and Mre11 recruitment to the DSB. A) Checkpoint activation. Protein extracts from JKM139 derivative strains containing the indicated centromeric plasmids were subjected to Western blot analysis with anti-Rad53 antibodies at different time points after HO induction. B) Sensitivity to phleomycin. Strains in (A) were serially diluted (1:10) and spotted out onto YEPD plates with or without phleomycin. C) DSB resection. YEPR exponentially growing cultures of JKM139 derivative cells were transferred to YEPRG at time zero. Gel blots of SspI-digested genomic DNA separated on alkaline agarose gel were

hybridized with a single-stranded RNA probe that anneals to the unresected strand on one side of the break. 5'–3' resection progressively eliminates SspI sites (S), producing larger SspI fragments (r1 through r7) detected by the probe. D) Densitometric analyses. The experiment as in (C) was independently repeated three times and the mean values are represented with error bars denoting SD (n = 3). E) Mre11-Myc recruitment at the HO-induced DSB. In all diagrams, data are expressed as fold enrichment at the HO-induced DSB over that at the non-cleaved *ARO1* locus, after normalization of ChIP signals to the corresponding input for each time point. The mean values are represented with error bars denoting SD (n = 3). *P < 0.01, t-test. F) MRX complex formation. Protein extracts were analyzed by Western blot with anti-Myc or anti-HA antibodies either directly (Total) or after Mre11-Myc immunoprecipitation (IPs) with anti-Myc antibodies. G) Mre11 recruitment at the HO-induced DSB in G1-arrested *xrn1Δ* cells. ChIP analysis was performed as in (E) except that HO was induced in α-factor-arrested JKM139 derivative cells kept arrested in G1 with α-factor throughout the experiment. qPCR was performed at 1.8 kb from the DSB. The mean values are represented with error bars denoting SD (n = 3). *P < 0.01, t-test.

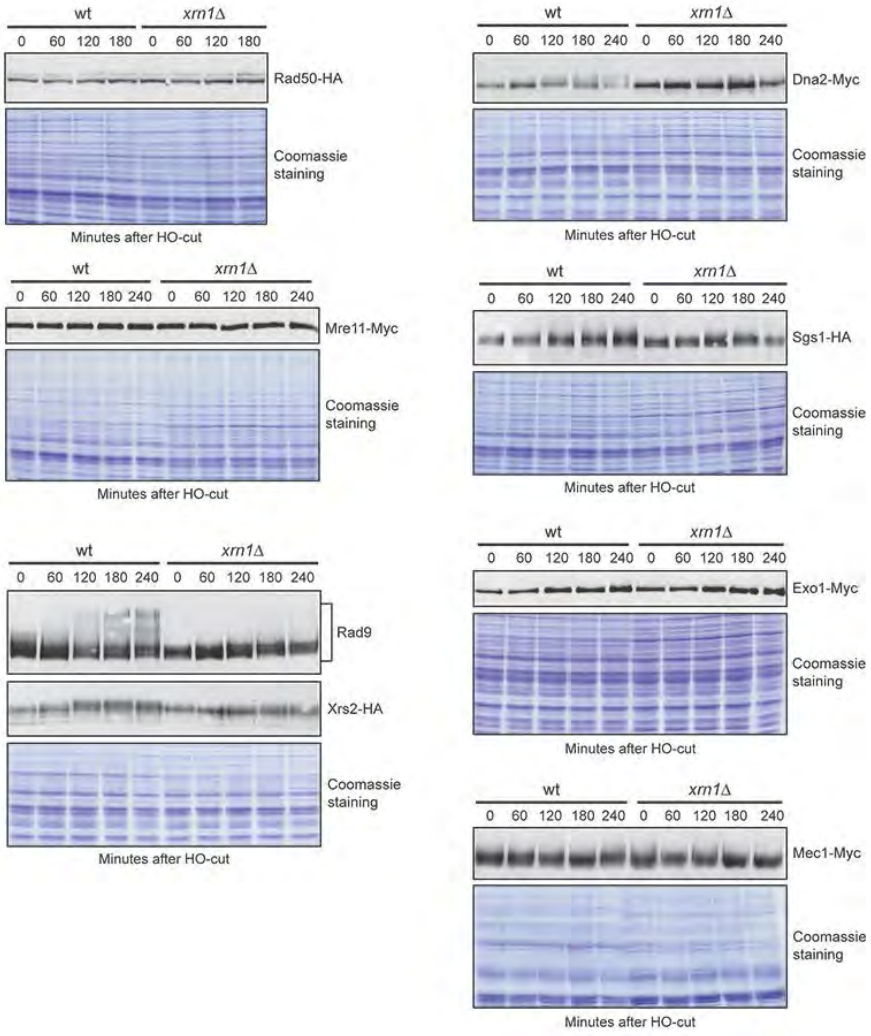

Figure 13. Levels of DDR proteins involved in DSB resection in *xrn1Δ* cells. Exponentially growing cell cultures of JKM139 derivative strains expressing the indicated tagged proteins were transferred to YEPGR at time zero to induce HO. Protein extracts at different time points after HO induction were subjected to western blot with antibodies specific for the indicated proteins or tags. The same amounts of protein extracts were separated by SDS-PAGE and stained with Coomassie as loading control.

Rrp6 and Trf4 promote the loading of RPA and Mec1 to the DSB

Resection intermediates accumulated with wild-type kinetics in *rrp6Δ* and *trf4Δ* cells (Figure 14A and B), indicating that the defective checkpoint response in these mutants cannot be ascribed to reduced generation of ssDNA at the DSB. As Mec1 recognizes and is activated by RPA-coated ssDNA (Zou and Elledge, 2003), the checkpoint defect of *rrp6Δ* and *trf4Δ* cells might be due to the inability of either Mec1 itself or RPA to bind ssDNA. Indeed, the lack of Rrp6 or Trf4 impaired Mec1 and Rpa1 association at the DSB (Figure 14C and D), although similar amounts of Mec1 (Figure 14E) and RPA complex (Figure 14F) can be detected in protein extracts from wild-type, *rrp6Δ* and *trf4Δ* cells. This decreased RPA recruitment to the DSB was not due to defects in either RPA complex formation (Figure 14G) or RPA sub-cellular localization (Figure 15A). Thus, Rrp6 and Trf4 appear to regulate Mec1 activation by promoting association to the DSB ends of RPA, and therefore of Mec1.

Interestingly, Rrp6 and Trf4 promoted Mec1 activation not only in response to a HO-induced DSB, but also after treatment with methyl methane sulfonate (MMS) or hydroxyurea (HU) (Figure 14H), suggesting that they favor RPA loading also to the ssDNA generated during replicative stress.

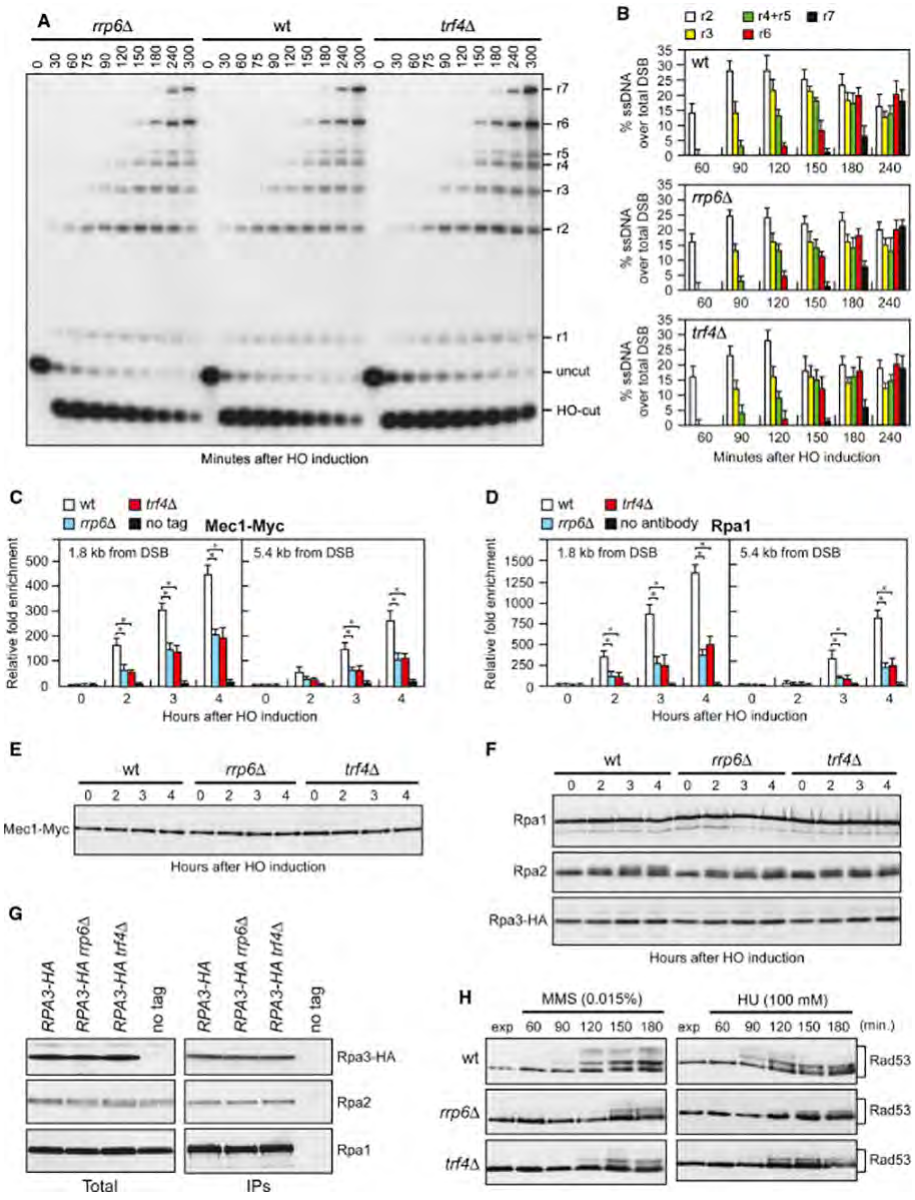

Figure 14. The lack of Rrp6 or Trf4 impairs RPA and Mec1 recruitment to the DSB without affecting DSB resection. A) DSB resection. Genomic DNA was analyzed for ssDNA formation as described in Figure 12C. B) Densitometric analyses. The experiment as in (A) was independently repeated three times and the mean values are represented with error bars denoting SD (n = 3). C) Mec1-Myc recruitment at the HO-induced DSB. In all diagrams, data are expressed as fold enrichment at the HO-induced DSB over that at the non-cleaved *ARO1* locus, after normalization of ChIP signals to the corresponding input for each time point. The mean values are

represented with error bars denoting SD (n = 3). *P < 0.01, t-test. D) Rpa1 recruitment at the HO-induced DSB. ChIP analysis was performed as in (C). The mean values are represented with error bars denoting SD (n = 3). *P < 0.01, t-test. E) Mec1 protein level. Western blot with anti-Myc antibodies of extracts used for the ChIP analysis shown in (C). F) Rpa1, Rpa2 and Rpa3 protein levels. Western blot with anti-Rpa1, anti-Rpa2 and anti-HA antibodies of extracts used for the ChIP analysis in (D). G) RPA complex formation. Protein extracts were analyzed by Western blotting with anti-HA (Rpa3), anti-Rpa1 or anti-Rpa2 antibodies either directly (Total) or afterRpa3-HA immunoprecipitation (IPs) with anti-HA antibodies. H) Checkpoint activation in response to HU and MMS treatment. Western blot analysis with anti-Rad53 antibodies of protein extracts prepared from exponentially growing cells that were treated with HU or MMS for the indicated time points.

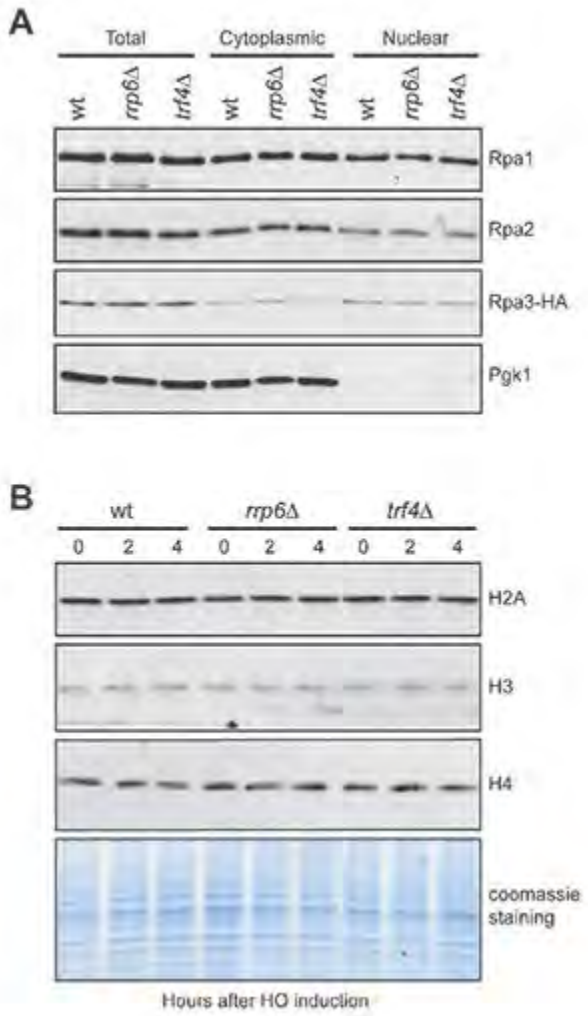

Figure 15. Sub-cellular localization of RPA and levels of histones H2A, H3, H4 in wild type, *rrp6*Δ and *trf4*Δ cells. A) Extracts from exponentially growing cell cultures were fractionated to determine total, cytoplasmic and nuclear fractions. Fractions were analyzed by western blot with anti-HA antibodies (Rpa3-HA) and antibodies specific for Rpa1 and Rpa2. Fractionation was controlled by using antibodies specific for Pgk1, which is known to be cytoplasmic. B) Exponentially growing cell cultures of JKM139 derivative strains were transferred to YEPRG at time zero to induce HO. Protein extracts at different time points after HO induction were subjected to western blot with antibodies specific for the indicated histone proteins. The same amounts of protein extracts were separated by SDS-PAGE and stained with Coomassie as loading control.

Rrp6 and Trf4 are not required for HR repair of a DSB

After covering ssDNA, RPA is displaced by Rad51 (Jasin and Rothstein, 2013). Reduced RPA binding in *rrp6Δ* and *trf4Δ* cells was due to a less efficient RPA loading rather than to a more efficient RPA displacement by Rad51 and/ or Rad52. In fact, RPA was still poorly recruited at the DSB ends in *rrp6Δ* and *trf4Δ* cells lacking either Rad51 or Rad52 (Figure 16A).

As RPA promotes localization of the recombination proteins Rad51 and Rad52 to initiate DSB repair by HR (Chen *et al.*, 2013), the lack of Rrp6 and/or Trf4 may affect the loading of Rad51 and/or Rad52 on the DSB. This does not seem to be the case, as similar amounts of Rad51 and Rad52 were detected in wild-type, *rrp6Δ* and *trf4Δ* cells, both in total protein extracts (Figure 16B) and bound at the DSB (Figure 16C and D). Rad51-dependent recombination leads to the formation of noncrossover or crossover products. We analyzed the formation of such recombination products using a haploid strain that bears a *MATα* sequence on chromosome V and an uncleavable *MATα-inc* sequence on chromosome III (Saponaro *et al.*,2010). Upon galactose addition, the HO-induced DSB can be repaired using the *MATα-inc* sequence as a donor, resulting in crossover and non-crossover products (Figure 16E).

Consistent with the finding that the lack of Rrp6 did not impair Rad51 and Rad52 loading at the DSB, the overall DSB repair efficiency in *rrp6Δ* cells was similar to that observed in wild-type cells (Figure 16F and G). By contrast, DSB repair efficiency was reduced in *xrn1Δ* cells (Figure 16F and G), in agreement with the finding that these cells were

defective in the generation of ssDNA (Figure 16C and D) that is necessary to catalyze strand invasion and base pairing.

Therefore, the lack of Rrp6 or Trf4 appears to specifically impair the loading at the DSB ends of RPA, but not of Rad51 and Rad52.

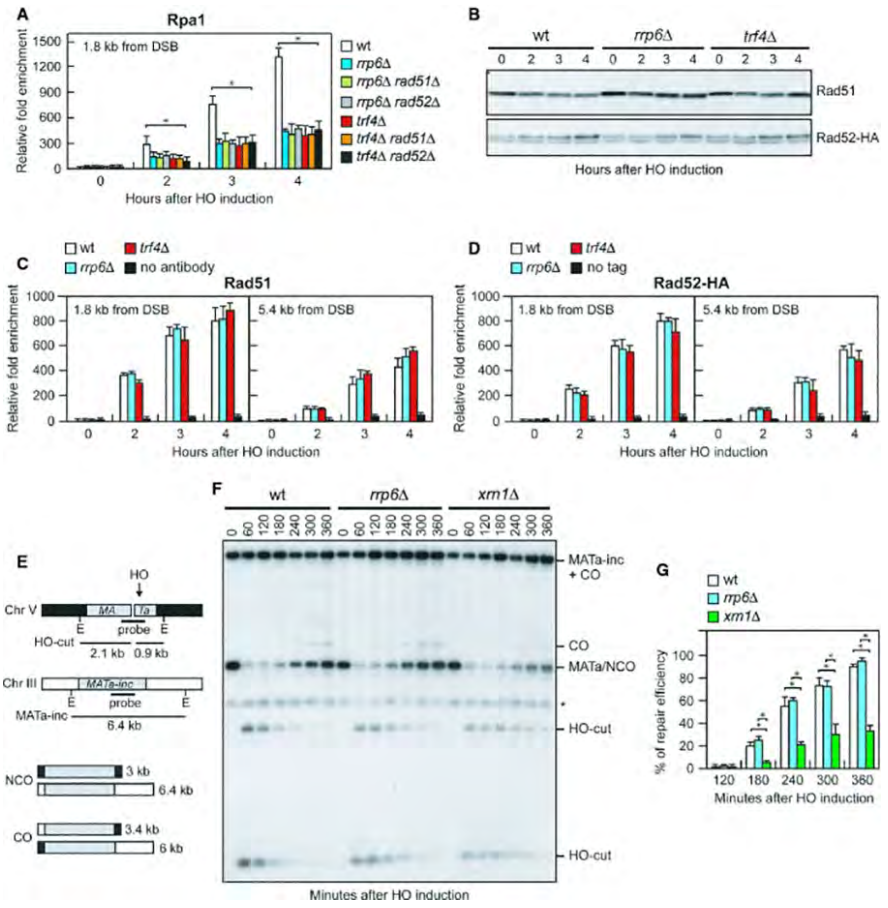

Figure 16. The lack of Rrp6 or Trf4 does not affect DSB repair by HR. A) Recruitment of Rpa1 at the HO-induced DSB. ChIP analysis was performed as in Figure 14D. The mean values are represented with error bars denoting SD (n = 3). *P < 0.01, t-test. B) Rad51 and Rad52 protein levels. Western blot with anti-Rad51 and anti-HA antibodies of extracts used for the ChIP analysis in (C) and (D), respectively. C), D) Recruitment of Rad51 and Rad52-HA at the HO-induced DSB. ChIP analysis was performed as in Figure 14. The mean values are represented with error bars denoting SD (n = 3). *P < 0.01, t-test. E) System to detect CO and NCO. Galactose-induced HO generates a DSB at the *MATα* locus on chromosome V that is repaired by using the homologous *MATα-inc* region on chromosome III. Sizes of EcoRI (E) DNA fragments detected by the probe are indicated. F) Detection of DSB repair products. EcoRI-digested genomic DNA from samples taken at the indicated times after HO induction was subjected to Southern blot analysis with the *MATα* probe depicted in (E). *indicates a cross hybridization signal. G) Densitometric analysis of the repair signals. The mean values are represented with error bars denoting SD (n = 3). *P < 0.01, t-test.

The lack of Xrn1, Rrp6 or Trf4 does not affect expression of most DDR genes

As the lack of Xrn1 or Rrp6/Trf4 might influence the recruitment of MRX or RPA, respectively, by regulating gene expression, we performed deep transcriptome analyses before and after generation of the HO-induced DSB. Biological duplicates of cells exponentially growing in raffinose (time zero) were shifted to galactose for 60 and 240 min to induce HO, and total RNA was subjected to strand-specific whole transcriptome analysis. The vast majority of proteincoding genes in a wild-type context showed no significant change of expression 60 min (Spearman's correlation coefficient 0.98; Figure 17A) and 240 min (Spearman's correlation coefficient 0.95; Figure 17B) after HO induction. Expression of genes coding for factors involved in DDR (see list in Table 1) also remained globally unchanged (Figure 17C and D), with 0.96-0.98 and 0.89-0.94 Spearman's correlation coefficients 60 min (Fig. R5A) and 240 min (Fig. R5B) after HO induction, respectively. Further differential expression analysis to obtain better statistical validation revealed that only 5 of 193 DDR genes were affected (fold change ≤ 0.5 or ≥ 2, $P \leq 0.001$) 240 min after HO induction (Figure 18A and B, see list in Table 2), indicating that the HO-induced DSB has little impact on the transcriptome.

When we performed similar analyses in strains lacking Xrn1, Rrp6 or Trf4, as previously reported (van Dijk *et al.*, 2011), we observed that inactivation of Xrn1 resulted in global stabilization of mRNAs (Figure 17C and D; Figure 18F). In contrast, mRNA levels in *rrp6Δ* and *trf4Δ* cells were similar to wild-type (Figure 17C and D, Figure 18G and H).

Importantly, in all tested strains and conditions, DDR genes showed expression similar to all genes (Figure 17D). Deeper differential expression analysis showed that the majority of DDR mRNAs remained unchanged (Figure 17C and Fig. Figure 18C–E), although some of them were misregulated in these mutants (3 in *rrp6Δ*, 22 in *xrn1Δ* and 27 in *trf4Δ*, Table 2). Further studies are required to assess whether these mRNA misregulations might account for the DSB resection defect of *xrn1Δ* cells, but the finding that Xrn1 acts in the checkpoint as a cytoplasmic exoribonuclease makes them potential candidates.

The only three genes (*SMC6*, *HPA2* and *RLF2*) that are downregulated in *rrp6Δ* cells are not affected in *trf4Δ* and vice versa (Table 2), making it unlikely that these altered mRNA levels may account for the reduced recruitment of RPA to the ssDNA ends displayed by both *rrp6Δ* and *trf4Δ* cells. In addition, while *SMC6* is essential for cell viability, deletion of *RLF2*, which encodes the largest subunit of the Chromatin Assembly Factor CAF-1, or *HPA2*, which encodes a histone acetyltransferase, did not impair checkpoint activation in response to the HO-induced DSB (Kim and Haber, 2009; data not shown). Of note, the lack of Trf4 increased the amount of mRNAs encoding histones H2A, H3 and H4 (Table 2). However, these upregulations did not cause any increase of the corresponding protein levels (Figure 15B), consistent with previous findings that RNA decay mutants accumulate mRNA intermediates that might not be efficiently translated (Nagarajan *et al.*, 2013; Houseley *et al.*, 2006).

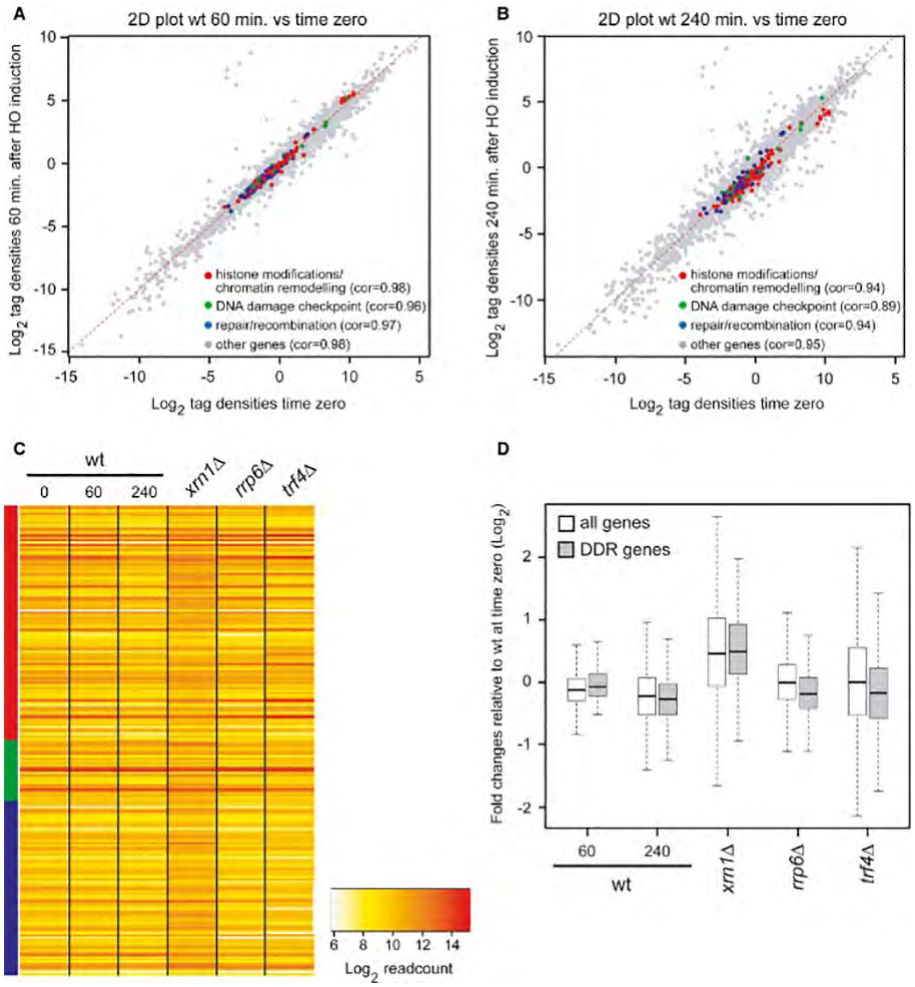

Figure 17. The lack of Xrn1, Rrp6 or Trf4 does not impair expression of most DDR genes. A) Expression of DDR genes in wild-type cells 60 min after HO induction. Scatter plot of tag density for genes encoding DDR factors in wild-type strain (JKM139) before (time zero) and after (60 min) HO induction. Results are presented as log_2 of density, expressed in tag per nucleotide. Spearman's correlation coefficients for each set of genes are indicated. B) Expression of DDR genes in wild-type cells 240 min after HO induction. Same as in (A) using JKM139 cells at time zero and 240 min after HO induction. C) Expression of DDR genes in wild-type cells at time zero, 60 and 240 min after HO induction, and in *xrn1Δ*, *rrp6Δ* and *trf4Δ* cells at time zero. Data are presented as a heatmap and genes are clustered according the classification used in (A), with the same color code. D) Global expression of all protein-coding and DDR genes upon HO induction or inactivation of RNA decay factors. Box plot representation of expression fold change for all protein-coding

(white) and DDR (gray) genes in wild-type cells 60 and 240 min after HO induction, and in *xrn1Δ*, *rrp6Δ* and *trf4Δ* mutants at time zero. All fold changes are relative to the wild-type at time zero. For each condition, the black line within the box corresponds to the median value, while the top and bottom lines of the box correspond to the upper quartile and lower quartile, respectively (n = 5,798 for all genes and n = 194 for the DDR genes). Outliers are not represented.

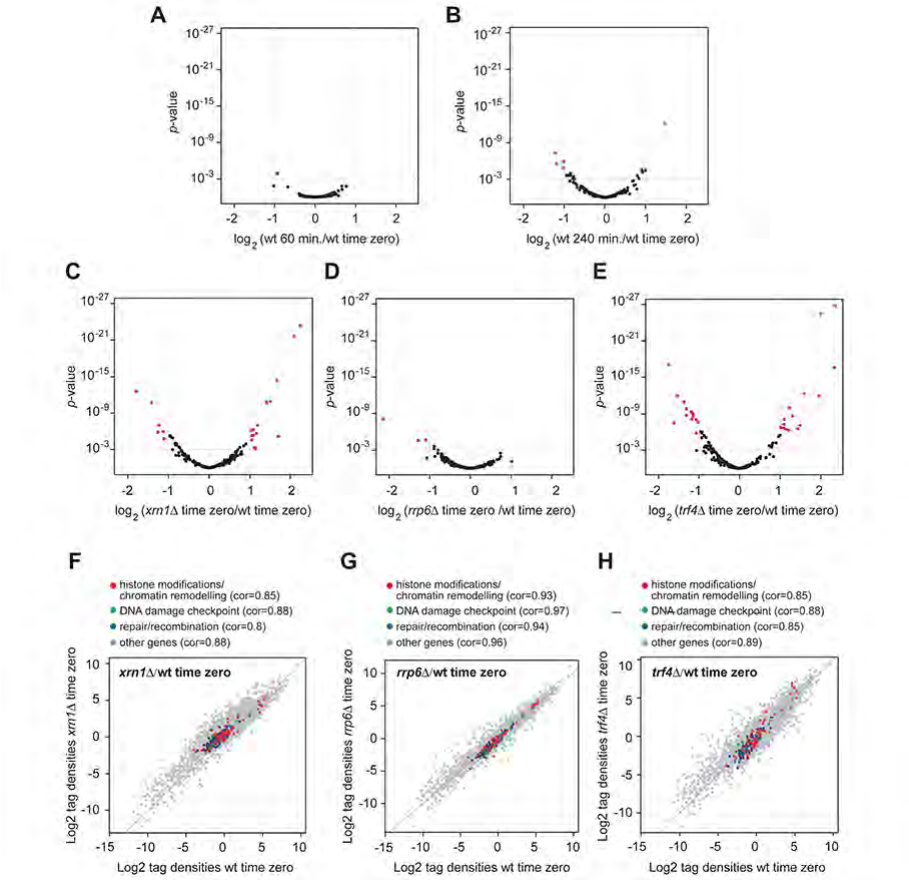

Figure 18. Expression of DDR genes upon DSB induction or inactivation of RNA decay factors. A), B) Expression of DDR genes in wild type cells 60 minutes (A) and 240 minutes (B) after DSB induction relative to wild type cells at time zero. For each of the DDR genes, expression fold change and *P*-value from DESeq analysis were determined. Genes showing significant differential expression (fold change ≤0.5 or ≥2, *P*-value ≤0.001) are highlighted in red (list in Table 2). C)-E) Expression of DDR genes in *xrn1Δ*, *rrp6Δ* and *trf4Δ* cells. As in (A) but showing *xrn1Δ* (C), *rrp6Δ* (D) and *trf4Δ* (E) cells at time zero relative to wild type cells at time zero. F)-H) Scatter plots of tag density (expressed in tag per nucleotide, $\log_2$ scale) for genes encoding proteins involved in histone modifications/chromatin remodelling (red dots), DNA damage checkpoint (green dots), DNA repair/recombination (blue dots) and all other protein-coding genes (grey dots) in *xrn1Δ* (F), *rrp6Δ* (G) and *trf4Δ* (H) cells at time zero relative to wild type cells at time zero. Spearman's correlation coefficients for each set of genes are indicated.

			Fold changes (relative to WT at time zero)				
ID	gene	Cellular function	WT T60	WT T240	*xrn1* T0	*rrp6* T0	*trf4* T0
YBL003C	HTA2	chromatin remodellers	1,5	0,5	0,4	1,4	3,9
YLR449W	FPR4	chromatin remodellers	0,5	0,4	0,5	0,8	0,5
YBR010W	HHT1	chromatin remodellers	1,3	0,5	0,6	1,2	2,7
YER030W	CHZ1	chromatin remodellers	1,0	0,9	0,6	1,0	4,0
YBR009C	HHF1	chromatin remodellers	1,4	0,5	0,6	1,4	2,3
YNL031C	HHT2	chromatin remodellers	1,3	0,7	0,6	1,2	2,8
YDR334W	SWR1	chromatin remodellers	0,8	0,6	0,7	1,0	0,7
YBR245C	ISW1	chromatin remodellers	0,9	0,9	0,7	0,7	0,5
YBR082C	UBC4	chromatin remodellers	1,0	1,1	0,8	1,5	1,2
YDR224C	HTB1	chromatin remodellers	1,3	0,4	0,8	1,4	0,8
YNL030W	HHF2	chromatin remodellers	1,3	0,6	0,8	1,4	5,1
YFR037C	RSC8	chromatin remodellers	0,9	0,8	0,8	0,7	0,9
YNL059C	ARP5	chromatin remodellers	0,9	0,7	0,9	0,8	0,6
YLR442C	SIR3	chromatin remodellers	0,8	0,8	0,9	0,6	0,7
YJL081C	ARP4	chromatin remodellers	1,0	0,9	0,9	0,9	1,0
YDL029W	ARP2	chromatin remodellers	1,2	1,5	0,9	1,0	1,3
YLR418C	CDC73	chromatin remodellers	1,0	0,8	0,9	1,0	0,8
YNL246W	VPS75	chromatin remodellers	0,8	0,7	0,9	0,8	0,9
YNL021W	HDA1	chromatin remodellers	0,9	0,6	0,9	0,8	0,6
YJL176C	SWI3	chromatin remodellers	1,0	0,8	0,9	0,8	0,8
YOR189W	IES4	chromatin remodellers	0,9	1,0	0,9	1,0	1,7
YDR303C	RSC3	chromatin remodellers	0,8	0,5	1,0	1,0	0,7
YMR033W	ARP9	chromatin remodellers	1,0	0,8	1,0	0,9	0,8
YGL150C	INO80	chromatin remodellers	0,9	1,0	1,0	0,7	0,6
YJR082C	EAF6	chromatin remodellers	0,8	0,9	1,1	0,8	2,0
YDL074C	BRE1	chromatin remodellers	0,9	0,6	1,1	1,0	0,7
YDL042C	SIR2	chromatin remodellers	0,9	0,4	1,1	0,7	0,4
YDR181C	SAS4	chromatin remodellers	0,9	0,8	1,1	0,8	0,5
YDR225W	HTA1	chromatin remodellers	1,1	0,5	1,1	1,1	1,6
YIL126W	STH1	chromatin remodellers	1,0	0,7	1,1	0,7	0,5
YPR018W	RLF2	chromatin remodellers	1,2	1,1	1,1	0,4	0,6
YBR215W	HPC2	chromatin remodellers	0,9	0,9	1,1	0,7	0,6
YCR052W	RSC6	chromatin remodellers	0,8	0,7	1,1	0,7	0,6
YDR207C	UME6	chromatin remodellers	0,8	0,4	1,2	0,8	0,4
YML127W	RSC9	chromatin remodellers	1,1	0,9	1,2	0,8	0,7
YER161C	SPT2	chromatin remodellers	0,8	0,7	1,2	0,7	0,6
YOR141C	ARP8	chromatin remodellers	0,9	0,7	1,2	0,7	0,6
YNL206C	RTT106	chromatin remodellers	0,9	0,7	1,2	0,9	0,9
YPL127C	HHO1	chromatin remodellers	1,5	1,1	1,2	1,0	2,1
YGL112C	TAF6	chromatin remodellers	0,9	1,0	1,2	0,8	0,8
YJR140C	HIR3	chromatin remodellers	1,0	1,0	1,2	0,7	0,7
YKR008W	RSC4	chromatin remodellers	1,0	0,8	1,2	1,2	0,8
YDR295C	HDA2	chromatin remodellers	0,9	0,8	1,2	1,2	0,7
YOR038C	HIR2	chromatin remodellers	1,0	0,7	1,2	0,9	0,8
YNL107W	YAF9	chromatin remodellers	0,8	0,7	1,2	1,0	1,3
YPL016W	SWI1	chromatin remodellers	0,9	0,6	1,3	1,7	2,0
YOL004W	SIN3	chromatin remodellers	1,0	1,0	1,3	0,9	0,9
YOR244W	ESA1	chromatin remodellers	0,9	0,8	1,3	1,0	2,4
YLR015W	BRE2	chromatin remodellers	1,0	0,9	1,3	0,7	0,8
YBL002W	HTB2	chromatin remodellers	1,6	0,5	1,3	1,2	0,6
YBR258C	SHG1	chromatin remodellers	1,0	0,9	1,3	1,4	1,7
YHR090C	YNG2	chromatin remodellers	0,8	0,5	1,3	1,0	0,8
YNL330C	RPD3	chromatin remodellers	1,0	0,8	1,4	0,9	1,2
YPL116W	HOS3	chromatin remodellers	0,9	0,5	1,4	1,1	1,7
YDR469W	SDC1	chromatin remodellers	1,0	1,0	1,4	1,6	1,0
YMR263W	SAP30	chromatin remodellers	0,9	0,9	1,4	0,9	1,1
YPR179C	HDA3	chromatin remodellers	1,0	0,9	1,4	1,2	2,1
YDR191W	HST4	chromatin remodellers	0,7	0,6	1,4	0,6	0,6
YOR025W	HST3	chromatin remodellers	0,6	0,6	1,4	0,7	0,4
YGR002C	SWC4	chromatin remodellers	0,9	0,8	1,5	1,0	0,7
YLR033W	RSC58	chromatin remodellers	0,9	0,6	1,5	1,1	0,7
YLR357W	RSC2	chromatin remodellers	1,0	0,6	1,5	0,9	0,3
YLL002W	RTT109	chromatin remodellers	1,2	1,2	1,5	0,8	1,1
YDR485C	VPS72	chromatin remodellers	1,0	0,7	1,5	1,2	0,9
YHR056C	RSC30	chromatin remodellers	1,0	0,7	1,6	1,0	0,8
YLR085C	ARP6	chromatin remodellers	0,9	1,0	1,6	0,8	0,8

YJL168C	set-02	chromatin remodellers	0,9	0,5	1,6	0,6	0,5
YPR031W	NTO1	chromatin remodellers	0,9	0,7	1,6	0,8	1,3
YEL056W	HAT2	chromatin remodellers	1,0	0,9	1,6	1,1	0,6
YPR034W	ARP7	chromatin remodellers	1,0	0,8	1,6	0,8	1,7
YPL138C	SPP1	chromatin remodellers	0,9	0,7	1,7	0,6	1,9
YPR193C	HPA2	chromatin remodellers	0,5	1,2	1,7	0,2	0,9
YHR119W	set-01	chromatin remodellers	0,9	0,7	1,7	1,0	0,9
YGR056W	RSC1	chromatin remodellers	0,8	0,5	1,8	0,8	0,4
YOR064C	YNG1	chromatin remodellers	0,8	0,4	1,8	0,7	1,1
YBL052C	SAS3	chromatin remodellers	1,2	1,0	1,8	0,9	1,2
YBR231C	SWC5	chromatin remodellers	0,8	0,7	1,8	0,8	0,8
YOL012C	HTZ1	chromatin remodellers	1,2	0,7	1,8	1,1	1,2
YMR223W	UBP8	chromatin remodellers	1,0	0,8	1,8	1,3	0,8
YOR290C	SNF2	chromatin remodellers	0,9	0,7	1,9	0,7	0,5
YFL024C	EPL1	chromatin remodellers	0,7	0,6	1,9	1,0	0,5
YLR052W	IES3	chromatin remodellers	0,8	0,7	2,0	1,4	0,8
YPL001W	HAT1	chromatin remodellers	1,1	0,9	2,0	1,2	2,1
YAL011W	SWC3	chromatin remodellers	1,0	0,9	2,0	0,9	0,9
YDL076C	RXT3	chromatin remodellers	0,9	0,6	2,1	1,4	1,2
YNL136W	EAF7	chromatin remodellers	1,0	1,0	2,2	1,0	1,3
YER169W	RPH1	chromatin remodellers	1,1	0,9	2,2	1,3	0,9
YFL013C	IES1	chromatin remodellers	0,9	0,9	2,2	0,9	0,8
YGR252W	GCN5	chromatin remodellers	0,9	0,8	2,2	1,1	5,2
YEL044W	IES6	chromatin remodellers	0,9	0,9	2,6	1,2	1,3
YOR213C	SAS5	chromatin remodellers	0,9	0,7	2,8	1,0	0,9
YMR127C	SAS2	chromatin remodellers	1,1	0,8	3,0	1,0	1,1
YCL010C	SGF29	chromatin remodellers	1,0	0,8	3,1	0,9	1,4
YPL047W	SGF11	chromatin remodellers	0,9	0,8	3,9	1,6	3,0
YBR175W	SWD3	chromatin remodellers	1,2	0,8	4,4	1,7	1,0
YMR069W	NAT4	chromatin remodellers	1,4	1,3	4,5	2,0	1,1
YOR023C	AHC1	chromatin remodellers	0,8	0,5	5,9	1,4	0,8
YNL201C	PSY2	DNA damage checkpoint	1,2	0,8	0,7	1,0	0,6
YER133W	GLC7	DNA damage checkpoint	0,8	0,8	0,7	1,3	1,1
YDR217C	RAD9	DNA damage checkpoint	0,9	0,9	0,7	0,7	0,7
YER177W	BMH1	DNA damage checkpoint	1,3	1,4	0,8	1,0	1,1
YOR217W	RFC1	DNA damage checkpoint	0,9	1,1	0,8	0,7	0,6
YDR099W	BMH2	DNA damage checkpoint	1,0	1,0	0,9	1,0	0,7
YDL101C	DUN1	DNA damage checkpoint	1,3	2,4	0,9	0,7	1,0
YPL194W	DDC1	DNA damage checkpoint	0,9	0,9	1,1	0,6	1,9
YPL153C	RAD53	DNA damage checkpoint	1,1	1,4	1,1	0,6	2,5
YOR368W	RAD17	DNA damage checkpoint	0,9	0,9	1,1	0,7	1,0
YBL046W	PSY4	DNA damage checkpoint	0,8	0,9	1,3	1,0	0,7
YNL273W	TOF1	DNA damage checkpoint	1,1	1,0	1,3	0,5	0,6
YDR440W	DOT1	DNA damage checkpoint	1,3	1,1	1,4	0,7	0,9
YCL061C	MRC1	DNA damage checkpoint	1,1	1,1	1,4	0,6	0,8
YGL058W	RAD6	DNA damage checkpoint	0,8	0,9	1,4	1,0	1,0
YBR136W	MEC1	DNA damage checkpoint	1,0	0,8	1,5	0,8	0,6
YML011C	RAD33	DNA damage checkpoint	0,8	0,7	1,6	0,8	1,1
YBR274W	CHK1	DNA damage checkpoint	0,8	0,8	1,6	1,0	0,8
YDR499W	LCD1	DNA damage checkpoint	1,0	0,6	1,6	0,9	1,0
YDR075W	PPH3	DNA damage checkpoint	1,2	0,6	1,6	1,2	0,7
YLR288C	MEC3	DNA damage checkpoint	0,8	0,5	1,7	0,7	0,8
YER089C	PTC2	DNA damage checkpoint	1,0	0,9	1,7	1,2	1,0
YBL051C	PIN4	DNA damage checkpoint	0,8	0,7	2,0	1,2	0,6
YER173W	RAD24	DNA damage checkpoint	1,0	0,7	2,9	0,9	1,1
YBL088C	TEL1	DNA damage checkpoint	1,0	1,0	3,0	1,0	0,7
YDR180W	SCC2	DNA repair/recombination	0,9	0,8	0,8	0,8	0,5
YNL250W	RAD50	DNA repair/recombination	0,9	0,9	0,8	0,6	0,5
YNL088W	TOP2	DNA repair/recombination	1,1	1,7	0,8	0,6	0,6
YAR007C	RFA1	DNA repair/recombination	1,2	1,1	0,8	0,7	0,9
YFL008W	SMC1	DNA repair/recombination	1,0	0,9	0,8	0,6	0,3
YEL037C	RAD23	DNA repair/recombination	0,7	0,7	0,9	0,8	0,7
YDL059C	RAD59	DNA repair/recombination	0,8	1,0	0,9	0,7	1,0
YER171W	RAD3	DNA repair/recombination	0,8	0,7	1,0	0,9	1,0
YAL019W	FUN30	DNA repair/recombination	0,7	0,7	1,0	0,9	0,4
YBR073W	RDH54	DNA repair/recombination	0,9	1,2	1,0	0,7	0,6
YDL200C	MGT1	DNA repair/recombination	0,9	0,7	1,0	0,9	1,3
YGR258C	RAD2	DNA repair/recombination	1,1	0,9	1,1	1,0	0,9
YJL173C	RFA3	DNA repair/recombination	1,3	1,6	1,1	1,2	1,4

YDR288W	NSE3	DNA repair/recombination	0,7	0,6	1,1	1,3	1,1
YLR032W	RAD5	DNA repair/recombination	0,8	0,7	1,1	0,6	0,5
YMR190C	SGS1	DNA repair/recombination	1,0	0,9	1,2	0,8	1,1
YDR369C	XRS2	DNA repair/recombination	1,0	0,9	1,2	0,8	1,0
YGL163C	RAD54	DNA repair/recombination	1,1	1,5	1,2	0,9	0,8
YOL006C	TOP1	DNA repair/recombination	0,9	0,6	1,2	0,9	1,4
YMR137C	PSO2	DNA repair/recombination	0,9	0,7	1,2	0,9	0,8
YMR106C	YKU80	DNA repair/recombination	0,9	0,7	1,3	0,8	0,5
YOL034W	SMC5	DNA repair/recombination	1,0	0,8	1,3	0,6	0,9
YMR284W	YKU70	DNA repair/recombination	0,8	0,9	1,3	1,0	1,4
YML061C	PIF1	DNA repair/recombination	1,1	1,0	1,3	0,7	1,0
YKL113C	RAD27	DNA repair/recombination	1,1	0,9	1,3	0,5	0,9
YLR383W	SMC6	DNA repair/recombination	1,2	1,1	1,3	0,5	0,8
YLR086W	SMC4	DNA repair/recombination	1,0	1,0	1,4	0,8	1,1
YFR031C	SMC2	DNA repair/recombination	1,1	1,1	1,4	0,7	1,1
YMR201C	RAD14	DNA repair/recombination	0,7	0,7	1,4	0,5	1,1
YNL312W	RFA2	DNA repair/recombination	1,1	1,4	1,5	1,0	1,0
YER162C	RAD4	DNA repair/recombination	0,8	0,6	1,5	0,8	0,3
YOR033C	EXO1	DNA repair/recombination	1,0	0,8	1,5	1,1	1,0
YJR052W	RAD7	DNA repair/recombination	0,9	1,0	1,5	1,1	1,3
YJR035W	RAD26	DNA repair/recombination	0,9	0,9	1,7	0,8	1,0
YDR314C	RAD34	DNA repair/recombination	0,9	1,0	1,7	1,0	1,4
YJL092W	SRS2	DNA repair/recombination	1,2	1,4	1,7	0,7	0,6
YDR386W	MUS81	DNA repair/recombination	0,9	0,8	1,7	0,9	1,1
YMR156C	TPP1	DNA repair/recombination	0,9	0,8	1,8	0,9	0,6
YHR164C	DNA2	DNA repair/recombination	0,9	1,0	1,8	0,9	0,9
YPL022W	RAD1	DNA repair/recombination	0,9	0,7	1,8	1,1	1,7
YMR224C	MRE11	DNA repair/recombination	1,0	0,8	1,8	0,8	0,7
YIL153W	RRD1	DNA repair/recombination	1,1	0,9	1,9	1,5	2,2
YBR098W	MMS4	DNA repair/recombination	1,1	1,2	1,9	0,8	1,1
YBR114W	RAD16	DNA repair/recombination	1,1	1,3	1,9	1,4	1,1
YER147C	SCC4	DNA repair/recombination	0,9	0,7	2,0	0,6	0,6
YEL019C	MMS21	DNA repair/recombination	1,1	0,7	2,0	0,9	0,7
YER116C	SLX8	DNA repair/recombination	0,7	0,7	2,0	0,9	1,2
YLR007W	NSE1	DNA repair/recombination	1,0	0,9	2,0	1,3	1,4
YPL128C	TBF1	DNA repair/recombination	1,1	0,6	2,0	0,9	1,0
YLR373C	VID22	DNA repair/recombination	1,3	1,1	2,1	0,8	0,5
YDL013W	SLX5	DNA repair/recombination	0,9	0,7	2,1	0,8	1,2
YDR004W	RAD57	DNA repair/recombination	0,7	0,5	2,1	0,7	0,8
YOR005C	DNL4	DNA repair/recombination	0,9	0,9	2,1	0,8	1,0
YDR030C	RAD28	DNA repair/recombination	1,0	0,9	2,1	1,1	1,4
YCR066W	RAD18	DNA repair/recombination	0,9	0,7	2,1	1,2	0,7
YER095W	RAD51	DNA repair/recombination	1,3	1,6	2,2	0,9	0,6
YPR164W	MMS1	DNA repair/recombination	1,2	1,1	2,2	0,9	1,1
YML023C	NSE5	DNA repair/recombination	1,2	1,0	2,2	0,7	0,9
YML095C	RAD10	DNA repair/recombination	1,1	1,0	2,3	1,3	0,9
YML032C	RAD52	DNA repair/recombination	1,0	0,7	2,3	0,8	0,8
YLR320W	MMS22	DNA repair/recombination	0,9	0,7	2,4	0,9	0,6
YDR076W	RAD55	DNA repair/recombination	1,0	0,8	2,4	0,8	0,5
YBR228W	SLX1	DNA repair/recombination	0,8	0,6	2,4	1,1	1,3
YGL175C	SAE2	DNA repair/recombination	1,0	1,0	2,4	0,7	0,9
YLR135W	SLX4	DNA repair/recombination	0,9	1,0	2,5	0,9	1,2
YER041W	YEN1	DNA repair/recombination	1,1	1,3	2,9	1,1	1,6
YLR234W	TOP3	DNA repair/recombination	1,2	1,5	3,0	0,5	0,8
YGL090W	LIF1	DNA repair/recombination	0,8	1,0	3,1	1,1	1,8
YBR223C	TDP1	DNA repair/recombination	0,9	0,7	3,2	0,8	0,7
YAR003W	SWD1	DNA repair/recombination	1,2	1,2	3,7	1,2	1,8
YBR275C	RIF1	DNA repair/recombination	1,2	1,1	3,7	0,7	0,6
YDL105W	NSE4	DNA repair/recombination	1,2	1,2	6,6	0,8	0,7

Table 1. List of the DDR genes. For each gene, expression fold change is indicated in the wild type strain 60 and 240 minutes after DSB induction, and in *xrn1Δ*, *rrp6Δ* and *trf4Δ* mutants at time zero. All fold changes are relative to the wild type at time zero.

Conditions	ID	Gene	Fold change	P-value
WT t240/WT t0	YDL101C	DUN1	2,8	8,44E-13
WT t240/WT t0	YLR449W	FPR4	0,5	1,37E-06
WT t240/WT t0	YDL042C	SIR2	0,4	5,20E-08
WT t240/WT t0	YDR207C	UME6	0,5	1,49E-05
WT t240/WT t0	YOR064C	YNG1	0,4	3,11E-06
rrp6/WT	YPR193C	HPA2	0,2	7,48E-09
rrp6/WT	YPR018W	RLF2	0,4	2,66E-05
rrp6/WT	YLR383W	SMC6	0,5	2,24E-05
trf4/WT	YER030W	CHZ1	4,0	3,47E-26
trf4/WT	YOR244W	ESA1	2,3	1,15E-10
trf4/WT	YLR449W	FPR4	0,5	9,71E-09
trf4/WT	YAL019W	FUN30	0,4	4,68E-10
trf4/WT	YGR252W	GCN5	5,1	1,59E-27
trf4/WT	YPL001W	HAT1	2,1	5,55E-08
trf4/WT	YPR179C	HDA3	2,1	2,19E-07
trf4/WT	YBR009C	HHF1	2,3	5,07E-07
trf4/WT	YNL030W	HHF2	5,0	2,30E-17
trf4/WT	YPL127C	HHO1	2,1	8,76E-09
trf4/WT	YBR010W	HHT1	2,7	2,98E-07
trf4/WT	YNL031C	HHT2	2,8	7,72E-08
trf4/WT	YOR025W	HST3	0,4	1,46E-10
trf4/WT	YBL003C	HTA2	3,9	1,08E-12
trf4/WT	YER162C	RAD4	0,3	3,21E-08
trf4/WT	YPL153C	RAD53	2,5	2,51E-09
trf4/WT	YNL250W	RAD50	0,5	2,42E-09
trf4/WT	YIL153W	RRD1	2,2	3,50E-07
trf4/WT	YGR056W	RSC1	0,4	1,16E-11
trf4/WT	YLR357W	RSC2	0,3	1,23E-12
trf4/WT	YDR180W	SCC2	0,5	2,43E-08
trf4/WT	YPL047W	SGF11	3,0	5,23E-13
trf4/WT	YDL042C	SIR2	0,4	7,92E-09
trf4/WT	YFL008W	SMC1	0,3	8,13E-18
trf4/WT	YIL126W	STH1	0,4	9,83E-10
trf4/WT	YPL016W	SWI1	2,0	1,80E-07
trf4/WT	YDR207C	UME6	0,4	1,77E-09
xrn1/WT	YOR023C	AHC1	4,3	2,41E-22
xrn1/WT	YER030W	CHZ1	0,4	9,12E-08
xrn1/WT	YLR449W	FPR4	0,4	1,84E-11
xrn1/WT	YBR009C	HHF1	0,5	1,10E-06
xrn1/WT	YBR010W	HHT1	0,4	1,37E-06
xrn1/WT	YNL031C	HHT2	0,5	1,61E-05
xrn1/WT	YBL003C	HTA2	0,3	2,67E-13
xrn1/WT	YGL090W	LIF1	2,2	0,00068156
xrn1/WT	YMR069W	NAT4	3,3	6,68E-06
xrn1/WT	YDL105W	NSE4	4,7	4,66E-24
xrn1/WT	YER173W	RAD24	2,1	4,84E-06
xrn1/WT	YBR275C	RIF1	2,7	2,05E-11
xrn1/WT	YMR127C	SAS2	2,1	4,46E-06
xrn1/WT	YOR213C	SAS5	2,0	7,56E-07
xrn1/WT	YPL047W	SGF11	2,8	1,20E-11
xrn1/WT	YCL010C	SGF29	2,2	2,14E-06
xrn1/WT	YAR003W	SWD1	2,7	1,51E-11
xrn1/WT	YBR175W	SWD3	3,2	4,45E-15
xrn1/WT	YBR223C	TDP1	2,3	9,50E-08
xrn1/WT	YBL088C	TEL1	2,1	5,62E-07
xrn1/WT	YLR234W	TOP3	2,2	0,00045833
xrn1/WT	YER041W	YEN1	2,1	2,68E-05

Table 2. List of differentially expressed DDR genes upon DSB formation or deletion of RNA decay factors. For each gene, expression fold change and *P*-value from DESeq analysis were determined in the wild type strain 60 and 240 minutes after DSB induction and in the *xrn1Δ*, *rrp6Δ* and *trf4Δ* mutants at time zero, relative to the wild type at time zero. Candidates showing significant differential expression (fold change ≤0.5 or ≥2, *P*-value ≤0.001) in one of the conditions are indicated, with their associated fold change and *P*-value. No significant candidate was found in the wild type 60 minutes after HO induction (see Figure 18A).

(Cesena *et al.*, 2017)

NUCLEIC ACIDS RESEARCH

February 2017 (Published online).

doi: 10.1093/nar/gkx072.

Regulation of telomere metabolism by the RNA processing protein Xrn1

Daniele Cesena[1], Corinne Cassani[1], Emanuela Rizzo[1], Michael Lisby[2], Diego Bonetti[1], Maria Pia Longhese[1]

[1]Dipartimento di Biotecnologie e Bioscienze, Università di Milano-Bicocca, Milan, Italy.

[2]Department of Biology, University of Copenhagen, DK-2200 Copenhagen N, Denmark.

Nucleoprotein complexes called telomeres are present at the ends of linear eukaryotic chromosomes, where they ensure replication of the chromosome ends and prevent their recognition as DNA double-strand breaks (DSBs) (Wellinger and Zakian, 2012; Bonetti *et al.*, 2014). Telomeric DNA in most eukaryotes consists of tandem arrays of short repeated sequences which are guanine-rich in the strand running 5'-3' from the centromere towards the chromosome end. The G-rich strand at both ends of a chromosome extends over the C-strand to form a 3'-ended single-stranded G-rich overhang (G-tail) (Henderson and Blackburn, 1989; Wellinger *et al.*, 1993). This G-tail is important for telomere replication, because it provides a substrate for the telomerase enzyme. Telomerase is a ribonucleoprotein complex that uses its RNA component as a template to elongate the telomere by addition of G-rich telomeric repeats to the G-tail (Wellinger and Zakian, 2012; Pfeiffer and Lingner, 2013). The telomerase-extended single-stranded DNA (ssDNA) must then be copied by the conventional replication machinery to reconstitute the double-stranded telomeric DNA.

In *S. cerevisiae*, single-stranded G-rich tails of 5-10 nt in length are present at telomeres throughout most of the cell cycle except in late S phase, when longer overhangs are detected (Wellinger *et al.*, 1993; Dionne and Wellinger, 1996; Wellinger *et al.*, 1996). Removal of the last RNA primers that are generated by lagging-strand synthesis appears to match the observed overhang length (Soudet *et al.*, 2014). By contrast, the telomeric C-strands generated by leading-strand synthesis are resected by about 30-40 nt before being filled in again to

leave DNA ends with a 3' overhang of about 10 nt (Soudet *et al.*, 2014; Faure *et al.*, 2010). This resection depends on the MRX (Mre11-Rad50-Xrs2) complex, on the exonuclease Exo1 and on the Sgs1-Dna2 helicase-nuclease complex (Diede and Gottschling, 2001; Larrivée *et al.*, 2004; Bonetti *et al.*, 2009).

G-tails at both leading- and lagging-strand telomeres are covered by the CST (Cdc13-Stn1-Ten1) complex, which is an RPA-like complex that binds with high affinity and sequence specificity to the telomeric ssDNA overhangs (Gao *et al.*, 2007). The CST complex drives the localization of telomerase to telomeres through a direct interaction between Cdc13 and the telomerase subunit Est1 (Nugent *et al.*, 1996; Evans and Lundblad, 1999; Pennock *et al.*, 2001; Bianchi *et al.*, 2004). MRX, in turn, ensures robust association of telomerase with telomeres by promoting the binding of the checkpoint kinase Tel1 via a specific interaction with the MRX subunit Xrs2 (Nakada *et al.*, 2003; Chang *et al.*, 2007; Hector *et al.*, 2007; Sabourin *et al.*, 2007; McGee *et al.*, 2010). It remains unclear whether Tel1 facilitates telomerase association directly by phosphorylating specific targets that promote telomerase recruitment, and/or indirectly by stimulating resection of the C-strand, thus generating a ssDNA substrate for telomerase action (Tseng *et al.*, 2006; Gao *et al.*, 2010; Wu *et al.*, 2013). Interestingly, Mre11 inactivation strongly reduces the binding to telomeres of the telomerase subunits Est1 and Est2, while it has a moderate effect on Cdc13 binding (Goudsouzian *et al.*, 2006). Further work has shown that the absence of Mre11 reduces Cdc13 binding only to the leading-strand telomere, while Cdc13 ability to bind to the lagging-strand

telomere is not affected (Faure *et al.*, 2010). This observation is consistent with the finding that Mre11 binds only to leading telomeres to generate the single-stranded overhangs (Faure *et al.*, 2010).

In addition to drive telomerase localization to telomeres, the CST complex also genetically and physically interacts with the DNA polymerase α/primase complex and promotes lagging strand synthesis during telomere replication (Qi and Zakian,2000; Grossi *et al.*, 2004). Furthermore, it prevents inappropriate generation of ssDNA at telomeric ends. Cdc13 inactivation through either the *cdc13-1* temperature sensitive allele or the *cdc13-td* conditional degron allele results in both degradation of the 5'-terminated DNA strand and checkpoint-dependent cell cycle arrest (Garvik *et al.*, 1995; Lydall and Weinert, 1995; Vodenicharov and Wellinger, 2006). Similarly, temperature sensitive alleles of either the *STN1* or *TEN1* gene cause telomere degradation and checkpoint-mediated cell cycle arrest at the nonpermissive temperature (Grandin *et al.*, 1997; Grandin *et al.*, 2001; Puglisi *et al.*, 2008; Xu *et al.*, 2009). DNA degradation in the *cdc13-1* mutant depends mainly on the 5'-3' nuclease Exo1 (Maringele and Lydall, 2002; Zubko *et al.*, 2004), suggesting that CST protects telomeric DNA from Exo1 activity.

There is emerging evidence that telomere metabolism is influenced by RNA processing pathways. In eukaryotes, RNA processing relies on two highly conserved pathways involving both 5'-3' and 3'-5' exoribonuclease activities (Parker, 2012). In particular, 5'-3' degradation is performed by the Xrn protein family, which comprises the cytoplasmic Xrn1 enzyme and the nuclear Rat1 enzyme (also

known as Xrn2) (Nagarajan *et al.*, 2013). The 3'-5' RNA processing activity is due to the exoribonuclease Rrp6 that belongs to the nuclear exosome (Houseley *et al.*, 2006). In addition, RNA molecules are subjected to a quality control system, which is called nonsense-mediated mRNA decay (NMD) and degrades nonfunctional RNAs that might otherwise give rise to defective protein products (Parker, 2012). RNA processing proteins have been recently implicated in telomere metabolism in both yeast and mammals, although the related mechanisms are poorly understood. In particular, Xrn1 has been identified in genome-wide screenings for *Saccharomyces cerevisiae* mutants with altered telomere length (Askree *et al.*, 2004; Ungar *et al.*, 2009). Moreover, proteins belonging to the mammalian NMD pathway have been found to bind telomeres and to control telomere length (Azzalin *et al.*, 2007; Chawla *et al.*, 2011). Similarly, the lack of the *S. cerevisiae* NMD proteins was shown to cause telomere shortening by increasing the amount of Stn1 and Ten1, which in turn inhibit telomerase activity by interfering with Est1-Cdc13 interaction (Lew *et al.*, 1998; Dahlseid *et al.*, 2003; Addinall *et al.*, 2011; Holstein *et al.*, 2014). Furthermore, both Xrn1 and the nuclear exosome control degradation of the RNA component of human telomerase (Shukla *et al.*, 2016). Finally, Rat1 and the NMD pathway control the level of a new class of noncoding RNAs called TERRA (telomeric repeat-containing RNA), which are transcribed from the subtelomeric sequences and likely regulate telomere length (Luke *et al.*, 2008; Pfeiffer and Lingner, 2012; Iglesias *et al.*, 2011).

Here we show that the lack of the *S. cerevisiae* RNA processing factors

Xrn1 or Rrp6 suppresses the temperature sensitivity of *cdc13-1* mutant cells by attenuating the activation of the DNA damage checkpoint response. In particular, Xrn1 is required to activate the checkpoint upon telomere uncapping because it promotes the generation of ssDNA. Furthermore, Xrn1 maintains telomere length independently of ssDNA generation by promoting Cdc13 association to telomeres through downregulation of the transcript encoding the telomerase inhibitor Rif1.

The lack of Xrn1 or Rrp6 partially suppresses the temperature sensitivity of *cdc13-1* cells

Protection of telomeres from degradation depends on the CST (Cdc13-Stn1-Ten1) complex, which specifically binds to the telomeric ssDNA overhangs (Gao *et al.*, 2007). We have previously shown that the RNA processing proteins Xrn1 and Rrp6 are required to fully activate the checkpoint kinase Mec1/ATR at intrachromosomal DSBs (Manfrini *et al.*, 2015). We then asked whether Xrn1 and/or Rrp6 regulate checkpoint activation also in response to telomere uncapping. To this end, we analyzed the effect of deleting either the *XRN1* or the *RRP6* gene in *cdc13-1* cells, which show temperature-dependent loss of telomere capping, ssDNA production, checkpoint activation and cell death (Garvik *et al.*, 1995; Lydall and Weinert, 1995). As expected, *cdc13-1* cells were viable at permissive temperature (25°C), but died at restrictive temperature (26-30°C) (Figure 19A). Deletion of either *XRN1* or *RRP6* partially suppressed the temperature sensitivity of *cdc13-1* cells, as it allowed *cdc13-1* cells to form colonies at 26-28°C

(Figure 19A). Xrn1 and Rrp6 appear to impair cell viability of *cdc13-1* cells by acting in two different pathways, as *xrn1Δ rrp6Δ cdc13-1* triple mutant cells formed colonies at 30°C more efficiently than both *xrn1Δ cdc13-1* and *xrn1Δ cdc13-1* double mutant cells (Figure 19B).

Xrn1 and Rrp6 control RNA degradation by acting as 5'-3' and 3'-5' exoribonucleases, respectively (Parker, 2012). The *xrn1-E176G* and *rrp6-D238A* alleles, encoding nuclease-defective Xrn1 or Rrp6 variants (Page *et al.*, 1998; Burkard and Butler, 2000), suppressed the temperature sensitivity of *cdc13-1* cells to an extent similar to that of *xrn1Δ* and *rrp6Δ*, respectively (Figure 19C). Therefore, Xrn1 and Rrp6 appear to impair viability in the presence of uncapped telomeres by acting as nucleases.

Xrn1 controls cytoplasmic RNA decay, whereas RNA processing in the nucleus depends on its nuclear paralog Rat1 (Johnson, 1997). Targeting Rat1 to the cytoplasm by deleting its nuclear localization sequence (*rat1-ΔNLS*) restores Xrn1-like function in RNA degradation (Johnson, 1997), prompting us to ask whether it could restore Xrn1 function in causing loss of viability of *cdc13-1* cells. Strikingly, *cdc13-1 xrn1Δ* cells expressing the *rat1-ΔNLS* allele on a centromeric plasmid formed colonies at 27°C much less efficiently than *cdc13-1 xrn1Δ* cells expressing wild type *RAT1* (Figure 19D). Thus, Xrn1 impairs viability in the presence of uncapped telomeres by controlling a cytoplasmic RNA decay pathway.

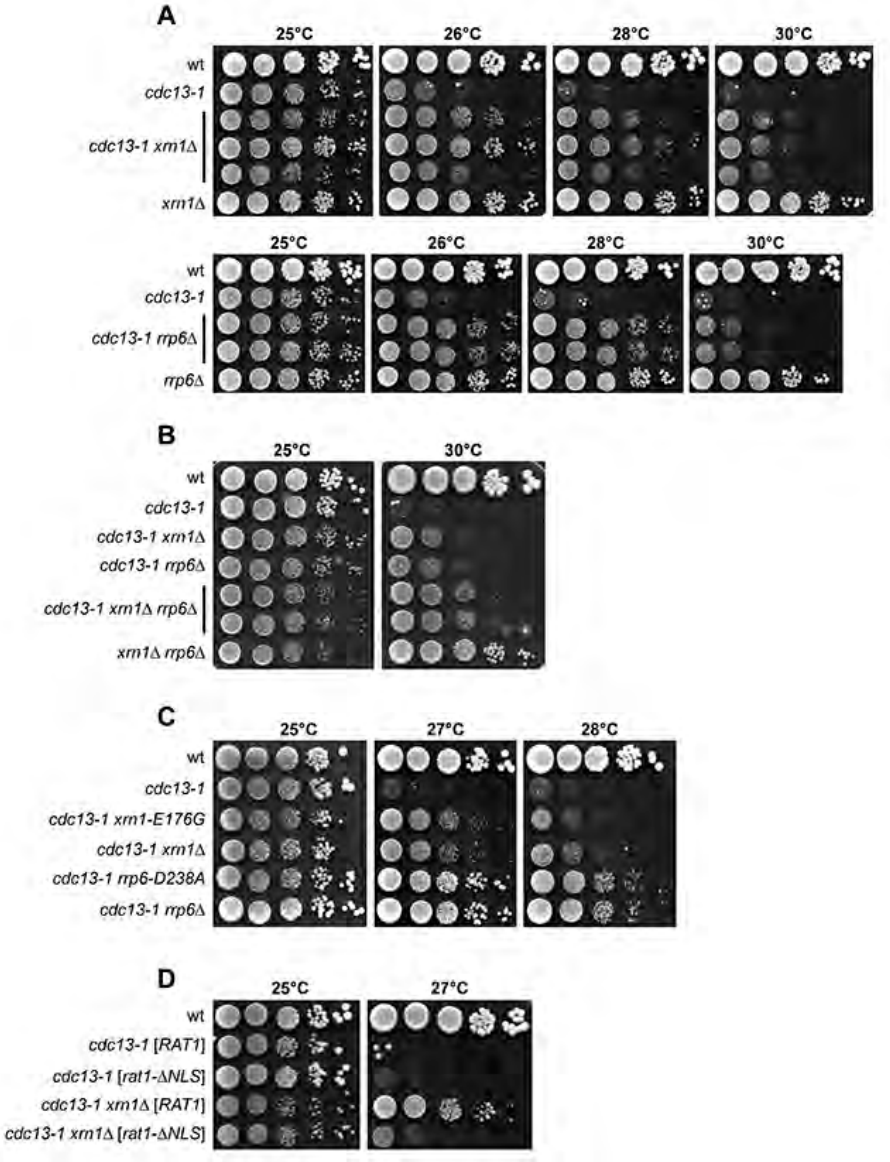

Figure 19. The lack of Xrn1 or Rrp6 partially suppresses the temperature sensitivity of cdc13-1 cells. A)-C) Cell cultures were grown overnight at 23°C and 10-fold serial dilutions were spotted onto YEPD plates. Bars point out independent clones. D) Cell cultures were grown overnight at 23°C in synthetic complete (S.C.) medium lacking leucine and 10-fold serial dilutions were spotted onto YEPD plates. Plates were incubated at the indicated temperatures before images were taken.

Xrn1 and Rrp6 are required to fully activate the checkpoint at uncapped telomeres

A checkpoint-dependent arrest of the metaphase to anaphase transition is observed in *cdc13-1* cells at high temperatures (Garvik *et al.*, 1995). Failure to turn on the checkpoint allows *cdc13-1* cells to form colonies at 28°C (Lydall and Weinert, 1995), indicating that checkpoint activation can partially account for the loss of viability of *cdc13-1* cells. We therefore asked whether the enhanced temperature resistance of *cdc13-1 xrn1*Δ and *cdc13-1 rrp6*Δ cells might be related to defective checkpoint activation. Cell cultures were arrested in G1 with α-factor at 23°C and then released from G1 arrest at 28°C, followed by monitoring nuclear division at different time points. As expected, *cdc13-1* cells remained arrested as large budded cells with a single nucleus throughout the experiment (Figure 20A). Conversely, although *xrn1*Δ and *rrp6*Δ single mutant cells slowed down nuclear division compared to wild type cells, *cdc13-1 xrn1*Δ and *cdc13-1 rrp6*Δ cells started to divide nuclei about 90 minutes after release (Figure 20A).

We then examined under the same conditions phosphorylation of the Rad53 checkpoint kinase that is necessary for checkpoint activation and can be detected as changes in Rad53 electrophoretic mobility. After release at 28°C from G1 arrest, Rad53 phosphorylation was strong in *cdc13-1* cells, as expected, whereas it was undetectable in *cdc13-1 xrn1*Δ cells and it was reduced in *cdc13-1 rrp6*Δ cells (Figure 20B). Taken together, these results indicate that Xrn1 and Rrp6 are

required to fully activate the checkpoint in response to telomere uncapping caused by defective Cdc13.

Xrn1 and Rrp6 regulate telomere capping through a mechanism that is distinct from that involving the NMD pathway

In both yeast and mammals, the NMD pathway is involved in quality control of gene expression by eliminating aberrant RNAs (Isken and Maquat, 2008). Interestingly, NMD inactivation was shown to suppress the temperature sensitivity of *cdc13-1* cells by increasing the levels of the Cdc13 interacting proteins Stn1 and Ten1, which likely stabilize the CST complex at telomeres (Dahlseid *et al.*, 2003; Addinall *et al.*, 2011; Enomoto *et al.*, 2004). These high levels of Stn1 and Ten1 are also responsible for the short telomere length phenotype of *nmdΔ* mutants, possibly because Stn1 and Ten1 inhibit telomerase activity by interfering with Est1-Cdc13 interaction (Pennock *et al.*, 2001; Puglisi *et al.*, 2008; Chandra *et al.*, 2001; Grandin *et al.*, 2000).

As 77% of the transcripts that are upregulated in *nmdΔ* cells are upregulated also in *xrn1Δ* cells (He *et al.*, 2003), we asked whether Xrn1 and/or Rrp6 action at telomeres might involve the same pathway that is regulated by NMD. To this purpose, we constructed fully functional Ten1-Myc and Stn1-HA alleles to analyze the levels of Ten1 and Stn1 in *xrn1Δ* and *rrp6Δ* cells. As expected, the amounts of Ten1-Myc and Stn1-HA were greatly increased in cells lacking the NMD protein Upf2 (Figure 20C and D). By contrast, the lack of Xrn1 or Rrp6 did not change the amount of Ten1-Myc (Figure 20C) and only very slightly increased the amount of Stn1-HA (Figure 20D). Furthermore,

Xrn1 and Rrp6 do not compensate for the absence of each other in controlling Ten1 and Stn1 levels, as the amount of Ten1-Myc (Figure 20E) and Stn1-HA (Figure 20F) in *xrn1Δ rrp6Δ* double mutant cells was similar to that in *xrn1Δ* and *rrp6Δ* single mutant cells.

The presence of the Myc or HA tag at the C-terminus of Ten1 and Stn1, respectively, did not affect the possible regulation of the corresponding mRNAs by Xrn1 or Rrp6, as the suppression of the temperature sensitivity of *cdc13-1* cells by *XRN1* or *RRP6* deletion was similar either in the presence or in the absence of the *TEN1-MYC* or *STN1-HA* allele (Figure 21).

We also analyzed the epistatic relationships between Xrn1/Rrp6 and NMD. The effect of deleting *UPF2* in *xrn1Δ cdc13-1* cells could not be assessed due to the poor viability of the triple mutant at 23-25°C. Nonetheless, deletion of *UPF2*, which partially suppressed the temperature sensitivity of *cdc13-1* cells, further improved the temperature resistance of *cdc13-1 rrp6Δ* double mutant cells at 32°C compared to both *cdc13-1 rrp6Δ* and *cdc13-1 upf2Δ* cells (Figure 20G). Altogether, these data suggest that Xrn1 and Rrp6 impair survival of *cdc13-1* by acting in a pathway that is different from that involving the NMD proteins.

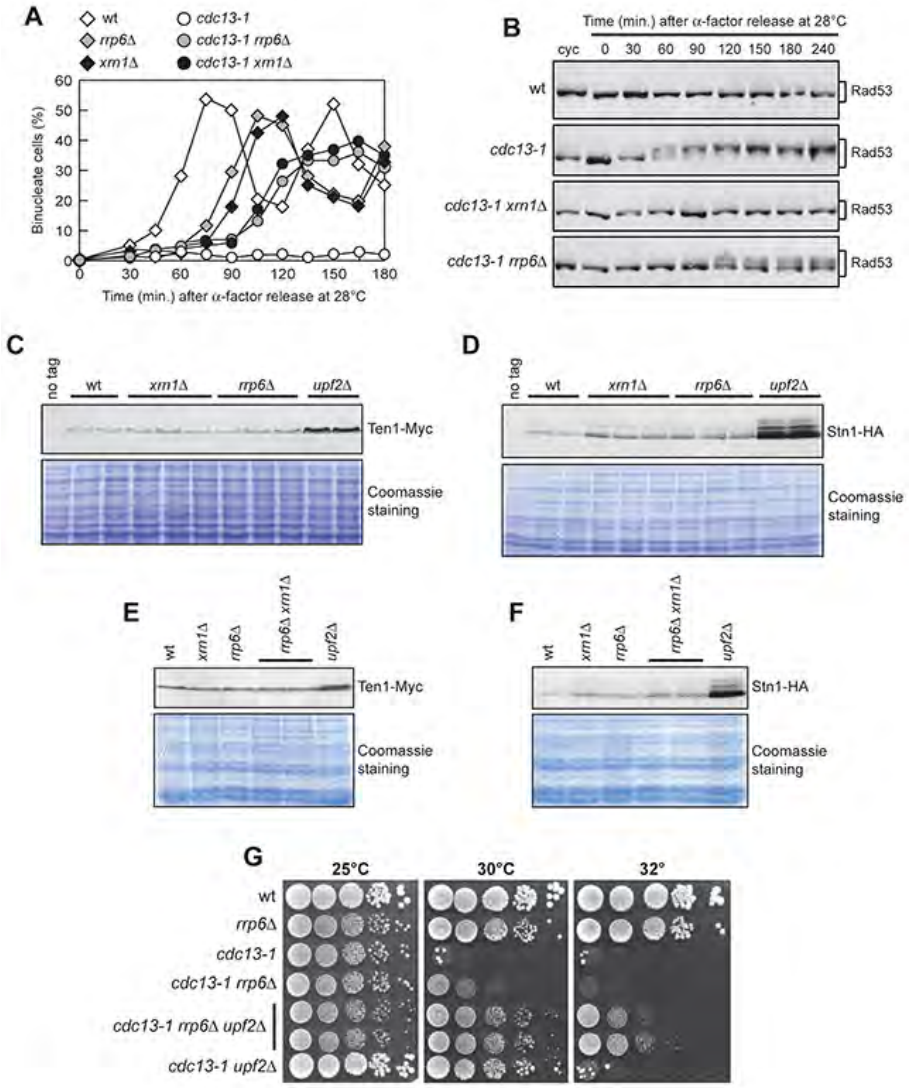

Figure 20. The lack of Xrn1 or Rrp6 reduces checkpoint activation in cdc13-1 cells and suppresses the temperature sensitivity of cdc13-1 cells by acting in a pathway different from NMD. A), B) Cell cultures exponentially growing at 23°C in YEPD (cyc) were arrested in G1 with α-factor and then released into the cell cycle at 28°C (time zero). Samples were taken at the indicated times after α-factor release to determine the kinetics of nuclear division (A), and for western blot analysis of protein extracts using anti-Rad53 antibodies (B). C)-F) Protein extracts prepared from cell cultures exponentially growing at 25°C in YEPD were subjected to western blot analysis with an anti-Myc (C,E) or anti-HA (D,F) antibody. The same amount of extracts was separated by SDS-PAGE and stained with Coomassie Blue as loading control. Bars

point out two or three independent cell cultures. G) Cell cultures were grown overnight at 23°C, and 10-fold serial dilutions were spotted onto YEPD plates. The bar points out two independent *cdc13-1 rrp6Δ upf2Δ* clones.

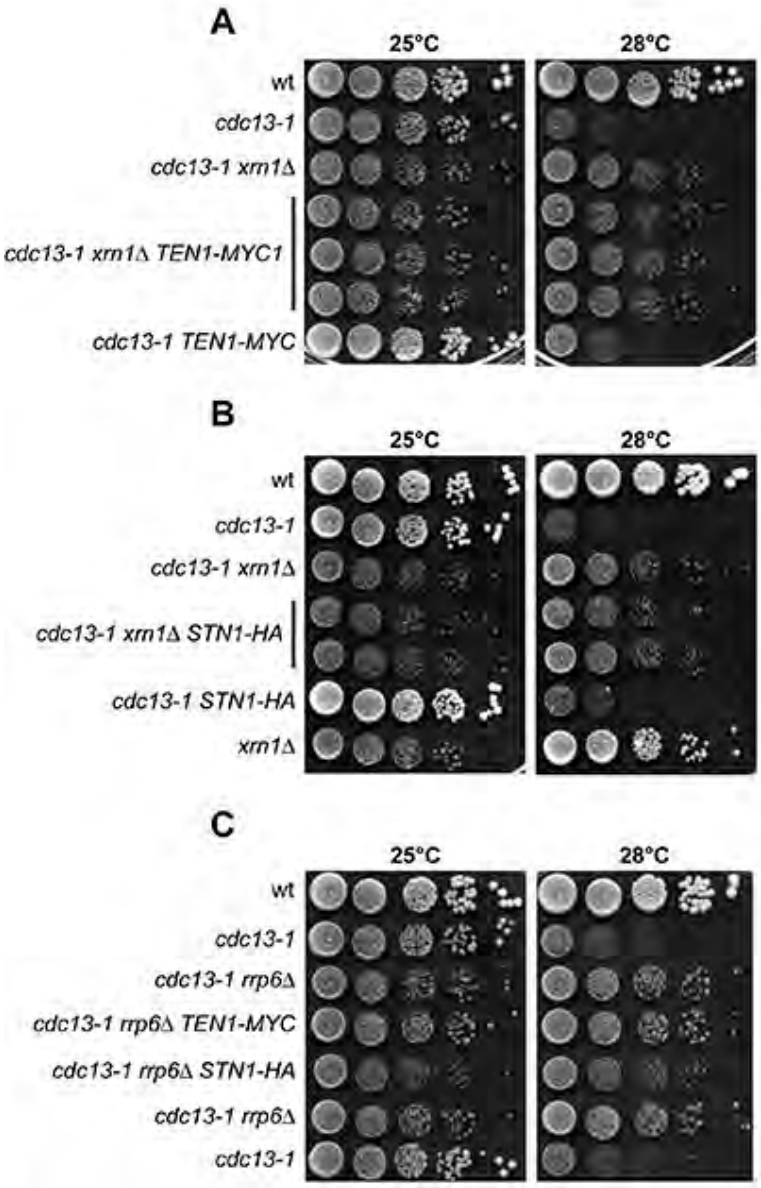

Figure 21. Ten1-MYC and Stn1-HA variants did not affect the suppression of *cdc13-1* by *XRN1* or *RRP6* deletion. Cell cultures were grown overnight at 23°C in YEPD medium and 10-fold serial dilutions were spotted onto YEPD plates.

Xrn1 is required to generate ssDNA at uncapped telomeres

It is known that cell death of *cdc13-1* cells at restrictive temperatures is due to generation of telomeric ssDNA that triggers checkpoint-mediated metaphase arrest (Garvik *et al.*, 1995; Lydall and Weinert, 1995). Hence, the improved temperature resistance of *cdc13-1 xrn1Δ* and *cdc13-1 rrp6Δ* cells might be due to a reduction of the amount of telomeric DNA that becomes single-stranded in *cdc13-1* cells at restrictive temperatures. We therefore assessed the presence of ssDNA at natural chromosome ends by analyzing genomic DNA prepared from exponentially growing cells. Non-denaturing in-gel hybridization with a C-rich radiolabelled oligonucleotide showed that the amount of telomeric ssDNA after incubation of cells at 28°C for 5 hours was lower in *cdc13-1 xrn1Δ* double mutant cells than in *cdc13-1* cells (Figure 22A). By contrast, the level of single-stranded TG sequences showed a very similar increase in both *cdc13-1* and *cdc13-1 rrp6Δ* mutant cells compared to wild type cells (Figure 22A).

The function of Cdc13 in telomere protection is mediated by its direct interaction with Stn1 and Ten1. In contrast to Cdc13, Stn1 inhibits telomerase action by competing with Est1 for binding to Cdc13 (Chandra *et al.*, 2001; Grandin *et al.*, 2000). As a consequence, cells lacking the Stn1 C-terminus (*stn1-ΔC*) display long telomeres because the Stn1-ΔC variant fails to compete with Est1 for binding to Cdc13. Furthermore, these same cells accumulate telomeric ssDNA, although the amount of this ssDNA is not enough to impair cell viability (Puglisi *et al.*, 2008; Chandra *et al.*, 2001; Petreaca *et al.*, 2007). We therefore evaluated the specificity of the genetic interactions between Cdc13,

Xrn1 and Rrp6 by analyzing the consequences of deleting *XRN1* or *RRP6* in *stn1*-Δ*C* cells. Like in *cdc13-1* cells, generation of telomeric ssDNA in *stn1*-ΔC cells was reduced by the lack of Xrn1, but not by *RRP6* deletion (Figure 22B). Thus, Xrn1 is required to generate ssDNA at dysfunctional telomeres, whereas Rrp6 does not, implying that the defective checkpoint response in *cdc13-1 rrp6*Δ cells cannot be ascribed to a reduced generation of telomeric ssDNA.

The data above suggest that the lack of Xrn1 might suppress the temperature sensitivity of *cdc13-1* cells by attenuating the generation of telomeric ssDNA. We then asked whether the overexpression of Exo1, which bypasses MRX requirement for intrachromosomal DSB end resection (Mantiero *et al.*, 2007), decreased the maximum permissive temperature of *cdc13-1 xrn1Δ* cells. Strikingly, *cdc13-1 xrn1Δ* cells containing the *EXO1* gene on a 2µ plasmid were more temperature-sensitive than *cdc13-1 xrn1Δ* cells containing the empty vector (Figure 22C). This finding supports the hypothesis that the lack of Xrn1 can partially bypass the requirement for CST in telomere capping because it attenuates the generation of telomeric ssDNA.

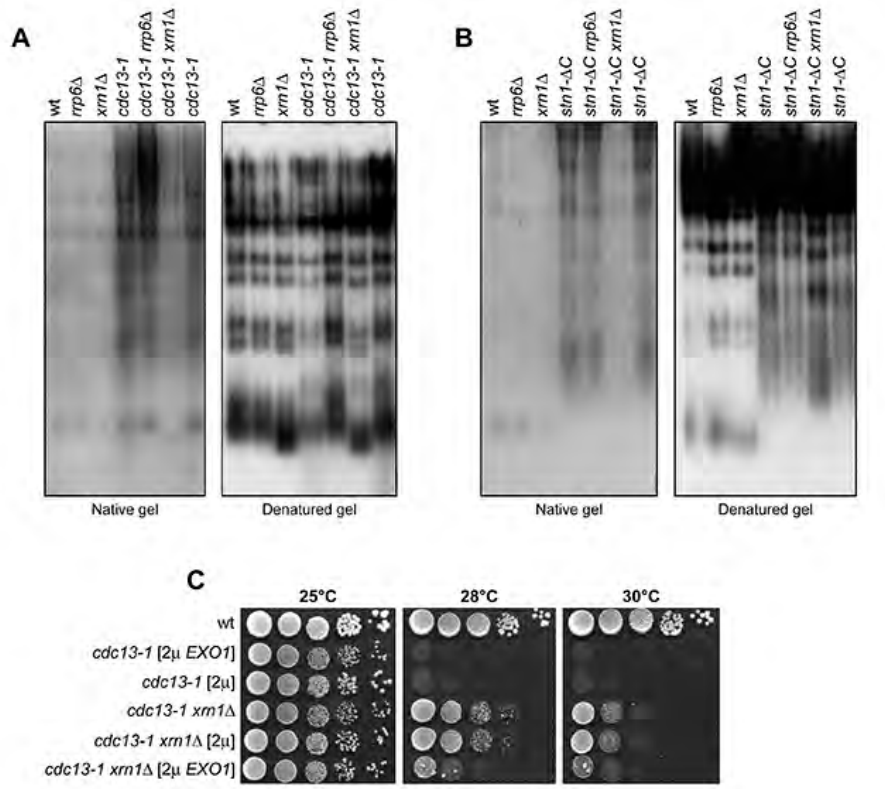

Figure 22. The lack of Xrn1 reduces ssDNA generation at uncapped telomeres. A), B) Cell cultures exponentially growing at 23°C were shifted to 28°C for 5 hours. Genomic DNA was digested with XhoI, and single-stranded G-tails were visualized by non-denaturing in-gel hybridization (native gel) using an end-labeled C-rich oligonucleotide as a probe. The gel was denatured and hybridized again with the same probe for loading control (denatured gel). C) Cell cultures were grown overnight in S.C. medium lacking uracil and 10-fold serial dilutions were spotted onto YEPD plates. Plates were incubated at the indicated temperatures before images were taken.

Xrn1 maintains telomere length by acting as a cytoplasmic nuclease

Xrn1 has been identified in genome-wide screenings for *Saccharomyces cerevisiae* mutants that are affected in telomere length (Askree *et al.*, 2004; Ungar *et al.*, 2009). We confirmed the requirement for Xrn1 in telomere elongation by using an inducible short telomere assay that allows the generation of a single short telomere without affecting the length of the other telomeres in the same cell (Diede and Gottschling, 2001). We used a strain that carried at the *ADH4* locus on chromosome VII an internal tract of telomeric DNA sequence (81 bp TG) adjacent to an HO endonuclease recognition sequence (Figure 23A) (Diede and Gottschling, 2001; Diede and Gottschling, 1999). Upon cleavage by HO, the fragment distal to the break is lost, and, over time, the TG side of the break is elongated by the telomerase. As shown in Figure 23B, sequence addition at the HO-derived telomere was clearly detectable after galactose addition in wild type cells, whereas it was strongly delayed and reduced in *xrn1Δ* cells, confirming the requirement of Xrn1 for telomere elongation.

Xrn1 controls telomere length by acting as cytoplasmic nuclease. In fact, expression of the Xrn1 nuclear paralog Rat1 lacking its nuclear localization sequence (*rat1-ΔNLS*) restored telomere length in *xrn1Δ* cells (Figure 23C). Furthermore, telomeres in *xrn1-E176G* cells expressing the nuclease defective Xrn1 variant were as short as in *xrn1Δ* cells (Figure 23D).

In a deep transcriptome analysis of the genes that are misregulated by the lack of Xrn1, *xrn1Δ* cells showed a ~3-fold reduction of the levels of *TLC1* (Manfrini *et al.*, 2015), the RNA component of the telomerase

enzyme. However, a 2µ plasmid overexpressing *TLC1* from a galactose inducible promoter did not allow *xrn1Δ* cells to elongate telomeres (Figure 24A), although wild type and *xrn1Δ* cells expressed similar amount of *TLC1* RNA (Figure 24B). Thus, telomere shortening in *xrn1Δ* cells cannot be simply explained by the reduction of *TLC1* RNA.

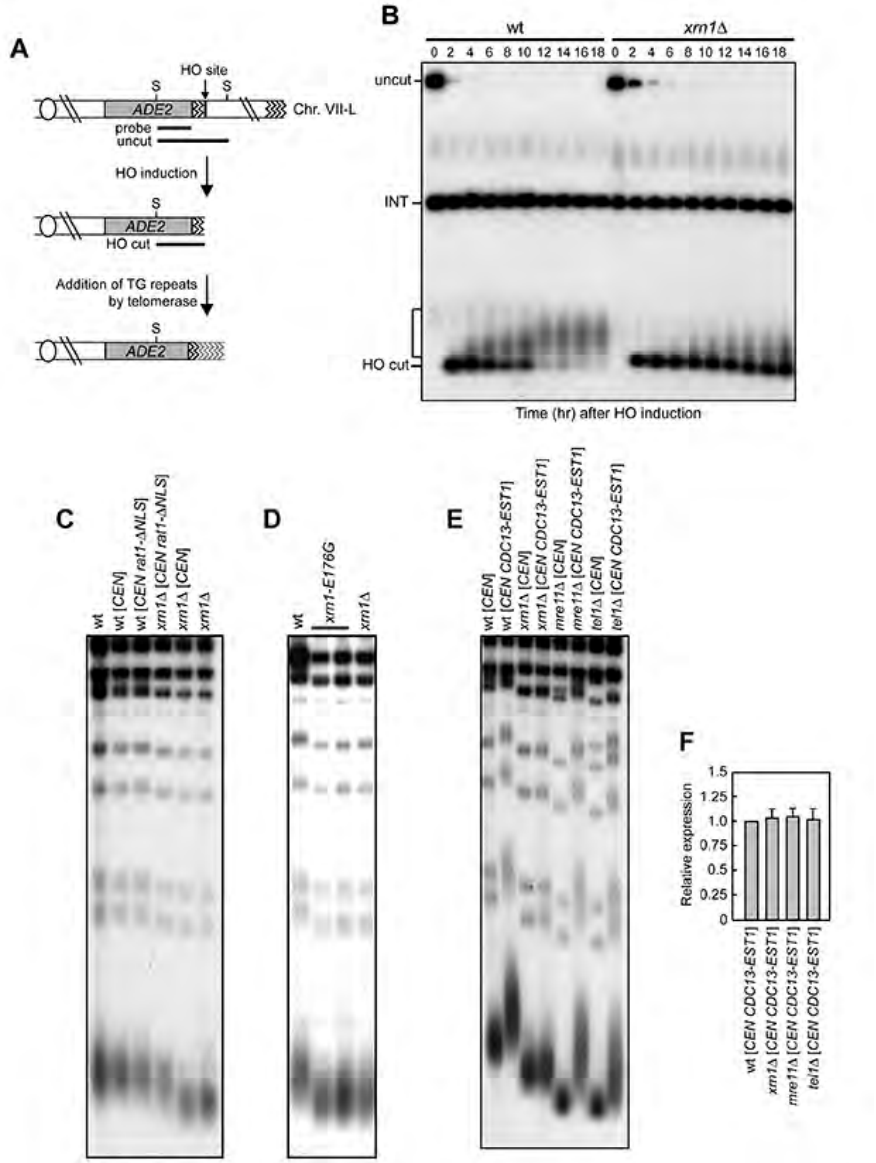

Figure 23. The lack of Xrn1 impairs telomere elongation. A) Schematic representation of the HO-induced short telomere system. The *ADH4* locus on chromosome VII was replaced with a fragment consisting of the *ADE2* gene and 81 bp of TG telomeric sequences (zigzag lines) flanking the recognition site for the HO endonuclease. The centromere is shown as a circle. S, SpeI. B) Elongation of the HO-induced telomere. Cell cultures carrying the system described in (A) and exponentially growing in raffinose were shifted to galactose at time zero to induce HO expression. SpeI-digested genomic DNA prepared at the indicated times was subjected to Southern blot analysis using an *ADE2* fragment as a probe. A bracket

points out new telomere repeats added to the exposed TG telomeric sequences. The band of about 1.6kb (INT) represents the endogenous *ade2-101* gene. C), D) XhoI-cut genomic DNA from exponentially growing cells was subjected to Southern blot analysis using a radiolabeled poly(GT) probe. The bar in (D) points out two independent *xrn1-E176G* cell cultures. E) Overexpression of *CDC13-EST1* fusion does not suppress the telomere shortening of *xrn1Δ* cells. XhoI-cut genomic DNA from exponentially growing cells was subjected to Southern blot analysis using a radiolabeled poly(GT) probe. F) RNA levels of *CDC13-EST1* from cells in (E) were evaluated by quantitative reverse transcriptase PCR (qRT-PCR). RNA levels were quantified using ΔΔCt method. Quantities were normalized to *ACT1* RNA levels and compared to that of wild type cells that was set up to 1. The mean values ±SD. are represented (n=3).

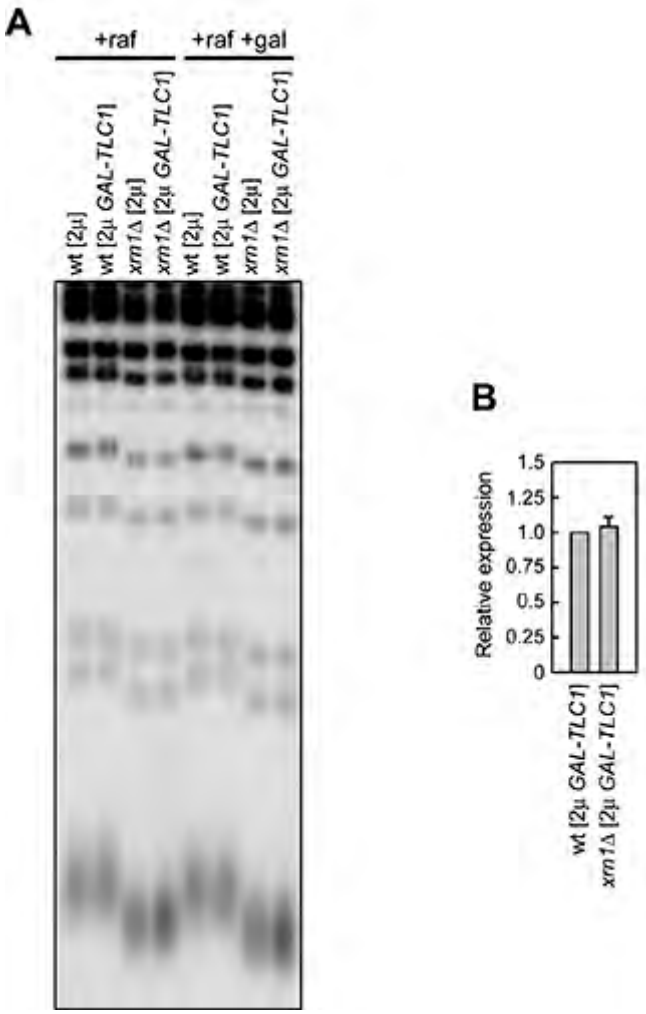

Figure 24. Overexpression of *TLC1* does not suppress telomere shortening of *xrn1Δ* cells. A) Cells exponentially growing cells in S.C.-Trp+raffinose were shifted to S.C.-Trp+galactose for 12 hours. XhoI-cut genomic DNA was subjected to Southern blot analysis using a radiolabeled poly(GT) probe. B) RNA levels of *TLC1* from cells in (A) shifted to galactose were evaluated by quantitative reverse transcriptase PCR (qRT-PCR). RNA levels were quantified using ΔΔCt method. Quantities were normalized to *ACT1* RNA levels and compared to that of wild type cells that was set up to 1. The mean values ±SD. are represented (n=3).

Xrn1 promotes Cdc13 association to telomeres independently of ssDNA generation

Productive association of telomerase to telomeres requires the generation of ssDNA that leads to the recruitment of Cdc13. Cdc13 in turn recruits the telomerase to telomeres by interacting with the telomerase subunit Est1 (Nugent *et al.*, 1996; Evans and Lundblad, 1999; Pennock *et al.*, 2001; Bianchi *et al.*, 2004). Binding of MRX to telomeres allows Tel1 recruitment that strengthens the association of telomerase to telomeres by phosphorylating unknown targets (Tseng *et al.*, 2006; Gao *et al.*, 2010; Wu *et al.*, 2013). The finding that telomere shortening in *mrxΔ* and *tel1Δ* cells can be suppressed by targeting the telomerase to telomeres through a Cdc13-Est1 protein fusion (Tsukamoto *et al.*, 2001) suggests that MRX/Tel1 promotes Cdc13-Est1 interaction rather than Cdc13 association to telomeres.

As Xrn1 was found to promote MRX association at intrachromosomal DSBs (Manfrini *et al.*, 2015), we asked whether the expression of a Cdc13-Est1 fusion could restore telomere length in *xrn1Δ* cells. A Cdc13-Est1 fusion expressed from a single-copy plasmid did not suppress the telomere length defect of *xrn1Δ* cells, although it was capable to elongate telomeres in wild type, *mre11Δ* and *tel1Δ* cells (Figure 23E) and all cell cultures expressed similar levels of *CDC13-EST1* mRNA (Figure 23F). This finding suggests that the telomere length defect of *xrn1Δ* cells is not due to MRX dysfunction.

The inability of the Cdc13-Est1 fusion protein to suppress the telomere length defect of *xrn1Δ* cells raises the possibility that Cdc13 itself cannot bind telomeres in the absence of Xrn1. As loss of telomerase is

known to be accompanied by recruitment of Cdc13 and Mre11 to telomeres (Khadaroo *et al.*, 2009), we analyzed the generation of Cdc13 and Mre11 foci before or after loss of telomerase in wild type and *xrn1Δ* cells. These cells expressed fully functional Cdc13-CFP (Cyan Fluorescent Protein) and Mre11-YFP (Yellow Fluorescent Protein) fusion proteins. As expected, telomerase removal by loss of a plasmid-borne copy of *EST2* resulted in a significant increase of both Mre11-YFP and Cdc13-CFP foci in wild type cells as early as 25-50 generations after loss of telomerase, with a subset of them colocalizing (Figure 25A-C). By contrast, *xrn1Δ* cells showed a reduction in the number of Cdc13-CFP foci (Figure 25A and B), but not of Mre11-YFP foci (Figure 25A and C), compared to wild type, suggesting a requirement for Xrn1 in promoting Cdc13 association to telomeres.

To investigate further this hypothesis, we analyzed the amount of Cdc13 bound at native telomeres in wild type and *xrn1Δ* cells that were released into a synchronous cell cycle from a G1 arrest (Figure 26A). Cdc13 binding to telomeres peaked in wild type cells 45 minutes after release, concomitantly with the completion of DNA replication, while it remained very low in *xrn1Δ* cells throughout the time course (Figure 26A and B), although both cell type extracts contained similar amount of Cdc13 (Figure 26C).

Because Cdc13 binds telomeric ssDNA and the lack of Xrn1 impairs ssDNA generation at uncapped telomeres, the reduced Cdc13 association at telomeres in *xrn1Δ* cells might be due to defective generation of telomeric single-stranded overhangs. To investigate this issue, XhoI-cut DNA prepared at different time points after release into

the cell cycle from a G1 arrest was subjected to native gel electrophoresis, followed by in-gel hybridization with a C-rich radiolabeled oligonucleotide. As shown in Figure 26D, both wild type and *xrn1Δ* cells showed similar amount of G-tail signals that reached their maximal levels 15-45 minutes after release, indicating that the lack of Xrn1 does not affect the generation of single-stranded overhangs at capped telomeres.

As generation of telomeric single-stranded overhangs requires the MRX complex (Diede and Gottschling, 2001; Larrivée *et al.*, 2004; Bonetti *et al.*, 2009; Chai *et al.*, 2006), we also analyzed Mre11 association at native telomeres. Wild type and *xrn1Δ* cells released into a synchronous cell cycle from a G1 arrest showed similar amount of telomere-bound Mre11 (Figure 26E), consistent with the finding that the lack of Xrn1 does not affect the generation of telomeric single-stranded overhangs. Altogether, these data indicate that Xrn1 promotes Cdc13 binding/association to telomeres independently of ssDNA generation.

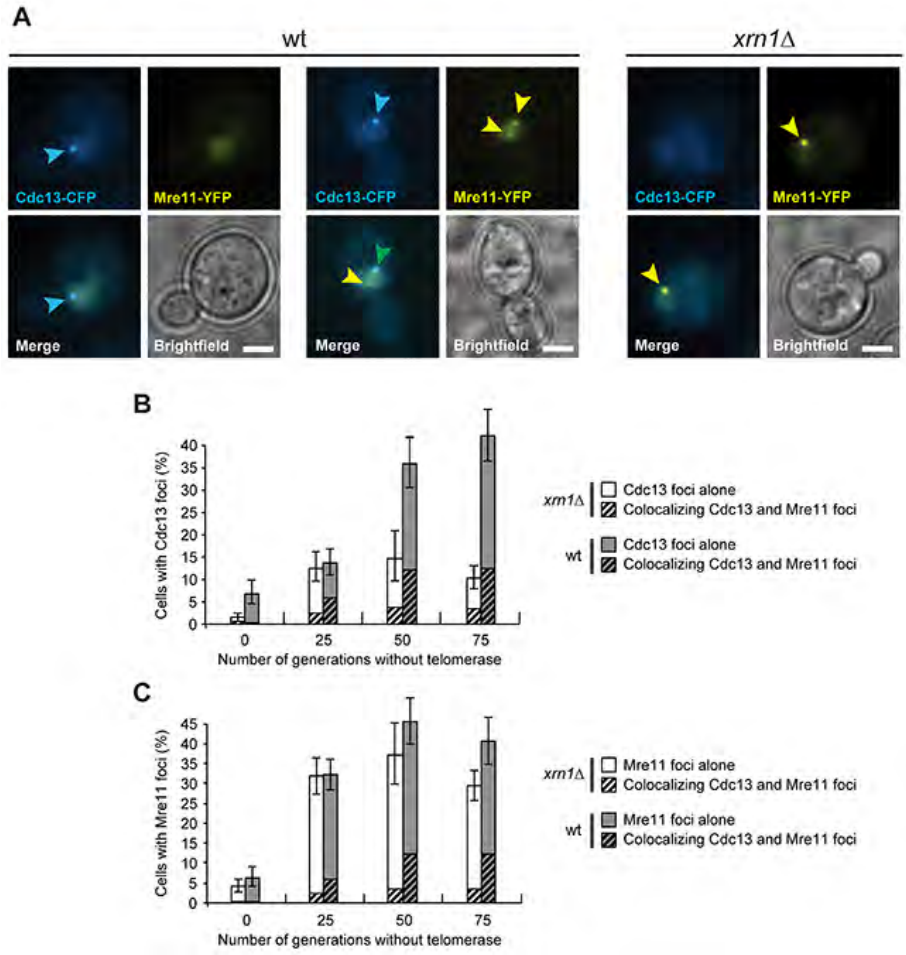

Figure 25. The lack of Xrn1 impairs Cdc13 focus formation. A) Cdc13 and Mre11 localization was examined in *XRN1* (ML968-1D) and *xrn1Δ* (ML968-3B) cells before or 25, 50 and 75 generations after loss of a telomerase-encoding plasmid (pVL291). Yellow arrowheads indicate Mre11-YFP foci, blue arrowheads indicate Cdc13-CFP foci and green arrowhead indicates colocalization between the two proteins. Scale bar: 3 µm. B) *xrn1Δ* cells are impaired for Cdc13 focus formation. Cells in panel (A) were quantified. Error bars represent 95% confidence intervals (n=200-600). C) *xrn1Δ* cells are proficient for Mre11 focus formation. Cells in panel (A) were quantified. Error bars represent 95% confidence intervals (n=200-600).

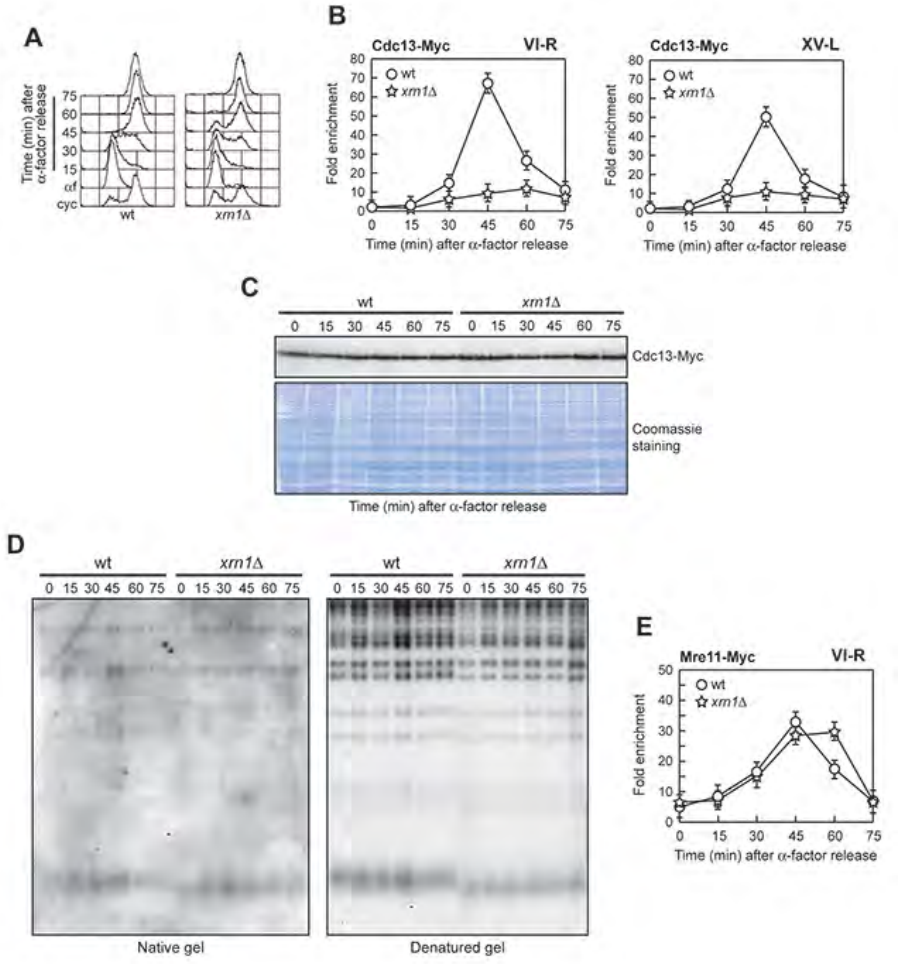

Figure 26. The lack of Xrn1 impairs Cdc13 association but not ssDNA generation at capped telomeres. A)-D) Exponentially growing cell cultures (cyc) were arrested in G1 with α-factor (αf) and released into the cell cycle. A) Samples were collected for fluorescence activated cell sorting (FACS). B) Chromatin samples taken at the indicated times after α-factor release were immunoprecipitated with an anti-Myc antibody. Coimmunoprecipitated DNA was analyzed by quantitative real-time PCR (qPCR) using primer pairs located at telomeres VI-R (right) and XV-L (left) and at the nontelomeric *ARO1* fragment of chromosome IV (CON). Data are expressed as relative fold enrichment of VI-R and XV-L telomere signals over CON signals after normalization to input signals for each primer set. The mean values ±SD. are represented (n=3). C) Western blot with anti-Myc antibodies of extracts used for the ChIP analysis shown in (B). D) Genomic DNA prepared from cell samples in (A) was

digested with XhoI and the single-strand telomere overhang was visualized by in-gel hybridization (native gel) using an end-labeled C-rich oligonucleotide. The same DNA samples were hybridized with a radiolabeled poly(GT) probe as loading control (denatured gel). E) Chromatin samples taken at the indicated times after α-factor release were immunoprecipitated with an anti-Myc antibody. Coimmunoprecipitated DNA was analyzed by qPCR using primer pairs located at VI-R telomere. Data are expressed as in (B).

Xrn1 promotes Cdc13 association at telomeres by downregulating Rif1 level

Deep transcriptome analysis showed that the *RIF1* mRNA level was ~3-fold higher in *xrn1Δ* cells than in wild type (Manfrini *et al.*, 2015). This mRNA upregulation caused an increase of the Rif1 protein level, as shown by Western blot analysis of wild type and *xrn1Δ* protein extracts (Figure 27A), prompting us to test whether this Rif1 upregulation can account for the telomere defects of *xrn1Δ* cells.

As expected from previous findings that Rif1 has a very slight effect on the generation of telomeric ssDNA (Bonetti *et al.*, 2010; Ribeyre and Shore, 2012), the increased Rif1 levels did not account for the increased temperature resistance of *cdc13-1 xrn1Δ* cells compared to *cdc13-1*. In fact, although *RIF1* deletion decreased the maximum permissive temperature of *cdc13-1* cells (Anbalagan *et al.*, 2011; Xue *et al.*, 2011), *cdc13-1 rif1Δ xrn1Δ* cells were more temperature-resistant than *cdc13-1 rif1*Δ cells (Figure 27B), indicating that the suppression of the temperature sensitivity of *cdc13-1* cells by *XRN1* deletion does not require Rif1.

Rif1 was originally identified as a telomere-binding protein that negatively regulates telomerase-mediated telomere elongation (Hardy *et al.*, 1992). Interestingly, the lack of Rif1, although causing a very slight increase of ssDNA formation, yet leads to considerably more Cdc13 binding at telomeres (Ribeyre and Shore, 2012). Therefore, Rif1 might block the association/accumulation of Cdc13 at telomeres through a direct mechanism. Consistent with this hypothesis, a 2µ plasmid carrying the *RIF1* gene counteracted the

ability of the Cdc13-Est1 fusion to elongate telomeres in wild type cells (Figure 27C). Thus, we investigated whether the upregulation of Rif1 in *xrn1Δ* cells could explain both the reduced Cdc13 binding and the telomere length defect of the same cells. As shown in Figure 27D, deletion of *RIF1* totally suppressed the telomere length defect of *xrn1Δ* cells. Telomere length in *rif1Δ xrn1Δ* cells was the same as in *rif1Δ* cells (Figure 27D), suggesting that Xrn1 acts in telomere length maintenance by counteracting the effects of Rif1.

As telomeres were much longer in *xrn1Δ rif1Δ* cells than in *xrn1Δ* cells, we could not compare the above cell types for Cdc13 association at native telomeres. Thus, we used the strain with the 81 bp TG repeat sequence adjacent to the HO endonuclease cut site (Figure 23A) (Diede and Gottschling, 2001), where HO induction generates an HO-derived telomere whose length is similar in both *xrn1Δ* and *xrn1Δ rif1Δ* cells. As expected (Ribeyre and Shore, 2012), ChIP analysis revealed that the amount of Cdc13 associated to the HO-induced telomere was higher in *rif1Δ* cells than in wild type (Figure 27E). Furthermore, although all cell type extracts contained similar amounts of Cdc13 (Figure 27F), the lack of Rif1 restored Cdc13 association to telomeres in *xrn1Δ* cells. In fact, the amount of Cdc13 bound at the HO-induced telomere in *xrn1Δ rif1Δ* cells was higher than in *xrn1Δ* cells (Figure 27E). Altogether, these findings indicate that Xrn1 promotes Cdc13 association to telomeres by controlling Rif1 levels.

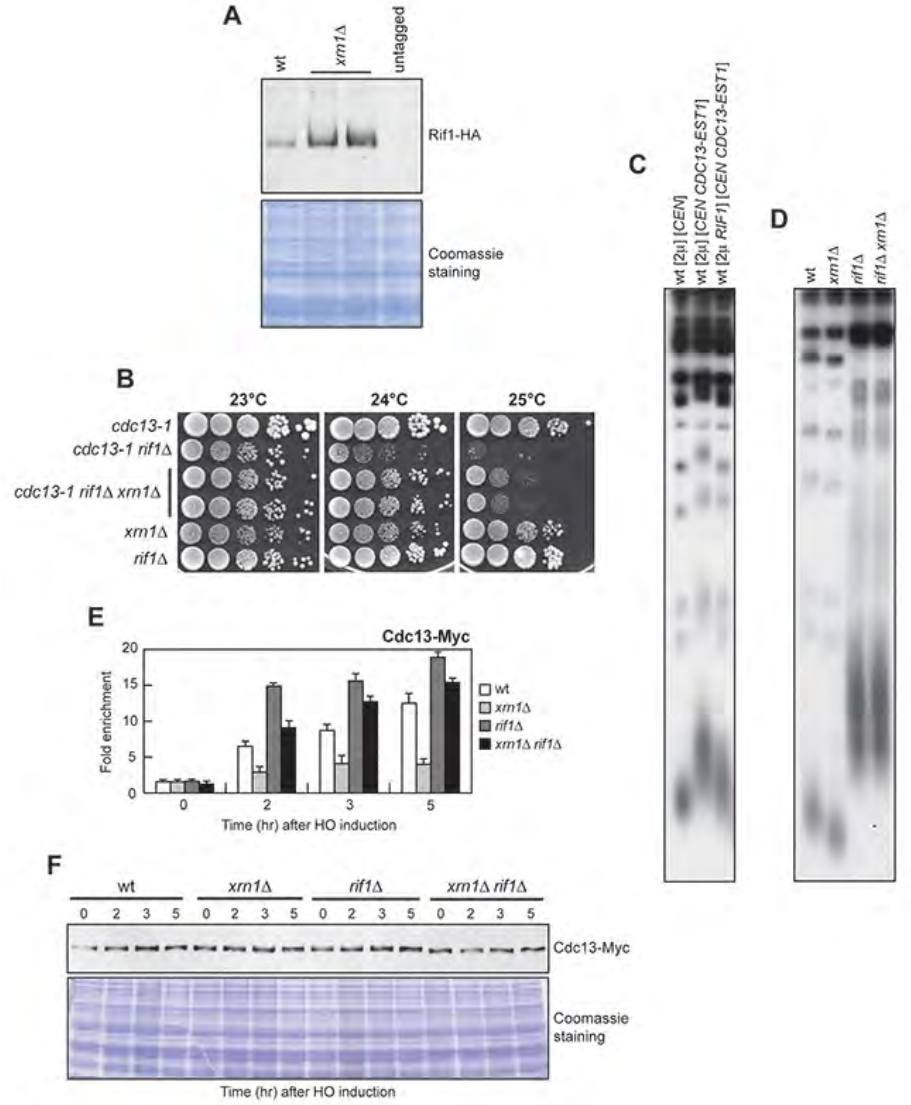

Figure 27. Functional interplays between Xrn1 and Rif1 in telomere length control. A) Protein extracts prepared from cell cultures exponentially growing in YEPD were subjected to western blot analysis with an anti-HA antibody. B) Cell cultures were grown overnight at 23°C in YEPD and 10-fold serial dilutions were spotted onto YEPD plates. C), D) XhoI-cut genomic DNA from exponentially growing cells was subjected to Southern blot analysis using a radiolabeled poly(GT) probe. E) HO expression was induced at time zero by galactose addition to yeast strains carrying the system described in Figure 23A. Chromatin samples taken at the indicated times after HO induction were immunoprecipitated with an anti-Myc antibody and coimmunoprecipitated DNA was analyzed by qPCR using primer pairs located 640 bp

centromere-proximal to the HO cutting site and at the non-telomeric *ARO1* fragment of chromosome IV (CON). Data are expressed as relative fold enrichment of TG-HO over CON signal after normalization to input signals for each primer set. The mean values ±SD are represented (n=3). F) Western blot with anti-Myc antibodies of extracts used for the ChIP analysis shown in (E).

DISCUSSION

DNA double-strand breaks (DSBs) are among the most dangerous types of DNA lesions because failure to repair them can result in genome rearrangements, which lead to the development of many diseases, including cancer. The DNA damage response (DDR) ensures the rapid detection and repair of DSBs in order to maintain genome integrity. Central to the DDR is the DNA damage checkpoint, which is conserved from yeasts to humans. When activated by DNA damage, this sophisticated surveillance mechanism induces transient cell cycle arrests, allowing sufficient time for DNA repair (Finn *et al.*, 2012). The checkpoint response to DSB is regulated by the protein kinases Tel1/ATM and Mec1/ATR. Recruitment of ATR/Mec1 at the DSB sites requires the presence of RPA-coated single-stranded DNA (ssDNA) 3' overhangs, which are generated by nuclease-mediated DSB resection (Gobbini *et al.*, 2013).

Recently, many evidences implicate RNA processing factors in the maintaining of genome stability. However, the precise DNA maintenance mechanisms involving these RNA decay factors remain poorly characterized. In *Saccharomyces cerevisiae*, RNA processing relies on a 5'-3' exoribonuclease activity that is due to the Xrn protein family, which comprises one cytoplasmic (Xrn1) and one nuclear enzyme (Rat1) (Nagarajan *et al.*, 2013). The nuclear exosome, whose activity is modulated by a set of cofactors including the poly(A) polymerase Trf4, is responsible for the 3'-5' RNA processing activity, which depends on the exoribonuclease Rrp6 (Kilchert *et al.*, 2016).

Starting from the evidence that *XRN1*, *RRP6* or *TRF4* deletion causes hypersensitivity to the DSB-inducing agent phleomycin in yeast cells,

in the first part of the thesis I have contributed to define the roles of RNA processing factors in the cellular response to DSBs (Manfrini N, Trovesi C, Wery M, Martina M, Cesena D, Descrimes M, Morillon A, d'Adda di Fagagna F, Longhese MP. RNA-processing proteins regulate Mec1/ATR activation by promoting generation of RPA-coated ssDNA. EMBO Rep., 2015). We show that Xrn1, Rrp6 and Trf4 proteins regulate Mec1 signaling activity by promoting the formation of RPA-coated ssDNA at the DSB ends, thus linking RNA processing to the checkpoint response. While Xrn1 is required to generate ssDNA by promoting MRX recruitment to the DSB, Rrp6 and Trf4 are required to recruit RPA, and therefore Mec1/ATR, to the ssDNA ends. Although the amount of RPA recruited at the DSB in *rrp6Δ* and *trf4Δ* cells appears to be below the threshold necessary for full checkpoint activation, it is enough for Rad51 and Rad52 loading to the DSB and for subsequent homologous recombination (HR) repair. Indeed, DSB repair by HR has been shown to require limited amount of ssDNA at the DSB ends (Jinks-Robertson *et al.*, 1993; Ira and Haber, 2002). This finding suggests that full Mec1 activation requires a higher amount of RPA-coated ssDNA than HR-mediated repair events, thus ensuring checkpoint activation only when the DSB cannot be rapidly repaired. How Rrp6 and Trf4 control the association of RPA with ssDNA requires further studies. One possibility is that the lack of Rrp6 or Trf4 increases the persistence around the DSB site of RNA molecules that can inhibit RPA recruitment by annealing with the ssDNA generated during DSB resection. However, overproduction of the Ribonuclease H1 Rnh1, which is known to decrease endogenous RNA:DNA hybrids *in vivo* (Gavaldá *et*

al., 2013), did not restore either Rad53 phosphorylation or RPA association to the DSB (data not shown) in *rrp6Δ* and *trf4Δ* cells. As RPA binds to ssDNA in two conformational states that differ both in affinity of the bound DNA and in the length of the contacted ssDNA (Fanning *et al.*, 2006), we favor the hypothesis that Rrp6 and Trf4 may modulate directly or indirectly these RPA conformational changes, and therefore RPA ability to bind ssDNA.

Since the eukaryotic chromosomes are linear DNA molecules with physical ends, cells need to distinguish them from intrachromosomal DSBs, thus preventing their repair that leads to chromosome fusion and genome instability. In order to accomplish this task, eukaryotic cells protect the chromosomes termini with particular structures called telomeres. Telomeres are nucleoprotein complexes that protect the natural ends of chromosomes from fusion and degradation and prevent them from eliciting a checkpoint response. Telomeric DNA consists of tandemly repeated G-rich sequences that terminate with a 3' single-stranded overhang (G-tail), which is important for telomere extension by the telomerase enzyme (Bonetti *et al.*, 2014). The protective function of telomeres, which is referred to as telomere capping, is largely mediated by telomere-binding proteins that suppress checkpoint activation and DNA repair activities. In particular, in yeast the CST (Cdc13-Stn1-Ten1) complex binds to the single-stranded G-tail, while the shelterin-like (composed of Rap1-Rif2-Rif1) complex binds to double-stranded telomeric DNA. These complexes are conserved from yeast to humans (Wellinger and Zakian, 2012). Telomere dysfunction through progressive shortening or removal of

capping proteins leads to a checkpoint-mediated block of cell proliferation, which acts as a cancer-suppressor mechanism (Gobbini *et al.*, 2014).

Emerging evidence indicates that RNA processing factors play critical, yet poorly understood, roles in telomere metabolism. Thus, in the second part of the thesis, I have investigated the roles of the RNA processing proteins Xrn1 and Rrp6 in telomere metabolism (Cesena D, Cassani C, Rizzo E, Lisby M, Bonetti D, Longhese MP. Regulation of telomere metabolism by the RNA processing protein Xrn1. Nucleic Acids Res., 2017). We found that the temperature sensitivity of *cdc13-1* mutant cells is partially suppressed by the lack of Rrp6 or Xrn1, as well as by Rrp6 or Xrn1 nuclease defective variants, independently of the NMD proteins. The increased temperature resistance of *cdc13-1 xrn1Δ* and *cdc13-1 rrp6Δ* cells is related to their inability to activate the checkpoint.

Checkpoint activation in *cdc13-1* cells is due to the accumulation at telomeres of ssDNA that turns on the checkpoint kinase Mec1. Our data indicate that the defective checkpoint response in *cdc13-1 rrp6Δ* double mutant cells cannot be ascribed to reduced ssDNA generation. Since we have shown that Rrp6 promotes the association of RPA at intrachromosomal DSBs, one possibility is that Rrp6 modulates directly or indirectly the association to telomeric ssDNA of protein(s) required for checkpoint activation. Alternatively, the lack of Rrp6 can lead to the generation of G-quadruplex structures at the telomeric ssDNA that impairs checkpoint activation and restore *cdc13-1* cells viability at restrictive temperature (Smith *et al.*, 2011). These structures could be

formed at the displaced DNA strand of an R-loop (Hamperl and Cimprich, 2014) located at telomeric ends in *rrp6Δ* cells, which are known to accumulate R-loops (Luna *et al.*, 2005; Gavaldá *et al.*, 2013; Wahba *et al.*, 2013). However, overproduction of the Ribonuclease H1 (Rnh1), which decreases R-loops at telomeres (Balk *et al.*, 2013), did not restore the temperature sensitivity in *cdc13-1 rrp6Δ* cells (data not shown). Nevertheless, short nucleotide sequences that form a structure comprising a G-quartet are able to inhibit eukaryotic ribonuclease H (Pileur *et al.*, 2003), suggesting that G-quadruplex structures can inhibit both checkpoint activation and degradation of the telomeric RNA:DNA hybrids in *cdc13-1 rrp6Δ* background. Thus, Rrp6 would be required to remove R-loops at telomeres in a context where Rnh1 could not exert its function for the persistence of G-quartet. Noteworthy, in human cells, the exosome is recruited at R-loops by interaction with the R-loop-associated helicase senataxin (SETX) and mutations which disrupt this interaction cause *ataxia with oculomotor apraxia 2* (AOA2), a disease associated with defects in the checkpoint response (Richard *et al.*, 2013).

By contrast and consistent with the finding that Xrn1 and Rrp6 impairs viability of *cdc13-1* cells by acting in two distinct pathways, the lack of Xrn1 reduces the generation of telomeric ssDNA upon telomere uncapping, like it does at intrachromosomal DSBs. This observation, together with the finding that *EXO1* overexpression decreases the maximum permissive temperature of *cdc13-1 xrn1Δ* cells, indicates that Xrn1 participates in checkpoint activation in response to telomere uncapping by promoting the generation of telomeric ssDNA. By

contrast, Xrn1 does not contribute to the generation of single-stranded overhangs at capped telomeres. This observation, together with our finding that Xrn1 promotes ssDNA generation also at intrachromosomal DSBs that are subjected to extensive resection and stimulates Mec1-dependent checkpoint activation similarly to telomeres following Cdc13 inactivation, suggests a role for Xrn1 in promoting resection specifically at DNA ends that elicit a DNA damage response.

Because Xrn1 acts in resection as a cytoplasmic nuclease, one possibility is that the lack of Xrn1 increases the persistence of non-coding RNAs that can inhibit the action of nucleases by annealing with the ssDNA molecules that are generated following telomere uncapping. However, overproduction of the Ribonuclease H1 (Rnh1), which decreases endogenous RNA:DNA hybrids *in vivo* as well as TERRA levels and R-loops at telomeres (Balk *et al.*, 2013; Gavaldá *et al.*, 2013; Arora *et al.*, 2014; Yu *et al.*, 2014), did not restore the temperature sensitivity in *cdc13-1 xrn1Δ* cells (data not shown). The deep transcriptome analysis has revealed that the amounts of the majority of mRNAs coding for DNA damage response proteins remained unchanged in *xrn1Δ* cells and the few genes that were misregulated are not obvious candidates. Therefore, further work will be required to identify the target(s) by which Xrn1 promotes ssDNA generation and checkpoint activation at uncapped telomeres.

We also show that Xrn1 acts as a cytoplasmic nuclease to maintain telomere length. Strikingly, the lack of Xrn1 dramatically reduces Cdc13 association to telomeres. This defective Cdc13 recruitment is

not due to reduced ssDNA generation, as the lack of Xrn1 does not impair ssDNA generation at capped telomeres. On the other hand, the lack of Xrn1 causes upregulation of the *RIF1* mRNA and subsequent increase of the Rif1 protein level. Rif1 was shown to decrease Cdc13 association at telomeres independently of ssDNA generation (Ribeyre and Shore, 2012), suggesting that the high Rif1 levels in *xrn1Δ* cells might explain the reduced Cdc13 binding and the telomere length defect of the same cells. Consistent with this hypothesis, we found that the lack of Rif1 completely suppresses the telomere length defect and restores Cdc13 association at telomeres in *xrn1Δ* cells. Altogether, these findings indicate that Xrn1 promotes Cdc13 association to telomeres and telomere elongation independently of ssDNA generation by controlling the amount of Rif1. By contrast, Rif1 is not the Xrn1 target in promoting ssDNA generation and checkpoint activation at uncapped telomeres, as the lack of Xrn1 still suppresses the temperature sensitivity of *cdc13-1 rif1Δ* cells. In conclusion, Xrn1 appears to have two separate functions at telomeres: (i) it facilitates the generation of ssDNA and checkpoint activation at uncapped telomeres; (ii) it maintains telomere length independently of ssDNA generation by downregulating the amount of Rif1, which in turn counteracts Cdc13 association to telomeres.

As RNA processing factors are evolutionarily conserved and telomere protection is critical for preserving genetic stability and counteracting cancer development, our findings highlight novel mechanisms through which RNA processing proteins can preserve genome integrity.

MATERIALS AND METHODS

Yeast and bacterial strains

Yeast strains and plasmids

The yeast strains used in this study are derivatives of JKM139, YFP17, tGI354, W303 and UCC5913 and are listed in Table 1. Strains JKM139, YFP17 and tGI354 were kindly provided by J. Haber (Brandeis University, Waltham, USA). Strains used for monitoring telomere addition were derivatives of strain UCC5913, kindly provided by D. Gottschling (Fred Hutchinson Cancer Research Center, Seattle, USA). Strains ML968-1D and ML968-3B are derivatives of ML8-9A, a *RAD5 ADE2* derivative of W303 (*MAT***a** *LYS2 ade2-1 can1-100 ura3-1 his3-11, 15 leu2-3, 112 trp1-1 rad5-535*). A plasmid carrying the *GAL1-RNH1* allele and the control vector plasmid *pGAL1* were kindly provided by A. Aguilera (University of Seville, Sevilla, Spain). Plasmid pAM140/pAJ228 (*CEN LEU2 rat1-ΔNLS*) was previously described (Johnson, 1997). Plasmids pAM144 (*CEN LEU2 xrn1-E176G*) and pAM145/pAJ37 (*CEN LEU2 XRN1*) were kindly provided by A.W. Johnson (University of Texas, Austin, USA). Plasmid pGFPRRP6H1 (*CEN6 URA3 pGFP-rrp6-D238A*) was kindly provided by J.S. Butler (University of Rochester Medical Center, Rochester, USA). Plasmid pTRP61 (2μ *TRP1 GAL1-TLC1*) was kindly provided by R. Wellinger (Université de Sherbrooke, Québec, Canada). Plasmid pVL1091 (*CEN LEU2 CDC13-EST1*) was kindly provided by V. Lundblad (Salk Institute, La Jolla, USA). All gene disruptions were carried out by PCR-based methods. The accuracy of all gene replacements and integrations was verified by Southern blot analysis or PCR. Strains expressing fully functional tagged protein alleles were constructed by one-step PCR.

Cells were grown in YEP medium (1% yeast extract, 2% bactopeptone, 50 mg/l adenine) supplemented with 2% glucose (YEPD) or 2% raffinose (YEPR) or 2% raffinose and 2% galactose (YEPRG).

***E. coli* strain**

E. coli DH5α™ strain (*F-, φ80 dlacZM15, D(lacZTA-argF) U169, deoR, recA1, endA1, hsdR17, (rK-,mK+) phoA supE44, λ−, thi-1, gyrA96, relA1*) was used as bacterial host for plasmid manipulation and amplification. *E. coli* DH5α™ competent cells to transformation were purchased from Invitrogen.

Strain	Relevant genotype	Source
JKM139	*MAT*a *hmlΔ*::*ADE1, hmrΔ::ADE1*, *ade1-100, lys5, leu2-3,112, trp1::hisG ura3-52, ho, ade3::GAL::HO*	Lee *et al.*, 1998
YLL3305.8	JKM139 *trf4Δ::NATMX*	This study
YLL3287.5	JKM139 *rrp6Δ::NATMX*	This study
YLL3288.11	JKM139 *xrn1Δ::KANMX4*	This study
YLL3012.1	JKM139 *DDC2-3HA*::*URA3*	This study
DMP5786/1B	JKM139 *DDC2-3HA*::*URA3 xrn1Δ::KANMX4*	This study
DMP5785/1A	JKM139 *DDC2-3HA*::*URA3 rrp6Δ::NATMX*	This study
DMP5796/1B	JKM139 *DDC2-3HA*::*URA3 trf4Δ::NATMX*	This study
YLL1769.1	JKM139 *mre11Δ::NATMX*	This study
DMP5921/1A	JKM139 *mre11Δ::NATMX xrn1Δ::KANMX4*	This study
YLL1854.2	JKM139 *MRE11-18MYC::TRP1*	This study
DMP5922/3B	JKM139 *MRE11-18MYC::TRP1 xrn1Δ::KANMX4*	This study
YLL1959.2	JKM139 *EXO1-18MYC::TRP1*	This study
DMP5946/2B	JKM139 *EXO1-18MYC::TRP1 xrn1Δ::KANMX4*	This study
DMP6097/1A	JKM139 *MRE11-18MYC::TRP1 XRS2-3HA::URA3*	This study
DMP6097/3C	JKM139 *MRE11-18MYC::TRP1 XRS2-3HA::URA3 xrn1Δ::KANMX4*	This study
YLL3187.1	JKM139 *XRS2-3HA::URA3*	This study
DMP6098/4A	JKM139 *MRE11-18MYC::TRP1 RAD50-3HA::URA3*	This study
DMP6098/9C	JKM139 *MRE11-18MYC::TRP1 RAD50-3HA::URA3 xrn1Δ::KANMX4*	This study
DMP6024/2A	JKM139 *RAD50-3HA::URA3*	This study
YLL3096.8	JKM139 *MEC1-9MYC::TRP1*	This study
DMP5771/7B	JKM139 *MEC1-9MYC::TRP1 rrp6Δ::NATMX*	This study
DMP5794/4C	JKM139 *MEC1-9MYC::TRP1 trf4Δ::NATMX*	This study
YLL3526.20	JKM139 *RFA3-3HA::TRP1*	This study
DMP5993/2A	JKM139 *RFA3-3HA::TRP1 rrp6Δ::NATMX*	This study

DMP5995/7D	JKM139 *RFA3-3HA::TRP1 trf4Δ::NATMX*	This study
DMP5961/3B	JKM139 *rad51Δ::HPHMX rrp6Δ::NATMX*	This study
DMP5962/10C	JKM139 *rad51Δ::HPHMX trf4Δ::NATMX*	This study
DMP5979/1D	JKM139 *rad52Δ::TRP1 rrp6Δ::NATMX*	This study
DMP5978/11A	JKM139 *rad52Δ::TRP1 trf4Δ::NATMX*	This study
YLL3495.71	JKM139 *RAD52-3HA::TRP1*	This study
DMP5966/5A	JKM139 *RAD52-3HA::TRP1 rrp6Δ::NATMX*	This study
DMP5965/10C	JKM139 *RAD52-3HA::TRP1 trf4Δ::NATMX*	This study
DMP5986/1B	JKM139 *XRS2-3HA::URA3 xrn1Δ::KANMX4*	This study
DMP6024/2D	JKM139 *RAD50-3HA::URA3 xrn1Δ::KANMX4*	This study
DMP5923/6A	JKM139 *DNA2-18MYC::TRP1*	This study
DMP5923/1C	JKM139 *DNA2-18MYC::TRP1 xrn1Δ::KANMX4*	This study
DMP6023/5A	JKM139 *SGS1-3HA::URA3*	This study
DMP6023/3C	JKM139 *SGS1-3HA::URA3 xrn1Δ::KANMX4*	This study
DMP5767/2A	JKM139 *MEC1-9MYC::TRP1 xrn1Δ::KANMX4*	This study
DMP5820/8B	JKM139 *RIF1-3HA::URA*	This study
DMP6077/3A	JKM139 *RIF1-3HA::URA xrn1Δ::KANMX*	This study
YFP17	*mataΔ::hisG hmlΔ::ADE1 hmrΔ::ADE1 ho ade3::GAL::HO leu2::HO site ura3-52*	Pâques *et al.*, 1998
YLL3419.1	YFP17 *xrn1Δ::KANMX4*	This study
YLL3418.2	YFP17 *rrp6Δ::NATMX*	This study
YLL3420.119	YFP17 *trf4Δ::NATMX*	This study
YLL3565.2	YFP17 *leu2prΔ::URA3*	This study
YLL3566.6	YFP17 *xrn1Δ::KANMX4 leu2prΔ::URA3*	This study
YLL3567.1	YFP17 *rrp6Δ::NATMX leu2prΔ::URA3*	This study
YLL3568.7	YFP17 *trf4Δ::NATMX leu2prΔ::URA3*	This study
tGI354	*ho hmlΔ::ADE1 MATa-inc hmrΔ::ADE1 ade1 leu2-3,112 lys5 trp1::hisG ura3-52 ade3::GAL::HO*	Saponaro *et al.*, 2010

	arg5,6::MATa::HPHMX	
YLL3437.11	tGI354 *rrp6Δ::NATMX*	This study
YLL3432.103	tGI354 *xrn1Δ::KANMX4*	This study
W303	*MATa/α ade2-1 can1-100 his3-11,15 leu2-3,112 trp1-1 ura3-1 rad5-535*	
YLL3334.8	W303 *rrp6Δ::NATMX*	This study
DMP2045/4A	W303 *cdc13-1*	This study
DMP5899/10D	W303 *cdc13-1 xrn1Δ::KANMX*	This study
DMP5897/9B	W303 *cdc13-1 rrp6Δ::NATMX*	This study
DMP6525/2B	W303 *cdc13-1 xrn1Δ::KANMX rrp6Δ::NATMX*	This study
DMP6508/3B	W303 *xrn1Δ::KANMX rrp6Δ::NATMX*	This study
DMP4523/89	W303 *TEN1-18MYC::HIS3*	This study
DMP5912/3A	W303 *TEN1-18MYC::HIS3 xrn1Δ::KANMX*	This study
DMP5913/5D	W303 *TEN1-18MYC::HIS3 rrp6Δ::NATMX*	This study
DMP5989/13A	W303 *TEN1-18MYC::HIS3 upf2Δ::KANMX*	This study
DMP6523/17A	W303 *TEN1-18MYC::HIS3 xrn1Δ::KANMX rrp6Δ::NATMX*	This study
YLL2614.7	W303 *STN1-3HA::URA3*	This study
DMP5904/3B	W303 *STN1-3HA::URA3 xrn1Δ::KANMX*	This study
DMP5905/2A	W303 *STN1-3HA::URA3 rrp6Δ::NATMX*	This study
DMP5929/8D	W303 *STN1-3HA::URA3 upf2Δ::KANMX*	This study
DMP6524/3C	W303 *STN1-3HA::URA3 xrn1Δ::KANMX rrp6Δ::NATMX*	This study
YLL3281.1	W303 *cdc13-1 upf2Δ::KANMX*	This study
DMP5916/2C	W303 *cdc13-1 upf2Δ::KANMX rrp6Δ::NATMX*	This study
YLL2804.1	W303 *stn1-ΔC::KANMX*	This study

DMP5998/1B	W303 *stn1-ΔC::KANMX rrp6Δ::NATMX*	This study
DMP6000/7C	W303 *stn1-ΔC::KANMX xrn1Δ::KANMX*	This study
YLL936.3	W303 *mre11Δ::HIS3*	This study
DMP3335/2A	W303 *tel1Δ::HIS3*	This study
ML968-1D	W303 *MRE11-LLAKKRKG-YFP CDC13-CFP est2Δ::LEU2*	This study
ML968-3B	W303 *MRE11-LLAKKRKG-YFP CDC13-CFP est2Δ::LEU2 xrn1Δ::KANMX*	This study
YLL3790.1	W303 *CDC13-18MYC::URA3*	This study
YLL3791.2	W303 *CDC13-18MYC::URA3 xrn1Δ::KANMX*	This study
YLL1139.32	W303 *MRE11-18MYC::TRP1*	This study
DMP6141/21C	W303 *MRE11-18MYC::TRP1 xrn1Δ::KANMX*	This study
DMP5126/5C	W303 *cdc13-1 rif1Δ::HIS3*	This study
DMP6089/15A	W303 *cdc13-1 rif1Δ::HIS3 xrn1Δ::KANMX*	This study
YLL1223.2	W303 *rif1Δ::HIS3*	This study
DMP6089/17B	W303 *rif1Δ::HIS3 xrn1Δ::KANMX*	This study
UCC5913	*MAT*a-*inc ade2-101 lys2-801 his3-Δ200 trp1-Δ63 ura3-52 leu2-Δ1::GAL1-HO-LEU2 VII-L::ADE2-TG(1-3)-HO site-LYS2*	Diede and Gottschling, 2001
YLL3595.2	UCC5913 *xrn1Δ::KANMX*	This study
YLL3794.4	UCC5913 *CDC13-18MYC::URA3*	This study
YLL3795.1	UCC5913 *CDC13-18MYC::URA3 xrn1Δ::KANMX*	This study
YLL3798.1	UCC5913 *CDC13-18MYC::URA3 xrn1Δ::KANMX rif1Δ::NATMX bar1Δ::HPHMX*	This study
YLL3797.1	UCC5913 *CDC13-18MYC::URA3 rif1Δ::NATMX bar1Δ::HPHMX*	This study

Table 3. *Saccharomyces cerevisiae* strains used in this study.

Growth media

S. cerevisiae media

YEP (Yeast-Extract Peptone) is the standard rich media for *S. cerevisiae* and contains 10 g/L yeast extract, 20 g/L peptone and 50 mg/L adenine. YEP must be supplemented with 2% glucose (YEPD), 2% raffinose (YEP+raf) or 2% raffinose and 2% galactose (YEP+raf+gal) as carbon source. YEP-based selective media are obtained including 400 µg/mL G418, 300 µg/mL hygromicin-B or 100 µg/mL nourseotricin. Solid media are obtained including 2% agar. Stock solutions are 50% glucose, 30% raffinose, 30% galactose, 80 mg/mL G418, 50 mg/mL hygromicin-B and 50 mg/mL nourseotricin. YEP and glucose stock solution are autoclave-sterilized and stored at RT. Sugars and antibiotics stock solutions are sterilized by microfiltration and stored at RT and 4°C respectively.

S.C. (Synthetic Complete) is the minimal growth media for *S. cerevisiae* and contains 1.7 g/L YNB (Yeast Nitrogen Base) without amino acids, 5 g/L ammonium sulphate, 200µM inositol, 25 mg/L uracil, 25 mg/L adenine, 25 mg/L hystidine, 25 mg/L leucine, 25 mg/L tryptophan. S.C. can be supplemented with drop-out solution (20 mg/L arginine, 60 mg/L isoleucine, 40 mg/L lysine, 10 mg/L methionine, 60 mg/L phenylalanine, 50 mg/L tyrosine) based on yeast strains requirements. Different carbon sources can be used in rich media (2% glucose, 2% raffinose or 2% raffinose and 3% galactose). One or more amino acid/base can be omitted to have S.C.-based selective media (e.g. S.C.-ura is S.C. lacking uracil). To obtain G418 or NAT S.C. selective medium the 5 g/L ammonium sulphate are replaced with 1 g/L monosodic

glutamic acid. Solid media are obtained by including 2% agar. Stock solutions are 17 g/L YNB + 50 g/L ammonium sulphate (or 10g/L monosodic glutamic acid), 5 g/L uracil, 5 g/L adenine, 5 g/L hystidine, 5 g/L leucine, 5 g/L tryptophan, 100X drop out solution (2 g/L arginine, 6 g/L isoleucine, 4 g/L lysine, 1 g/L methionine, 6 g/L phenylalanine, 5 g/L tyrosine), 20mM inositol. All of these solutions are sterilized by micro-filtration and stored at 4°C.

VB sporulation medium contains 13.6 g/L sodium acetate, 1.9 g/L KCl, 0.35 g/L MgSO4, 1.2 g/L NaCl. pH is adjusted to 7.0. To obtain solid medium include 2% agar. pH is adjusted to 7.0. Sterilization by autoclavation.

***E. coli* media**

LD is the standard growth medium for *E. coli.* LD medium contains 10 g/L tryptone, 5 g/L yeast extract and 5 g/L NaCl. Solid medium is obtained by including 1% agar. LD+Amp selective medium is obtained including 50 µg/mL Ampicillin. LD is autoclave-sterilized and stored at RT. Ampicillin stock solution (2.5 g/L) is sterilized by micro-filtration and stored at 4°C.

Conservation and storage of *S. cerevisiae* and *E. coli* strains

Yeast cells are grown 2-3 days at 30°C on YEPD plates, resuspended in 15% glycerol and stored at -80°C. Bacteria are grown o/n at 37°C on LD+Amp plates, resuspended in 50% glycerol and stored at -80°C. Yeast and bacteria cells can be stored for years in these conditions.

Molecular biology techniques

Agarose gel electrophoresis

Agarose gel elctrophoresis is the easiest and common way of separating and analyzing DNA molecules. This technique allows the separation of DNA fragments based on their different molecular weight (or length in kb). The purpose of this technique might be to visualize the DNA, to quantify it or to isolate a particular DNA fragment. The DNA is visualized by the addition in the gel of ethidium bromide, which is a fluorescent dye that intercalates between bases of nucleic acids. Ethidium bromide absorbs UV light and transmits the energy as visible orange light, revealing the DNA molecules to which is bound.

To pour a gel, agarose powder is mixed with TAE (0.04M TrisAcetate 0.001M EDTA) to the desired concentration, and the solution is microwaved until completely melted. Most gels are made between 0.8% and 2% agarose. A 0.8% gel will show good resolution of large DNA fragments (5-10 Kb) and a 2% gel will show good resolution for small fragments (0.2-1 Kb). Ethidium bromide is added to the gel at a final concentration of 1 μg/mL to facilitate visualization of DNA after electrophoresis. After cooling the solution to about 60°C, it is poured into a casting tray containing a sample comb and allowed to solidify at RT or at 4°C. The comb is then removed and the gel is placed into an electrophoresis chamber and just covered with the buffer (TAE). Sample containing DNA mixed with loading buffer are then pipetted into the sample wells. The loading buffer contains 0.05% bromophenol blue and 5% glycerol, which give color and density to the sample. A

marker containing DNA fragments of known length and concentration is loaded in parallel to determine size and quantity of DNA fragments in the samples. Then current is applied and DNA will migrate toward the positive electrode. When adequate migration has occurred, DNA fragments are visualized by placing the gel on a UV trans illuminator.

DNA extraction from agarose gels (paper strip method)

This method allows to isolate a DNA fragment of interest. Using a scalpel blade cut a slit immediately in front of the band to be extracted. Cut a piece of GF-C filter to size to fit inside the slit. Place the paper strip in the slit and switch on the current for 1-2 minutes at 150 V. The DNA runs onward into the paper and is delayed in the smaller mesh size of the paper. Remove the strip of paper and place it into a 0.5 mL micro centrifuge tube. Make a tiny hole in the bottom of the tube using a syringe needle, place the 0.5 mL tube inside a 1.5 mL tube and spin for 30 seconds. Buffer and DNA are retained in the 1.5 mL tube. Extract the DNA with 1 volume of phenol/chloroform and precipitate the DNA with 100mM sodium acetate and 3 volumes of 100% ethanol. After micro centrifugation re-dissolve DNA in an appropriate volume of water, TRIS (10mM Tris HCl pH 8.5) or TE (10mM Tris HCl, 1mM EDTA pH7.4) buffer.

Restriction endonucleases

Type II endonucleases (also known as restriction endonucleases or restriction enzymes) cut DNA molecules at defined positions close to their recognitions sequences in a reaction known as enzymatic

digestion. They produce discrete DNA fragments that can be separated by agarose gel electrophoresis, generating distinct gel banding patterns. For these reasons they are used for DNA analysis and gene cloning. Restriction enzymes are generally stored at -20°C in a solution containing 50% glycerol, in which they are stable but not active. Glycerol concentration in the reaction mixture must be below 5% in order to allow enzymatic reaction to occur. They generally work at 37°C with some exceptions (e.g. ApaI activity is maximal at 25°C) and they must be supplemented with a reaction buffer provided by the manufacturer, and in some cases with Bovin Serum Albumin. We use restriction endonucleases purchased from NEB and PROMEGA.

Ligation

DNA is previously purified from agarose gel with the paper strip method, phenol/chloroform extracted, ethanol precipitated and resuspended in the appropriate volume of water or TE buffer. The ligation reaction is performed in the following conditions: DNA fragment and vector are incubated overnight at 16°C with 1 µl T4 DNA Ligase (PROMEGA) and T4 DNA Ligase Buffer (PROMEGA).

The ligation reaction is then used to transform competent *E. coli* cells. Plasmids are recovered from Amp+ transformants and subjected to restriction analysis.

Polymerase Chain Reaction (PCR)

PCR allows to obtain high copy number of a specific DNA fragment of interest starting from very low quantity of DNA fragment. The reaction

is directed to a specific DNA fragment by using a couple of oligonucleotides flanking the DNA sequence of interest. These oligonucleotides work as primers for the DNA polymerase. The reaction consists of a number of polymerization cycles which are based on 3 main temperature-dependent steps: denaturation of DNA (which occur over 90°C), primer annealing to DNA (typically take place at 45-55°C depending on primer characteristic), synthesis of the DNA sequence of interest by a thermophilic DNA polymerase (which usually works at 68 or 72°C). Different polymerases with different properties (processivity, fidelity, working temperature, etc) are commercially available and suitable for different purpose. Taq polymerase works at 72°C and is generally used for analytical PCR. Polymerases with higher fidelity like Pfx and VENT polymerases, which work respectively at 68 and 72°C, are generally employed when 100% polymerization accuracy is required.

The typical 50 µL PCR mixture contains 1µL of template DNA, 0.5 µM each primer, 200µM dNTPs, 5 µL of 10X Reaction Buffer, 1mM MgCl2, 1-2 U DNA polymerase and water to 50 µL. The typical cycle-program for a reaction is: 1. 2 minutes' denaturation at 94-95°C; 2. 30 seconds denaturation at 94-95°C; 3. 30 seconds annealing at primers Tm (melting temperature); 4. 1 minute polymerization per kb at 68 or 72°C (depending on polymerase); 5. repeat 30 times from step 2; 6. 51-minutes polymerization at 68-72°C. The choice of primer sequences determines the working Tm, which depends on the length (L) and GC% content of the oligonucleotides and can be calculated as follows: Tm = 59.9 + 0.41(GC%) – 675/L.

Preparation of yeast genomic DNA for PCR

Resuspend yeast cells in 200 µL Yeast Lysis Buffer (2% TRITON X100, 1% SDS, 100mM NaCl, 10mM Tris HCl pH 8, 1mM EDTA pH 8), add 200 µL glass beads, 200 µL phenol/chloroform and vortex 3 minutes. Ethanol precipitate the aqueous phase obtained after 5 minutes' centrifugation. Resuspend DNA in the appropriate volume of water and use 1 µL as a template for PCR.

Plasmid DNA extraction from *E. coli* (I): minipreps boiling

E. coli cells (2mL overnight culture) are harvested by centrifugation and resuspended in 500 µL STET buffer (8% sucrose, 5% TRITON X-100, 50mM EDTA, 50mM Tris-HCl, pH 8). Bacterial cell wall is digested boiling the sample for 2 minutes with 1 mg/mL lysozyme. Cellular impurities are removed by centrifugation and DNA is precipitated with isopropanol and resuspended in the appropriate volume of water or TE.

Plasmid DNA extraction from *E. coli* (II): minipreps with QIAGEN columns

This protocol allows the purification of up to 20 µg high copy plasmid DNA from 1-5 mL overnight *E. coli* culture in LD medium. Cells are pelleted by centrifugation and resuspended in 250 µL buffer P1 (100 µg/mL RNase, 50mM Tris HCl pH 8, 10mM EDTA pH 8). After addition of 250 µL buffer P2 (200mM NaOH, 1% SDS) the solution is mixed thoroughly by inverting the tube 4-6 times, and the lysis reaction occur in 5 minutes at RT. 350 µL N3 buffer (QIAGEN) are added to the

solution, which is then centrifuged for 10 minutes. The supernatant is applied to a QIAprep spin column which is washed once with PB buffer (QIAGEN) and once with PE buffer (QIAGEN). The DNA is eluted with EB buffer (10mM Tris HCl pH 8.5) or water.

Transformation of *E. coli* DH5α

DH5α competent cells are thawed on ice. Then, 50-100 µL cells are incubated 30 minutes in ice with 1 µL plasmid DNA. Cells are then subjected to heat shock at 37°C for 30 seconds and then incubated on ice for 2 minutes. Finally, 900 µL LD are added to the tube and cells are incubated 30 minutes at 37°C to allow expression of ampicillin resistance. Cells are then plated on LD+Amp and overnight incubated at 37°C.

Transformation of *S. cerevisiae*

YEPD exponentially growing yeast cells are harvested by centrifugation and washed with 1 mL 1M lithium acetate (LiAc) pH 7.5. Cells are then resuspended in 1M LiAc pH 7.5 to obtain a cells/LiAc 1:1 solution. 12 µL cells/LiAc are incubated 30-45 minutes at RT with 45 µL 50% PEG (PolyEthyleneGlycol) 3350, 4 µL carrier DNA (salmon sperm DNA) and 1-4 µL DNA of interest (double each quantity when transform with PCR products). After addition of 6 µL 60% glycerol cells are incubated at RT for 30-45 minutes, heat-shocked at 42°C for 5-10 minutes and plated on appropriate selective medium.

Extraction of yeast genomic DNA (Teeny yeast DNA preps)

Yeast cells are harvested from overnight cultures by centrifugation, washed with 1 mL of 0.9M sorbytol 0.1M EDTA pH 7.5 and resuspended in 0.4 mL of the same solution supplemented with 14mM β-mercaptoethanol. Yeast cell wall is digested by 45 minutes' incubation at 37°C with 0.4 mg/mL 20T zimoliase. Spheroplasts are harvested by 30 seconds centrifugation and resuspended in 400 µL TE. After addition of 90 µL of a solution containing EDTA pH 8.5, Tris base and SDS, spheroplasts are incubated 30 minutes at 65°C. Samples are kept on ice for 1 hour following addition of 80 µL 5M potassium acetate. Cell residues are eliminated by 15 minutes' centrifugation at 4°C. DNA is precipitated with chilled 100% ethanol, resuspended in 500 µL TE and incubated 30 minutes with 25 µL 1 mg/mL RNase to eliminate RNA. DNA is then precipitated with isopropanol and resuspended in the appropriate volume (typically 50 µL) of TE.

Southern blot analysis

Yeast genomic DNA prepared with standard methods is digested with the appropriate restriction enzyme(s). The resulting DNA fragments are separated by agarose gel electrophoresis in a 0.8% agarose gel. When adequate migration has occurred, gel is washed 40 minutes with a denaturation buffer (0.2N NaOH, 0.6M NaCl), and 40 minutes with a neutralization buffer (1.5M NaCl, 1M Tris HCl, pH 7.4). DNA is blotted onto a positively charged nylon membrane by overnight capillary transfer with 10X SSC buffer (20X SSC: 3M sodium chloride, 0.3M sodium citrate, pH 7.5). Membrane is then washed with 4X SSC and

UV-crosslinked. Hybridization is carried out by incubating membrane for 5 hours at 50°C with pre-hybridization buffer (50% formamide, 5X SSC, 0.1% N-lauroylsarcosine, 0.02% SDS, 2% Blocking reagent) following by o/n incubation at 50°C with pre-hybridization buffer + probe. The probe is obtained by random priming method (DECAprime^{TM} kit by Ambion) on a suitable DNA template and with 32P d-ATP. Filter is then washed (45 minutes + 15 minutes) at 55°C with a washing solution (0.2M sodium phosphate buffer pH 7.2, SDS 1%, water), air dried and then exposed to an autoradiography film.

Southern blot analysis of telomere length

The length of HO-induced telomeres was determined as previously described (Bonetti *et al.*, 2010). Briefly, yeast DNA was digested with SpeI and the resulting DNA fragments were separated by 0.8% agarose gel electrophoresis and hybridized with ^{32}P-labelled probes corresponding to a 500 bp *ADE2* fragment.

To determine the length of native telomeres, XhoI-digested yeast DNA was subjected to 0.8% agarose gel electrophoresis and hybridized with a ^{32}P-labelled poly(GT) probe. Standard hybridization conditions were used.

In-Gel Hybridization

Visualization of the single-stranded overhangs at native telomeres was done by in-gel hybridization as previously described (Dionne and Wellinger, 1996). The same gel was denatured and hybridized with the end-labeled C-rich oligonucleotide for loading control.

DSB end resection

DSB end resection at the *MAT* locus in JKM139 derivative strains was analyzed on alkaline agarose gels as described in (Clerici *et al.*, 2008), by using a single-stranded RNA (ssRNA) probe complementary to the unresected DSB strand. The ssRNA probe was obtained by *in vitro* transcription using Promega Riboprobe System-T7 and a pGEM-7Zf-based plasmid as a template. Quantitative analysis of DSB resection was performed by calculating the ratio of band intensities for ssDNA and total amount of DSB products.

DSB repair

DSB repair in tGI354 strain was detected as previously described (Saponaro *et al.*, 2010). To determine the amount of noncrossover and crossover products, the normalized intensity of the corresponding bands at different time points after DSB formation was divided by the normalized intensity of the uncut *MATa* band at time zero before HO induction (100%). The repair efficiency (NCO+CO) was normalized with respect to the efficiency of DSB formation by subtracting the value calculated at the time point of maximum DSB formation efficiency from the values calculated at the subsequent time points after galactose addition.

qRT-PCR

Total RNA was extracted from cells using the Bio-Rad (Hercules, CA) Aurum total RNA mini kit. First strand cDNA synthesis was performed with the Bio-Rad iScript cDNA Synthesis Kit. qRT-PCR was performed

on a MiniOpticon Real-time PCR system (Bio-Rad) and RNA levels were quantified using the ΔΔCt method. Quantities were normalized to *ACT1* RNA levels and compared to that of wild type cells that was set up to 1.

Total RNA-Seq analysis

Total RNA was extracted using standard hot phenol procedure. Ribosomal RNAs were depleted from total RNA using the RiboMinusTM Eukaryote Kit for RNA-Seq (Life Technologies). Efficiency of the depletion and quality of rRNA-depleted RNA was assessed by analysis in RNA Pico 6000 chips for 2100 Bioanalyzer (Agilent). Total RNA-Seq libraries were prepared from 125 ng of rRNA-depleted RNA, using the TruSeq® Stranded Total RNA Sample Preparation Kit (Illumina) according manufacturer's instruction. Paired-end sequencing (2x50 nt) of the libraries was performed on a HiSeq 2500 sequencer. Reads were mapped to the *S. cerevisiae* S288C reference genome (retrieved from SGD) using the version 1.4.1 of TopHat, with a tolerance of 4 mismatches and a maximum size for introns of 2 Kb. All subsequent bioinformatics analysis used reads uniquely mapped on the reference genome. Tags densities were normalized on the total number of reads mapped on ORFs. Differential expression analysis was performed by using DESeq (Anders and Huber, 2010).

Sub-cellular fractionation

Fractioning was performed as described in (Keogh *et al.*, 2006). Briefly, cells were collected by centrifugation and washed with PSB (20mM Tris-HCl pH 7.4, 2mM EDTA, 100mM NaCl, 10mM ß-ME) and SB (1M Sorbitol, 20mM Tris-HCl pH 7.4). Cells were then incubated at 30°C for 30 minutes in 1ml SB + 125µl Zymolase 20T (10mg/ml). Spheroplasts were pelletted at 4°C and resuspended in 500µl EBX (20mM Tris-HCl pH 7.4, 100mM NaCl, 0.25% Triton X-100, 15mM ß-ME, 0,005% Phenol red, protease/phosphatase inhibitors). Triton X-100 concentration was adjusted to 0.5% to lyse the outer cell membrane, and samples were kept on ice with gentle mixing. After taking an aliquot for total protein extract, the lysate was transferred in 1ml NIB (20mM Tris-HCl pH 7.4, 100mM NaCl, 1.2M Sucrose, 15mM β-mercaptoethanol, protease/phosphatase inhibitors) and centrifuged at 12000rpm at 4°C. A sample of the upper cytoplasmic protein fraction was taken and the rest of the supernatant discarded. The nuclear pellet was gently resuspended in 100µl EBX, and Triton X-100 concentration was adjusted to 1% to lyse the nuclear membrane. Samples were kept on ice with gentle mixing and aliquots of the nuclear extract were taken. To each fraction an equal volume of 2x SDS-PAGE loading buffer (60mM Tris pH 6.8, 2% SDS, 10% Glycerol, 0.2% bromophenol blue, 200mM DTT) was added. After 5 min at 95°C, samples were centrifuged and the supernatant collected for SDS-PAGE and Western blot analyses.

Chromatin ImmunoPrecipitation (ChIP) analysis

ChIP assays were performed as previously described (Viscardi *et al.*, 2007). Exponentially growing cells (50 mL of $8x10^6$-$1x10^7$) were treated with 1.4 mL of 37% formaldehyde for 5 minutes while shaking, in order to create DNA-protein and protein-protein covalent bounds (cross-link). Then 2.5 mL of 2.5M glycine were added for other 5 minutes while shaking. Treated cells were kept on ice until centrifugation at 1800 rpm for 5 minutes at 4°C. Cell pellet was then washed first with HBS buffer (50mM HEPES pH 7.5, 140mM NaCl) and then with ChIP buffer (50mM HEPES pH 7.5, 140mM NaCl, 1mM EDTA pH 8, 1% IGEPAL CA-630, 0.1% Sodium deoxycholate, 1mM PMSF). Before each wash cells were pelleted by centrifugation at 1800 rpm for 5 minutes at 4°C. After the wash with ChIP buffer and subsequent centrifugation, the supernatant was carefully and completely removed. Then 0.4 mL of ChIP buffer + complete anti-proteolitic tablets (Roche) was added and samples were stored at -80°C until the following day. After breaking cells for 30 minutes at 4°C with glass beads, the latter were eliminated. This passage was followed by centrifugation at 4°C for 30 minutes. Pellet was resuspended in 0.5 mL ChIP buffer + antiproteolitics and then sonicated, in order to share DNA in 500-1000 bp fragments (4 cycles of 25 seconds). At this point 5 µL as "input DNA" for PCR reactions and 20 µL as "input" for western blot analysis were taken. Then 400 µL of the remaining solution was immunoprecipitated with specific Dynabeads-coated antibodies. After proper incubation with desired antibodies, Dynabeads could be washed RT as follow: 2X with SDS buffer (50mM HEPES pH 7.5, 1mM EDTA pH 8, 140mM NaCl,

0.025% SDS), 1X with High-salt buffer (50mM HEPES pH 7.5, 1mM EDTA pH 8, 1M NaCl), 1X with T/L buffer (20mM Tris-Cl, pH 7.5, 250mM LiCl, 1mM EDTA pH 8, 0.05% sodium deoxycholate, 0.5%IGEPAL-CA630), and then 2X with T/E buffer (20mM Tris-Cl pH 7.5, 0.1mM EDTA pH 8). All washes were done by pulling down Dynabeads 1 minute and then nutating for 4 minutes with the specific buffer. After the last wash Dynabeads were resuspended in 145 µL TE + 1% SDS buffer, shaked on a vortex, put at 65°C for 2 minutes, shaked on vortex again and then pulled down. Then 120 µL of the supernatant were put at 65°C over-night for reverse cross-linking, while 20 µL were stored as sample for western blot analysis of the immunoprecipitated protein amount. Previously taken input DNA samples must be put at 65°C over-night with 115 µL of TE + 1% SDS buffer. The next day DNA must be purified for PCR analysis with QIAGEN columns.

Quantification of immunoprecipitated DNA was achieved by quantitative real-time (qPCR) on a Bio-Rad MiniOpticon apparatus. qPCR at the HO-induced DSB was carried out by using primer pairs located at different distances from the HO-induced DSB and at the *ARO1* fragment of chromosome IV. Data were expressed as fold enrichment at the HO-induced DSB over that at the non-cleaved *ARO1* locus, after normalization of each ChIP signals to the corresponding amount of immunoprecipitated protein and input for each time point. Fold enrichment was then normalized to the efficiency of DSB induction. qPCR at the HO-induced telomere was carried out by using primer pairs located at 640 bp centromere-proximal to the HO cutting site at chromosome VII and at the nontelomeric *ARO1* fragment of

chromosome IV (CON). qPCR at native telomeres was carried out by using primer pairs located at 70 bp and 139 bp from the TG sequences on telomeres VI-R (right) and XV-L (left), respectively. Data are expressed as fold enrichment over the amount of CON in the immunoprecipitates after normalization to input signals for each primer set.

Coimmunoprecipitations

Coimmunoprecipitations were performed as described in (Hegnauer *et al.*, 2012). Cells were collected by centrifugation and put on ice. Cell pellet was then resuspended in 200 µL cold breaking buffer (50 mM HEPES pH 8.0, 150 mM NaCl, 5 mM EDTA, 20% glycerol, 1mM sodium orthovanadate, 60 mM β-Glycerophosphate, supplemented with protease inhibitors). After addition of glass beads, cells were disrupted by vortexing for 7 minutes. The supernatant was collected in a new tube and centrifuged for 20 minutes at 4° C. Proteins extracts were quantified by direct UV A280 measurements and normalized to OD=12. At this point 10 µL as "input" were taken, mixed with 10 µL of Laemmli buffer (0.62M Tris, 2% SDS, 10% glycine, 0.001% Bfb, 100mM DTT) and boiled for 3 minutes. Specific antibodies were added to the remaining solution and left at 4°C with gentle mixing for 1 hour. Then 50 µL protein G conjugatd Dynabeads was added to the solution and kept at 4°C with gentle mixing for another hour. After centrifugation and removal of the supernatant, the Dynabeads were washed 3 times with breaking buffer and 3 times with PBS. After the last wash Dynabeads were resuspended in 40 µL 2x Laemmli buffer and boiled

for 3 minutes. Finally, proteins of interest in the supernatant were analyzed by SDS-PAGE and Western blot.

Synchronization of yeast cells

Synchronization of yeast cells with α-factor

α-factor allows to synchronize a population of yeast cells in G1 phase. This pheromone activates a signal transduction cascade which arrests yeast cells in G1 phase. Only *MATa* cells are responsive to α-factor. To synchronize in G1 a population of exponentially growing yeast cells in YEPD, 2 μg/mL α-factor is added to $6x10^6$ cells/mL culture. As the percentage of budded cells will fall below 5% cells are considered to be G1-arrested. Cells are then washed and resuspended in fresh medium with or without 3 μg/mL α-factor to keep cells G1-arrested or release them into the cell cycle respectively. At this time cell cultures can be either treated with genotoxic agents or left untreated. If cells carry the deletion of *BAR1* gene, that encodes a protease that degrades the α-factor, 0.5 μg/mL α-factor is sufficient to induce a G1-arrest that lasts several hours.

Synchronization of yeast cells with nocodazole

Nocodazole allows to synchronize a population of yeast cells in G2 phase. This drug causes the depolimerization of microtubules, thus activating the mitotic checkpoint which arrests cells at the metaphase to anaphase transition (G2 phase). To synchronize in G2 a population of exponentially growing yeast cells in YEPD, 0.5 μg/mL nocodazole is added to $6x10^6$ cells/mL culture together with DMSO at a final

concentration of 1% (use a stock solution of 100X nocodazole in 100% DMSO). As the percentage of dumbbell cells will reach 95% cells are considered to be G2-arrested. Cells are then washed and resuspended in fresh medium with or without 1.5 µg/mL nocodazole to keep cells G2-arrested or release them into the cell cycle respectively. At this time cell cultures can be either treated with genotoxic agents or left untreated.

Other techniques

FACS analysis of DNA contents

FACS (Fluorescence-Activated Cell Sorting) analysis allows to determine the DNA content of every single cell of a given population of yeast cells. $6x10^6$ cells are harvested by centrifugation, resuspended in 70% ethanol and incubated at RT for 1 hour. Cells are then washed with 1 mL 50mM Tris pH 7.5 and incubated overnight at 37°C in the same solution with 1 mg/mL RNase. Samples are centrifuged and cells are incubated at 37°C for 30 minutes with 5 mg/mL pepsin in 55mM HCl, washed with 1 mL FACS Buffer and stained in 0.5 mL FACS buffer with 50 µg/mL propidium iodide. 100 µL of each sample are diluted in 1 mL 50mM Tris pH 7.5 and analyzed with a BectonDickinson FACS-Scan. The same samples can also be analyzed by fluorescence microscopy to score nuclear division.

Total protein extracts

Total protein extracts were prepared from 10^8 cells collected from exponentially growing yeast cultures. Cells are harvested by

centrifugation and washed with 20% trichloracetic acid (TCA) in order to prevent proteolysis and resuspended in 50 µL 20% TCA. After addition of 200 µL of glass beads, cells are disrupted by vortexing for 8 minutes. Glass beads are washed with 400 µL 5% TCA, and the resulting extract are centrifuged at 3000 rpm for 10 minutes. The pellet is resuspended in 70 µL Laemmli buffer (0.62M Tris, 2% SDS, 10% glycine, 0.001% Bfb, 100mM DTT), neutralized with 30 µL 1M Tris base, boiled for 3 minutes, and finally clarified by centrifugation.

SDS-PAGE and western blot analysis

Protein extracts for western blot analysis were prepared by TCA precipitation. Protein extracts are loaded in 10% polyacrylamide gels (composition). Proteins are separated based on their molecular weight by polyacrylamide gel electrophoresis in the presence of sodium dodecyl sulphate (SDS-PAGE). When adequate migration has occurred proteins are blotted onto nitrocellulose membrane. Membrane is saturated by 1-hour incubation with 4% milk in TBS containing 0.2% TRITON X-100 and incubated for 2 hours with primary antibodies. Membrane is washed three times with TBS for 10 minutes, incubated for 1 hour with secondary antibodies and again washed with TBS. Detection is performed with ECL (Enhanced ChemiLuminescence - Genespin) and X-ray films according to the manufacturer.

Primary monoclonal 12CA5 anti-HA and 9E10 anti-MYC antibodies are purchased at GE Healthcare, as well as peroxidase conjucated IgG anti-rabbit and anti-mouse secondary antibodies. Rad53 and Rad51 were detected by using anti-Rad53 (ab104232) and anti-Rad51 (ab63798)

polyclonal antibodies, respectively, from Abcam. Rpa1 and Rpa2 subunits of the RPA complex were detected by using polyclonal antibodies kindly provided by B. Stillman (Cold Spring Harbor, New York, USA). Rad9 was detected using polyclonal antibodies kindly provided by N. Lowndes (National University of Ireland Galway, Ireland). Histone H2A was detected by using anti-H2A polyclonal antibodies from Active Motif. Histone H3 was detected by using anti-H3 polyclonal antibodies from Abcam (ab1791). Histone H4 was detected by using anti-H4 polyclonal antibodies from Upstate Biotechnology. Pgk1 was detected by using anti-Pgk1 antibodies from Invitrogen (cat No. 459250).

Drop test

For spot assays, exponentially growing overnight cultures were counted, and 10-fold serial dilutions of equivalent cell numbers were spotted onto plates containing the indicated media.

Fluorescence microscopy

Yeast cells were grown and processed for fluorescence microscopy as described previously (Eckert-Boulet *et al.*, 2011). Fluorophores were cyan fluorescent protein (CFP, clone W7) (Heim and Tsien, 1996) and yellow fluorescent protein (YFP, clone 10C) (Ormo *et al.*, 1996). Fluorophores were visualized on a Deltavision Elite microscope (Applied Precision, Inc) equipped with a 100x objective lens (Olympus U-PLAN S-APO, NA 1.4), a cooled Evolve 512 EMCCD camera (Photometrics, Japan), and an Insight solid state illumination source

(Applied Precision, Inc). Pictures were processed with Volocity software (PerkinElmer). Images were acquired using softWoRx (Applied Precision, Inc) software.

REFERENCES

Addinall SG, Holstein EM, Lawles C, Yu M, Chapman K, Banks AP, Ngo HP, Maringele L, Taschuk M, Young A, Ciesiolka A, Lister AL, Wipat A, Wilkinson DJ, Lydall D (2011) Quantitative fitness analysis shows that NMD proteins and many other protein complexes suppress or enhance distinct telomere cap defects. *PLoS Genet., 7*, e1001362.

Adkins NL, Niu H, Sung P, Peterson CL (2013) Nucleosome dynamics regulates DNA processing. *Nat. Struct. Mol. Biol., 20*, 836–842.

Aguilera A, García-Muse T (2012) R loops: from transcription byproducts to threats to genome stability. *Mol. Cell, 46*, 115-24.

Amrani N, Dong S, He F, Ganesan R, Ghosh S, Kervestin S, Li C, Mangus DA, Spatrick P, Jacobson A (2006) Aberrant termination triggers nonsense-mediated mRNA decay. *Biochem. Soc. Trans., 34*, 39-42.

Amrani N, Ganesan R, Kervestin S, Mangus DA, Ghosh S, Jacobson A (2004) A faux 3'-UTR promotes aberrant termination and triggers nonsense-mediated mRNA decay. *Nature, 432*, 112-118.

Anbalagan S, Bonetti D, Lucchini G, Longhese MP (2011) Rif1 supports the function of the CST complex in yeast telomere capping. *PLoS Genet., 7*, e1002024.

Anders S, Huber W (2010). Differential expression analysis for sequence count data. *Genome Biol., 11*, R106.

Aparicio T, Baer R, Gautier J (2014) DNA double-strand break repair pathway choice and cancer. *DNA Repair (Amst), 19*, 169-175.

Arora R, Lee Y, Wischnewski H, Brun CM, Schwarz T, Azzalin CM (2014) RNaseH1 regulates TERRA-telomeric DNA hybrids and telomere maintenance in ALT tumour cells. *Nat. Commun., 5*, 5220.

Askree SH, Yehuda T, Smolikov S, Gurevich R, Hawk J, Coker C, Krauskopf A, Kupiec M, McEachern MJ (2004) A genome-wide screen for *Saccharomyces cerevisiae* deletion mutants that affect telomere length. *Proc. Natl. Acad. Sci. USA, 101*, 8658-8663.

Azzalin CM, Lingner J (2006). The double life of UPF1 in RNA and DNA stability pathways. *Cell Cycle, 5*, 1496-8.

Azzalin CM, Reichenbach P, Khoriauli L, Giulotto E, Lingner J (2007) Telomeric repeat containing RNA and RNA surveillance factors at mammalian chromosome ends. *Science, 318*, 798-801.

Badis G, Saveanu C, Fromont-Racine M, Jacquier A (2004) Targeted mRNA degradation by deadenylation-independent decapping. *Mol. Cell, 15*, 5-15.

Balk B, Maicher A, Dees M, Klermund J, Luke-Glaser S, Bender K, Luke B (2013) Telomeric RNA-DNA hybrids affect telomere-length dynamics and senescence. *Nat. Struct. Mol. Biol., 20*, 1199-1205.

Bhargava R, Onyango DO, Stark JM (2016) Regulation of Single-Strand Annealing and its Role in Genome Maintenance. *Trends Genet., 32*, 566-575.

Bianchi A, Negrini S, Shore D (2004) Delivery of yeast telomerase to a DNA break depends on the recruitment functions of Cdc13 and Est1. *Mol. Cell, 16*, 139-146.

Bizard AH, Hickson ID (2014) The dissolution of double Holliday junctions. *Cold Spring Harb. Perspect. Biol., 6*, a016477.

Bonetti D, Clerici M, Anbalagan S, Martina M, Lucchini G, Longhese MP (2010) Shelterin-like proteins and Yku inhibit nucleolytic processing of *Saccharomyces cerevisiae* telomeres. *PLoS Genet., 6*, e1000966.

Bonetti D, Clerici M, Manfrini N, Lucchini G, Longhese MP (2010) The MRX complex plays multiple functions in resection of Yku- and Rif2-protected DNA ends. *PLoS One, 5*, e14142.

Bonetti D, Martina M, Clerici M, Lucchini G, Longhese MP (2009) Multiple pathways regulate 3' overhang generation at *S. cerevisiae* telomeres. *Mol. Cell, 35*, 70-81.

Bonetti D, Martina M, Falcettoni M, Longhese MP (2014) Telomere-end processing: mechanisms and regulation. *Chromosoma, 123*, 57-66.

Bonetti D, Villa M, Gobbini E, Cassani C, Tedeschi G, Longhese MP (2015) Escape of Sgs1 from Rad9 inhibition reduces the requirement for Sae2 and functional MRX in DNA end resection. *EMBO Rep., 16*, 351-361.

Bonneau F, Basquin J, Ebert J, Lorentzen E, Conti E (2009) The yeast exosome functions as a macromolecular cage to channel RNA substrates for degradation. *Cell, 139*, 547-559.

Burkard KT, Butler JS (2000) A nuclear 3'-5' exonuclease involved in mRNA degradation interacts with Poly(A) polymerase and the hnRNA protein Npl3p. *Mol. Cell. Biol., 20*, 604-616.

Cannavo E, Cejka P (2014) Sae2 promotes dsDNA endonuclease activity within Mre11-Rad50-Xrs2 to resect DNA breaks. *Nature, 514*, 122-125.

Cassani C, Gobbini E, Wang W et al (2016) Tel1 and Rif2 regulate MRX functions in end-tethering and repair of DNA double-strand breaks. *PLoS Biol., 14*, e1002387.

Cejka P (2015) DNA End Resection, Nucleases Team Up with the Right Partners to Initiate Homologous Recombination. *J. Biol. Chem., 290*, 22931-8.

Cejka P, Cannavo E, Polaczek P, Masuda-Sasa T, Pokharel S, Campbell JL, Kowalczykowski SC. (2010) DNA end resection by Dna2-Sgs1-RPA and its stimulation by Top3-Rmi1 and Mre11Rad50-Xrs2. *Nature, 467*, 112-116.

Cejka P, Kowalczykowski SC (2010) The full-length *Saccharomyces cerevisiae* Sgs1 protein is a vigorous DNA helicase that preferentially unwinds Holliday junctions. *J. Biol. Chem., 285*, 8290-8301.

Celli GB, de Lange T (2005) DNA processing is not required for ATM-mediated telomere damage response after TRF2 deletion. *Nat. Cell Biol., 7*,712-718.

Chai W, Sfeir AJ, Hoshiyama H, Shay JW, Wright WE (2006) The involvement of the Mre11/Rad50/Nbs1 complex in the generation of G-overhangs at human telomeres. *EMBO Rep., 7*, 225-230.

Chan YA, Hieter P, Stirling PC (2014) Mechanisms of genome instability induced by RNA-processing defects. Trends Genet., 30, 245-253.

Chandra A, Hughes TR, Nugent CI, Lundblad V (2001) Cdc13 both positively and negatively regulates telomere replication. *Genes Dev., 15*, 404-414.

Chang M, Arneric M, Lingner J (2007) Telomerase repeat addition processivity is increased at critically short telomeres in a Tel1-dependent manner in *Saccharomyces cerevisiae*. *Genes Dev., 21*, 2485-2494.

Chawla R, Redon S, Raftopoulou C, Wischnewski H, Gagos S, Azzalin CM (2011) Human UPF1 interacts with TPP1 and telomerase and sustains telomere leading-strand replication. *EMBO J., 30*, 4047-4058.

Chen H, Lisby M, Symington LS (2013) RPA coordinates DNA end resection and prevents formation of DNA hairpins. *Mol. Cell, 50*, 589-600.

Chen X, Niu H, Chung WH, Zhu Z, Papusha A, Shim EY, Lee SE, Sung P, Ira G (2011) Cell cycle regulation of DNA double-strand break end resection by Cdk1-dependent Dna2 phosphorylation. *Nat. Struct. Mol. Biol., 18*, 1015-1019.

Chiruvella KK, Liang Z, Wilson TE (2013) Repair of double-strand breaks by end joining. *Cold Spring Harb. Perspect. Biol., 5*, a012757.

Chow TT, Zhao Y, Mak SS, Shay JW, Wright WE (2012) Early and late steps in telomere overhang processing in normal human cells: the position of the final RNA primer drives telomere shortening. *Genes Dev., 26*, 1167-78.

Ciccia A, Elledge SJ (2010) The DNA damage response: making it safe to play with knives. *Mol. Cell, 40*, 179-204.

Clerici M, Mantiero D, Guerini I, Lucchini G, Longhese MP (2008) The Yku70-Yku80 complex contributes to regulate double-strand break processing and checkpoint activation during the cell cycle. *EMBO Rep., 9*, 810-818.

Clerici M, Mantiero D, Lucchini G, Longhese MP (2005) The *Saccharomyces cerevisiae* Sae2 protein promotes resection and bridging of double strand break ends. *J. Biol. Chem., 280*, 38631-8.

Counter CM, Avilion AA, LeFeuvre CE, Stewart NG, Greider CW, Harley CB, Bacchetti S (1992) Telomere shortening associated with

chromosome instability is arrested in immortal cells which express telomerase activity. *EMBO J., 11*, 1921-9.

Czaplinski K, Ruiz-Echevarria MJ, Paushkin SV, Han X, Weng Y, Perlick HA, Dietz HC, Ter-Avanesyan MD, Peltz SW (1998) The surveillance complex interacts with the translation release factors to enhance termination and degrade aberrant mRNAs. *Genes Dev., 12*, 1665-1677.

Dahlseid JN, Lew-Smith J, Lelivelt MJ, Enomoto S, Ford A, Desruisseaux M, McClellan M, Lue N, Culbertson MR, Berman J (2003) mRNAs encoding telomerase components and regulators are controlled by *UPF* genes in *Saccharomyces cerevisiae*. *Eukaryot. Cell, 2*, 134-142.

Daley JM, Gaines WA, Kwon YH, Sung P (2014) Regulation of DNA pairing in homologous recombination. *Cold Spring Harb. Perspect. Biol., 6*, a017954.

Davis AJ, Chen DJ (2013) DNA double strand break repair via non-homologous end-joining. *Transl. Cancer Res.*, 2, 130-143.

de Lange T (2009) How telomeres solve the end-protection problem. *Science, 326*, 948-952.

Diede SJ, Gottschling DE (1999) Telomerase-mediated telomere addition in vivo requires DNA primase and DNA polymerases alpha and delta. *Cell, 99*, 723-733.

Diede SJ, Gottschling DE (2001) Exonuclease activity is required for sequence addition and Cdc13p loading at a de novo telomere. *Curr.*

Biol., 11, 1336-1340.

Dionne I, Wellinger RJ (1996) Cell cycle-regulated generation of single-stranded G-rich DNA in the absence of telomerase. *Proc. Natl. Acad. Sci. USA, 93*, 13902-13907.

Dionne I, Wellinger RJ (1998) Processing of telomeric DNA ends requires the passage of a replication fork. *Nucleic Acids Res., 26*, 5365-5371.

Doksani Y, Wu JY, de Lange T, Zhuang X (2013) Super-resolution fluorescence imaging of telomeres reveals TRF2-dependent T-loop formation. *Cell, 155*, 345-56.

Dutertre M, Lambert S, Carreira A, Amor-Guéret M, Vagner S (2014) DNA damage: RNA-binding proteins protect from near and far. *Trends Biochem. Sci., 39*, 141-149.

Eberle AB, Lykke-Andersen S, Muhlemann O, Jensen TH (2009) SMG6 promotes endonucleolytic cleavage of nonsense mRNA in human cells. *Nat. Struct. Mol. Biol., 16*, 49-55.

Eckert-Boulet N, Rothstein R, Lisby M (2011) Cell biology of homologous recombination in yeast. *Methods Mol. Biol., 745*, 523-536.

Enomoto S, Glowczewski L, Lew-Smith J, Berman JG (2004) Telomere cap components influence the rate of senescence in telomerase-deficient yeast cells. *Mol. Cell. Biol., 24*, 837-845.

Evans SK, Lundblad V (1999) Est1 and Cdc13 as comediators of telomerase access. *Science, 286*, 117-120.

Fanning E, Klimovich V, Nager AR (2006) A dynamic model for replication protein A (RPA) function in DNA processing pathways. *Nucleic Acids Res., 34*, 4126-4137.

Faure V, Coulon S, Hardy J, Géli V (2010) Cdc13 and telomerase bind through different mechanisms at the lagging- and leading-strand telomeres. *Mol. Cell, 38*, 842-852.

Ferrari M, Dibitetto D, De Gregorio G, Eapen VV, Rawal CC, Lazzaro F, Tsabar M, Marini F, Haber JE, Pellicioli A (2015) Functional interplay between the 53BP1-ortholog Rad9 and the Mre11 complex regulates resection, end-tethering and repair of a double-strand break. *PLoS Genet., 11*, e1004928.

Flynn RL, Centore RC, O'Sullivan RJ, Rai R, Tse A, Songyang Z, Chang S, Karlseder J, Zou L (2011) TERRA and hnRNPA1 orchestrate an RPA-to-POT1 switch on telomeric single-stranded DNA. *Nature, 471*, 532-536.

Foster SS, Balestrini A, Petrini JH (2011) Functional interplay of the Mre11 nuclease and Ku in the response to replication-associated DNA damage. *Mol. Cell. Biol., 31*, 4379-4389.

Francia S, Michelini F, Saxena A, Tang D, de Hoon M, Anelli V, Mione M, Carninci P, d'Adda di Fagagna F (2012) Site-specific DICER and DROSHA RNA products control the DNA-damage response. *Nature,*

488, 231-235.

Frank CJ, Hyde M, Greider CW (2006) Regulation of telomere elongation by the cyclin-dependent kinase CDK1. *Mol. Cell, 24*, 423-32.

Gao H, Cervantes RB, Mandell EK, Otero JH, Lundblad V (2007) RPA-like proteins mediate yeast telomere function. *Nat. Struct. Mol. Biol., 14*, 208-214.

Gao H, Toro TB, Paschini M, Braunstein-Ballew B, Cervantes RB, Lundblad V (2010) Telomerase recruitment in *Saccharomyces cerevisiae* is not dependent on Tel1-mediated phosphorylation of Cdc13. *Genetics, 186*, 1147-1159.

Gao M, Wei W, Li MM, Wu YS, Ba Z, Jin KX, Li MM, Liao YQ, Adhikari S, Chong Z, Zhang T, Guo CX, Tang TS, Zhu BT, Xu XZ, Mailand N, Yang YG, Qi Y, Rendtlew Danielsen JM (2014) Ago2 facilitates Rad51 recruitment and DNA double-strand break repair by homologous recombination. *Cell Res., 24*, 532-541.

Garvik B, Carson M, Hartwell L (1995) Single-stranded DNA arising at telomeres in *cdc13* mutants may constitute a specific signal for the *RAD9* checkpoint. *Mol. Cell. Biol., 15*, 6128-6138.

Gavaldá S, Gallardo M, Luna R, Aguilera A (2013) R-loop mediated transcription-associated recombination in *trf4Δ* mutants reveals new links between RNA surveillance and genome integrity. *PLoS One, 8*, e65541.

Ginno PA, Lim YW, Lott PL, Korf I, Chédin F (2013) GC skew at the 5′ and 3′ ends of human genes links R-loop formation to epigenetic regulation and transcription termination. *Genome Res., 23*, 1590-1600.

Gobbini E, Cesena D, Galbiati A, Lockhart A, Longhese MP (2013) Interplays between ATM/Tel1 and ATR/Mec1 in sensing and signaling DNA double-strand breaks. *DNA Repair (Amst), 12*, 791-799.

Gobbini E, Trovesi C, Cassani C, Longhese MP (2014) Telomere uncapping at the crossroad between cell cycle arrest and carcinogenesis. *Mol. Cell. Oncol., 1*, e29901.

Gong Y, de Lange T (2010) A Shld1-controlled POT1a provides support for repression of ATR signaling at telomeres through RPA exclusion. *Mol. Cell, 40*, 377-387.

Goudsouzian LK, Tuzon CT, Zakian VA (2006) *S. cerevisiae* Tel1p and Mre11p are required for normal levels of Est1p and Est2p telomere association. *Mol. Cell, 24*, 603-610.

Grandin N, Damon C, Charbonneau M (2000) Cdc13 cooperates with the yeast Ku proteins and Stn1 to regulate telomerase recruitment. *Mol. Cell. Biol., 20*, 8397-8408.

Grandin N, Damon C, Charbonneau M (2001) Ten1 functions in telomere end protection and length regulation in association with Stn1 and Cdc13. *EMBO J., 20*, 1173-1183.

Grandin N, Reed SI, Charbonneau M (1997) Stn1, a new *Saccharomyces cerevisiae* protein, is implicated in telomere size regulation in association with Cdc13. *Genes Dev., 11*, 512-527.

Greider CW, Blackburn EH (1985) Identification of a specific telomere terminal transferase activity in *Tetrahymena* extracts. *Cell, 43*, 405-413.

Grenon M, Costelloe T, Jimeno S, O'Shaughnessy A, Fitzgerald J, Zgheib O, Degerth L, Lowndes NF (2007) Docking onto chromatin via the Saccharomyces cerevisiae Rad9 Tudor domain. *Yeast, 24*, 105-19.

Grossi S, Puglisi A, Dmitriev PV, Lopes M, Shore D (2004) Pol12, the B subunit of DNA polymerase alpha, functions in both telomere capping and length regulation. *Genes Dev., 18*, 992-1006.

Hammet A, Magill C, Heierhorst J, Jackson SP (2007) Rad9 BRCT domain interaction with phosphorylated H2AX regulates the G1 checkpoint in budding yeast. *EMBO Rep., 8*, 851-857.

Hamperl S, Cimprich KA (2014) The contribution of co-transcriptional RNA:DNA hybrid structures to DNA damage and genome instability. *DNA Repair (Amst), 19*, 84-94.

Hardwick, SW, Luisi BF (2013) Rarely at rest: RNA helicases and their busy contributions to RNA degradation, regulation and quality control. *RNA Biol., 10*, 56-70.

Hardy CF, Sussel L, Shore D (1992) A RAP1-interacting protein involved

in transcriptional silencing and telomere length regulation. *Genes Dev., 6*, 801-814.

Harley CB, Futcher AB, Greider CW (1990) Telomeres shorten during ageing of human fibroblasts. *Nature, 345*, 458-460.

He F, Brown AH, Jacobson A (1997). Upf1p, Nmd2p, and Upf3p are interacting components of the yeast nonsense-mediated mRNA decay pathway. *Mol. Cell. Biol., 17*, 1580-94.

He F, Li X, Spatrick P, Casillo R, Dong S, Jacobson A (2003) Genome-wide analysis of mRNAs regulated by the nonsense-mediated and 5' to 3' mRNA decay pathways in yeast. *Mol. Cell, 12*, 1439-1452.

Hector RE, Shtofman RL, Ray A, Chen BR, Nyun T, Berkner KL, Runge KW (2007) Tel1p preferentially associates with short telomeres to stimulate their elongation. *Mol. Cell, 27*, 851-858.

Hegnauer AM, Hustedt N, Shimada K, Pike BL, Vogel M, Amsler P, Rubin SM, van Leeuwen F, Guénolé A, van Attikum H, Thomä NH, Gasser SM (2012) An N-terminal acidic region of Sgs1 interacts with Rpa70 and recruits Rad53 kinase to stalled forks. *EMBO J., 31*, 3768-3783.

Heim R, Tsien RY (1996) Engineering green fluorescent protein for improved brightness, longer wavelengths and fluorescence resonance energy transfer. *Curr. Biol., 6*, 178-182.

Henderson ER, Blackburn EH (1989) An overhanging 3' terminus is a

conserved feature of telomeres. *Mol. Cell. Biol., 9*, 345-348.

Hirano Y, Sugimoto K (2007) Cdc13 telomere capping decreases Mec1 association but does not affect Tel1 association with DNA ends. Mol. Biol. Cell, 18, 2026-2036.

Hockemeyer D, Sfeir AJ, Shay JW, Wright WE, de Lange T (2005) POT1 protects telomeres from a transient DNA damage response and determines how human chromosomes end. *EMBO J., 24*, 2667-2678.

Hohl M, Kwon Y, Galván SM, Xue X, Tous C, Aguilera A, Sung P, Petrini JH (2011) The Rad50 coiled-coil domain is indispensable for Mre11 complex functions. *Nat. Struct. Mol. Biol., 18*, 1124-1131.

Holstein EM, Clark KR, Lydall D (2014) Interplay between nonsense-mediated mRNA decay and DNA damage response pathways reveals that Stn1 and Ten1 are the key CST telomere-cap components. *Cell Rep., 7*, 1259-1269.

Houseley J, LaCava J, Tollervey D (2006) RNA-quality control by the exosome. *Nat. Rev. Mol. Cell. Biol., 7*, 529-539.

Huertas P, Cortés-Ledesma F, Sartori AA, Aguilera A, Jackson SP (2008) CDK targets Sae2 to control DNA-end resection and homologous recombination. *Nature, 455*, 689-692.

Iglesias N, Redon S, Pfeiffer V, Dees M, Lingner J, Luke B (2011) Subtelomeric repetitive elements determine TERRA regulation by Rap1/Rif and Rap1/Sir complexes in yeast. *EMBO Rep., 12*, 587-593.

Ira G, Haber JE (2002) Characterization of RAD51-independent break-induced replication that acts preferentially with short homologous sequences. *Mol. Cell. Biol., 22*, 6384-92.

Ira G, Pellicioli A, Balijja A, Wang X, Fiorani S, Carotenuto W, Liberi G, Bressan D, Wan L, Hollingsworth NM et al (2004) DNA end resection, homologous recombination and DNA damage checkpoint activation require CDK1. *Nature, 431*, 1011-1017.

Isken O, Maquat LE (2008) The multiple lives of NMD factors: balancing roles in gene and genome regulation. *Nat. Rev. Genet., 9*, 699-712.

Jackson SP, Bartek J (2009) The DNA-damage response in human biology and disease. *Nature, 461*, 1071-1078.

Jasin M, Rothstein R (2013) Repair of strand breaks by homologous recombination. *Cold Spring Harb. Perspect. Biol., 5*, a012740.

Jinek M, Coyle SM, Doudna JA (2011) Coupled 5' nucleotide recognition and processivity in Xrn1-mediated mRNA decay. *Mol. Cell*, 41, 600-8.

Jinks-Robertson S, Michelitch M, Ramcharan S (1993) Substrate length requirements for efficient mitotic recombination in *Saccharomyces cerevisiae*. *Mol. Cell. Biol., 13*, 3937-50.

Johnson AW (1997) Rat1p and Xrn1p are functionally interchangeable exoribonucleases that are restricted to and required in the nucleus and cytoplasm, respectively. *Mol. Cell. Biol., 17*, 6122-6130.

Kaygun H, Marzluff WF (2005) Regulated degradation of replication-dependent histone mRNAs requires both ATR and Upf1. *Nat. Struct. Mol. Biol., 12*, 794-800.

Keogh MC, Kim JA, Downey M, Fillingham J, Chowdhury D, Harrison JC, Onishi M, Datta M, Galicia S, Emili A, Lieberman J, Shen X, Buratowski S, Haber JE, Durocher D, Greenblatt JF, Krogan NJ (2006) A phosphatase complex that dephosphorylates γH2AX regulates DNA damage checkpoint recovery. *Nature, 439*, 497-501.

Khadaroo B, Teixeira MT, Luciano P, Eckert-Boulet N, Germann SM, Simon MN, Gallina I, Abdallah P, Gilson E, Géli V, Lisby M (2009) The DNA damage response at eroded telomeres and tethering to the nuclear pore complex. *Nat. Cell Biol., 11*, 980-987.

Kim JA, Haber JE (2009) Chromatin assembly factors Asf1 and CAF-1 have overlapping roles in deactivating the DNA damage checkpoint when DNA repair is complete. *Proc. Natl. Acad. Sci. USA, 106*, 1151-1156.

Kim NW, Piatyszek MA, Prowse KR, Harley CB, West MD, Ho PL, Coviello GM, Wright WE, Weinrich SL, Shay JW (1994) Specific association of human telomerase activity with immortal cells and cancer. *Science, 266*, 2011-5.

LaCava J, Houseley J, Saveanu C, Petfalski E, Thompson E, Jacquier A, Tollervey D (2005) RNA degradation by the exosome is promoted by a nuclear polyadenylation complex. *Cell, 121*, 713-724.

Larrivée M, LeBel C, Wellinger RJ (2004) The generation of proper constitutive G-tails on yeast telomeres is dependent on the MRX complex. *Genes Dev., 18*, 1391-1396.

Lazzaro F, Sapountzi V, Granata M, Pellicioli A, Vaze M, Haber JE, Plevani P, Lydall D, Muzi-Falconi M (2008) Histone methyltransferase Dot1 and Rad9 inhibit single-stranded DNA accumulation at DSBs and uncapped telomeres. *EMBO J., 27*, 1502-12.

Lazzerini Denchi E, de Lange T (2007) Protection of telomeres through independent control of ATM and ATR by TRF2 and POT1. *Nature, 448*, 1068-1071.

Lee SE, Moore JK, Holmes A, Umezu K, Kolodner RD, Haber JE (1998) Saccharomyces Ku70, Mre11/Rad50 and RPA proteins regulate adaptation to G2/M arrest after DNA damage. *Cell, 94*, 399-409.

Lee TI, Young RA (2013) Transcriptional regulation and its misregulation in disease. *Cell, 152*, 1237-1251.

Lew JE, Enomoto S, Berman J (1998) Telomere length regulation and telomeric chromatin require the nonsense-mediated mRNA decay pathway. *Mol. Cell. Biol., 18*, 6121-6130.

Lisby M, Barlow JH, Burgess RC, Rothstein R (2004) Choreography of the DNA damage response, spatiotemporal relationships among checkpoint and repair proteins. *Cell, 118*, 699-713.

Liu SW, Jiao X, Liu H, Gu M, Lima CD, Kiledjian M (2004) Functional analysis of mRNA scavenger decapping enzymes. *RNA, 10*, 1412-22.

Longhese MP, Bonetti D, Manfrini N, Clerici M (2010) Mechanisms and regulation of DNA end resection. *EMBO J., 29*, 2864-2874.

Luke B, Panza A, Redon S, Iglesias N, Li Z, Lingner J (2008) The Rat1p 5' to 3' exonuclease degrades telomeric repeat-containing RNA and promotes telomere elongation in *Saccharomyces cerevisiae*. *Mol. Cell, 32*, 465-77.

Luna R, Jimeno S, Marín M, Huertas P, García-Rubio M, Aguilera A (2005) Interdependence between transcription and mRNP processing and export, and its impact on genetic stability. *Mol. Cell, 18*, 711-722.

Lundblad V, Szostak JW (1989) A mutant with a defect in telomere elongation leads to senescence in yeast. *Cell, 57*, 633-43.

Lydall D, Weinert T (1995) Yeast checkpoint genes in DNA damage processing: implications for repair and arrest. *Science, 270*, 1488-1491.

Majka J, Niedziela-Majka A, Burgers PM (2006) The checkpoint clamp activates Mec1 kinase during initiation of the DNA damage checkpoint. *Mol. Cell, 24*, 891-901.

Makarov VL, Hirose Y, Langmore JP (1997) Long G tails at both ends of human chromosomes suggest a C-strand degradation mechanism for telomere shortening. *Cell, 88*, 657-66.

Malkova A, Ira G (2013) Break-induced replication: functions and molecular mechanism. *Curr. Opin. Genet. Dev., 23*, 271-279.

Mantiero D, Clerici M, Lucchini G, Longhese MP (2007) Dual role for *Saccharomyces cerevisiae* Tel1 in the checkpoint response to double-strand breaks. *EMBO Rep., 8*, 380-387.

Marcand S, Pardo B, Gratias A, Cahun S, Callebaut I (2008) Multiple pathways inhibit NHEJ at telomeres. *Genes Dev., 22*, 1153-8.

Maringele L, Lydall D (2002) *EXO1*-dependent single-stranded DNA at telomeres activates subsets of DNA damage and spindle checkpoint pathways in budding yeast *yku70*Δ mutants. *Genes Dev., 16*, 1919-1933.

Marin-Vicente C, Domingo-Prim J, Eberle AB, Visa N (2015) RRP6/EXOSC10 is required for the repair of DNA double-strand breaks by homologous recombination. *J. Cell Sci., 128*, 1097-1107.

Mathiasen DP, Lisby M (2014) Cell cycle regulation of homologous recombination in *Saccharomyces cerevisiae*. *FEMS Microbiol. Rev., 38*, 172-184.

McGee JS, Phillips JA, Chan A, Sabourin M, Paeschke K, Zakian VA (2010) Reduced Rif2 and lack of Mec1 target short telomeres for elongation rather than double-strand break repair. *Nat. Struct. Mol. Biol., 17*, 1438-1445.

Mehta A, Haber JE (2014) Sources of DNA double-strand breaks and models of recombinational DNA repair. *Cold Spring Harb. Perspect. Biol., 6*, a016428.

Mimitou EP, Symington LS (2008) Sae2, Exo1 and Sgs1 collaborate in DNA double-strand break processing. *Nature, 455*, 770-774.

Mimitou EP, Symington LS (2010) Ku prevents Exo1 and Sgs1dependent resection of DNA ends in the absence of a functional MRX complex or Sae2. *EMBO J., 29*, 3358-3369.

Muhlrad D, Parker R (2005) The yeast EDC1 mRNA undergoes deadenylation-independent decapping stimulated by Not2p, Not4p, and Not5p. *EMBO J., 24*, 1033-1045.

Nagarajan VK, Jones CI, Newbury SF, Green PJ (2013) XRN 5'-3' exoribonucleases: structure, mechanisms and functions. *Biochim. Biophys. Acta, 1829*, 590-603.

Nakada D, Matsumoto K, Sugimoto K (2003) ATM-related Tel1 associates with double-strand breaks through an Xrs2-dependent mechanism. *Genes Dev., 17*, 1957-1962.

Nimonkar AV, Genschel J, Kinoshita E, Polaczek P, Campbell JL, Wyman C, Modrich P, Kowalczykowski SC (2011) BLM-DNA2-RPA-MRN and EXO1-BLM-RPA-MRN constitute two DNA end resection machineries for human DNA break repair. *Genes Dev., 25*, 350-362.

Nugent CI, Hughes TR, Lue NF, Lundblad V (1996) Cdc13p: a single-strand telomeric DNA-binding protein with a dual role in yeast telomere maintenance. *Science, 274*, 249-252.

Ormo M, Cubitt AB, Kallio K, Gross LA, Tsien RY, Remington SJ (1996) Crystal structure of the Aequorea victoria green fluorescent protein. *Science, 273*, 1392-1395.

Page AM, Davis K, Molineux C, Kolodner RD, Johnson AW (1998) Mutational analysis of exoribonuclease I from *Saccharomyces cerevisiae*. *Nucleic Acids Res., 26*, 3707-3716.

Palmbos PL, Wu D, Daley JN, Wilson TE (2008) Recruitment of *Saccharomyces cerevisiae* Dnl4-Lif1 complex to a double-strand break requires interactions with Yku80 and the Xrs2 FHA domain. *Genetics, 180*, 1809-1819.

Pâques F, Leung WY, Haber JE (1998) Expansions and contractions in a tandem repeat induced by double-strand break repair. *Mol. Cell. Biol., 18*, 2045-2054.

Parker R (2012) RNA degradation in *Saccharomyces cerevisae*. *Genetics, 191*, 671-702.

Paull TT, Gellert M (1998) The 3’ to 5’ exonuclease activity of Mre11 facilitates repair of DNA double-strand breaks. *Mol. Cell, 1*, 969-979.

Peccarelli M, Kebaara BW (2014) Regulation of natural mRNAs by the nonsense-mediated mRNA decay pathway. *Eukaryot. Cell, 13*, 1126-35.

Pefanis E, Wang J, Rothschild G, Lim J, Chao J, Rabadan R, Economides AN, Basu U (2014) Noncoding RNA transcription targets AID to divergently transcribed loci in B cells. Nature, 514, 389-393.

Pellicioli A, Foiani M (2005) Signal transduction: how Rad53 kinase is activated. *Curr. Biol., 15*, R769-71.

Pennock E, Buckley K, Lundblad V (2001) Cdc13 delivers separate complexes to the telomere for end protection and replication. *Cell, 104*, 387-396.

Petreaca RC, Chiu HC, Nugent CI (2007) The role of Stn1p in *Saccharomyces cerevisiae* telomere capping can be separated from its interaction with Cdc13p. *Genetics, 177*, 1459-1474.

Pfeiffer V, Lingner J (2012) TERRA promotes telomere shortening through exonuclease 1-mediated resection of chromosome ends. *PLoS Genet., 8*, e1002747.

Pfeiffer V, Lingner J (2013) Replication of telomeres and the regulation of telomerase. *Cold Spring Harb. Perspect. Biol., 5*, a010405.

Pileur F, Andreola ML, Dausse E, Michel J, Moreau S, Yamada H, Gaidamakov SA, Crouch RJ, Toulmé JJ, Cazenave C (2003) Selective

inhibitory DNA aptamers of the human RNase H1. *Nucleic Acids Res., 31*, 5776-88.

Popp MW, Maquat LE (2013) Organizing principles of mammalian nonsense-mediated mRNA decay. *Annu. Rev. Genet., 47*, 139-165.

Price CM, Boltz KA, Chaiken MF, Stewart JA, Beilstein MA, Shippen DE (2010) Evolution of CST function in telomere maintenance. *Cell Cycle, 9*, 3157-3165.

Puglisi A, Bianchi A, Lemmens L, Damay P, Shore D (2008) Distinct roles for yeast Stn1 in telomere capping and telomerase inhibition. *EMBO J., 27*, 2328-2339.

Putnam CD, Jaehnig EJ, Kolodner RD (2009) Perspectives on the DNA damage and replication checkpoint responses in *Saccharomyces cerevisiae*. *DNA Repair (Amst), 8*, 974-82.

Qi H, Zakian VA (2000) The *Saccharomyces* telomere-binding protein Cdc13p interacts with both the catalytic subunit of DNA polymerase alpha and the telomerase-associated est1 protein. *Genes Dev., 14*, 1777-1788.

Ribeyre C, Shore D (2012) Anticheckpoint pathways at telomeres in yeast. *Nat. Struct. Mol. Biol., 19*, 307-313.

Richard P, Feng S, Manley JL (2013) A SUMO-dependent interaction between Senataxin and the exosome, disrupted in the

neurodegenerative disease AOA2, targets the exosome to sites of transcription-induced DNA damage. *Genes Dev., 27*, 2227-32.

Sabourin M, Tuzon CT, Zakian VA (2007) Telomerase and Tel1p preferentially associate with short telomeres in *S. cerevisiae*. *Mol. Cell, 27*, 550-561.

Sadoff BU, Heath-Pagliuso S, Castaño IB, Zhu Y, Kieff FS, Christman MF (1995) Isolation of mutants of Saccharomyces cerevisiae requiring DNA topoisomerase I. *Genetics, 141*, 465-479.

Saponaro M, Callahan D, Zheng X, Krejci L, Haber JE, Klein HL, Liberi G (2010) Cdk1 targets Srs2 to complete synthesis-dependent strand annealing and to promote recombinational repair. *PLoS Genet., 6*, e1000858.

Sartori AA, Lukas C, Coates J, Mistrik M, Fu S, Bartek J, Baer R, Lukas J, Jackson SP (2007) Human CtIP promotes DNA end resection, *Nature, 450*, 509-514.

Seeber A, Hauer M, Gasser SM (2013) Nucleosome remodelers in double-strand break repair. *Curr. Opin. Genet. Dev., 23*, 174-184.

Segurado M, Tercero JA (2009) The S-phase checkpoint: targeting the replication fork. *Biol. Cell, 101*, 617-27.

Sfeir A, de Lange T (2012) Removal of shelterin reveals the telomere end-protection problem. *Science, 336*, 593-597.

Sfeir A, Kabir S, van Overbeek M, Celli GB, de Lange T (2010) Loss of Rap1 induces telomere recombination in the absence of NHEJ or a DNA damage signal. *Science, 327*, 1657-1661.

Shi T, Bunker RD, Mattarocci S, Ribeyre C, Faty M, Gut H, Scrima A, Rass U, Rubin SM, Shore D, Thomä NH (2013) Rif1 and Rif2 shape telomere function and architecture through multivalent Rap1 interactions. *Cell, 153*, 1340-1353.

Shim EY, Chung WH, Nicolette ML, Zhang Y, Davis M, Zhu Z, Paull TT, Ira G, Lee SE (2010) Saccharomyces cerevisiae Mre11/Rad50/Xrs2 and Ku proteins regulate association of Exo1 and Dna2 with DNA breaks. *EMBO J., 29*, 3370- 3380.

Shiotani B, Zou L (2009) Single-stranded DNA orchestrates an ATM-to-ATR switch at DNA breaks. *Mol. Cell, 33*, 547-558.

Shukla S, Schmidt JC, Goldfarb KC, Cech TR, Parker R (2016) Inhibition of telomerase RNA decay rescues telomerase deficiency caused by dyskerin or PARN defects. *Nat. Struct. Mol. Biol., 23*, 286-292.

Siwaszek A, Ukleja M, Dziembowski A (2014) Proteins involved in the degradation of cytoplasmic mRNA in the major eukaryotic model systems. *RNA Biol., 11*, 1122-36.

Smith JS, Chen Q, Yatsunyk LA, Nicoludis JM, Garcia MS, Kranaster R, Balasubramanian S, Monchaud D, Teulade-Fichou MP, Abramowitz L, Schultz DC, Johnson FB (2011) Rudimentary G-quadruplex-based

telomere capping in *Saccharomyces cerevisiae*. *Nat. Struct. Mol. Biol., 18*, 478-485.

Soudet J, Jolivet P, Teixeira MT (2014) Elucidation of the DNA end-replication problem in *Saccharomyces cerevisiae*. *Mol. Cell, 53*, 954-964.

Sun J, Lee KJ, Davis AJ, Chen DJ (2012) Human Ku70/80 protein blocks exonuclease 1-mediated DNA resection in the presence of human Mre11 or Mre11/Rad50 protein complex. *J. Biol. Chem., 287*, 4936-45.

Symington LS, Gautier J (2011) Double-strand break end resection and repair pathway choice. *Annu. Rev. Genet., 45*, 247-71.

Takai H, Smogorzewska A, de Lange T (2003) DNA damage foci at dysfunctional telomeres. *Curr. Biol., 13*, 1549-56.

Tishkoff DX, Rockmill B, Roeder GS, Kolodner RD (1995) The sep1 mutant of Saccharomyces cerevisiae arrests in pachytene and is deficient in meiotic recombination. *Genetics, 139*, 495- 509.

Tomecki R, Dziembowski A (2010) Novel endoribonucleases as central players in various pathways of eukaryotic RNA metabolism. *RNA, 16*, 1692–724.

Tran PT, Erdeniz N, Dudley S, Liskay RM (2002) Characterization of nuclease-dependent functions of Exo1p in *Saccharomyces cerevisiae*. *DNA Repair (Amst), 1*, 895-912.

Trujillo KM, Yuan SS, Lee EY, Sung P (1998) Nuclease activities in a complex of human recombination and DNA repair factors Rad50, Mre11, and p95. *J. Biol. Chem., 273*, 21447-50.

Tseng SF, Lin JJ, Teng SC (2006) The telomerase-recruitment domain of the telomere binding protein Cdc13 is regulated by Mec1p/Tel1p-dependent phosphorylation. *Nucleic Acids Res., 34*, 6327-6336.

Tsukamoto Y, Taggart AK, Zakian VA (2001) The role of the Mre11-Rad50-Xrs2 complex in telomerase- mediated lengthening of *Saccharomyces cerevisiae* telomeres. *Curr. Biol., 11*, 1328-1335.

Ungar L, Yosef N, Sela Y, Sharan R, Ruppin E, Kupiec M (2009) A genome-wide screen for essential yeast genes that affect telomere length maintenance. *Nucleic Acids Res., 37*, 3840-3849.

Valencia-Sanchez MA, Liu J, Hannon GJ, Parker R (2006) Control of translation and mRNA degradation by miRNAs and siRNAs. *Genes Dev., 20*, 515–524.

van Dijk EL, Chen CL, d'Aubenton-Carafa Y, Gourvennec S, Kwapisz M, Roche V, Bertrand C, Silvain M, Legoix-Né P, Loeillet S, Nicolas A, Thermes C, Morillon A (2011) XUTs are a class of Xrn1-sensitive antisense regulatory non-coding RNA in yeast. *Nature, 475*, 114-117.

Van Overbeek M, de Lange T (2006) Apollo, an Artemis-related nuclease, interacts with TRF2 and protects human telomeres in S phase. *Curr. Biol., 16*, 1295-1302.

Villa M, Cassani C, Gobbini E, Bonetti D, Longhese MP (2016) Coupling end resection with the checkpoint response at DNA double-strand breaks. *Cell. Mol. Life Sci., 73*, 3655-3663.

Viscardi V, Bonetti D, Cartagena-Lirola H, Lucchini G, Longhese MP (2007) MRX-dependent DNA damage response to short telomeres. *Mol. Biol. Cell, 18*, 3047-3058.

Vodenicharov MD, Laterreur N, Wellinger RJ (2010) Telomere capping in non-dividing yeast cells requires Yku and Rap1. *EMBO J., 29*, 3007-19.

Vodenicharov MD, Wellinger RJ (2006) DNA degradation at unprotected telomeres in yeast is regulated by the CDK1 (Cdc28/Clb) cell-cycle kinase. *Mol. Cell, 24*, 127-137.

Wahba L, Gore SK, Koshland D (2013) The homologous recombination machinery modulates the formation of RNA-DNA hybrids and associated chromosome instability. Elife, 2, e00505.

Webb CJ, Wu Y, Zakian VA (2013) DNA repair at telomeres: keeping the ends intact. *Cold Spring Harb. Perspect. Biol., 5*, a012666.

Wei W, Ba Z, Gao M, Wu Y, Ma Y, Amiard S, White CI, Rendtlew Danielsen JM, Yang YG, Qi Y (2012) A role for small RNAs in DNA double-strand break repair. *Cell, 149*, 101-112.

Wellinger RJ, Ethier K, Labrecque P, Zakian VA (1996) Evidence for a new step in telomere maintenance. *Cell, 85*, 423-433.

Wellinger RJ, Wolf AJ, Zakian VA (1993) *Saccharomyces* telomeres acquire single-strand TG_{1-3} tails late in S phase. *Cell, 72*, 51-60.

Wellinger RJ, Zakian VA (2012) Everything you ever wanted to know about *Saccharomyces cerevisiae* telomeres: beginning to end. *Genetics, 191*, 1073-1105.

Wu D, Tooper LM, Wilson TE (2008) Recruitment and dissociation of nonhomologous end joining proteins at a DNA double-strand break in *Saccharomyces cerevisiae*. *Genetics, 178*, 1237-1249.

Wu L, Multani AS, He H, Cosme-Blanco W, Deng Y, Deng JM, Bachilo O, Pathak S, Tahara H, Bailey SM, Deng Y, Behringer RR, Chang S (2006) Pot1 deficiency initiates DNA damage checkpoint activation and aberrant homologous recombination at telomeres. *Cell, 126*, 49-62.

Wu P, Takai H, de Lange T (2012) Telomeric 3' overhangs derive from resection by Exo1 and Apollo and fill-in by POT1b-associated CST. *Cell, 150*, 39-52.

Wu Y, DiMaggio PA Jr, Perlman DH, Zakian VA, Garcia BA (2013) Novel phosphorylation sites in the *S. cerevisiae* Cdc13 protein reveal new targets for telomere length regulation. *J. Proteome Res., 12*, 316-327.

Wyatt HDM, West SC (2014) Holliday junction resolvases. *Cold Spring Harb. Perspect. Biol., 6*, a023192.

Xu L, Petreaca RC, Gasparyan HJ, Vu S, Nugent CI (2009) *TEN1* is essential for *CDC13*-mediated telomere capping. *Genetics, 183*, 793-810.

Xue Y, Rushton MD, Maringele L (2011) A novel checkpoint and RPA inhibitory pathway regulated by Rif1. *PLoS Genet., 7*, e1002417.

Yu TY, Kao YW, Lin JJ (2014) Telomeric transcripts stimulate telomere recombination to suppress senescence in cells lacking telomerase. *Proc. Natl. Acad. Sci. USA, 111*, 3377-3382.

Zhang K, Dion N, Fuchs B, Damron T, Gitelis S, Irwin R, O'Connor M, Schwartz H, Scully SP, Rock MG, Bolander ME, Sarkar G (2002) The human homolog of yeast SEP1 is a novel candidate tumor suppressor gene in osteogenic sarcoma, *Gene, 298*, 121-7.

Zhu Z, Chung WH, Shim EY, Lee SE, Ira G (2008) Sgs1 helicase and two nucleases Dna2 and Exo1 resect DNA double-strand break ends. *Cell, 134*, 981-994.

Zou L, Elledge SJ (2003) Sensing DNA damage through ATRIP recognition of RPA-ssDNA complexes. *Science, 300*, 1542-1548.

Zubko MK, Guillard S, Lydall D (2004) Exo1 and Rad24 differentially regulate generation of ssDNA at telomeres of *Saccharomyces cerevisiae cdc13-1* mutants. *Genetics, 168*, 103-115.

Scientific Report

SOURCE DATA | TRANSPARENT PROCESS

EMBO reports

RNA-processing proteins regulate Mec1/ATR activation by promoting generation of RPA-coated ssDNA

Nicola Manfrini[1], Camilla Trovesi[1], Maxime Wery[2], Marina Martina[1], Daniele Cesena[1], Marc Descrimes[2], Antonin Morillon[2,*], Fabrizio d'Adda di Fagagna[3,4,**] & Maria P Longhese[1,***]

Abstract

Eukaryotic cells respond to DNA double-strand breaks (DSBs) by activating a checkpoint that depends on the protein kinases Tel1/ATM and Mec1/ATR. Mec1/ATR is activated by RPA-coated single-stranded DNA (ssDNA), which arises upon nucleolytic degradation (resection) of the DSB. Emerging evidences indicate that RNA-processing factors play critical, yet poorly understood, roles in genomic stability. Here, we provide evidence that the *Saccharomyces cerevisiae* RNA decay factors Xrn1, Rrp6 and Trf4 regulate Mec1/ATR activation by promoting generation of RPA-coated ssDNA. The lack of Xrn1 inhibits ssDNA generation at the DSB by preventing the loading of the MRX complex. By contrast, DSB resection is not affected in the absence of Rrp6 or Trf4, but their lack impairs the recruitment of RPA, and therefore of Mec1, to the DSB. Rrp6 and Trf4 inactivation affects neither Rad51/Rad52 association nor DSB repair by homologous recombination (HR), suggesting that full Mec1 activation requires higher amount of RPA-coated ssDNA than HR-mediated repair. Noteworthy, deep transcriptome analyses do not identify common misregulated gene expression that could explain the observed phenotypes. Our results provide a novel link between RNA processing and genome stability.

Keywords DNA damage checkpoint; DNA double-strand breaks; Rrp6; Trf4; Xrn1

Subject Categories DNA Replication, Repair & Recombination; RNA Biology

DOI 10.15252/embr.201439458 | Received 18 August 2014 | Revised 21 November 2014 | Accepted 24 November 2014

Introduction

DNA double-strand breaks (DSBs) undergo 5′–3′ nucleolytic degradation (resection) of their 5′-ending strands, to generate 3′-ended ssDNA overhangs, which are bound by the RPA complex [1]. RPA-coated ssDNA enables the checkpoint kinase Mec1/ATR to recognize DSBs [2] and facilitates the formation of continuous Rad51 filaments that initiate homologous recombination (HR) [3]. DSB resection is initiated by the MRX (Mre11-Rad50-Xrs2)/MRN (Mre11-Rad50-Nbs1) complex that acts in concert with Sae2/CtIP [4–6]. Subsequent long-range resection of the 5′ strand can occur by one of two pathways that depend on either the 5′–3′ exonuclease Exo1/hEXO1 or the Sgs1/BLM helicase in conjunction with the nuclease Dna2/hDNA2 [5,6].

Recent data indicate that RNA-processing proteins contribute to maintain genome stability either by controlling the turnover of specific transcripts or preventing accumulation of harmful DNA:RNA hybrids [7]. RNA processing can be directly involved in the DNA damage response (DDR), as some endoribonucleases have been implicated in the formation around the DSB of small non-coding RNAs that control DDR activation in both mammals and *Arabidopsis* [8,9]. Furthermore, in mammals, the endoribonuclease Ago2 facilitates the recruitment of the recombination protein Rad51 to the DSB ends [10], while the exosome recruits the activation-induced cytidine deaminase (AID) to ssDNA regions generated at divergently transcribed loci in B cells [11].

In *Saccharomyces cerevisiae*, RNA processing relies on a 5′–3′ exoribonuclease activity that is due to the Xrn protein family, which comprises one cytoplasmic (Xrn1) and one nuclear enzyme (Rat1) [12]. The nuclear exosome, whose activity is modulated by a set of cofactors including the poly(A) polymerase Trf4, is responsible for the 3′–5′ RNA-processing activity, which depends on the exoribonuclease Rrp6 [13]. Xrn1, Rrp6 and Trf4 have been shown to prevent DNA:RNA hybrid-mediated genome instability and transcription-associated hyperrecombination [14–16]. Furthermore, the lack of Trf4 leads to sensitivity to camptothecin [17], while *XRN1* deletion impairs meiotic recombination [18]. However, the precise DNA maintenance mechanisms involving these RNA decay factors remain poorly characterized. Here, we show that Xrn1, Rrp6 and

1 Dipartimento di Biotecnologie e Bioscienze, Università di Milano-Bicocca, Milan, Italy
2 Institut Curie, CNRS UMR3244, Université Pierre et Marie Curie, Paris Cedex 05, France
3 IFOM Foundation-FIRC Institute of Molecular Oncology Foundation, Milan, Italy
4 Istituto di Genetica Molecolare, Consiglio Nazionale delle Ricerche, Pavia, Italy
*Corresponding author. Tel: +33 156246570; Fax: +33 156246674; E-mail: antonin.morillon@curie.fr
**Corresponding author. Tel: +39 02574303227; Fax: +39 02574303231; E-mail: fabrizio.dadda@ifom.eu
***Corresponding author. Tel: +39 0264483425; Fax: +39 0264483565; E-mail: mariapia.longhese@unimib.it

Trf4 participate in the activation of the checkpoint kinase Mec1 by promoting the formation of RPA-coated ssDNA at DSB ends. These findings reveal a novel role for RNA decay factors in the maintenance of genome integrity.

Results and Discussion

Xrn1, Rrp6 and Trf4 are necessary for Mec1/ATR activation in response to a DSB

To investigate the role of Xrn1, Rrp6 and Trf4 in the DDR, yeast strains carrying the deletion of the corresponding genes were tested for sensitivity to DNA damaging agents. The *xrn1*Δ, *rrp6*Δ and *trf4*Δ mutants were hypersensitive to the DSB-inducing agent phleomycin, with *xrn1*Δ cells showing the strongest sensitivity (Fig 1A), suggesting that the corresponding proteins are involved, directly or indirectly, in the cellular response to DSBs.

Next, we asked whether *xrn1*Δ, *rrp6*Δ and *trf4*Δ cells were defective in checkpoint activation in response to a single DSB. To address this question, we deleted *XRN1*, *RRP6* or *TRF4* in a haploid strain carrying the *HO* gene under the control of a galactose-inducible promoter. In this strain, induction of HO by galactose addition leads to the generation at the *MAT* locus of a single DSB that cannot be repaired by HR due to the lack of the homologous donor loci *HML* and *HMR* [19]. *HO* expression was induced by transferring to galactose wild-type, *xrn1*Δ, *rrp6*Δ and *trf4*Δ cells exponentially growing in raffinose. Checkpoint activation was monitored by following Rad53 phosphorylation, which is required for Rad53 activation and is detectable as a decrease of its electrophoretic mobility. As shown in Fig 1B, the amount of phosphorylated Rad53 after HO induction was much lower in *xrn1*Δ, *rrp6*Δ and *trf4*Δ than in wild-type cells. Furthermore, when the same strains were arrested in G1 with α-factor and then spotted on galactose-containing plates to induce HO, *xrn1*Δ, *rrp6*Δ and *trf4*Δ cells formed microcolonies with more than 2 cells more efficiently than similarly treated wild-type cells (Fig 1C), indicating a defect in DSB-induced cell cycle arrest. Although *xrn1*Δ, *rrp6*Δ and *trf4*Δ cells slightly delayed the G1/S transition under unperturbed conditions (Fig 1D), their checkpoint defect was not due to altered cell cycle progression, as *xrn1*Δ, *rrp6*Δ and *trf4*Δ were defective in Rad53 phosphorylation also when the HO cut was induced in G2-arrested cells that were kept arrested in G2 throughout the experiment (Fig 1E).

The requirement of Xrn1, Rrp6 and Trf4 for DSB-induced checkpoint activation was not locus specific, as *xrn1*Δ, *rrp6*Δ and *trf4*Δ cells were defective in Rad53 phosphorylation also when the HO-induced DSB was generated at the *LEU2* locus (Fig 1F). Neither it was influenced by the level of transcription of the DNA region in which the DSB occurs, as the amount of Rad53 phosphorylation in wild-type, *xrn1*Δ, *rrp6*Δ and *trf4*Δ cells after HO-induced DSB formation into the *LEU2* gene was similar to that detected when the DSB was generated into the *LEU2* gene lacking its promoter (Supplementary Fig S1).

Xrn1 and Rrp6 promote checkpoint activation by acting as exoribonucleases. In fact, cells carrying the *xrn1-E176G* or the *rrp6-D238A* allele, encoding nuclease-defective Xrn1 [20] or Rrp6 [21] variants, were as defective in HO-induced Rad53 phosphorylation as *xrn1*Δ and *rrp6*Δ cells, respectively (Fig 1G).

In *S. cerevisiae*, checkpoint activation in response to a single DSB is completely dependent on Mec1 [22], suggesting that *xrn1*Δ, *rrp6*Δ and *trf4*Δ cells might be defective in Mec1 activation. Indeed, *xrn1*Δ, *rrp6*Δ and *trf4*Δ cells were defective in phosphorylation of the Mec1 specific target Ddc2 after HO induction (Fig 1H), indicating that the lack of Xrn1, Rrp6 or Trf4 impairs Mec1 signaling activity.

Xrn1 promotes resection of DNA ends

While Xrn1 controls cytoplasmic RNA decay, RNA processing into the nucleus depends on its nuclear paralog Rat1 [23]. Targeting Rat1 into the cytoplasm by deleting its nuclear localization sequence (*rat1-ΔNLS*) restores Xrn1-like function in mRNA degradation [23], prompting us to test whether it could restore Rad53 phosphorylation after DSB formation in *xrn1*Δ cells. Strikingly, expression of the *rat1-ΔNLS* allele on a centromeric plasmid, but not of wild-type *RAT1*, suppressed both the Rad53 phosphorylation defect (Fig 2A) and the hypersensitivity to phleomycin (Fig 2B) of *xrn1*Δ cells, indicating that Xrn1 controls checkpoint activation by acting in the cytoplasm.

Mec1 activation requires formation of RPA-coated ssDNA, which arises from 5′ to 3′ nucleolytic degradation of the DSB ends [2]. To assess whether the inability of *xrn1*Δ cells to activate Mec1/ATR

Figure 1. The lack of Xrn1, Rrp6 or Trf4 impairs Mec1 checkpoint signaling in response to a DSB.

A Sensitivity to phleomycin. Serial dilutions (1:10) of exponentially growing cell cultures were spotted out onto YEPD plates with or without phleomycin (phleo).

B Rad53 phosphorylation after a DSB at the *MAT* locus. YEPR exponentially growing cell cultures of JKM139 derivative strains, carrying the HO cut site at the *MAT* locus, were transferred to YEPRG at time zero. Protein extracts from samples taken at the indicated times after HO induction were subjected to Western blot analysis with anti-Rad53 antibodies.

C Checkpoint-mediated cell cycle arrest. G1-arrested JKM139 derivative cells were plated on galactose-containing plates at time zero. Two hundred cells for each strain were analyzed to determine the frequency of cells that were unbudded, large budded or forming microcolonies with more than two cells.

D Analysis of cell cycle progression in unperturbed conditions. Cell cultures arrested in G1 with α-factor were released into YEPD at time zero. FACS analysis of DNA content.

E Checkpoint activation in G2-arrested cells. As in (B) except that HO was induced in nocodazole-arrested JKM139 derivative cells that were kept arrested in G2 in the presence of nocodazole throughout the experiment.

F Rad53 phosphorylation after a DSB at the *LEU2* locus. As in (B), but inducing HO expression in YFP17 derivative strains, which carry the HO cut site at the *LEU2* locus.

G Checkpoint activation. Protein extracts from JKM139 derivative strains containing the indicated centromeric plasmids were subjected to Western blot analysis with anti-Rad53 antibodies at different time points after HO induction.

H Ddc2 phosphorylation after a DSB at the *MAT* locus. Protein extracts from JKM139 derivative strains expressing fully functional Ddc2-HA were subjected to Western blot analysis with anti-HA antibodies at different time points after HO induction.

Source data are available online for this figure.

could be related to defects in DSB resection, we directly monitored ssDNA generation at the DSB ends. Cells exponentially growing in raffinose were transferred to galactose to induce HO and genomic DNA was analyzed at different time points after HO induction. Because ssDNA is resistant to cleavage by restriction enzymes, 5′ strand resection can be measured by following the loss of SspI restriction fragments by Southern blot analysis under alkaline conditions using a ssRNA probe that anneals to the unresected strand on

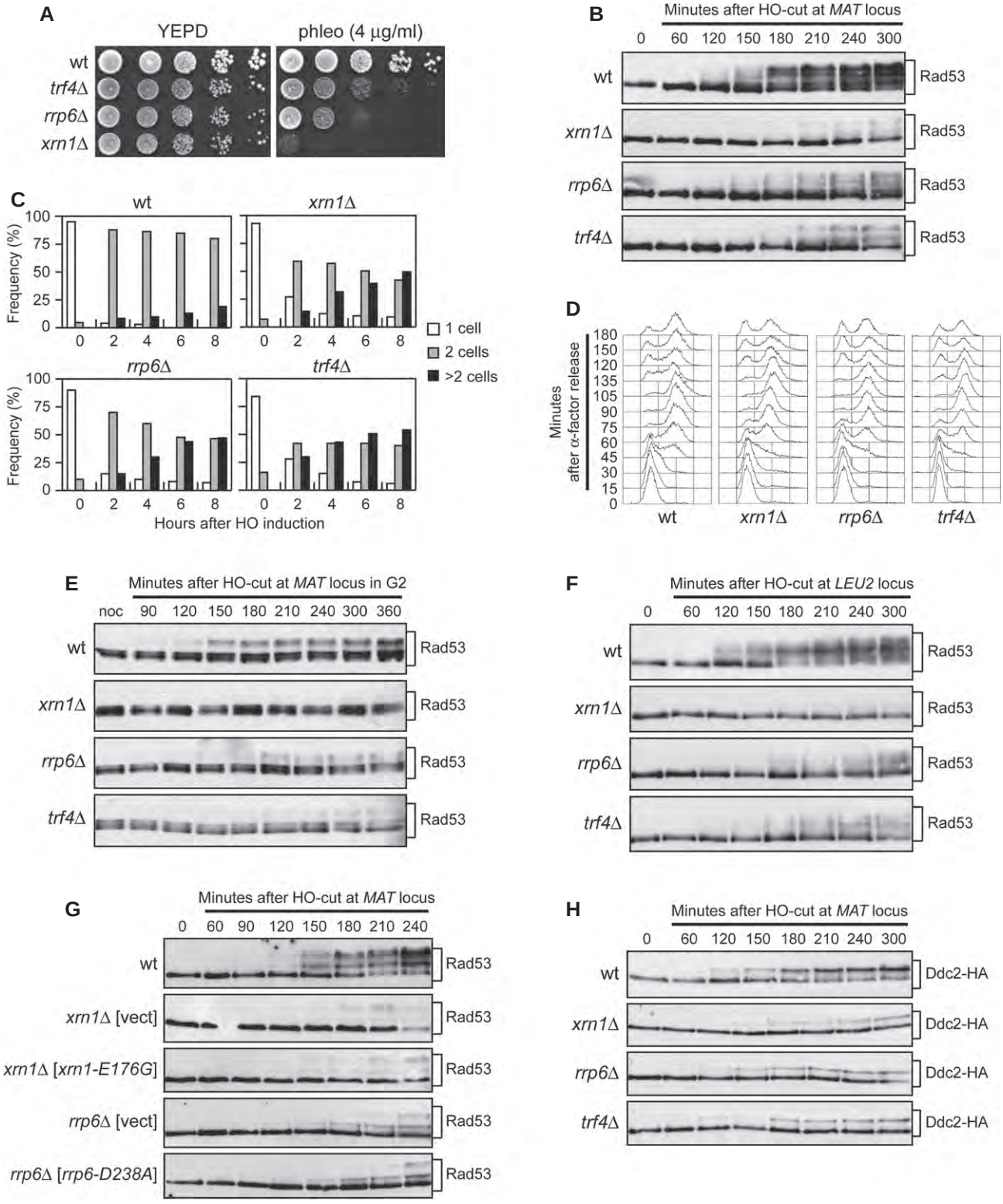

Figure 1.

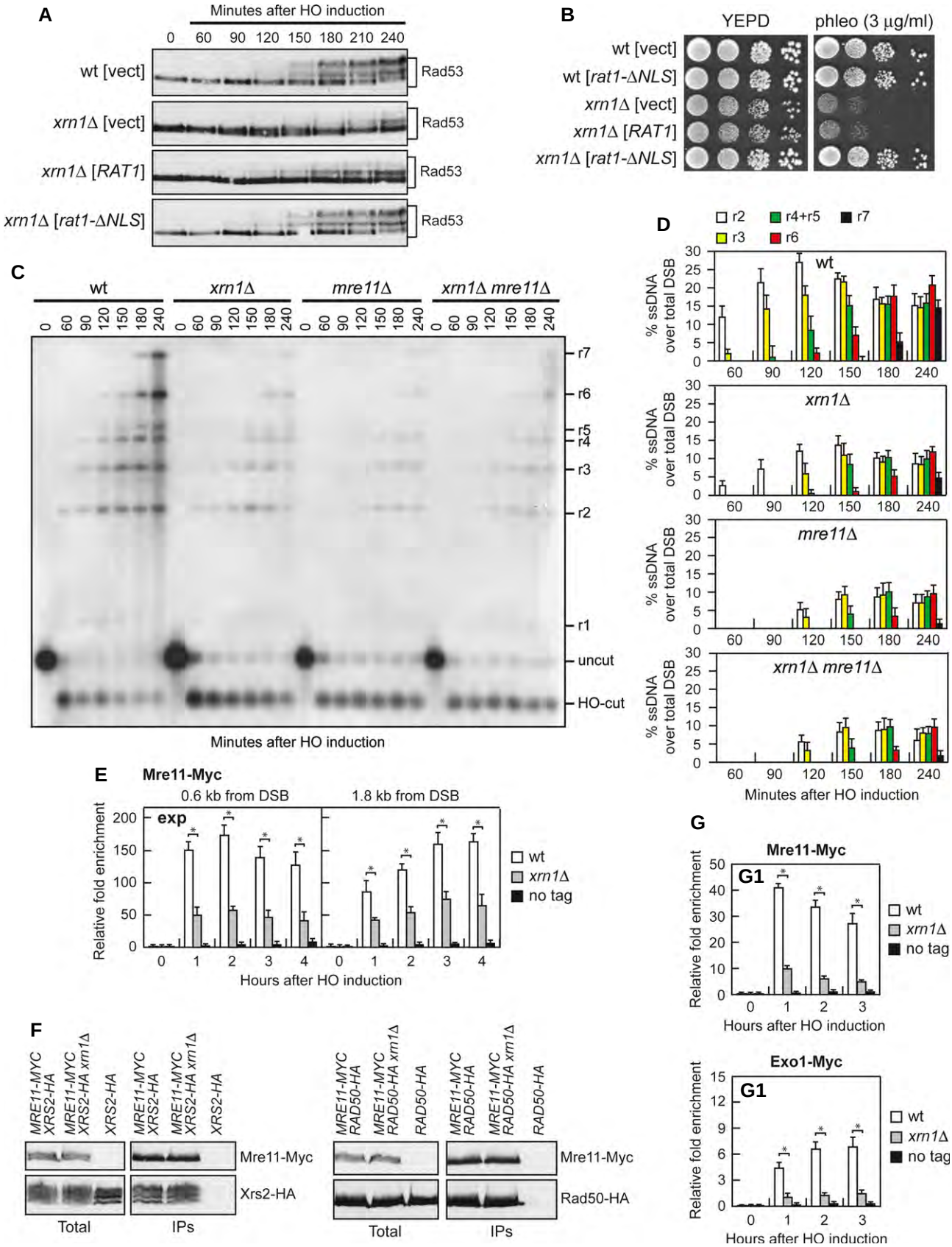

Figure 2.

Figure 2. The lack of Xrn1 impairs DSB resection and Mre11 recruitment to the DSB.

A Checkpoint activation. Protein extracts from JKM139 derivative strains containing the indicated centromeric plasmids were subjected to Western blot analysis with anti-Rad53 antibodies at different time points after HO induction.

B Sensitivity to phleomycin. Strains in (A) were serially diluted (1:10) and spotted out onto YEPD plates with or without phleomycin.

C DSB resection. YEPR exponentially growing cultures of JKM139 derivative cells were transferred to YEPRG at time zero. Gel blots of SspI-digested genomic DNA separated on alkaline agarose gel were hybridized with a single-stranded RNA probe that anneals to the unresected strand on one side of the break. 5′–3′ resection progressively eliminates SspI sites (S), producing larger SspI fragments (r1 through r7) detected by the probe.

D Densitometric analyses. The experiment as in (C) was independently repeated three times and the mean values are represented with error bars denoting SD ($n = 3$).

E Mre11-Myc recruitment at the HO-induced DSB. In all diagrams, data are expressed as fold enrichment at the HO-induced DSB over that at the non-cleaved *ARO1* locus, after normalization of ChIP signals to the corresponding input for each time point. The mean values are represented with error bars denoting SD ($n = 3$). *$P < 0.01$, *t*-test.

F MRX complex formation. Protein extracts were analyzed by Western blot with anti-Myc or anti-HA antibodies either directly (Total) or after Mre11-Myc immunoprecipitation (IPs) with anti-Myc antibodies.

G Mre11 recruitment at the HO-induced DSB in G1-arrested *xrn1*Δ cells. ChIP analysis was performed as in (E) except that HO was induced in α-factor-arrested JKM139 derivative cells kept arrested in G1 with α-factor throughout the experiment. qPCR was performed at 1.8 kb from the DSB. The mean values are represented with error bars denoting SD ($n = 3$). *$P < 0.01$, *t*-test.

Source data are available online for this figure.

one side of the break. The appearance of ssDNA intermediates was delayed in galactose-induced *xrn1*Δ cells compared to wild-type (Fig 2C and D), indicating that the lack of Xrn1 impairs generation of ssDNA at the DSB ends.

DSB resection is under the control of several proteins, which act as positive (Mre11, Rad50, Xrs2, Dna2, Sgs1 and Exo1) or negative (Rad9) regulators [1]. The resection defect of *xrn1*Δ was not due to lower amounts of the above proteins, as similar amounts of Mre11, Rad50, Xrs2, Sgs1, Exo1 and Rad9 proteins could be detected in both wild-type and *xrn1*Δ cells (Supplementary Fig S2). The amount of Dna2 was higher in *xrn1*Δ than in wild-type cells (Supplementary Fig S2), but this effect did not account by itself for the DSB resection defect of *xrn1*Δ cells, as *DNA2* overexpression did not affect either checkpoint activation or generation of ssDNA at the DSB ends in wild-type cells (data not shown).

Xrn1 supports MRX function in DSB resection

As the lack of Xrn1 impairs initiation of DSB processing, which is known to require the MRX complex, we investigated whether it might affect MRX function. Epistasis analysis revealed that DSB resection in the *xrn1*Δ *mre11*Δ double mutant was as defective as in the *mre11*Δ single mutant (Fig 2C and D), indicating that Xrn1 and MRX promote DSB resection by acting in the same pathway. Chromatin immunoprecipitation (ChIP) and quantitative real-time PCR showed that Mre11 association at the HO-induced DSB was lower in *xrn1*Δ than in wild-type cells (Fig 2E). This decreased binding was not due to lower Mre11 protein level (Supplementary Fig S2) or altered MRX complex formation (Fig 2F). Neither it was due to different resection kinetics, as the lack of Xrn1 impaired Mre11 recruitment even when the DSB was induced in G1-arrested cells (Fig 2G), where DSB resection is very poor due to low Cdk1 activity [24]. Consistent with MRX being required to load Exo1 and Dna2 at the DSB [25], Exo1 association at the HO-induced DSB was lower in *xrn1*Δ than in wild-type cells (Fig 2G), and similar results were obtained for Dna2 (data not shown). Thus, Xrn1 regulates DSB resection likely by promoting MRX recruitment to the DSB.

Rrp6 and Trf4 promote the loading of RPA and Mec1 to the DSB

Resection intermediates accumulated with wild-type kinetics in *rrp6*Δ and *trf4*Δ cells (Fig 3A and B), indicating that the defective checkpoint response in these mutants cannot be ascribed to reduced generation of ssDNA at the DSB. As Mec1 recognizes and is activated by RPA-coated ssDNA [2], the checkpoint defect of *rrp6*Δ and *trf4*Δ cells might be due to the inability of either Mec1 itself or RPA to bind ssDNA. Indeed, the lack of Rrp6 or Trf4 impaired Mec1 and Rpa1 association at the DSB (Fig 3C and D), although similar amounts of Mec1 (Fig 3E) and RPA complex (Fig 3F) can be detected in protein extracts from wild-type, *rrp6*Δ and *trf4*Δ cells. This decreased RPA recruitment to the DSB was not due to defects in either RPA complex formation (Fig 3G) or RPA sub-cellular localization (Supplementary Fig S3A). Thus, Rrp6 and Trf4 appear to regulate Mec1 activation by promoting association to the DSB ends of RPA, and therefore of Mec1.

Interestingly, Rrp6 and Trf4 promoted Mec1 activation not only in response to a HO-induced DSB, but also after treatment with methyl methane sulfonate (MMS) or hydroxyurea (HU) (Fig 3H), suggesting that they favor RPA loading also to the ssDNA generated during replicative stress.

Rrp6 and Trf4 are not required for HR repair of a DSB

After covering ssDNA, RPA is displaced by Rad51 [3]. Reduced RPA binding in *rrp6*Δ and *trf4*Δ cells was due to a less efficient RPA loading rather than to a more efficient RPA displacement by Rad51 and/or Rad52. In fact, RPA was still poorly recruited at the DSB ends in *rrp6*Δ and *trf4*Δ cells lacking either Rad51 or Rad52 (Fig 4A).

As RPA promotes localization of the recombination proteins Rad51 and Rad52 to initiate DSB repair by HR [26], the lack of Rrp6 and/or Trf4 may affect the loading of Rad51 and/or Rad52 on the DSB. This does not seem to be the case, as similar amounts of Rad51 and Rad52 were detected in wild-type, *rrp6*Δ and *trf4*Δ cells, both in total protein extracts (Fig 4B) and bound at the DSB (Fig 4C and D).

Rad51-dependent recombination leads to the formation of noncrossover or crossover products. We analyzed the formation of such recombination products using a haploid strain that bears a *MATa* sequence on chromosome V and an uncleavable *MATa-inc* sequence on chromosome III [27]. Upon galactose addition, the HO-induced DSB can be repaired using the *MATa-inc* sequence as a donor, resulting in crossover and non-crossover products (Fig 4E). Consistent with the finding that the lack of Rrp6 did not impair Rad51 and Rad52 loading at the DSB, the overall DSB repair

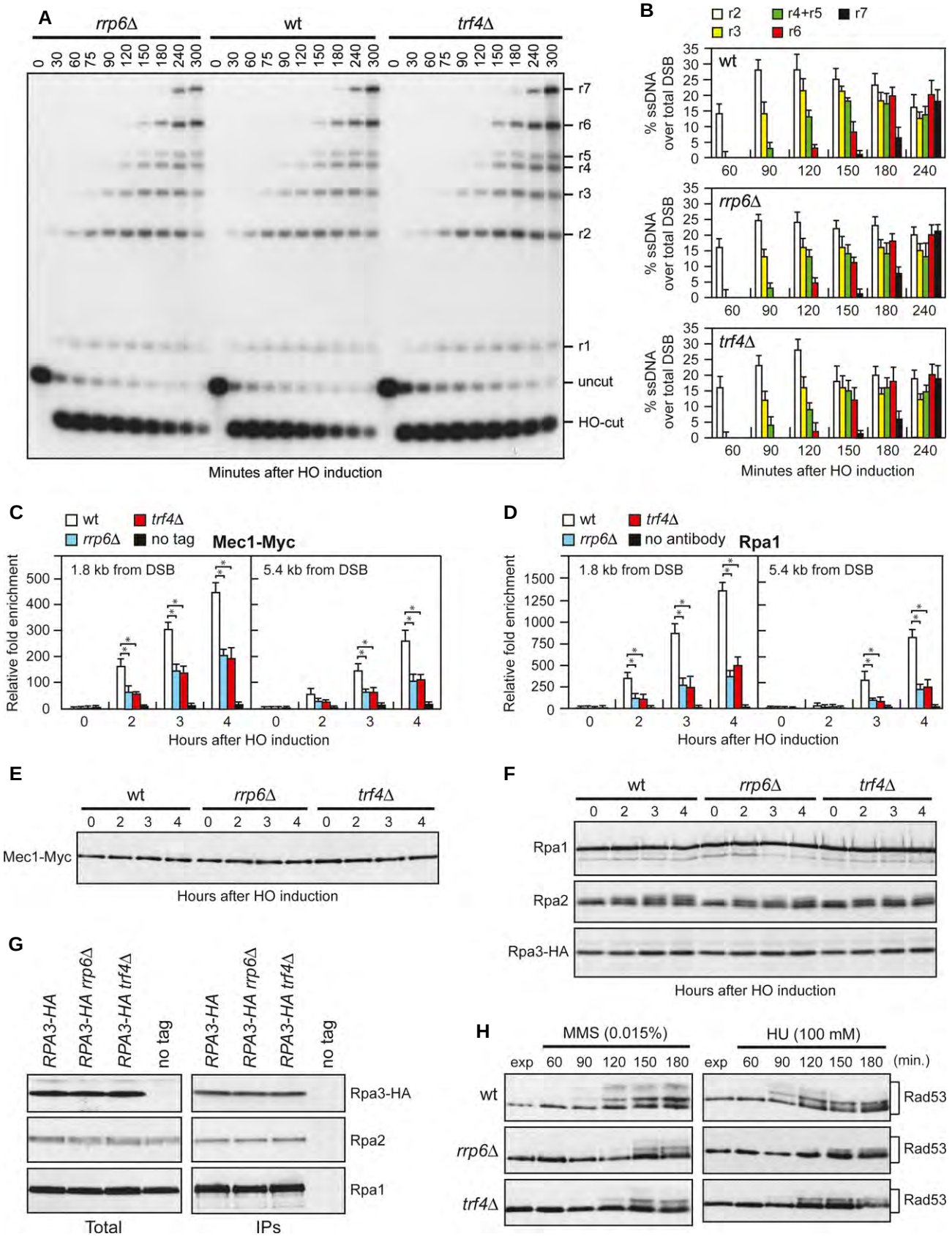

Figure 3.

Figure 3. The lack of Rrp6 or Trf4 impairs RPA and Mec1 recruitment to the DSB without affecting DSB resection.

A DSB resection. Genomic DNA was analyzed for ssDNA formation as described in Fig 2C.

B Densitometric analyses. The experiment as in (A) was independently repeated three times and the mean values are represented with error bars denoting SD (n = 3).

C Mec1-Myc recruitment at the HO-induced DSB. In all diagrams, data are expressed as fold enrichment at the HO-induced DSB over that at the non-cleaved *ARO1* locus, after normalization of ChIP signals to the corresponding input for each time point. The mean values are represented with error bars denoting SD (n = 3). *$P < 0.01$, t-test.

D Rpa1 recruitment at the HO-induced DSB. ChIP analysis was performed as in (C). The mean values are represented with error bars denoting SD (n = 3). *$P < 0.01$, t-test.

E Mec1 protein level. Western blot with anti-Myc antibodies of extracts used for the ChIP analysis shown in (C).

F Rpa1, Rpa2 and Rpa3 protein levels. Western blot with anti-Rpa1, anti-Rpa2 and anti-HA antibodies of extracts used for the ChIP analysis in (D).

G RPA complex formation. Protein extracts were analyzed by Western blotting with anti-HA (Rpa3), anti-Rpa1 or anti-Rpa2 antibodies either directly (Total) or after Rpa3-HA immunoprecipitation (IPs) with anti-HA antibodies.

H Checkpoint activation in response to HU and MMS treatment. Western blot analysis with anti-Rad53 antibodies of protein extracts prepared from exponentially growing cells that were treated with HU or MMS for the indicated time points.

Source data are available online for this figure.

efficiency in *rrp6*Δ cells was similar to that observed in wild-type cells (Fig 4F and G). By contrast, DSB repair efficiency was reduced in *xrn1*Δ cells (Fig 4F and G), in agreement with the finding that these cells were defective in the generation of ssDNA (Fig 2C and D) that is necessary to catalyze strand invasion and base pairing. Therefore, the lack of Rrp6 or Trf4 appears to specifically impair the loading at the DSB ends of RPA, but not of Rad51 and Rad52.

The lack of Xrn1, Rrp6 or Trf4 does not affect expression of most DDR genes

As the lack of Xrn1 or Rrp6/Trf4 might influence the recruitment of MRX or RPA, respectively, by regulating gene expression, we performed deep transcriptome analyses before and after generation of the HO-induced DSB. Biological duplicates of cells exponentially growing in raffinose (time zero) were shifted to galactose for 60 and 240 min to induce HO, and total RNA was subjected to strand-specific whole transcriptome analysis. The vast majority of protein-coding genes in a wild-type context showed no significant change of expression 60 min (Spearman's correlation coefficient 0.98; Fig 5A) and 240 min (Spearman's correlation coefficient 0.95; Fig 5B) after HO induction. Expression of genes coding for factors involved in DDR (see list in Supplementary Table S1) also remained globally unchanged (Fig 5C and D), with 0.96–0.98 and 0.89–0.94 Spearman's correlation coefficients 60 min (Fig 5A) and 240 min (Fig 5B) after HO induction, respectively. Further differential expression analysis to obtain better statistical validation revealed that only 5 of 193 DDR genes were affected (fold change ≤ 0.5 or ≥ 2, $P \leq 0.001$) 240 min after HO induction (Supplementary Fig S4A and B, see list in Supplementary Table S2), indicating that the HO-induced DSB has little impact on the transcriptome.

When we performed similar analyses in strains lacking Xrn1, Rrp6 or Trf4, as previously reported [28], we observed that inactivation of Xrn1 resulted in global stabilization of mRNAs (Fig 5C and D; Supplementary Fig S4F). In contrast, mRNA levels in *rrp6*Δ and *trf4*Δ cells were similar to wild-type (Fig 5C and D, Supplementary Fig S4G and H). Importantly, in all tested strains and conditions, DDR genes showed expression similar to all genes (Fig 5D). Deeper differential expression analysis showed that the majority of DDR mRNAs remained unchanged (Fig 5C and Supplementary Fig S4C–E), although some of them were misregulated in these mutants (3 in *rrp6*Δ, 22 in *xrn1*Δ and 27 in *trf4*Δ, Supplementary Table S2). Further studies are required to assess whether these mRNA misregulations might account for the DSB resection defect of *xrn1*Δ cells, but the finding that Xrn1 acts in the checkpoint as a cytoplasmic exoribonuclease makes them potential candidates.

The only three genes (*SMC6*, *HPA2* and *RLF2*) that are downregulated in *rrp6*Δ cells are not affected in *trf4*Δ and vice versa (Supplementary Table S2), making it unlikely that these altered mRNA levels may account for the reduced recruitment of RPA to the ssDNA ends displayed by both *rrp6*Δ and *trf4*Δ cells. In addition, while *SMC6* is essential for cell viability, deletion of *RLF2*, which encodes the largest subunit of the Chromatin Assembly Factor CAF-1, or *HPA2*, which encodes a histone acetyltransferase, did not impair checkpoint activation in response to the HO-induced DSB [29, data not shown]. Of note, the lack of Trf4 increased the amount of mRNAs encoding histones H2A, H3 and H4 (Supplementary Table S2). However, these upregulations did not cause any increase of the corresponding protein levels (Supplementary Fig S3B), consistent with previous findings that RNA decay mutants accumulate mRNA intermediates that might not be efficiently translated [12,13].

In summary, our data show that Xrn1, Rrp6 and Trf4 proteins regulate Mec1 signaling activity by promoting formation of RPA-coated ssDNA at the DSB ends, thus linking RNA processing to the checkpoint response. While Xrn1 is required to generate ssDNA by promoting MRX recruitment to the DSB, Rrp6 and Trf4 are required to recruit RPA, and therefore Mec1/ATR, to the ssDNA ends. Although the amount of RPA recruited at the DSB in *rrp6*Δ and *trf4*Δ cells appears to be below the threshold necessary for full checkpoint activation, it is enough for Rad51 and Rad52 loading to the DSB and for subsequent HR repair. This finding suggests that full Mec1 activation requires a higher amount of RPA-coated ssDNA than HR-mediated repair events, thus ensuring checkpoint activation only when the DSB cannot be rapidly repaired. How Rrp6 and Trf4 control the association of RPA with ssDNA requires further studies. One possibility is that the lack of Rrp6 or Trf4 increases the persistence around the DSB site of RNA molecules that can inhibit RPA recruitment by annealing with the ssDNA generated during DSB resection. However, overproduction of the Ribonuclease H1 Rnh1, which is known to decrease endogenous RNA:DNA hybrids *in vivo* [15], did not restore either Rad53 phosphorylation or RPA association to the DSB (Supplementary Fig S5A and B) in *rrp6*Δ and *trf4*Δ cells. As RPA binds to ssDNA in two conformational states that differ both in affinity of the bound DNA and in the length of the contacted ssDNA [30], we favor the hypothesis that Rrp6 and Trf4

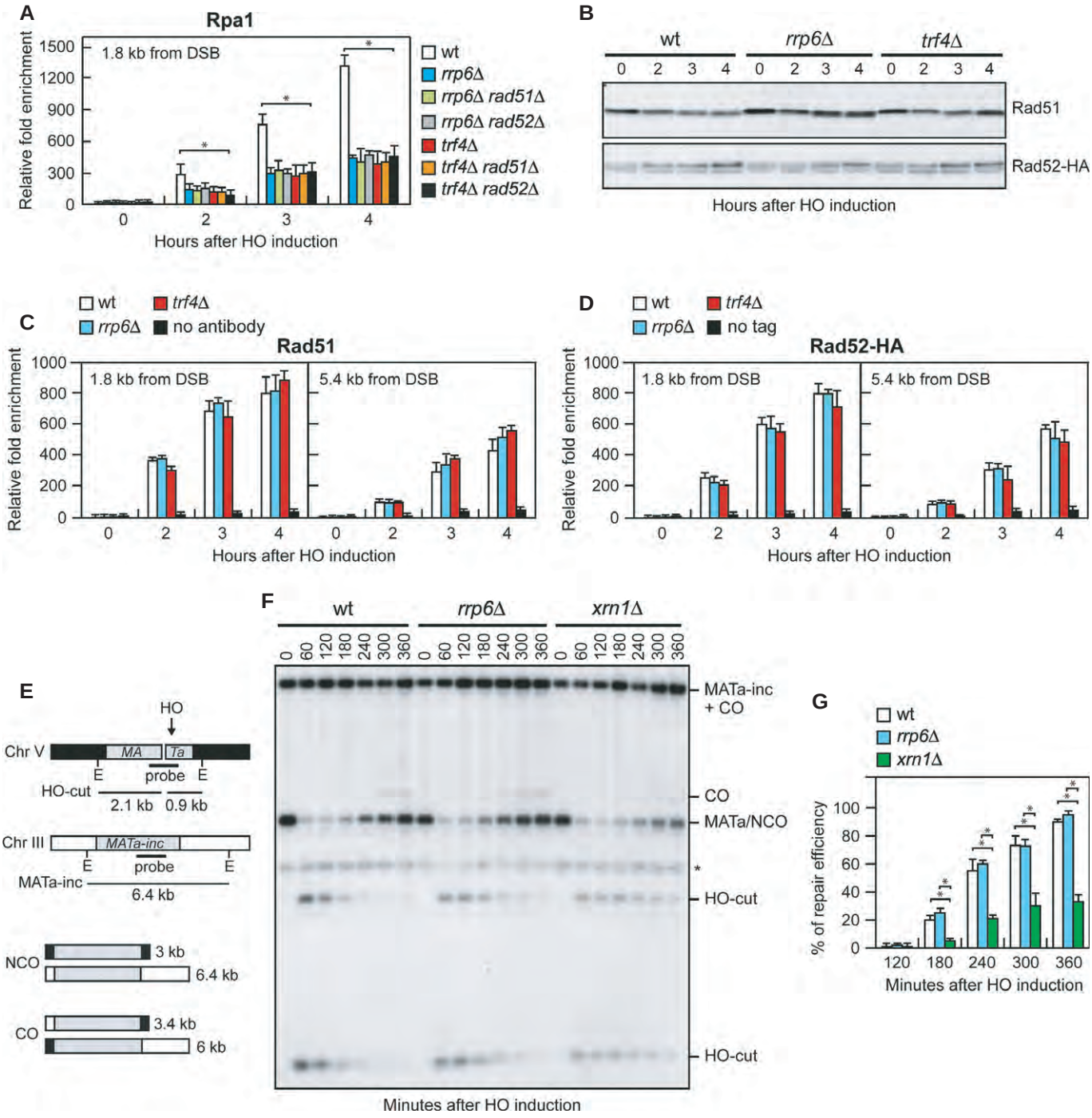

Figure 4. The lack of Rrp6 or Trf4 does not affect DSB repair by HR.

A Recruitment of Rpa1 at the HO-induced DSB. ChIP analysis was performed as in Fig 3D. The mean values are represented with error bars denoting SD (n = 3). *P < 0.01, t-test.

B Rad51 and Rad52 protein levels. Western blot with anti-Rad51 and anti-HA antibodies of extracts used for the ChIP analysis in (C) and (D), respectively.

C, D Recruitment of Rad51 and Rad52-HA at the HO-induced DSB. ChIP analysis was performed as in Fig 3. The mean values are represented with error bars denoting SD (n = 3). *P < 0.01, t-test.

E System to detect CO and NCO. Galactose-induced HO generates a DSB at the *MATa* locus on chromosome V that is repaired by using the homologous *MATa-inc* region on chromosome III. Sizes of EcoRI (E) DNA fragments detected by the probe are indicated.

F Detection of DSB repair products. EcoRI-digested genomic DNA from samples taken at the indicated times after HO induction was subjected to Southern blot analysis with the *MATa* probe depicted in (E). *indicates a cross hybridization signal.

G Densitometric analysis of the repair signals. The mean values are represented with error bars denoting SD (n = 3). *P < 0.01, t-test.

Source data are available online for this figure.

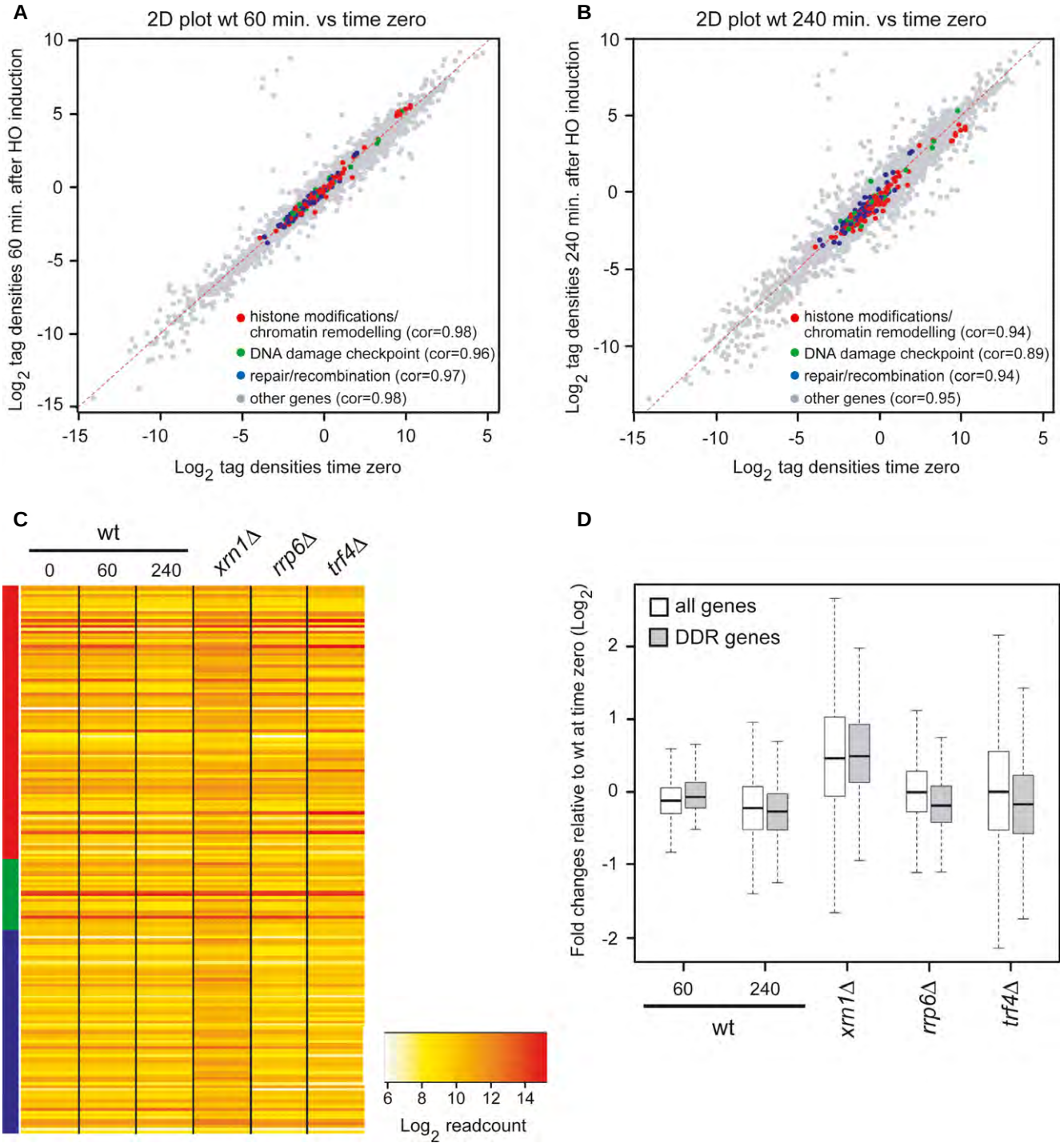

Figure 5. The lack of Xrn1, Rrp6 or Trf4 does not impair expression of most DDR genes.

A Expression of DDR genes in wild-type cells 60 min after HO induction. Scatter plot of tag density for genes encoding DDR factors in wild-type strain (JKM139) before (time zero) and after (60 min) HO induction. Results are presented as $\log_2$ of density, expressed in tag per nucleotide. Spearman's correlation coefficients for each set of genes are indicated.

B Expression of DDR genes in wild-type cells 240 min after HO induction. Same as in (A) using JKM139 cells at time zero and 240 min after HO induction.

C Expression of DDR genes in wild-type cells at time zero, 60 and 240 min after HO induction, and in *xrn1Δ*, *rrp6Δ* and *trf4Δ* cells at time zero. Data are presented as a heatmap and genes are clustered according the classification used in (A), with the same color code.

D Global expression of all protein-coding and DDR genes upon HO induction or inactivation of RNA decay factors. Box plot representation of expression fold change for all protein-coding (white) and DDR (gray) genes in wild-type cells 60 and 240 min after HO induction, and in *xrn1Δ*, *rrp6Δ* and *trf4Δ* mutants at time zero. All fold changes are relative to the wild-type at time zero. For each condition, the black line within the box corresponds to the median value, while the top and bottom lines of the box correspond to the upper quartile and lower quartile, respectively (n = 5,798 for all genes and n = 194 for the DDR genes). Outliers are not represented.

may modulate directly or indirectly these RPA conformational changes, and therefore RPA ability to bind ssDNA. As RNA-processing factors are evolutionary conserved, our findings highlight a novel important mechanism through which RNA-processing proteins can preserve genome integrity.

Materials and Methods

Yeast strains and plasmids

Strain genotypes are listed in Supplementary Table S3. Cells were grown in YEP medium (1% yeast extract, 2% bactopeptone) supplemented with 2% glucose (YEPD), 2% raffinose (YEPR) or 2% raffinose and 3% galactose (YEPRG).

DSB resection and repair

DSB end resection at the *MAT* locus in JKM139 derivative strains was analyzed on alkaline agarose gels. Quantitative analysis of DSB resection was performed by calculating the ratio of band intensities for ssDNA and total amount of DSB products.

ChIP analysis

Data are expressed as fold enrichment at the HO-induced DSB over that at the non-cleaved *ARO1* locus, after normalization of ChIP signals to the corresponding input for each time point. Fold enrichment was then normalized to the efficiency of DSB induction.

Total RNA-Seq analysis

For each yeast strain and condition, total RNA-Seq analysis was performed from two biological replicates. Sequence data are publicly available at Gene Expression Omnibus (GEO) (accession number GSE63444) and at http://vm-gb.curie.fr/dsb/.

For more detailed Materials and Methods see the Supplementary Information.

Supplementary information for this article is available online: http://embor.embopress.org

Acknowledgements

We thank A. Aguilera, J.S. Butler, J. Haber and A.W. Johnson for strains and plasmids; N. Lowndes and B. Stillman for antibodies; G. Lucchini for critical reading of the manuscript. M.P.L. is supported by Associazione Italiana per la Ricerca sul Cancro (AIRC) (grant IG15210), and PRIN 2010–2011. A.M. is supported by the ANR "REGULncRNA" and ERC "EpincRNA" starting grant. F.d'A.d.F. is supported by AIRC (grant IG12971), Human Frontier Science Program (contract number: RGP 0014/2012), Cariplo Foundation (grant number 2010.0818), FP7 PEOPLE 2012 ITN (CodAge), Telethon (GGP12059), AICR, PRIN 2010-2011, MIUR EPIGEN Project and European Research Council advanced grant (322726). High-throughput sequencing was performed by the NGS platform of Institut Curie, supported by the grants ANR-10-EQPX-03 and ANR10-INBS-09-08 from the Agence Nationale de la Recherche (investissements d'avenir) and by the Canceropôle Ile-de-France. NM and CT were supported by fellowships from Fondazione Italiana per la Ricerca sul Cancro (FIRC).

Author contributions

Fd'AdF conceived the project. NM, AM, Fd'AdF and MPL conceived and designed the experiments. NM, CT, MW, MM and DC performed the experiments. NM, CT, MW, MD, AM, Fd'AdF and MPL analyzed the data. MPL wrote the paper.

Conflict of interest

The authors declare that they have no conflict of interest.

References

1. Longhese MP, Bonetti D, Manfrini N, Clerici M (2010) Mechanisms and regulation of DNA end resection. *EMBO J* 29: 2864 – 2874
2. Zou L, Elledge SJ (2003) Sensing DNA damage through ATRIP recognition of RPA-ssDNA complexes. *Science* 300: 1542 – 1548
3. Jasin M, Rothstein R (2013) Repair of strand breaks by homologous recombination. *Cold Spring Harb Perspect Biol* 5: a012740
4. Cannavo E, Cejka P (2014) Sae2 promotes dsDNA endonuclease activity within Mre11-Rad50-Xrs2 to resect DNA breaks. *Nature* 514: 122 – 125
5. Mimitou EP, Symington LS (2008) Sae2, Exo1 and Sgs1 collaborate in DNA double-strand break processing. *Nature* 455: 770 – 774
6. Zhu Z, Chung WH, Shim EY, Lee SE, Ira G (2008) Sgs1 helicase and two nucleases Dna2 and Exo1 resect DNA double-strand break ends. *Cell* 134: 981 – 994
7. Dutertre M, Lambert S, Carreira A, Amor-Guéret M, Vagner S (2014) DNA damage: RNA-binding proteins protect from near and far. *Trends Biochem Sci* 39: 141 – 149
8. Francia S, Michelini F, Saxena A, Tang D, de Hoon M, Anelli V, Mione M, Carninci P, d'Adda di Fagagna F (2012) Site-specific DICER and DROSHA RNA products control the DNA-damage response. *Nature* 488: 231 – 235
9. Wei W, Ba Z, Gao M, Wu Y, Ma Y, Amiard S, White CI, Rendtlew Danielsen JM, Yang YG, Qi Y (2012) A role for small RNAs in DNA double-strand break repair. *Cell* 149: 101 – 112
10. Gao M, Wei W, Li MM, Wu YS, Ba Z, Jin KX, Li MM, Liao YQ, Adhikari S, Chong Z *et al* (2014) Ago2 facilitates Rad51 recruitment and DNA double-strand break repair by homologous recombination. *Cell Res* 24: 532 – 541
11. Pefanis E, Wang J, Rothschild G, Lim J, Chao J, Rabadan R, Economides AN, Basu U (2014) Noncoding RNA transcription targets AID to divergently transcribed loci in B cells. *Nature* 514: 389 – 393
12. Nagarajan VK, Jones CI, Newbury SF, Green PJ (2013) XRN 5′→3′ exoribonucleases: structure, mechanisms and functions. *Biochim Biophys Acta* 1829: 590 – 603
13. Houseley J, LaCava J, Tollervey D (2006) RNA-quality control by the exosome. *Nat Rev Mol Cell Biol* 7: 529 – 539
14. Luna R, Jimeno S, Marín M, Huertas P, García-Rubio M, Aguilera A (2005) Interdependence between transcription and mRNP processing and export, and its impact on genetic stability. *Mol Cell* 18: 711 – 722
15. Gavaldá S, Gallardo M, Luna R, Aguilera A (2013) R-loop mediated transcription-associated recombination in *trf4*Δ mutants reveals new links between RNA surveillance and genome integrity. *PLoS ONE* 8: e65541
16. Wahba L, Gore SK, Koshland D (2013) The homologous recombination machinery modulates the formation of RNA-DNA hybrids and associated chromosome instability. *Elife* 2: e00505
17. Sadoff BU, Heath-Pagliuso S, Castaño IB, Zhu Y, Kieff FS, Christman MF (1995) Isolation of mutants of *Saccharomyces cerevisiae* requiring DNA topoisomerase I. *Genetics* 141: 465 – 479

18. Tishkoff DX, Rockmill B, Roeder GS, Kolodner RD (1995) The *sep1* mutant of *Saccharomyces cerevisiae* arrests in pachytene and is deficient in meiotic recombination. *Genetics* 139: 495 – 509
19. Lee SE, Moore JK, Holmes A, Umezu K, Kolodner RD, Haber JE (1998) *Saccharomyces* Ku70, Mre11/Rad50 and RPA proteins regulate adaptation to G2/M arrest after DNA damage. *Cell* 94: 399 – 409
20. Page AM, Davis K, Molineux C, Kolodner RD, Johnson AW (1998) Mutational analysis of exoribonuclease I from *Saccharomyces cerevisiae*. *Nucleic Acids Res* 26: 3707 – 3716
21. Burkard KT, Butler JS (2000) A nuclear 3′–5′ exonuclease involved in mRNA degradation interacts with Poly(A) polymerase and the hnRNA protein Npl3p. *Mol Cell Biol* 20: 604 – 616
22. Mantiero D, Clerici M, Lucchini G, Longhese MP (2007) Dual role for *Saccharomyces cerevisiae* Tel1 in the checkpoint response to double-strand breaks. *EMBO Rep* 8: 380 – 387
23. Johnson AW (1997) Rat1p and Xrn1p are functionally interchangeable exoribonucleases that are restricted to and required in the nucleus and cytoplasm, respectively. *Mol Cell Biol* 17: 6122 – 6130
24. Ira G, Pellicioli A, Balijja A, Wang X, Fiorani S, Carotenuto W, Liberi G, Bressan D, Wan L, Hollingsworth NM *et al* (2004) DNA end resection, homologous recombination and DNA damage checkpoint activation require CDK1. *Nature* 431: 1011 – 1017
25. Shim EY, Chung WH, Nicolette ML, Zhang Y, Davis M, Zhu Z, Paull TT, Ira G, Lee SE (2010) *Saccharomyces cerevisiae* Mre11/Rad50/Xrs2 and Ku proteins regulate association of Exo1 and Dna2 with DNA breaks. *EMBO J* 29: 3370 – 3380
26. Chen H, Lisby M, Symington LS (2013) RPA coordinates DNA end resection and prevents formation of DNA hairpins. *Mol Cell* 50: 589 – 600
27. Saponaro M, Callahan D, Zheng X, Krejci L, Haber JE, Klein HL, Liberi G (2010) Cdk1 targets Srs2 to complete synthesis-dependent strand annealing and to promote recombinational repair. *PLoS Genet* 6: e1000858
28. van Dijk EL, Chen CL, d'Aubenton-Carafa Y, Gourvennec S, Kwapisz M, Roche V, Bertrand C, Silvain M, Legoix-Né P, Loeillet S *et al* (2011) XUTs are a class of Xrn1-sensitive antisense regulatory non-coding RNA in yeast. *Nature* 475: 114 – 117
29. Kim JA, Haber JE (2009) Chromatin assembly factors Asf1 and CAF-1 have overlapping roles in deactivating the DNA damage checkpoint when DNA repair is complete. *Proc Natl Acad Sci USA* 106: 1151 – 1156
30. Fanning E, Klimovich V, Nager AR (2006) A dynamic model for replication protein A (RPA) function in DNA processing pathways. *Nucleic Acids Res* 34: 4126 – 4137

Nucleic Acids Research, 2017 **1**
doi: 10.1093/nar/gkx072

Regulation of telomere metabolism by the RNA processing protein Xrn1

Daniele Cesena[1], Corinne Cassani[1], Emanuela Rizzo[1], Michael Lisby[2], Diego Bonetti[1] and Maria Pia Longhese[1,*]

[1]Dipartimento di Biotecnologie e Bioscienze, Università di Milano-Bicocca, Milan 20126, Italy and [2]Department of Biology, University of Copenhagen, DK-2200 Copenhagen N, Denmark

Received July 4, 2016; Revised January 23, 2017; Editorial Decision January 25, 2017; Accepted January 25, 2017

ABSTRACT

Telomeric DNA consists of repetitive G-rich sequences that terminate with a 3′-ended single stranded overhang (G-tail), which is important for telomere extension by telomerase. Several proteins, including the CST complex, are necessary to maintain telomere structure and length in both yeast and mammals. Emerging evidence indicates that RNA processing factors play critical, yet poorly understood, roles in telomere metabolism. Here, we show that the lack of the RNA processing proteins Xrn1 or Rrp6 partially bypasses the requirement for the CST component Cdc13 in telomere protection by attenuating the activation of the DNA damage checkpoint. Xrn1 is necessary for checkpoint activation upon telomere uncapping because it promotes the generation of single-stranded DNA. Moreover, Xrn1 maintains telomere length by promoting the association of Cdc13 to telomeres independently of ssDNA generation and exerts this function by downregulating the transcript encoding the telomerase inhibitor Rif1. These findings reveal novel roles for RNA processing proteins in the regulation of telomere metabolism with implications for genome stability in eukaryotes.

INTRODUCTION

Nucleoprotein complexes called telomeres are present at the ends of linear eukaryotic chromosomes, where they ensure replication of the chromosome ends and prevent their recognition as DNA double-strand breaks (DSBs) (1,2). Telomeric DNA in most eukaryotes consists of tandem arrays of short repeated sequences which are guanine-rich in the strand running 5′-3′ from the centromere toward the chromosome end. The G-rich strand at both ends of a chromosome extends over the C-strand to form a 3′-ended single-stranded G-rich overhang (G-tail) (3,4). This G-tail is important for telomere replication, because it provides a substrate for the telomerase enzyme. Telomerase is a ribonucleoprotein complex that uses its RNA component as a template to elongate the telomere by addition of G-rich telomeric repeats to the G-tail (1,5). The telomerase-extended single-stranded DNA (ssDNA) must then be copied by the conventional replication machinery to reconstitute the double-stranded telomeric DNA.

In *Saccharomyces cerevisiae*, single-stranded G-rich tails of 5–10 nt in length are present at telomeres throughout most of the cell cycle except in late S phase, when longer overhangs are detected (4,6,7). Removal of the last RNA primers that are generated by lagging-strand synthesis appears to match the observed overhang length (8). By contrast, the telomeric C-strands generated by leading-strand synthesis are resected by about 30–40 nt before being filled in again to leave DNA ends with a 3′ overhang of about 10 nt (8,9). This resection depends on the MRX (Mre11-Rad50-Xrs2) complex, on the exonuclease Exo1 and on the Sgs1-Dna2 helicase-nuclease complex (10–12).

G-tails at both leading- and lagging-strand telomeres are covered by the CST (Cdc13-Stn1-Ten1) complex, which is an RPA-like complex that binds with high affinity and sequence specificity to the telomeric ssDNA overhangs (13). The CST complex drives the localization of telomerase to telomeres through a direct interaction between Cdc13 and the telomerase subunit Est1 (14–17). MRX, in turn, ensures robust association of telomerase with telomeres by promoting the binding of the checkpoint kinase Tel1 via a specific interaction with the MRX subunit Xrs2 (18–22). It remains unclear whether Tel1 facilitates telomerase association directly by phosphorylating specific targets that promote telomerase recruitment, and/or indirectly by stimulating resection of the C-strand, thus generating a ssDNA substrate for telomerase action (23–25). Interestingly, Mre11 inactivation strongly reduces the binding to telomeres of the telomerase subunits Est1 and Est2, while it has a moderate effect on Cdc13 binding (26). Further work has shown that the absence of Mre11 reduces Cdc13 binding only to the leading-strand telomere, while Cdc13 ability to bind to the lagging-strand telomere is not affected (9). This observation

*To whom correspondence should be addressed. Tel: +39 02 64 483 425; Fax: +39 02 64 483 565; Email: mariapia.longhese@unimib.it

is consistent with the finding that Mre11 binds only to leading telomeres to generate the single-stranded overhangs (9).

In addition to drive telomerase localization to telomeres, the CST complex also genetically and physically interacts with the DNA polymerase α/primase complex and promotes lagging strand synthesis during telomere replication (27,28). Furthermore, it prevents inappropriate generation of ssDNA at telomeric ends. Cdc13 inactivation through either the *cdc13-1* temperature sensitive allele or the *cdc13-td* conditional degron allele results in both degradation of the 5′-terminated DNA strand and checkpoint-mediated cell cycle arrest (29–31). Similarly, temperature sensitive alleles of either the *STN1* or *TEN1* gene cause telomere degradation and checkpoint-dependent cell cycle arrest at the non-permissive temperature (32–35). DNA degradation in the *cdc13-1* mutant depends mainly on the 5′-3′ nuclease Exo1 (36,37), suggesting that CST protects telomeric DNA from Exo1 activity.

There is emerging evidence that telomere metabolism is influenced by RNA processing pathways. In eukaryotes, RNA processing relies on two highly conserved pathways involving both 5′-3′ and 3′-5′ exoribonuclease activities (38). In particular, 5′-3′ degradation is performed by the Xrn protein family, which comprises the cytoplasmic Xrn1 enzyme and the nuclear Rat1 enzyme (also known as Xrn2) (39). The 3′-5′ RNA processing activity is due to the exoribonuclease Rrp6 that belongs to the nuclear exosome (40). In addition, RNA molecules are subjected to a quality control system, which is called nonsense-mediated mRNA decay (NMD) and degrades non-functional RNAs that might otherwise give rise to defective protein products (38).

RNA processing proteins have been recently implicated in telomere metabolism in both yeast and mammals, although the related mechanisms are poorly understood. In particular, Xrn1 has been identified in genome-wide screenings for *S. cerevisiae* mutants with altered telomere length (41,42). Moreover, proteins belonging to the mammalian NMD pathway have been found to bind telomeres and to control telomere length (43,44). Similarly, the lack of the *S. cerevisiae* NMD proteins was shown to cause telomere shortening by increasing the amount of Stn1 and Ten1, which in turn inhibit telomerase activity by interfering with Est1–Cdc13 interaction (45–48). Furthermore, both Xrn1 and the nuclear exosome control degradation of the RNA component of human telomerase (49). Finally, Rat1 and the NMD pathway control the level of a new class of non-coding RNAs called TERRA (telomeric repeat-containing RNA), which are transcribed from the subtelomeric sequences and likely regulate telomere length (50–52).

Here we show that the lack of the *S. cerevisiae* RNA processing factors Xrn1 or Rrp6 suppresses the temperature sensitivity of *cdc13-1* mutant cells by attenuating the activation of the DNA damage checkpoint response. In particular, Xrn1 is required to activate the checkpoint upon telomere uncapping because it promotes the generation of ssDNA. Furthermore, Xrn1 maintains telomere length independently of ssDNA generation by promoting Cdc13 association to telomeres through downregulation of the transcript encoding the telomerase inhibitor Rif1.

MATERIALS AND METHODS

Strains and plasmids

Strain genotypes are listed in Supplementary Table S1. Strains used for monitoring telomere addition were derivatives of strain UCC5913, kindly provided by D. Gottschling (Fred Hutchinson Cancer Research Center, Seattle, USA). Strains ML968-1D and ML968-3B are derivatives of ML8-9A, a *RAD5 ADE2* derivative of W303 (*MAT***a** *LYS2 ade2-1 can1-100 ura3-1 his3-11,15 leu2-3, 112 trp1-1 rad5-535*). A plasmid carrying the *GAL1-RNH1* allele and the control vector plasmid *pGAL1* were kindly provided by A. Aguilera (University of Seville, Sevilla, Spain). Plasmids pAM140/pAJ228 (*CEN LEU2 rat1-ΔNLS*), pAM144 (*CEN LEU2 xrn1-E176G*) and pAM145/pAJ37 (*CEN LEU2 XRN1*) were kindly provided by A.W. Johnson (University of Texas, Austin, USA). Plasmid pGFPRRP6H1 (*CEN URA3* pGFP-*rrp6-D238A*) was kindly provided by J.S. Butler (University of Rochester Medical Center, Rochester, USA). Plasmid pTRP61 (2μ *TRP1 GAL1-TLC1*) was kindly provided by R. Wellinger (Université de Sherbrooke, Québec, Canada). Plasmid pVL1091 (*CEN LEU2 CDC13-EST1*) was kindly provided by V. Lundblad (Salk Institute, La Jolla, USA). All gene disruptions were carried out by polymerase chain reaction (PCR)-based methods. The accuracy of all gene replacements and integrations was verified by Southern blot analysis or PCR. Cells were grown in YEP medium (1% yeast extract, 2% bactopeptone, 50 mg/l adenine) supplemented with 2% glucose (YEPD) or 2% raffinose (YEPR) or 2% raffinose and 2% galactose (YEPRG).

Southern blot analysis of telomere length

The length of HO (Homothallic)-induced telomeres was determined as previously described (53). Briefly, yeast DNA was digested with SpeI and the resulting DNA fragments were separated by 0.8% agarose gel electrophoresis and hybridized with a ^{32}P-labeled probe corresponding to a 500 bp *ADE2* fragment. To determine the length of native telomeres, XhoI-digested yeast DNA was subjected to 0.8% agarose gel electrophoresis and hybridized with a ^{32}P-labeled poly(GT) probe. Standard hybridization conditions were used.

ChIP and qPCR

ChIP analysis was performed as previously described (54). Quantification of immunoprecipitated DNA was achieved by quantitative real-time PCR (qPCR) on a Bio-Rad MiniOpticon apparatus. Triplicate samples in 20 μl reaction mixture containing 10 ng of template DNA, 300 nM for each primer, 2× SsoFast™ EvaGreen® supermix (Bio-rad #1725201) were run in white 48-well PCR plates Multiplate™ (Bio-Rad #MLL4851). The qPCR program was as follows: step 1, 98°C for 2 min; step 2, 98°C for 5 s; step 3, 60°C for 10 s; step 4, return to step 2 and repeat 30 times. At the end of the cycling program, a melting program (from 65 to 95°C with a 0.5°C increment every 5 s) was run to test the specificity of each qPCR. qPCR at the HO-induced telomere was carried out by using primer pairs located at 640 bp

centromere-proximal to the HO cutting site at chromosome VII and at the non-telomeric *ARO1* fragment of chromosome IV (CON). qPCR at native telomeres was carried out by using primer pairs located at 70 and 139 bp from the TG sequences on telomeres VI-R (right) and XV-L (left), respectively. Data are expressed as fold enrichment over the amount of CON in the immunoprecipitates after normalization to input signals for each primer set.

qRT-PCR

Total RNA was extracted from cells using the Bio-Rad Aurum total RNA mini kit. First strand cDNA synthesis was performed with the Bio-Rad iScript™ cDNA Synthesis Kit. qRT-PCR was performed on a MiniOpticon Real-time PCR system (Bio-Rad) and RNA levels were quantified using the ΔΔCt method. Quantities were normalized to *ACT1* RNA levels and compared to that of wild-type cells that was set up to 1. Primer sequences are available upon request.

Fluorescence microscopy

Yeast cells were grown and processed for fluorescence microscopy as described previously (55). Fluorophores were cyan fluorescent protein (CFP, clone W7) (56) and yellow fluorescent protein (YFP, clone 10C) (57). Fluorophores were visualized on a Deltavision Elite microscope (Applied Precision, Inc) equipped with a 100× objective lens (Olympus U-PLAN S-APO, NA 1.4), a cooled Evolve 512 EM-CCD camera (Photometrics, Japan) and an Insight solid state illumination source (Applied Precision, Inc). Pictures were processed with Volocity software (PerkinElmer). Images were acquired using softWoRx (Applied Precision, Inc) software.

Other techniques

Visualization of the single-stranded overhangs at native telomeres was done as previously described (6). The same gel was denatured and hybridized with the end-labeled C-rich oligonucleotide for loading control. Protein extracts to detect Rad53 were prepared by trichloroacetic acid (TCA) precipitation. Rad53 was detected using anti-Rad53 polyclonal antibodies from Abcam. Secondary antibodies were purchased from Amersham and proteins were visualized by an enhanced chemiluminescence system according to the manufacturer.

RESULTS

The lack of Xrn1 or Rrp6 partially suppresses the temperature sensitivity of *cdc13-1* cells

Protection of telomeres from degradation depends on the CST (Cdc13-Stn1-Ten1) complex, which specifically binds to the telomeric ssDNA overhangs (13). We have previously shown that the RNA processing proteins Xrn1 and Rrp6 are required to fully activate the checkpoint kinase Mec1/ATR at intrachromosomal DSBs (58). We then asked whether Xrn1 and/or Rrp6 regulate checkpoint activation also in response to telomere uncapping. To this end, we analyzed the effect of deleting either the *XRN1* or the *RRP6* gene in *cdc13-1* cells, which show temperature-dependent loss of telomere capping, ssDNA production, checkpoint activation and cell death (29,30). As expected, *cdc13-1* cells were viable at permissive temperature (25°C), but died at restrictive temperature (26–30°C) (Figure 1A). Deletion of either *XRN1* or *RRP6* partially suppressed the temperature sensitivity of *cdc13-1* cells, as it allowed *cdc13-1* cells to form colonies at 26–28°C (Figure 1A). Xrn1 and Rrp6 appear to impair cell viability of *cdc13-1* cells by acting in two different pathways, as *xrn1Δ rrp6Δ cdc13-1* triple mutant cells formed colonies at 30°C more efficiently than both *xrn1Δ cdc13-1* and *xrn1Δ cdc13-1* double mutant cells (Figure 1B).

Xrn1 and Rrp6 control RNA degradation by acting as 5′-3′ and 3′-5′ exoribonucleases, respectively (38). The *xrn1-E176G* and *rrp6-D238A* alleles, encoding nuclease-defective Xrn1 or Rrp6 variants (59,60), suppressed the temperature sensitivity of *cdc13-1* cells to an extent similar to that of *xrn1Δ* and *rrp6Δ*, respectively (Figure 1C). Therefore, Xrn1 and Rrp6 appear to impair viability in the presence of uncapped telomeres by acting as nucleases.

Xrn1 controls cytoplasmic RNA decay, whereas RNA processing in the nucleus depends on its nuclear paralog Rat1 (61). Targeting Rat1 to the cytoplasm by deleting its nuclear localization sequence (*rat1-ΔNLS*) restores Xrn1-like function in RNA degradation (61), prompting us to ask whether it could restore Xrn1 function in causing loss of viability of *cdc13-1* cells. Strikingly, *cdc13-1 xrn1Δ* cells expressing the *rat1-ΔNLS* allele on a centromeric plasmid formed colonies at 27°C much less efficiently than *cdc13-1 xrn1Δ* cells expressing wild type *RAT1* (Figure 1D). Thus, Xrn1 impairs viability in the presence of uncapped telomeres by controlling a cytoplasmic RNA decay pathway.

Xrn1 and Rrp6 are required to fully activate the checkpoint at uncapped telomeres

A checkpoint-dependent arrest of the metaphase to anaphase transition is observed in *cdc13-1* cells at high temperatures (29). Failure to turn on the checkpoint allows *cdc13-1* cells to form colonies at 28°C (30), indicating that checkpoint activation can partially account for the loss of viability of *cdc13-1* cells. We therefore asked whether the enhanced temperature resistance of *cdc13-1 xrn1Δ* and *cdc13-1 rrp6Δ* cells might be related to defective checkpoint activation. Cell cultures were arrested in G1 with α-factor at 23°C and then released from G1 arrest at 28°C, followed by monitoring nuclear division at different time points. As expected, *cdc13-1* cells remained arrested as large budded cells with a single nucleus throughout the experiment (Figure 2A). Conversely, although *xrn1Δ* and *rrp6Δ* single mutant cells slowed down nuclear division compared to wild type cells, *cdc13-1 xrn1Δ* and *cdc13-1 rrp6Δ* cells started to divide nuclei about 90 min after release (Figure 2A).

We then examined under the same conditions phosphorylation of the Rad53 checkpoint kinase that is necessary for checkpoint activation and can be detected as changes in Rad53 electrophoretic mobility. After release at 28°C from G1 arrest, Rad53 phosphorylation was strong in *cdc13-1* cells, as expected, whereas it was undetectable in *cdc13-1 xrn1Δ* cells and it was reduced in *cdc13-1 rrp6Δ* cells (Figure 2B). Taken together, these results indicate that Xrn1

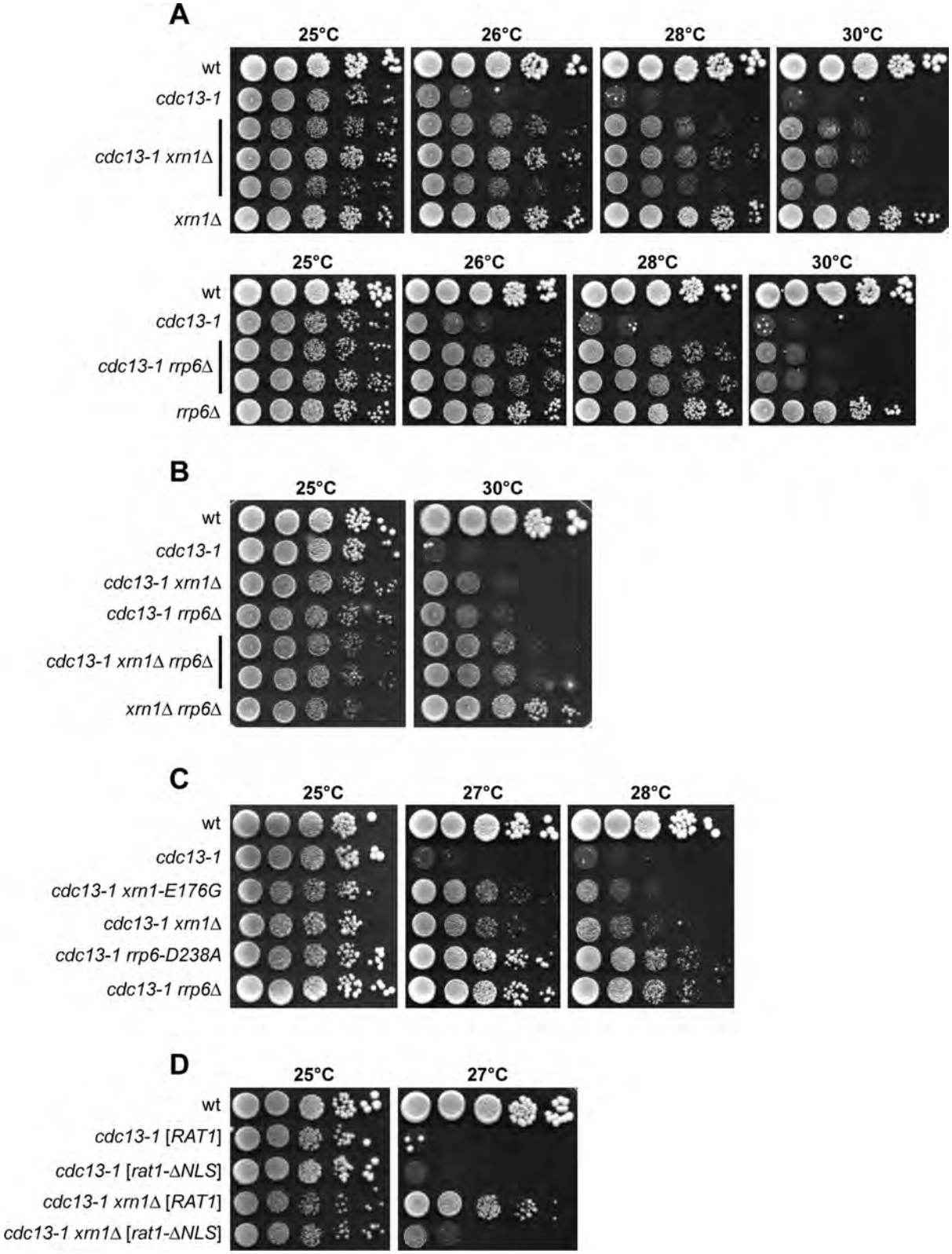

Figure 1. The lack of Xrn1 or Rrp6 partially suppresses the temperature sensitivity of *cdc13-1* cells. (**A**–**D**) Cell cultures were grown overnight at 23°C and 10-fold serial dilutions were spotted onto YEPD plates. Bars point out independent clones. Plates were incubated at the indicated temperatures before images were taken.

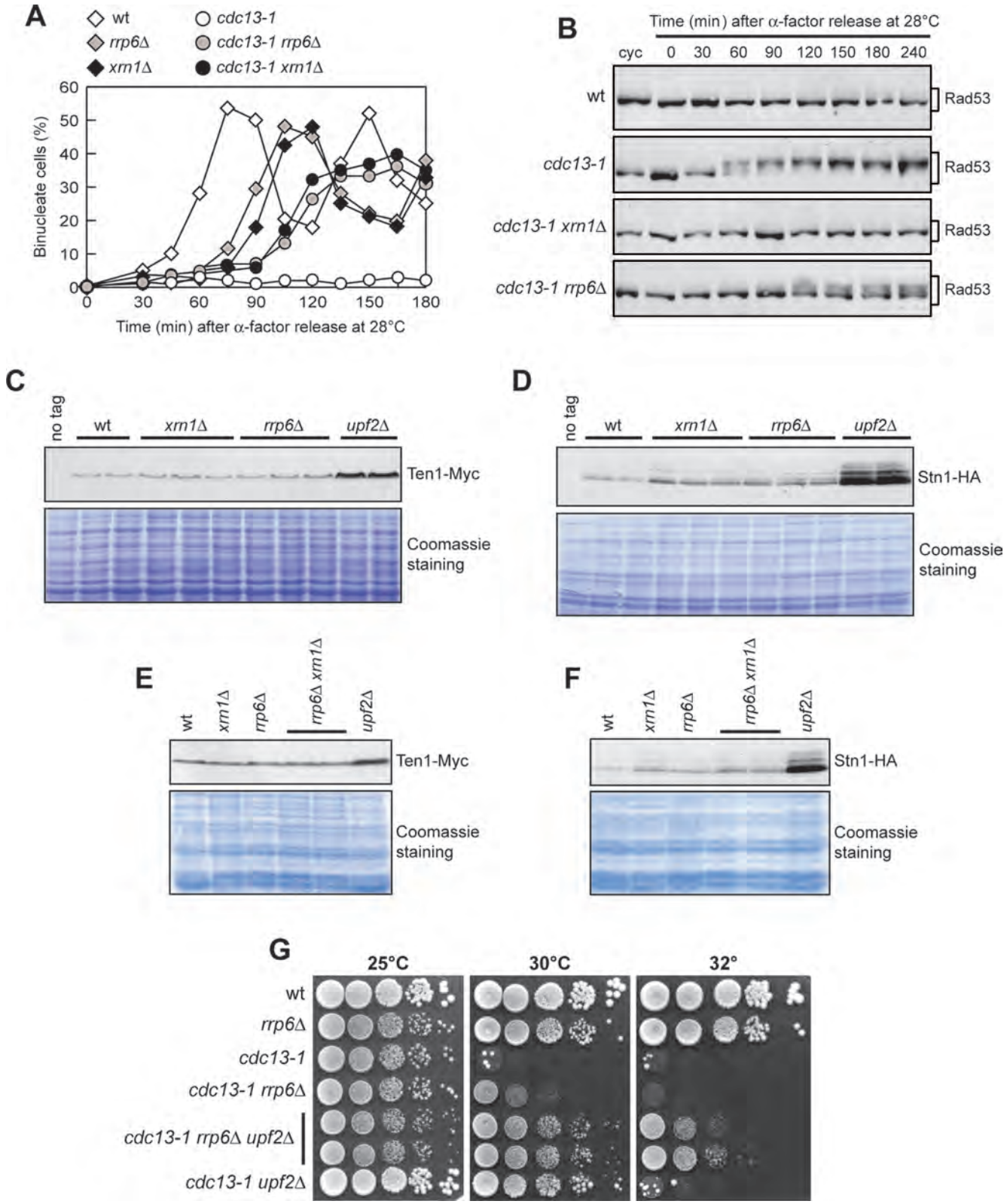

Figure 2. The lack of Xrn1 or Rrp6 reduces checkpoint activation in *cdc13-1* cells and suppresses the temperature sensitivity of *cdc13-1* cells by acting in a pathway different from NMD. (**A** and **B**) Cell cultures exponentially growing at 23°C in YEPD (cyc) were arrested in G1 with α-factor and then released into the cell cycle at 28°C (time zero). Samples were taken at the indicated times after α-factor release to determine the kinetics of nuclear division (**A**), and for western blot analysis of protein extracts using anti-Rad53 antibodies (**B**). (**C**–**F**) Protein extracts prepared from cell cultures exponentially growing at 25°C in YEPD were subjected to western blot analysis with anti-Myc (C and E) and anti-HA (D and F) antibodies. The same amount of extracts was separated by SDS-PAGE and stained with Coomassie Blue as loading control. Bars point out two or three independent cell cultures. (**G**) Cell cultures were grown overnight at 23°C and 10-fold serial dilutions were spotted onto YEPD plates. The bar points out two independent clones.

and Rrp6 are required to fully activate the checkpoint in response to telomere uncapping caused by defective Cdc13.

Xrn1 and Rrp6 regulate telomere capping through a mechanism that is distinct from that involving the NMD pathway

In both yeast and mammals, the NMD pathway is involved in quality control of gene expression by eliminating aberrant RNAs (62). Interestingly, NMD inactivation was shown to suppress the temperature sensitivity of *cdc13-1* cells by increasing the levels of the Cdc13 interacting proteins Stn1 and Ten1, which likely stabilize the CST complex at telomeres (46,47,63). These high levels of Stn1 and Ten1 are also responsible for the short telomere length phenotype of *nmdΔ* mutants, possibly because Stn1 and Ten1 inhibit telomerase activity by interfering with Est1–Cdc13 interaction (16,34,64,65).

As 77% of the transcripts that are upregulated in *nmdΔ* cells are upregulated also in *xrn1Δ* cells (66), we asked whether Xrn1 and/or Rrp6 action at telomeres might involve the same pathway that is regulated by NMD. To this purpose, we constructed fully functional Ten1-Myc and Stn1-HA alleles to analyze the levels of Ten1 and Stn1 in *xrn1Δ* and *rrp6Δ* cells. As expected, the amounts of Ten1-Myc and Stn1-HA were greatly increased in cells lacking the NMD protein Upf2 (Figure 2C and D). By contrast, the lack of Xrn1 or Rrp6 did not change the amount of Ten1-Myc (Figure 2C) and only very slightly increased the amount of Stn1-HA (Figure 2D). Furthermore, Xrn1 and Rrp6 do not compensate for the absence of each other in controlling Ten1 and Stn1 levels, as the amount of Ten1-Myc (Figure 2E) and Stn1-HA (Figure 2F) in *xrn1Δ rrp6Δ* double mutant cells was similar to that in *xrn1Δ* and *rrp6Δ* single mutant cells.

The presence of the Myc or HA tag at the C-terminus of Ten1 and Stn1, respectively, did not affect the possible regulation of the corresponding mRNAs by Xrn1 or Rrp6, as the suppression of the temperature sensitivity of *cdc13-1* cells by *XRN1* or *RRP6* deletion was similar either in the presence or in the absence of the *TEN1-MYC* or *STN1-HA* allele (Supplementary Figure S1).

We also analyzed the epistatic relationships between Xrn1/Rrp6 and NMD. The effect of deleting *UPF2* in *xrn1Δ cdc13-1* cells could not be assessed due to the poor viability of the triple mutant at 23–25°C. Nonetheless, deletion of *UPF2*, which partially suppressed the temperature sensitivity of *cdc13-1* cells, further improved the temperature resistance of *cdc13-1 rrp6Δ* double mutant cells at 32°C compared to both *cdc13-1 rrp6Δ* and *cdc13-1 upf2Δ* cells (Figure 2G). Altogether, these data suggest that Xrn1 and Rrp6 impair survival of *cdc13-1* by acting in a pathway that is different from that involving the NMD proteins.

Xrn1 is required to generate ssDNA at uncapped telomeres

It is known that cell death of *cdc13-1* cells at restrictive temperatures is due to generation of telomeric ssDNA that triggers checkpoint-mediated metaphase arrest (29,30). Hence, the improved temperature resistance of *cdc13-1 xrn1Δ* and *cdc13-1 rrp6Δ* cells might be due to a reduction of the amount of telomeric DNA that becomes single-stranded in *cdc13-1* cells at restrictive temperatures. We therefore assessed the presence of ssDNA at natural chromosome ends by analyzing genomic DNA prepared from exponentially growing cells. Non-denaturing in-gel hybridization with a C-rich radiolabeled oligonucleotide showed that the amount of telomeric ssDNA after incubation of cells at 28°C for 5 h was lower in *cdc13-1 xrn1Δ* double mutant cells than in *cdc13-1* cells (Figure 3A). By contrast, the level of single-stranded TG sequences showed a very similar increase in both *cdc13-1* and *cdc13-1 rrp6Δ* mutant cells compared to wild type cells (Figure 3A).

The function of Cdc13 in telomere protection is mediated by its direct interaction with Stn1 and Ten1. In contrast to Cdc13, Stn1 inhibits telomerase action by competing with Est1 for binding to Cdc13 (64,65). As a consequence, cells lacking the Stn1 C-terminus (*stn1-ΔC*) display long telomeres because the Stn1-ΔC variant fails to compete with Est1 for binding to Cdc13. Furthermore, these same cells accumulate telomeric ssDNA, although the amount of this ssDNA is not enough to impair cell viability (34,64,67). We therefore evaluated the specificity of the genetic interactions between Cdc13, Xrn1 and Rrp6 by analyzing the consequences of deleting *XRN1* or *RRP6* in *stn1-ΔC* cells. Like in *cdc13-1* cells, generation of telomeric ssDNA in *stn1-ΔC* cells was reduced by the lack of Xrn1, but not by *RRP6* deletion (Figure 3B). Thus, Xrn1 is required to generate ssDNA at dysfunctional telomeres, whereas Rrp6 does not, implying that the defective checkpoint response in *cdc13-1 rrp6Δ* cells cannot be ascribed to a reduced generation of telomeric ssDNA.

The data above suggest that the lack of Xrn1 might suppress the temperature sensitivity of *cdc13-1* cells by attenuating the generation of telomeric ssDNA. We then asked whether the overexpression of Exo1, which bypasses MRX requirement for intrachromosomal DSB end resection (68), decreased the maximum permissive temperature of *cdc13-1 xrn1Δ* cells. Strikingly, *cdc13-1 xrn1Δ* cells containing the *EXO1* gene on a 2μ plasmid were more temperature-sensitive than *cdc13-1 xrn1Δ* cells containing the empty vector (Figure 3C). This finding supports the hypothesis that the lack of Xrn1 can partially bypass the requirement for CST in telomere capping because it attenuates the generation of telomeric ssDNA.

Xrn1 maintains telomere length by acting as a cytoplasmic nuclease

Xrn1 has been identified in genome-wide screenings for *S. cerevisiae* mutants that are affected in telomere length (41,42). We confirmed the requirement for Xrn1 in telomere elongation by using an inducible short telomere assay that allows the generation of a single short telomere without affecting the length of the other telomeres in the same cell (10). We used a strain that carried at the *ADH4* locus on chromosome VII an internal tract of telomeric DNA sequence (81 bp TG) adjacent to an HO endonuclease recognition sequence (Figure 4A) (10,69). Upon cleavage by HO, the fragment distal to the break is lost, and, over time, the TG side of the break is elongated by the telomerase. As shown in Figure 4B, sequence addition at the HO-derived telomere was clearly detectable after galactose addition in

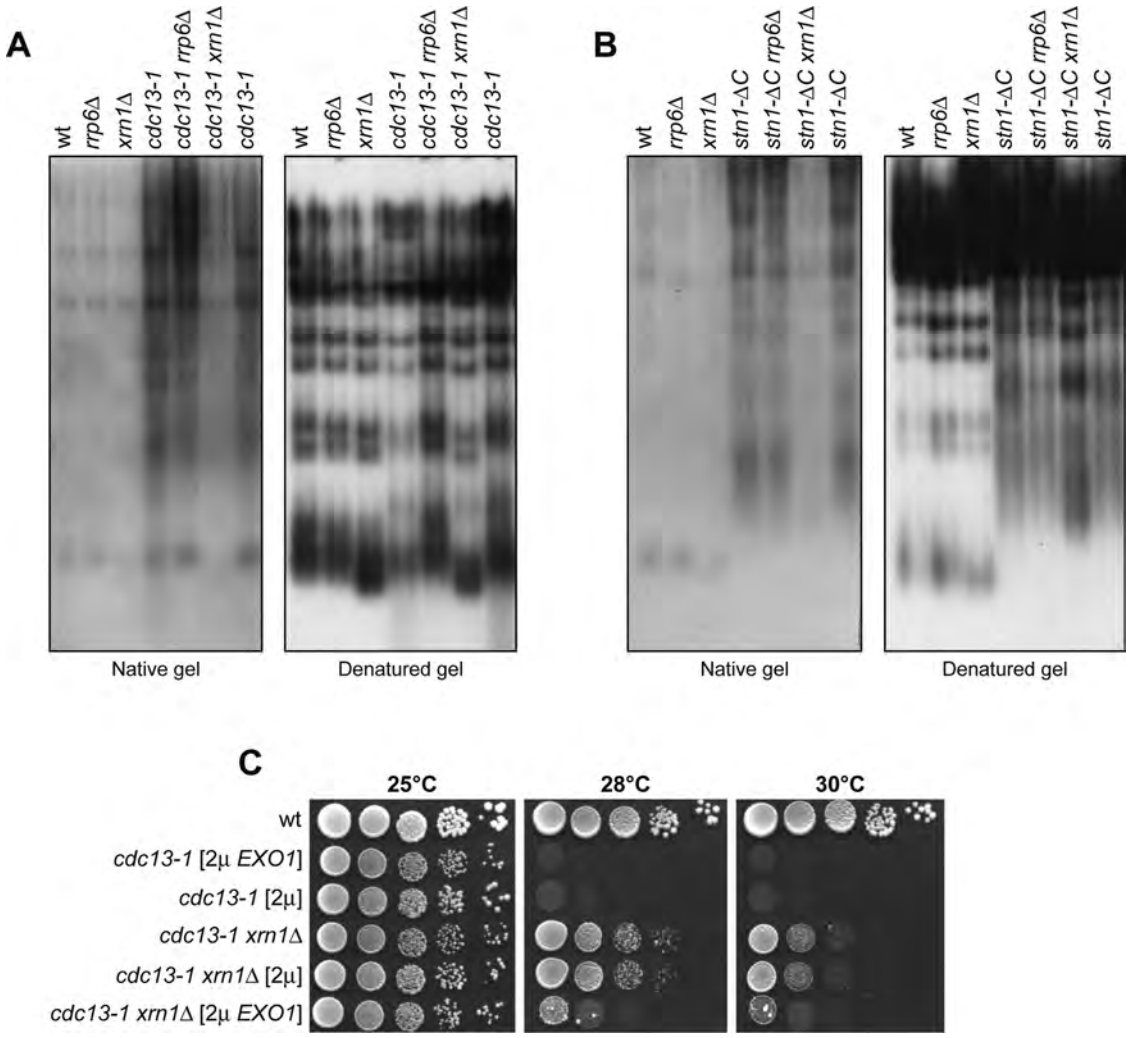

Figure 3. The lack of Xrn1 reduces ssDNA generation at uncapped telomeres. (**A** and **B**) Cell cultures exponentially growing at 23°C were shifted to 28°C for 5 h. Genomic DNA was digested with XhoI, and single-stranded G-tails were visualized by non-denaturing in-gel hybridization (native gel) using an end-labeled C-rich oligonucleotide as a probe. The gel was denatured and hybridized again with the same probe for loading control (denatured gel). (**C**) Cell cultures were grown overnight and 10-fold serial dilutions were spotted onto YEPD plates. Plates were incubated at the indicated temperatures before images were taken.

wild type cells, whereas it was strongly delayed and reduced in *xrn1Δ* cells, confirming the requirement for Xrn1 in telomere elongation.

Xrn1 controls telomere length by acting as cytoplasmic nuclease. In fact, expression of the Xrn1 nuclear paralog Rat1 lacking its nuclear localization sequence (*rat1-ΔNLS*) restored telomere length in *xrn1Δ* cells (Figure 4C). Furthermore, telomeres in *xrn1-E176G* cells expressing the nuclease defective Xrn1 variant were as short as in *xrn1Δ* cells (Figure 4D).

In a deep transcriptome analysis of the genes that are misregulated by the lack of Xrn1, *xrn1Δ* cells showed ∼3-fold reduction of the levels of *TLC1* (58), the RNA component of the telomerase enzyme. However, a 2μ plasmid overexpressing *TLC1* from a galactose inducible promoter did not allow *xrn1Δ* cells to elongate telomeres (Supplementary Figure S2A), although wild-type and *xrn1Δ* cells expressed similar amount of *TLC1* RNA (Supplementary Figure S2B). Thus, telomere shortening in *xrn1Δ* cells cannot be simply explained by the reduction of *TLC1* RNA.

Xrn1 promotes Cdc13 association to telomeres independently of ssDNA generation

Productive association of telomerase to telomeres requires the generation of ssDNA that leads to the recruitment of Cdc13. Cdc13 in turn recruits the telomerase to telomeres by interacting with the telomerase subunit Est1 (14–17). Binding of MRX to telomeres allows Tel1 recruitment that strengthens the association of telomerase to telomeres by phosphorylating unknown targets (23–25). The finding that telomere shortening in *mrxΔ* and *tel1Δ* cells can be suppressed by targeting the telomerase to telomeres through a Cdc13-Est1 protein fusion (70) suggests that MRX/Tel1 promotes Cdc13-Est1 interaction rather than Cdc13 association to telomeres.

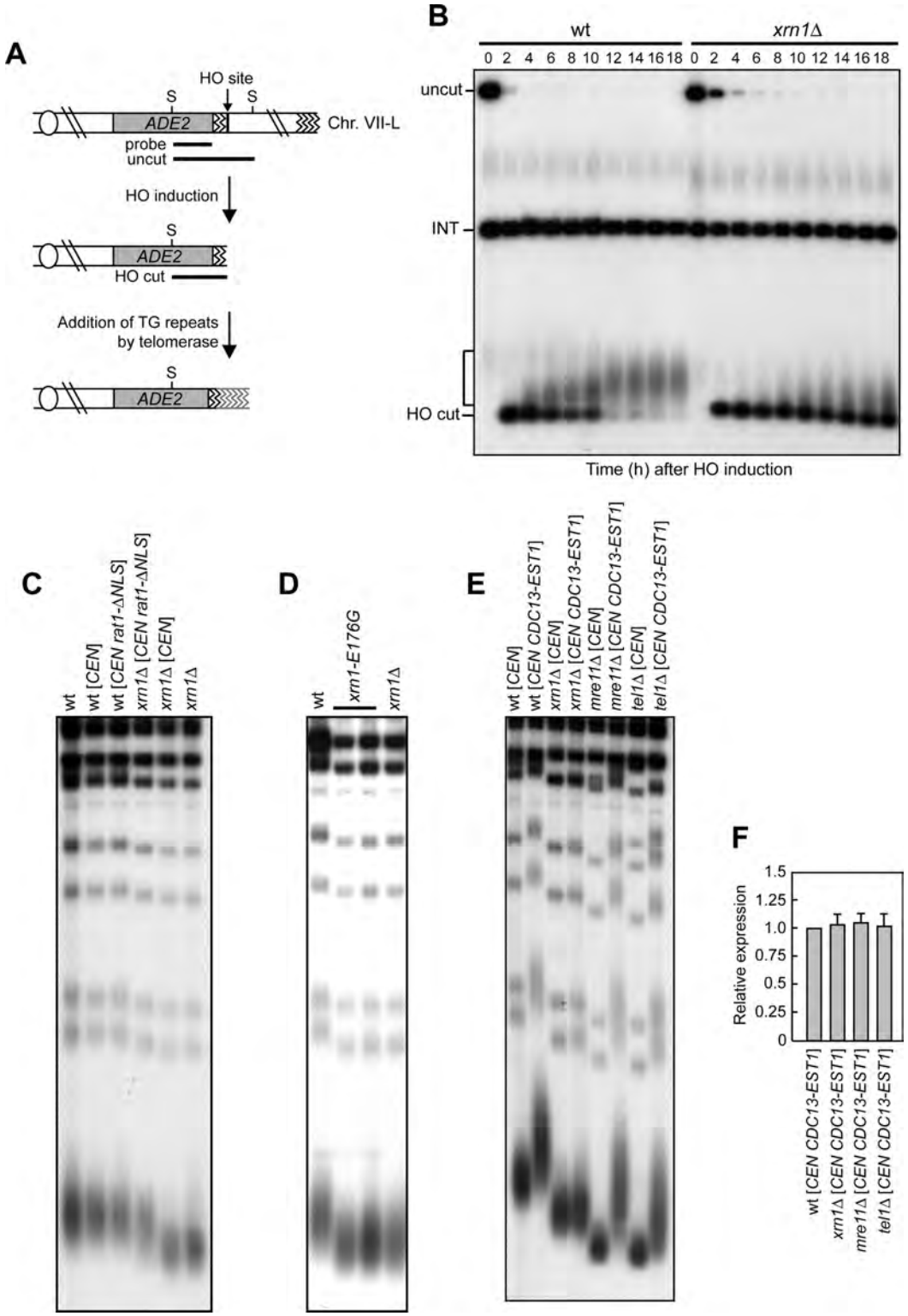

Figure 4. The lack of Xrn1 impairs telomere elongation. (**A**) Schematic representation of the HO-induced short telomere system. The *ADH4* locus on chromosome VII was replaced with a fragment consisting of the *ADE2* gene and 81 bp of TG telomeric sequences (zigzag lines) flanking the recognition site for the HO endonuclease. The centromere is shown as a circle. S, SpeI. (**B**) Elongation of the HO-induced telomere. Cell cultures carrying the system described in A and exponentially growing in raffinose were shifted to galactose at time zero to induce HO expression. SpeI-digested genomic DNA was subjected to Southern blot analysis using an *ADE2* fragment as a probe. A bracket points out new telomere repeats added to the TG telomeric sequences. The band of about 1.6kb (INT) represents the endogenous *ade2-101* gene. (**C**–**E**) XhoI-cut genomic DNA from exponentially growing cells was subjected to Southern blot analysis using a radiolabeled poly(GT) probe. The bar in (D) points out two independent *xrn1-E176G* cell cultures. (**F**) RNA levels of *CDC13-EST1* from cells in (E) were evaluated by quantitative reverse transcriptase PCR (qRT-PCR). Quantities were normalized to *ACT1* RNA levels and compared to that of wild-type cells that was set up to 1. The mean values ±s.d. are represented ($n = 3$).

As Xrn1 was found to promote MRX association at intrachromosomal DSBs (58), we asked whether the expression of a Cdc13-Est1 fusion could restore telomere length in *xrn1Δ* cells. A Cdc13-Est1 fusion expressed from a single-copy plasmid did not suppress the telomere length defect of *xrn1Δ* cells, although it was capable to elongate telomeres in wild type, *mre11Δ* and *tel1Δ* cells (Figure 4E) and all cell cultures expressed similar levels of *CDC13-EST1* mRNA (Figure 4F). This finding suggests that the telomere length defect of *xrn1Δ* cells is not due to MRX dysfunction.

The inability of the Cdc13-Est1 fusion protein to suppress the telomere length defect of *xrn1Δ* cells raises the possibility that Cdc13 itself cannot bind telomeres in the absence of Xrn1. As loss of telomerase is known to be accompanied by recruitment of Cdc13 and Mre11 to telomeres (71), we analyzed the generation of Cdc13 and Mre11 foci before or after loss of telomerase in wild-type and *xrn1Δ* cells. These cells expressed fully functional Cdc13-CFP and Mre11-YFP fusion proteins. As expected, telomerase removal by loss of a plasmid-borne copy of *EST2* resulted in a significant increase of both Mre11-YFP and Cdc13-CFP foci in wild-type cells as early as 25–50 generations after loss of telomerase, with only a subset of them colocalizing (Figure 5A–C). By contrast, *xrn1Δ* cells showed a reduction in the number of Cdc13-CFP foci (Figure 5A and B), but not of Mre11-YFP foci (Figure 5A and C), compared to wild-type, suggesting a requirement for Xrn1 in promoting Cdc13 association to telomeres.

To investigate further this hypothesis, we analyzed the amount of Cdc13 bound at native telomeres in wild-type and *xrn1Δ* cells that were released into a synchronous cell cycle from a G1 arrest (Figure 6A). Cdc13 binding to telomeres peaked in wild type cells 45 min after release, concomitantly with the completion of DNA replication, while it remained very low in *xrn1Δ* cells throughout the time course (Figure 6A and B), although both cell type extracts contained similar amount of Cdc13 (Figure 6C).

Because Cdc13 binds telomeric ssDNA and the lack of Xrn1 impairs ssDNA generation at uncapped telomeres, the reduced Cdc13 association at telomeres in *xrn1Δ* cells might be due to defective generation of telomeric single-stranded overhangs. To investigate this issue, XhoI-cut DNA prepared at different time points after release into the cell cycle from a G1 arrest was subjected to native gel electrophoresis, followed by in-gel hybridization with a C-rich radiolabeled oligonucleotide. As shown in Figure 6D, both wild type and *xrn1Δ* cells showed similar amount of G-tail signals that reached their maximal levels 15–45 min after release, indicating that the lack of Xrn1 does not affect the generation of single-stranded overhangs at capped telomeres.

As generation of telomeric single-stranded overhangs requires the MRX complex (10–12,72), we also analyzed Mre11 association at native telomeres. Wild-type and *xrn1Δ* cells released into a synchronous cell cycle from a G1 arrest showed similar amount of telomere-bound Mre11 (Figure 6E), consistent with the finding that the lack of Xrn1 does not affect the generation of telomeric single-stranded overhangs. Altogether, these data indicate that Xrn1 promotes Cdc13 binding/association to telomeres independently of ssDNA generation.

Xrn1 promotes Cdc13 association at telomeres by downregulating Rif1 level

Deep transcriptome analysis showed that the *RIF1* mRNA level was ∼3-fold higher in *xrn1Δ* cells than in wild-type (58). This mRNA upregulation caused an increase of the Rif1 protein level, as shown by western blot analysis of wild type and *xrn1Δ* protein extracts (Figure 7A), prompting us to test whether this Rif1 upregulation can account for the telomere defects of *xrn1Δ* cells.

As expected from previous findings that Rif1 has a very slight effect on the generation of telomeric ssDNA (73,74), the increased Rif1 levels did not account for the increased temperature resistance of *cdc13-1 xrn1Δ* cells compared to *cdc13-1*. In fact, although *RIF1* deletion decreased the maximum permissive temperature of *cdc13-1* cells (75,76), *cdc13-1 rif1Δ xrn1Δ* cells were more temperature-resistant than *cdc13-1 rif1Δ* cells (Figure 7B), indicating that the suppression of the temperature sensitivity of *cdc13-1* cells by *XRN1* deletion does not require Rif1.

Rif1 was originally identified as a telomere-binding protein that negatively regulates telomerase-mediated telomere elongation (77). Interestingly, the lack of Rif1, although causing a very slight increase of ssDNA formation, yet leads to considerably more Cdc13 binding at telomeres (74). Therefore, Rif1 might block the association/accumulation of Cdc13 at telomeres through a direct mechanism. Consistent with this hypothesis, a 2μ plasmid carrying the *RIF1* gene counteracted the ability of the Cdc13-Est1 fusion to elongate telomeres in wild-type cells (Figure 7C). Thus, we investigated whether the upregulation of Rif1 in *xrn1Δ* cells could explain both the reduced Cdc13 binding and the telomere length defect of the same cells. As shown in Figure 7D, deletion of *RIF1* totally suppressed the telomere length defect of *xrn1Δ* cells. Telomere length in *rif1Δ xrn1Δ* cells was the same as in *rif1Δ* cells (Figure 7D), suggesting that Xrn1 acts in telomere length maintenance by counteracting the effects of Rif1.

As telomeres were much longer in *xrn1Δ rif1Δ* cells than in *xrn1Δ* cells, we could not compare the above cell types for Cdc13 association at native telomeres. Thus, we used the strain with the 81 bp TG repeat sequence adjacent to the HO endonuclease cut site (Figure 4A) (10), where HO induction generates an HO-derived telomere whose length is similar in both *xrn1Δ* and *xrn1Δ rif1Δ* cells. As expected (74), ChIP analysis revealed that the amount of Cdc13 associated to the HO-induced telomere was higher in *rif1Δ* cells than in wild-type (Figure 7E). Furthermore, although all cell type extracts contained similar amounts of Cdc13 (Figure 7F), the lack of Rif1 restored Cdc13 association to telomeres in *xrn1Δ* cells. In fact, the amount of Cdc13 bound at the HO-induced telomere in *xrn1Δ rif1Δ* cells was higher than in *xrn1Δ* cells (Figure 7E). Altogether, these findings indicate that Xrn1 promotes Cdc13 association to telomeres by controlling Rif1 levels.

DISCUSSION

Here we provide evidence that the RNA processing proteins Xrn1 and Rrp6 are involved in telomere metabolism. In particular, we found that the temperature sensitivity of *cdc13-1* mutant cells is partially suppressed by the lack of Rrp6 or

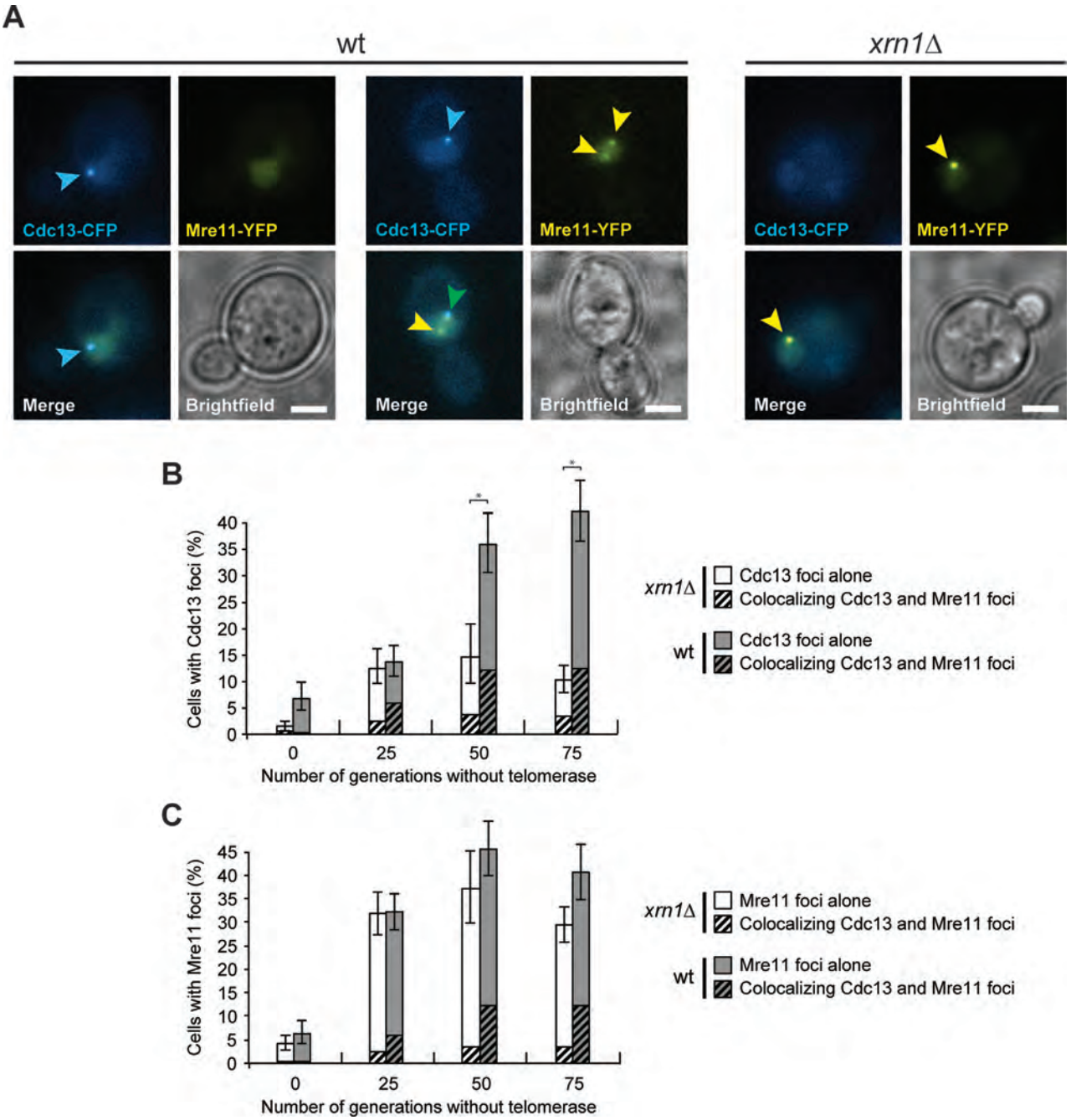

Figure 5. The lack of Xrn1 impairs Cdc13 focus formation. (**A**) Cdc13 and Mre11 localization was examined in *XRN1* (ML968-1D) and *xrn1Δ* (ML968-3B) cells before or 25, 50 and 75 generations after loss of a telomerase-encoding plasmid (pVL291). Yellow arrowheads indicate Mre11-YFP foci, blue arrowheads indicate Cdc13-CFP foci and green arrowhead indicates colocalization between the two proteins. Scale bar: 3 μm. (**B**) *xrn1Δ* cells are impaired for Cdc13 focus formation. Cells in panel A were quantified. Error bars represent 95% confidence intervals ($n = 200$–600). *$P < 0.05$, *t*-test. (**C**) *xrn1Δ* cells are proficient for Mre11 focus formation. Cells in panel A were quantified. Error bars represent 95% confidence intervals ($n = 200$–600).

Xrn1, as well as by Rrp6 or Xrn1 nuclease defective variants, independently of the NMD proteins. The increased temperature resistance of *cdc13-1 xrn1Δ* and *cdc13-1 rrp6Δ* cells is related to their inability to activate the checkpoint.

Checkpoint activation in *cdc13-1* cells is due to the accumulation at telomeres of ssDNA that turns on the checkpoint kinase Mec1. Our data indicate that the defective checkpoint response in *cdc13-1 rrp6Δ* double mutant cells cannot be ascribed to reduced ssDNA generation. Interestingly, Rrp6 was shown to promote the association of RPA (58) and Rad51 (78) at intrachromosomal DSBs in yeast and mammals, respectively, by an unknown mechanism. Thus, one possibility is that Rrp6 modulates directly or indirectly the association to telomeric ssDNA of protein(s) required for checkpoint activation.

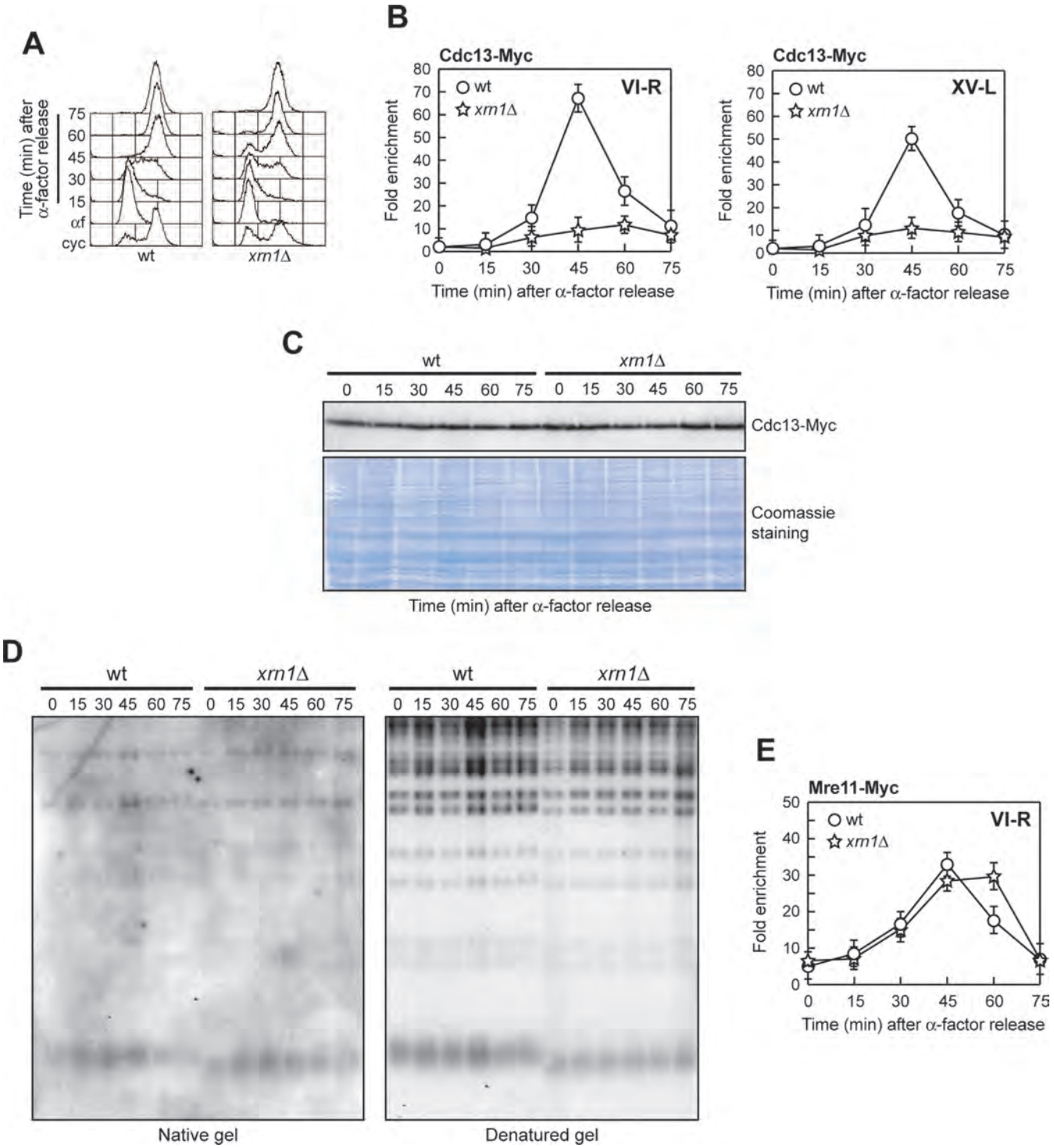

Figure 6. The lack of Xrn1 impairs Cdc13 association but not ssDNA generation at capped telomeres. (**A**–**D**) Exponentially growing cell cultures (cyc) were arrested in G1 with α-factor (αf) and released into the cell cycle. (A) Samples were collected for fluorescence activated cell sorting (FACS). (B) Chromatin samples taken at the indicated times after α-factor release were immunoprecipitated with anti-Myc antibodies. Coimmunoprecipitated DNA was analyzed by quantitative real-time PCR (qPCR) using primer pairs located at telomeres VI-R and XV-L and at the non-telomeric *ARO1* fragment of chromosome IV (CON). Data are expressed as relative fold enrichment of VI-R and XV-L telomere signals over CON signals after normalization to input signals for each primer set. The mean values ±s.d. are represented ($n = 3$). (**C**) Western blot with anti-Myc antibodies of extracts used for the ChIP analysis shown in (B). (D) Genomic DNA prepared from cell samples in (A) was digested with XhoI and the single-strand telomere overhang was visualized by in-gel hybridization (native gel) using an end-labeled C-rich oligonucleotide. The same DNA samples were hybridized with a radiolabeled poly(GT) probe as loading control (denatured gel). (**E**) Chromatin samples taken at the indicated times after α-factor release were immunoprecipitated with anti-Myc antibodies. Coimmunoprecipitated DNA was analyzed by qPCR using primer pairs located at VI-R telomere. Data are expressed as in (B).

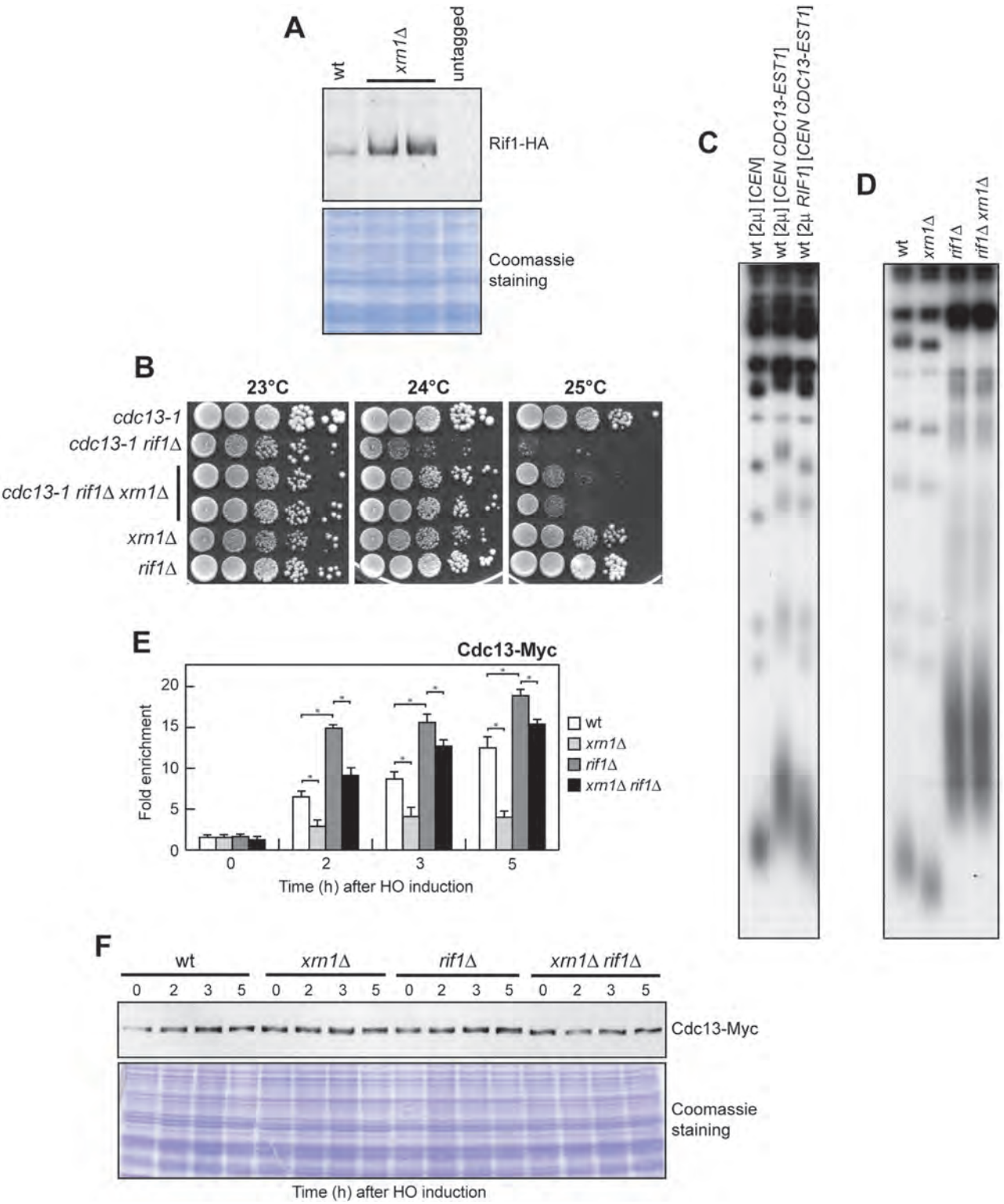

Figure 7. Functional interplays between Xrn1 and Rif1 in telomere length control. (**A**) Protein extracts prepared from exponentially growing cells were subjected to western blot analysis with anti-HA antibodies. (**B**) Cell cultures were grown overnight at 23°C in YEPD and 10-fold serial dilutions were spotted onto YEPD plates. (**C** and **D**) XhoI-cut genomic DNA from exponentially growing cells was subjected to Southern blot analysis using a radiolabeled poly(GT) probe. (**E**) HO expression was induced at time zero by galactose addition to yeast strains carrying the system described in Figure 4A. Chromatin samples taken at the indicated times after HO induction were immunoprecipitated with anti-Myc antibodies and coimmunoprecipitated DNA was analyzed by qPCR using primer pairs located 640 bp centromere-proximal to the HO cutting site and at the non-telomeric *ARO1* fragment of chromosome IV (CON). Data are expressed as relative fold enrichment of TG-HO over CON signal after normalization to input signals for each primer set. The mean values ±s.d. are represented ($n = 3$). *$P < 0.05$, *t*-test. (**F**) Western blot with anti-Myc antibodies of extracts used for the ChIP analysis shown in (E).

By contrast and consistent with the finding that Xrn1 and Rrp6 impairs viability of *cdc13-1* cells by acting in two distinct pathways, the lack of Xrn1 reduces the generation of telomeric ssDNA upon telomere uncapping. This observation, together with the finding that *EXO1* overexpression decreases the maximum permissive temperature of *cdc13-1 xrn1Δ* cells, indicates that Xrn1 participates in checkpoint activation in response to telomere uncapping by promoting the generation of telomeric ssDNA. Interestingly, Xrn1 contributes to generate ssDNA also at intrachromosomal DSBs that are subjected to extensive resection and stimulates Mec1-dependent checkpoint activation, similarly to telomeres following Cdc13 inactivation (29,30,58). By contrast, Xrn1 does not contribute to the generation of single-stranded overhangs at capped telomeres, suggesting a role for Xrn1 in promoting resection specifically at DNA ends that elicit a DNA damage response. Because Xrn1 acts in resection as a cytoplasmic nuclease, one possibility is that the lack of Xrn1 increases the persistence of non-coding RNAs that can inhibit the action of nucleases by annealing with the ssDNA molecules that are generated following telomere uncapping. However, overproduction of the Ribonuclease H1 (Rnh1), which decreases endogenous RNA:DNA hybrids in vivo as well as TERRA levels and R loops at telomeres (79–82), did not restore the temperature sensitivity in *cdc13-1 xrn1Δ* cells (Supplementary Figure S3). A previous deep transcriptome analysis has revealed that the amounts of the majority of mRNAs coding for DNA damage response proteins remained unchanged in *xrn1Δ* cells and the few genes that were misregulated are not obvious candidates (58). Therefore, further work will be required to identify the target(s) by which Xrn1 promotes ssDNA generation and checkpoint activation at uncapped telomeres.

We also show that Xrn1 acts as a cytoplasmic nuclease to maintain telomere length. Strikingly, the lack of Xrn1 dramatically reduces Cdc13 association to telomeres. This defective Cdc13 recruitment is not due to reduced ssDNA generation, as the lack of Xrn1 does not impair ssDNA generation at capped telomeres. On the other hand, the lack of Xrn1 causes upregulation of the *RIF1* mRNA and subsequent increase of the Rif1 protein level. Rif1 was shown to decrease Cdc13 association at telomeres independently of ssDNA generation (74), suggesting that the high Rif1 levels in *xrn1Δ* cells might explain the reduced Cdc13 binding and the telomere length defect of the same cells. Consistent with this hypothesis, we found that the lack of Rif1 completely suppresses the telomere length defect and restores Cdc13 association at telomeres in *xrn1Δ* cells. Altogether, these findings indicate that Xrn1 promotes Cdc13 association to telomeres and telomere elongation independently of ssDNA generation by controlling the amount of Rif1. By contrast, Rif1 is not the Xrn1 target in promoting ssDNA generation and checkpoint activation at uncapped telomeres, as the lack of Xrn1 still suppresses the temperature sensitivity of *cdc13-1 rif1Δ* cells.

In conclusion, Xrn1 appears to have two separate functions at telomeres: (i) it facilitates the generation of ssDNA and checkpoint activation at uncapped telomeres; (ii) it maintains telomere length independently of ssDNA generation by downregulating the amount of Rif1, which in turn counteracts Cdc13 association to telomeres. As RNA-processing factors are evolutionarily conserved and telomere protection is critical for preserving genetic stability and counteracting cancer development, our findings highlight novel mechanisms through which RNA processing proteins can preserve genome integrity.

SUPPLEMENTARY DATA

Supplementary Data are available at NAR Online.

ACKNOWLEDGEMENTS

We are grateful to A. Aguilera, J.S. Butler, D. Gottschling, A.W. Johnson, V. Lundblad and R. Wellinger for strains and plasmids. We thank G. Lucchini for critical reading of the manuscript.

FUNDING

Associazione Italiana per la Ricerca sul Cancro (AIRC) [IG grant 15210]; Progetti di Ricerca di Interesse Nazionale (PRIN) 2015 [to M.P.L.]; Danish Council for Independent Research and the Villum Foundation (to M.L.); Fellowship from Fondazione Italiana per la Ricerca sul Cancro (FIRC) (to C.C.). Funding for open access charge: AIRC [IG grant 15210 to M.P.L].
Conflict of interest statement. None declared.

REFERENCES

1. Wellinger,R.J. and Zakian,V.A. (2012) Everything you ever wanted to know about *Saccharomyces cerevisiae* telomeres: beginning to end. *Genetics*, **191**, 1073–1105.
2. Bonetti,D., Martina,M., Falcettoni,M. and Longhese,M.P. (2014) Telomere-end processing: mechanisms and regulation. *Chromosoma*, **123**, 57–66.
3. Henderson,E.R. and Blackburn,E.H. (1989) An overhanging 3′ terminus is a conserved feature of telomeres. *Mol. Cell. Biol.*, **9**, 345–348.
4. Wellinger,R.J., Wolf,A.J. and Zakian,V.A. (1993) *Saccharomyces* telomeres acquire single-strand TG_{1-3} tails late in S phase. *Cell*, **72**, 51–60.
5. Pfeiffer,V. and Lingner,J. (2013) Replication of telomeres and the regulation of telomerase. *Cold Spring Harb. Perspect. Biol.*, **5**, a010405.
6. Dionne,I. and Wellinger,R.J. (1996) Cell cycle-regulated generation of single-stranded G-rich DNA in the absence of telomerase. *Proc. Natl. Acad. Sci. U.S.A.*, **93**, 13902–13907.
7. Wellinger,R.J., Ethier,K., Labrecque,P. and Zakian,V.A. (1996) Evidence for a new step in telomere maintenance. *Cell*, **85**, 423–433.
8. Soudet,J., Jolivet,P. and Teixeira,M.T. (2014) Elucidation of the DNA end-replication problem in *Saccharomyces cerevisiae*. *Mol. Cell*, **53**, 954–964.
9. Faure,V., Coulon,S., Hardy,J. and Géli,V. (2010) Cdc13 and telomerase bind through different mechanisms at the lagging- and leading-strand telomeres. *Mol. Cell*, **38**, 842–852.
10. Diede,S.J. and Gottschling,D.E. (2001) Exonuclease activity is required for sequence addition and Cdc13p loading at a de novo telomere. *Curr. Biol.*, **11**, 1336–1340.
11. Larrivée,M., LeBel,C. and Wellinger,R.J. (2004) The generation of proper constitutive G-tails on yeast telomeres is dependent on the MRX complex. *Genes Dev.*, **18**, 1391–1396.
12. Bonetti,D., Martina,M., Clerici,M., Lucchini,G. and Longhese,M.P. (2009) Multiple pathways regulate 3′ overhang generation at *S. cerevisiae* telomeres. *Mol. Cell*, **35**, 70–81.
13. Gao,H., Cervantes,R.B., Mandell,E.K., Otero,J.H. and Lundblad,V. (2007) RPA-like proteins mediate yeast telomere function. *Nat. Struct. Mol. Biol.*, **14**, 208–214.

14. Nugent,C.I., Hughes,T.R., Lue,N.F. and Lundblad,V. (1996) Cdc13p: a single-strand telomeric DNA-binding protein with a dual role in yeast telomere maintenance. *Science*, **274**, 249–252.
15. Evans,S.K. and Lundblad,V. (1999) Est1 and Cdc13 as comediators of telomerase access. *Science*, **286**, 117–120.
16. Pennock,E., Buckley,K. and Lundblad,V. (2001) Cdc13 delivers separate complexes to the telomere for end protection and replication. *Cell*, **104**, 387–396.
17. Bianchi,A., Negrini,S. and Shore,D. (2004) Delivery of yeast telomerase to a DNA break depends on the recruitment functions of Cdc13 and Est1. *Mol. Cell*, **16**, 139–146.
18. Nakada,D., Matsumoto,K. and Sugimoto,K. (2003) ATM-related Tel1 associates with double-strand breaks through an Xrs2-dependent mechanism. *Genes Dev.*, **17**, 1957–1962.
19. Chang,M., Arneric,M. and Lingner,J. (2007) Telomerase repeat addition processivity is increased at critically short telomeres in a Tel1-dependent manner in *Saccharomyces cerevisiae*. *Genes Dev.*, **21**, 2485–2494.
20. Hector,R.E., Shtofman,R.L., Ray,A., Chen,B.R., Nyun,T., Berkner,K.L. and Runge,K.W. (2007) Tel1p preferentially associates with short telomeres to stimulate their elongation. *Mol. Cell*, **27**, 851–858.
21. Sabourin,M., Tuzon,C.T. and Zakian,V.A. (2007) Telomerase and Tel1p preferentially associate with short telomeres in *S. cerevisiae*. *Mol. Cell*, **27**, 550–561.
22. McGee,J.S., Phillips,J.A., Chan,A., Sabourin,M., Paeschke,K. and Zakian,V.A. (2010) Reduced Rif2 and lack of Mec1 target short telomeres for elongation rather than double-strand break repair. *Nat. Struct. Mol. Biol.*, **17**, 1438–1445.
23. Tseng,S.F., Lin,J.J. and Teng,S.C. (2006) The telomerase-recruitment domain of the telomere binding protein Cdc13 is regulated by Mec1p/Tel1p-dependent phosphorylation. *Nucleic Acids Res.*, **34**, 6327–6336.
24. Gao,H., Toro,T.B., Paschini,M., Braunstein-Ballew,B., Cervantes,R.B. and Lundblad,V. (2010) Telomerase recruitment in *Saccharomyces cerevisiae* is not dependent on Tel1-mediated phosphorylation of Cdc13. *Genetics*, **186**, 1147–1159.
25. Wu,Y., DiMaggio,P.A. Jr, Perlman,D.H., Zakian,V.A. and Garcia,B.A. (2013) Novel phosphorylation sites in the *S. cerevisiae* Cdc13 protein reveal new targets for telomere length regulation. *J. Proteome Res.*, **12**, 316–327.
26. Goudsouzian,L.K., Tuzon,C.T. and Zakian,V.A. (2006) *S.cerevisiae* Tel1p and Mre11p are required for normal levels of Est1p and Est2p telomere association. *Mol. Cell*, **24**, 603–610.
27. Qi,H. and Zakian,V.A. (2000) The *Saccharomyces* telomere-binding protein Cdc13p interacts with both the catalytic subunit of DNA polymerase alpha and the telomerase-associated est1 protein. *Genes Dev.*, **14**, 1777–1788.
28. Grossi,S., Puglisi,A., Dmitriev,P.V., Lopes,M. and Shore,D. (2004) Pol12, the B subunit of DNA polymerase alpha, functions in both telomere capping and length regulation. *Genes Dev.*, **18**, 992–1006.
29. Garvik,B., Carson,M. and Hartwell,L. (1995) Single-stranded DNA arising at telomeres in *cdc13* mutants may constitute a specific signal for the *RAD9* checkpoint. *Mol. Cell. Biol.*, **15**, 6128–6138.
30. Lydall,D. and Weinert,T. (1995) Yeast checkpoint genes in DNA damage processing: implications for repair and arrest. *Science*, **270**, 1488–1491.
31. Vodenicharov,M.D. and Wellinger,R.J. (2006) DNA degradation at unprotected telomeres in yeast is regulated by the CDK1 (Cdc28/Clb) cell-cycle kinase. *Mol. Cell*, **24**, 127–137.
32. Grandin,N., Reed,S.I. and Charbonneau,M. (1997) Stn1, a new *Saccharomyces cerevisiae* protein, is implicated in telomere size regulation in association with Cdc13. *Genes Dev.*, **11**, 512–527.
33. Grandin,N., Damon,C. and Charbonneau,M. (2001) Ten1 functions in telomere end protection and length regulation in association with Stn1 and Cdc13. *EMBO J.*, **20**, 1173–1183.
34. Puglisi,A., Bianchi,A., Lemmens,L., Damay,P. and Shore,D. (2008) Distinct roles for yeast Stn1 in telomere capping and telomerase inhibition. *EMBO J.*, **27**, 2328–2339.
35. Xu,L., Petreaca,R.C., Gasparyan,H.J., Vu,S. and Nugent,C.I. (2009) *TEN1* is essential for *CDC13*-mediated telomere capping. *Genetics*, **183**, 793–810.
36. Maringele,L. and Lydall,D. (2002) *EXO1*-dependent single-stranded DNA at telomeres activates subsets of DNA damage and spindle checkpoint pathways in budding yeast *yku70Δ* mutants. *Genes Dev.*, **16**, 1919–1933.
37. Zubko,M.K., Guillard,S. and Lydall,D. (2004) Exo1 and Rad24 differentially regulate generation of ssDNA at telomeres of *Saccharomyces cerevisiae cdc13-1* mutants. *Genetics*, **168**, 103–115.
38. Parker,R. (2012) RNA degradation in *Saccharomyces cerevisae*. *Genetics*, **191**, 671–702.
39. Nagarajan,V.K., Jones,C.I., Newbury,S.F. and Green,P.J. (2013) XRN 5′-3′ exoribonucleases: structure, mechanisms and functions. *Biochim. Biophys. Acta*, **1829**, 590–603.
40. Houseley,J., LaCava,J. and Tollervey,D. (2006) RNA-quality control by the exosome. *Nat. Rev. Mol. Cell Biol.*, **7**, 529–539.
41. Askree,S.H., Yehuda,T., Smolikov,S., Gurevich,R., Hawk,J., Coker,C., Krauskopf,A., Kupiec,M. and McEachern,M.J. (2004) A genome-wide screen for *Saccharomyces cerevisiae* deletion mutants that affect telomere length. *Proc. Natl. Acad. Sci. U.S.A.*, **101**, 8658–8663.
42. Ungar,L., Yosef,N., Sela,Y., Sharan,R., Ruppin,E. and Kupiec,M. (2009) A genome-wide screen for essential yeast genes that affect telomere length maintenance. *Nucleic Acids Res.*, **37**, 3840–3849.
43. Azzalin,C.M., Reichenbach,P., Khoriauli,L., Giulotto,E. and Lingner,J. (2007) Telomeric repeat containing RNA and RNA surveillance factors at mammalian chromosome ends. *Science*, **318**, 798–801.
44. Chawla,R., Redon,S., Raftopoulou,C., Wischnewski,H., Gagos,S. and Azzalin,C.M. (2011) Human UPF1 interacts with TPP1 and telomerase and sustains telomere leading-strand replication. *EMBO J.*, **30**, 4047–4058.
45. Lew,J.E., Enomoto,S. and Berman,J. (1998) Telomere length regulation and telomeric chromatin require the nonsense-mediated mRNA decay pathway. *Mol. Cell. Biol.*, **18**, 6121–6130.
46. Dahlseid,J.N., Lew-Smith,J., Lelivelt,M.J., Enomoto,S., Ford,A., Desruisseaux,M., McClellan,M., Lue,N., Culbertson,M.R. and Berman,J. (2003) mRNAs encoding telomerase components and regulators are controlled by *UPF* genes in *Saccharomyces cerevisiae*. *Eukaryot. Cell*, **2**, 134–142.
47. Addinall,S.G., Holstein,E.M., Lawles,C., Yu,M., Chapman,K., Banks,A.P., Ngo,H.P., Maringele,L., Taschuk,M., Young,A. *et al.* (2011) Quantitative fitness analysis shows that NMD proteins and many other protein complexes suppress or enhance distinct telomere cap defects. *PLoS Genet.*, **7**, e1001362.
48. Holstein,E.M., Clark,K.R. and Lydall,D. (2014) Interplay between nonsense-mediated mRNA decay and DNA damage response pathways reveals that Stn1 and Ten1 are the key CST telomere-cap components. *Cell Rep.*, **7**, 1259–1269.
49. Shukla,S., Schmidt,J.C., Goldfarb,K.C., Cech,T.R. and Parker,R. (2016) Inhibition of telomerase RNA decay rescues telomerase deficiency caused by dyskerin or PARN defects. *Nat. Struct. Mol. Biol.*, **23**, 286–292.
50. Luke,B., Panza,A., Redon,S., Iglesias,N., Li,Z. and Lingner,J. (2008) The Rat1p 5′ to 3′ exonuclease degrades telomeric repeat-containing RNA and promotes telomere elongation in *Saccharomyces cerevisiae*. *Mol. Cell*, **32**, 465–477.
51. Pfeiffer,V. and Lingner,J. (2012) TERRA promotes telomere shortening through exonuclease 1-mediated resection of chromosome ends. *PLoS Genet.*, **8**, e1002747.
52. Iglesias,N., Redon,S., Pfeiffer,V., Dees,M., Lingner,J. and Luke,B. (2011) Subtelomeric repetitive elements determine TERRA regulation by Rap1/Rif and Rap1/Sir complexes in yeast. *EMBO Rep.*, **12**, 587–593.
53. Bonetti,D., Clerici,M., Manfrini,N., Lucchini,G. and Longhese,M.P. (2010) The MRX complex plays multiple functions in resection of Yku- and Rif2-protected DNA ends. *PLoS One*, **5**, e14142.
54. Viscardi,V., Bonetti,D., Cartagena-Lirola,H., Lucchini,G. and Longhese,M.P. (2007) MRX-dependent DNA damage response to short telomeres. *Mol. Biol. Cell*, **18**, 3047–3058.
55. Eckert-Boulet,N., Rothstein,R. and Lisby,M. (2011) Cell biology of homologous recombination in yeast. *Methods Mol. Biol.*, **745**, 523–536.
56. Heim,R. and Tsien,R.Y. (1996) Engineering green fluorescent protein for improved brightness, longer wavelengths and fluorescence resonance energy transfer. *Curr. Biol.*, **6**, 178–182.

57. Ormo,M., Cubitt,A.B., Kallio,K., Gross,L.A., Tsien,R.Y. and Remington,S.J. (1996) Crystal structure of the Aequorea victoria green fluorescent protein. *Science*, **273**, 1392–1395.
58. Manfrini,N., Trovesi,C., Wery,M., Martina,M., Cesena,D., Descrimes,M., Morillon,A., d'Adda di Fagagna,F. and Longhese,M.P. (2015) RNA-processing proteins regulate Mec1/ATR activation by promoting generation of RPA-coated ssDNA. *EMBO Rep.*, **16**, 221–231.
59. Page,A.M., Davis,K., Molineux,C., Kolodner,R.D. and Johnson,A.W. (1998) Mutational analysis of exoribonuclease I from *Saccharomyces cerevisiae*. *Nucleic Acids Res.*, **26**, 3707–3716.
60. Burkard,K.T. and Butler,J.S. (2000) A nuclear 3′-5′ exonuclease involved in mRNA degradation interacts with Poly(A) polymerase and the hnRNA protein Npl3p. *Mol. Cell. Biol.*, **20**, 604–616.
61. Johnson,A.W. (1997) Rat1p and Xrn1p are functionally interchangeable exoribonucleases that are restricted to and required in the nucleus and cytoplasm, respectively. *Mol. Cell. Biol.*, **17**, 6122–6130.
62. Isken,O. and Maquat,L.E. (2008) The multiple lives of NMD factors: balancing roles in gene and genome regulation. *Nat. Rev. Genet.*, **9**, 699–712.
63. Enomoto,S., Glowczewski,L., Lew-Smith,J. and Berman,J.G. (2004) Telomere cap components influence the rate of senescence in telomerase-deficient yeast cells. *Mol. Cell. Biol.*, **24**, 837–845.
64. Chandra,A., Hughes,T.R., Nugent,C.I. and Lundblad,V. (2001) Cdc13 both positively and negatively regulates telomere replication. *Genes Dev.*, **15**, 404–414.
65. Grandin,N., Damon,C. and Charbonneau,M. (2000) Cdc13 cooperates with the yeast Ku proteins and Stn1 to regulate telomerase recruitment. *Mol. Cell. Biol.*, **20**, 8397–8408.
66. He,F., Li,X., Spatrick,P., Casillo,R., Dong,S. and Jacobson,A. (2003) Genome-wide analysis of mRNAs regulated by the nonsense-mediated and 5′ to 3′ mRNA decay pathways in yeast. *Mol. Cell*, **12**, 1439–1452.
67. Petreaca,R.C., Chiu,H.C. and Nugent,C.I. (2007) The role of Stn1p in *Saccharomyces cerevisiae* telomere capping can be separated from its interaction with Cdc13p. *Genetics*, **177**, 1459–1474.
68. Mantiero,D., Clerici,M., Lucchini,G. and Longhese,M.P. (2007) Dual role for *Saccharomyces cerevisiae* Tel1 in the checkpoint response to double-strand breaks. *EMBO Rep.*, **8**, 380–387.
69. Diede,S.J. and Gottschling,D.E. (1999) Telomerase-mediated telomere addition in vivo requires DNA primase and DNA polymerases alpha and delta. *Cell*, **99**, 723–733.
70. Tsukamoto,Y., Taggart,A.K. and Zakian,V.A. (2001) The role of the Mre11-Rad50-Xrs2 complex in telomerase- mediated lengthening of *Saccharomyces cerevisiae* telomeres. *Curr. Biol.*, **11**, 1328–1335.
71. Khadaroo,B., Teixeira,M.T., Luciano,P., Eckert-Boulet,N., Germann,S.M., Simon,M.N., Gallina,I., Abdallah,P., Gilson,E., Géli,V. and Lisby,M. (2009) The DNA damage response at eroded telomeres and tethering to the nuclear pore complex. *Nat. Cell Biol.*, **11**, 980–987.
72. Chai,W., Sfeir,A.J., Hoshiyama,H., Shay,J.W. and Wright,W.E. (2006) The involvement of the Mre11/Rad50/Nbs1 complex in the generation of G-overhangs at human telomeres. *EMBO Rep.*, **7**, 225–230.
73. Bonetti,D., Clerici,M., Anbalagan,S., Martina,M., Lucchini,G. and Longhese,M.P. (2010) Shelterin-like proteins and Yku inhibit nucleolytic processing of *Saccharomyces cerevisiae* telomeres. *PLoS Genet.*, **6**, e1000966.
74. Ribeyre,C. and Shore,D. (2012) Anticheckpoint pathways at telomeres in yeast. *Nat. Struct. Mol. Biol.*, **19**, 307–313.
75. Anbalagan,S., Bonetti,D., Lucchini,G. and Longhese,M.P. (2011) Rif1 supports the function of the CST complex in yeast telomere capping. *PLoS Genet.*, **7**, e1002024.
76. Xue,Y., Rushton,M.D. and Maringele,L. (2011) A novel checkpoint and RPA inhibitory pathway regulated by Rif1. *PLoS Genet.*, **7**, e1002417.
77. Hardy,C.F., Sussel,L. and Shore,D. (1992) A RAP1-interacting protein involved in transcriptional silencing and telomere length regulation. *Genes Dev.*, **6**, 801–814.
78. Marin-Vicente,C., Domingo-Prim,J., Eberle,A.B. and Visa,N. (2015) RRP6/EXOSC10 is required for the repair of DNA double-strand breaks by homologous recombination. *J. Cell Sci.*, **128**, 1097–1107.
79. Balk,B., Maicher,A., Dees,M., Klermund,J., Luke-Glaser,S., Bender,K. and Luke,B. (2013) Telomeric RNA-DNA hybrids affect telomere-length dynamics and senescence. *Nat. Struct. Mol. Biol.*, **20**, 1199–1205.
80. Gavaldá,S., Gallardo,M., Luna,R. and Aguilera,A. (2013) R-loop mediated transcription-associated recombination in *trf4Δ* mutants reveals new links between RNA surveillance and genome integrity. *PLoS One*, **8**, e65541.
81. Arora,R., Lee,Y., Wischnewski,H., Brun,C.M., Schwarz,T. and Azzalin,C.M. (2014) RNaseH1 regulates TERRA-telomeric DNA hybrids and telomere maintenance in ALT tumour cells. *Nat. Commun.*, **5**, 5220–5230.
82. Yu,T.Y., Kao,Y.W. and Lin,J.J. (2014) Telomeric transcripts stimulate telomere recombination to suppress senescence in cells lacking telomerase. *Proc. Natl. Acad. Sci. U.S.A.*, **111**, 3377–3382.